UiT Noregs arktiske universitet

Faculty of Science and Technology
Department of Computer Science

Near-optimality and robustness in energy systems modelling

A wealth of suboptimal alternatives for the energy transition

Koen van Greevenbroek

Philosophiae Doctor in Science, June 2024

Cover photo: Havøygavlen vindpark, Koen van Greevenbroek.

This thesis document was typeset using the *UiT Thesis LaTeX Template*.

Abstract

To avert a climate disaster, the global energy system quickly needs to transition to net-zero emissions. This will involve drastic reductions in the use of fossil fuels on one hand and electrification based on renewable energy on the other hand. Research has shown that the transition is technically feasible, but presents us with difficult trade-offs and compromises. Since renewable energy is more exposed to variability, the future will also present us with new robustness challenges.

Energy systems optimisation models, used to investigate possible future energy system designs, by default optimise for the least total cost. However, recent research has shown that near-optimal solutions, which are feasible and only slightly more expensive than cost-optimal ones, open up more options and create space for exploring factors that are hard to quantify. In this thesis, we develop a new methodology for approximating the space of all near-optimal solutions. It is applied to mapping out regional planning flexibility in Europe, analysing possible pathways for European green hydrogen production and studying how weather years impact the space of system designs. Across the board, the results show a wealth of options, creating much-needed space for public debate.

The advances in near-optimal methods are balanced by contributions towards improving robustness in energy systems design. We introduce a new method for identifying extreme weather events in energy systems with high shares of renewables, and use it to find the weather regimes posing the greatest risk of blackouts to a future European power system. By intersecting near-optimal spaces, we explore European energy system designs that are not only robust against different weather years but also various scenarios, including changing technology costs and land-use restrictions. In a case study on Norwegian hydrogen exports, we show that while technically feasible, the systemic impact of exports would face significant challenges in terms of land-use, social acceptance and equity. By taking a holistic perspective, energy systems modelling can help us brace for an uncertain future.

How to read this thesis

This thesis consists of a collection of articles and an accompanying introduction. The introduction sets up the context and motivation for the included articles, and provides time and space for the discussion of research methods, philosophical reflections and background material. It also includes an executive summary of the main results of the included articles, showing how they answer the overarching research questions of the thesis.

Chapter 1 (the "introduction to the introduction", as it were) is written in an more accessible style than the rest of the thesis. If you are curious about the topic of this thesis but are not an expert in energy systems research, you should still find this section interesting.

Chapter 2 (Background) covers the most essential theory needed to understand the methodology and results of the included articles. Chapter 3 contains a brief technical summary of the main findings in the included articles, organised thematically. Chapter 4 contextualises the results and points to future research directions.

Samandrag

For å unngå ein total klimakrise er det kritisk at det globale energisystemet går mot netto null utslepp so raskt som mogleg. Dette vil innebere ein drastisk nedgang i bruken av fossile brennstoff på den ein side, og auka elektrifisering basert på fornybar kraft på den andre. Forskinga viser at det let seg gjera, reint teknisk sett, men at overgangen vil by på vanskelege kompromiss og avvegingar. Fordi fornybar kraft er meir variabel, får me også større utfordringar knytt til pålitelegheit.

Energisystemmodellar blir brukte til å analysere framtidige energisystem, og blir vanlegvis optimaliserte for lågast totalkostnad. Nyare forsking har derimot peika på nær-optimale løysingar, som er funksjonelle og berre litt dyrare enn dei kostnads-optimale, som interessante. Dei opnar opp for fleire moglegheitar, og skapar rom for å utforska faktorar som er vanskelege å kvantifisere. I denne avhandlinga utviklar me ein ny metodikk for å kartleggja rommet av alle nær-optimale løysingar til ein modell. Metoden blir nytta til å kasta lys på regional planleggingsfleksibilitet i Europa, til å analysere moglege framtider for Europeisk produksjon av grønt hydrogen, samt til å forske på korleis vêret påverkar moglege energisystemløysingar.

Framgangen i nær-optimale metodar vert balansert av bidrag til forskinga rundt robuste energisystem. Me introduserer ein ny måte å identifisere dei mest utfordrande vêrsituasjonane for energisystem med ein høg grad av fornybar kraft, og brukar resultata til å peike på kva type vêrregime som vil kunne føre til straumkutt i framtidas Europa. Ved å rekna ut snittet av fleire nær-optimale rom finn me løysingar for det Europeiske energisystemet som er robuste, ikkje berre mot endrande vêr men òg ulike kostnadar og areal-avgrensingar. Til slutt ser me på norsk eksport av hydrogen; dette synar seg å vera mogleg i stor skala, men dei gjennomgripande konsekvensane for arealbruk, sosial aksept og fordelingspolitikk vil utgjera store hinder. Ved å ta omsyn til heilheita kan energisystemmodellering hjelpa oss gå ei usikker framtid i møte.

Korleis lesa denne avhandlinga?

Denne avhandlinga består av ein artikkelsamling samt ein introduksjon eller "kappe" til samlinga. Kappa kontekstualiserer og motiverer artiklane, og tek tida til å diskutera forskingsmetodane, drøfte forskingsfilosofi og presentera bakgrunnsmateriale. Den inneheld òg eit samandrag av hovudresultata i artiklane, og viser korleis dei svarar på forskingsspørsmåla i avhandlinga.

Kapittel 1, introduksjonen til kappa, er skreve i eit mindre teknisk språk enn resten av avhandlinga. Dersom du er interessert i temaet til avhandlinga, men ikkje er ekspert på energisystemmodellering, bør denne delen likevel kunne by på noko.

Kapittel 2 dekker det viktigaste bakgrunnsmaterialet som trengs til å forstå artiklane. Kapittel 3 inneheld ein kort og tematisk oppsummering av dei viktigaste resultata i artiklane. Kapittel 4 set alt i ein større kontekst og peikar på nokre moglege områder for framtidig forsking.

Acknowledgements

I am writing the final words of this thesis at an auspicious time, the day before the 10-year reunion of my high school class at UWC Atlantic College, sitting atop a cliff in southern Wales. If not at the start of my contract in Tromsø, one could trace the roots of the present work all the way back to those tumultuous and glorious years, which fuelled so much of the idealism and ambition to change the world that also drove me to pursue a PhD on just this topic. Who could have guessed then where I would be now, and what would be written on these pages? Certainly not I. Of course, the future is uncertain (see also Section 2.4), but another reason why I could not have know is that a thesis, to some extent, is the product of many influences from many different people, as well as places and events. Indeed, while sometimes being a solitary endeavour, the success of a PhD stands and falls with the support of the people around the candidate. I am immensely grateful for the support of everyone mentioned below, whether you played a large or small role in helping me in my efforts.

First, I would like to sincerely thank my supervisors. Alexander, thank you for adopting my project, and for always being available for a chat about anything. Marianne, thank you for all your advice — always on point and with a keen sense of what is relevant and what is not. Working with the both of you, I have felt supported and my ideas appreciated.

I was also privileged to work with a number of other co-authors. Aleks, words cannot do justice to my appreciation of our collaboration. Fred, your enthusiasm is always motivating; your feedback insightful. Hannah, you are the reason I now check the ECMWF extended range weather regime forecasts; it has been a pleasure and privilege to learn from you and work with you. Johannes, it has been inspiring to zero in on the (hopefully) right idea with you; I am really enjoying our collaboration. Isabelle, working with you is as refreshing as it is productive. Claudia, you have given me the outside perspective I needed and wanted, and your perfectionism is really paying off. I am very much looking forward to continue working with any and all of you in the future.

Others should be thanked precisely because they *didn't* work with me on my papers — thank you Marc, Martin and all the other kind co-workers at the

computer science department who have kept the spirits high and kept me from sinking into complete modelling obsession at work. I would also like to thank all supporting staff at my department, faculty and university; thank you for your work in cleaning, administration, gardening, snow-shovelling, maintaining the coffee supply and everything else that goes into running a successful research operation.

I did not study engineering or energy systems modelling but mathematics, as can probably be noticed from some of the exposition in this thesis. Throughout my studies, I have had incredibly inspiring and influential teachers and supervisors, without whom the present work also would not exist (or would contain deadly mathematical flaws or unintelligible writing). To Paul, Marni, Jonathan and Anne in particular: I am so grateful.

At the risk of stretching out these already long acknowledgements too far, I want to extend an to ode to Tromsø/Romsa: ground zero for this thesis. It is a cliché to claim that Tromsø possesses magic, but it certainly has *something* to it. This island, this remotest of cultural melting pots through the centuries, and the majestic and breath-taking nature around it, have grown very dear to me. Living "on top of Europe" at 69°N, so far away, affords a unique perspective which has influenced this work and my understanding of my home country. At the same time, the skiing, northern lights and cloudberries may just have distracted from my research.

Els, Jente, Grete og Bjørn: tusen takk for all støtta og kjærleiken over dei fire siste åra. Takk for at de har vore med meg heile vegen, at eg kunne ha heimekontor hjå dykk og for dei flotte feriane og høgtidane me har hatt ilag. Eg er veldig glad i dykk.

Voor Hein — de wind in mijn zeilen

Contents

1 Introduction

Many times I've gazed along the open road
Many times I've lied and many times I've listened
Many times I've wondered how much there is to know
Many dreams come true, and some have silver linings
— Led Zeppelin, Over the Hills and Far Away

The world is going through unprecedented climate change, prompting the declaration of a climate crisis. Global warming has already reached +1.1°C[1], leading to widespread negative impacts including reduced food security, lethal heat waves and infrastructure damage, among others.[1] These climate risks will only intensify and become more complex to manage at +2°C warming and beyond.

In one sense, avoiding future disaster is simple: greenhouse gas emissions must go down as soon as possible. While subject to great uncertainty, unmitigated climate change has been estimated to reduce global GDP by 19% by 2050[2] and 50% by the end of the century[3] (compared to a no-warming baseline). This can be translated to a *social cost of carbon dioxide* (SCC/SCCO_2), equivalent to the expected economic damage done by each tonne of CO_2 emitted and variously estimated at anywhere between 200–1000 EUR/tCO_2.[3]–[5] This cost is currently not fully accounted for[2], and a switch to renewable energy can cut

1. Specifically, the global surface temperature was 1.1°C higher in 2011–2020 than in the 1850–1900 period.[1]
2. The average price for emissions allowances in the EU emissions trading scheme (a cap-

emissions at a price significantly below the $SCCO_2$.[7]

On the other hand, cutting emissions presents many crossroads, choices and difficult trade-offs. For example, CO_2-emissions from the transportation sector could be reduced by a shift from cars to public transport, by switching from combustion engine cars to electric cars, by the increased use of bio-fuels or by a combination of the above and other measures. Each option involves a variety of different parties with different interests and can have wide-ranging impacts beyond the transportation sector alone (e.g. land use of bio-fuel production, mining of materials for batteries), making the choice a difficult political question. This may explain part of the substantial gap[1] between current climate policies and the targets set in the Paris agreement, intended to keep global warming "well below +2°C".[8]

More immediately relevant to this thesis, there are many different ways to decarbonise the energy sector. Both solar, wind, hydroelectric and nuclear power are major sources of low-emissions energy, but the ideal balance between these technologies is by no means a given. Decarbonisation involves some major open engineering questions, for instance, how to maintain system robustness and resilience under increasing shares of variable renewables such as solar and wind power; a question to which we return. On the whole, however, it has been amply demonstrated that net-zero emission energy systems are technically feasible.[9]–[11]

Arguably, the more pressing questions surrounding the energy transition are of a socio-political nature. Which technologies are deemed socially acceptable from a perspective of visual disturbance, equity and energy independence? Which industries are set to lose and gain? Where does the transition lead to job creation and losses?

The central aim of this thesis is to explore and expand our understanding of which future system designs are feasible and which are not. Mathematical models called *energy system optimisation models* (ESOMs) are a useful tool in this context, simulating the operations of an energy system with resolution needed to capture the variability of solar and wind power. Most research thus far, however, has focussed on exploring cost-optimal energy system solutions. These solutions can be fragile; by design they have the minimal needed capacities in order to meet modelled demands. This means they can be vulnerable to shocks that are not or cannot be accounted for in modelling, such as extreme weather, natural disasters, import disruptions or political upheaval. Moreover, purely cost-optimal solutions are often less socially or politically acceptable than slightly more expensive alternatives — cost is not everything. A major

and-trade mechanism for reducing emissions in the EU) was 84 EUR/tCO_2 in 2023.[6]

focus in this work is to look beyond cost-optimality in an effort to create space for public debate and acceptable trade-offs.

1.1 A crash course in near-optimality

The 20th century saw the breakthrough and widespread application of mathematical optimisation in planning and logistics, enabled by advances in both mathematical theory and computers. The modern academic discipline embodying this practice is called *operations research*, and has its roots in World War II.[12] Typical problems addressed in operations research include the optimisation of scheduling, flows of goods and placement of redistribution centres.

In the context of operations research, one usually takes the perspective of a central planner: the scope of the problem at hand is limited to choosing the best (e.g. cheapest, most efficient) solution among many possible alternatives. Strikingly often, such problems can be reduced to or may be related to so-called *linear programs*: a special type of optimisation problem where the space of alternatives (the *feasible space*) is bounded by linear constraints and the objective function (i.e. the thing to be optimised) is also linear. Linear programs can be solved particularly efficiently (a feat of much research; see e.g.Smith *et al.*[13]), meaning that even problem instances with thousands or millions of variables can be solved relatively quickly.

Planning and operation of an energy system[3] can in many cases be approximated by a linear program. Such a linear program, called an *energy system optimisation model* (ESOM) in this context, can be used to optimise both operations (hour to hour, day to day) *and* planning (e.g. where to place which power plants, where to strengthen the transmission grid by how much) simultaneously. The set of possible operations and planning choices is the feasible space in this case, and solving the linear program means finding the point in that space which optimises a given objective function. In the vast majority of cases, this objective function is total system cost[4].

Energy system optimisation models of this kind have a history of actual use in

3. For now, regard an energy system as being composed of the major components producing, converting, storing and transporting energy in a given geographical region. For example, the European energy system would encompass the transmission grid, the natural gas network and reserves and all power plants producing electricity. The exact delineation (i.e. which elements are and are not a part of the energy system) can be tailored to the problem at hand.
4. Typically calculated as the sum of annual operational costs and annualised investment costs

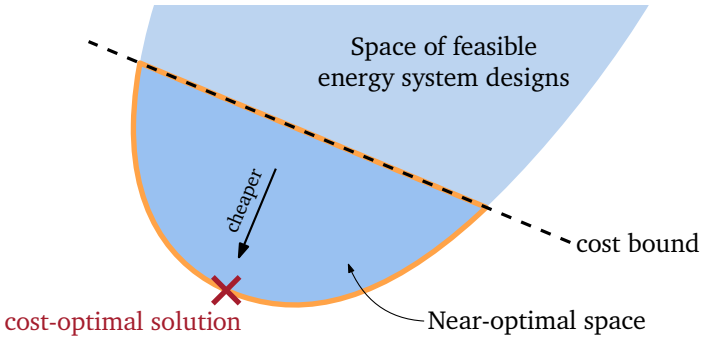

Figure 1.1: Abstract illustration of the near-optimal space of an energy system optimisation model. There is just one cost-optimal solution, but there are many different solutions (point in the near-optimal space) that are also feasible and only a little more expensive.

public administrations. The MARKAL family of models was one of the first,[14] being developed in an international collaboration under the International Energy Agency, and subsequently evolving into the TIMES model,[15] versions of which are still in use today. The current research field includes a large array of different models all following the same basic mathematical structure.[16]

Such models, however, essentially only strive for operational feasibility and cost minimisation. As we have seen, questions around the energy transition can be highly political; an axis that cannot easily be expressed as minimising total system cost and which is largely unaccounted for in ESOMs. An over-reliance on cost-optimisation could divert attention away from real alternatives, and at worst endanger the success of a rapid energy transition with all due consequences.

A key idea underpinning this thesis is to look not only for a single cost-optimal solution, but rather to look for a wide range of alternative solutions. These solutions should still be feasible (i.e. they should "work" from a technical point of view) and should not be too expensive. Figure 1.1 illustrates such a space of alternative solutions; it is commonly called a *near-optimal (feasible) space*. The idea is not new in itself, having roots in a paper by Brill from 1979[17] and being applied for the first time to energy systems by DeCarolis in 2011.[18] While subsequently developed,[19]–[21] the present work makes significant advances in techniques to systematically map out near-optimal solutions, as well as highlighting novel applications.

The vantage point afforded by near-optimal solutions can lead to important and useful insights into the ongoing energy transition. Broadly speaking, the wealth of different options that become possible at only slight cost increases is striking, and goes under the radar when focusing on cost-optimality only.

At the same time, working with near-optimal spaces presents its own challenges in the form of added complexity (making dissemination more difficult) and computational burden. Finally, while mapping out near-optimal spaces increases the number of energy system solutions under consideration, it is crucial to simultaneously address robustness to variable weather, climate change, changing costs, unexpected crises and other factors.

1.2 Robustness and feasibility

Energy systems can be fragile to changes and shocks from within and without. This is certainly not a new phenomenon — the 1973 oil shock,[22] triggered by the Yom Kippur War and characterised by a sudden quadrupling of global oil prices, had wide-reaching immediate and long term consequences. More recently, the Russian invasion of Ukraine in 2022 has led to a gas crisis in Europe with a tenfold increase in gas prices at its peak, inducing a sharp reduction in gas demand.[23] Both of the above take the form of a supply shock first and foremost; another common type of shock is extreme weather or natural disaster leading to power grid black-outs. A notable recent incident is the winter storm Uri which caused wide-spread black-outs across the isolated Texas electricity grid, resulting in dozens of deaths due to hypothermia and at least $130 billion in damages.[24]

Future energy systems may need to be robust to different kinds of shocks, especially as ever larger fractions of primary energy are sourced from renewables, and as climate change leads to more extreme weather. The variability of most renewable energy sources presents challenges on multiple time scales, from the daily[25],[26] and yearly[27],[28] to decadal,[29] and the question of how to brace for this variability is far from solved. Less of a shock but more of a long-term risk is that of climate change affecting both energy demand and renewable generation.[30]–[33] As the total cost of energy supply shifts more to capital expenditure (wind turbines, solar panels, etc.) and less to operational expenditure (fuels such as oil and gas), different kinds of supply shocks may take hold, hitting renewable energy generation supply chains.

"Robustness" can mean a variety of things in the context of energy systems planning. Loosely speaking, one can say that a particular energy system is *robust* against a certain set of events when these events do not significantly impact the ability of the system to satisfy a given energy demand at reasonable cost. Robustness against completely predictable events is usually a given, but events whose nature and frequency of impact are uncertain are more difficult to plan for. Some events may not be predictable exactly, but we might still have good statistical models for them. At the other extreme are "black swan" events:[34]

completely unforeseen events whose timing and consequences cannot be predicted using current knowledge and methods, such as a major political crisis, war or pandemic.

Energy system optimisation models often incorporate some variability, such as simulating operations over one or a few years of historical weather. Furthermore, common tactics used to enhance robustness of model solutions include accounting for possible transmission grid failure, ensuring available backup generation and more. However, how best to deal with the various types of shocks and risks in energy systems modelling is still an open field of research.

Feasibility does not have a precise definition in the context of energy systems modelling;[9] it is sometimes taken to mean what is "technically possible" in the world of physics, while viability also takes socio-economic constraints into account. In the context of this thesis, we refer to an energy system design being *feasible* in a particular model when the design is able to deliver on energy demand in that model. Feasibility as thus relative to any given model, and a solution that is feasible is only robust to the events and shocks represented in that model.

1.3 Research questions

The primary motivation of this thesis is to explore different options for the energy transition, going beyond cost-optimality. We formulate this as the following research question:

Question 1. *How can we map out which energy system designs are feasible and affordable, and which are not?*

In light of the above discussion on feasibility, this question should be interpreted relative to an energy systems model. Note that we leave it slightly open to interpretation what it means to "map out"; in Chapter 2 we see that the mathematical space of all feasible solutions is sufficiently complicated that only a simplified representation can be approximated in most cases.

If energy system models do not sufficiently account for robustness, their results run the risk of being overly optimistic and vulnerable to extreme events and shocks. This weakness extends to any answers to Question 1. It is therefore crucial to pursue robustness in modelling in parallel.

Question 2. *How can we find energy system designs that are robust against changing weather, climate, costs, political conditions and other factors?*

Finally, it is important not to lose sight of the eventual goal of energy systems modelling research: to inform effective policy decisions. Advances in modelling are mainly useful to the extent that they lead to more effective decision support (directly or indirectly),[35] and therefore we explicitly ask about the policy-relevance of methodological development.

Question 3. *What are the most relevant implications for energy policy resulting from advances in energy systems modelling?*

1.4 Overview over research contributions

1.4.1 Research articles

This thesis includes five research articles exploring the stated research questions from various angles. Here we provide a brief overview outlining how each article helps answer the above research questions; Chapter 3 gives a more technical and thematically organised summary of the main results. For ease of exposition, we refer to each article by single-word labels as listed in Table 1.1.

The first article, "1: Intersections", addresses Question 1 directly, laying out a new framework for working with near-optimal spaces in the context of energy systems modelling. Previous work on near-optimal spaces had employed various ad-hoc methods for producing collections of near-optimal energy system designs. "1: Intersections" stresses the interpretation of a suitable low-dimensional representation of a near-optimal space as a geometric object (a convex polytope) that can be mapped out as a whole. This systematic approach reveals large tracts of system designs that have previously largely gone under the radar. A novel technique enabled by the geometric perspective is computing the intersection of multiple near-optimal spaces, effectively cataloguing solutions that are feasible and near-optimal under different scenarios. This technique was showcased with the specific application of finding energy system designs that are robust against many different weather conditions, thus also addressing Question 2.

"2: Weather" further develops the topic of weather resilience by proposing a special class of energy system model output variables to identify extreme periods. In particular, this article builds on the premise of a future decarbonised European power grid with most electricity being produced by wind and solar power. Such a scenario induces vulnerability to cold periods with low winds, potentially leading to blackouts. In the article, we[5] show that electricity trans-

5. The academic "we" is used as a common custom; the articles included in this thesis also have multiple co-authors. See "Notes on included articles" in the appendix.

Label	Title	Status / reference
1: Intersections	*Intersecting near-optimal spaces: European power systems with more resilience to weather variability*	Published in *Energy Economics*[36]
2: Weather	*Using power system modelling outputs to identify weather-induced extreme events in highly renewable systems*	Published in *Environmental Research Letters*[37]
3: Trade-offs	*Trade-offs between regional and continental energy system design flexibility*	Under review at *Nature Sustainability*[38]
4: Pathways	*Diverse pathways for green hydrogen production in Europe*	Manuscript[39]
5: Exports	*The competitive edge of Norway's hydrogen by 2030: Socio-environmental considerations*	Published in the *International Journal of Hydrogen Energy*[40]

Table 1.1: Papers included in this thesis.

mission and storage infrastructure play a crucial role in such periods, and that the most severe events occur on a continental scale. This in turn influences what kinds of weather (i.e. what types of large-scale pressure systems) are critical for the electricity grid. The article improves our understanding of climate and weather resilience in energy systems planning, addressing an important part of Question 2.

"3: Trade-offs" introduces a novel application of near-optimal spaces (building on the theory developed in "1: Intersections") to the problem of regional design flexibility. Especially focusing on implications for European cooperation towards the 2050 target of net carbon neutrality (thus addressing Question 3), the article systematically maps out the regional/spatial variety of feasible European energy system designs. A surprising amount of design flexibility is revealed, showing that most studied regions have vast ranges of options in terms of renewable energy development and energy import/export balance. Importantly, however, key regions and technologies are revealed to have a disproportionate importance for the success of the overall European energy transition.

Taking a different, narrower perspective on European energy policy, "4: Pathways" considers the ways forward for European green hydrogen production specifically. Green hydrogen[6] is a major question mark in European energy

6. Hydrogen is a gas which can be used as an effective energy carrier (i.e. to store and transport energy) and as an alternative to for instance natural gas. It can be produced by

policy towards 2040 and 2050; it could play a large role in reducing CO_2 emissions, but competes with carbon capture and storage in this regard. We use near-optimal techniques to map out the breadth of different trajectories that European green hydrogen production could take over the 2025-2050 time horizon. This is the first time near-optimal techniques have been used to study the development of energy systems over a sequence of time horizons. Consistent with the theme of "1: Intersections" and "3: Trade-offs", we find a large range of possibilities even with a moderate total cost increase. An extensive scenario analysis reveals which factors are the most significant for green hydrogen development in terms of minimum and maximum viable production. Combining methodological development with insights for policy, this article touches on both Question 1 and 3.

Finally, "5: Exports" approaches the emerging European hydrogen sector from a different angle, investigating the prospects for Norwegian hydrogen exports to continental Europe. Break-even price ranges are obtained for three different overall export scenarios and a large variety of input cost assumptions. Rather than focusing specifically on mapping out the "entire" option space for hydrogen exports, however, this article addresses the limitations of modelling for cost-optimality. While blue[7] and green hydrogen exports are feasible from a technological perspective, a variety of concerns including public perception of onshore wind power, conflicts of interest with indigenous land use and fierce competition for any newly available electricity combine to cast doubt on the prospects for hydrogen exports.

Together, the five articles included in this thesis form a holistic approach to energy systems design, connecting developments in both theory and application. Moreover, "2: Weather" and "5: Exports" especially are examples of interdisciplinary work, connecting energy systems modelling with meteorology and social science, respectively. Questions 1 and 2 are complementary in the sense that the first asks how more options can be found, while the second considers which options might have to be struck out for lacking robustness (Figure 1.2). Seen together, the thesis attempts to strike a balance.

different means; "green" hydrogen is hydrogen produced by electrolysis using renewable electricity.

7. "Blue" hydrogen is produced from natural gas using steam methane reforming combined with carbon capture and storage.

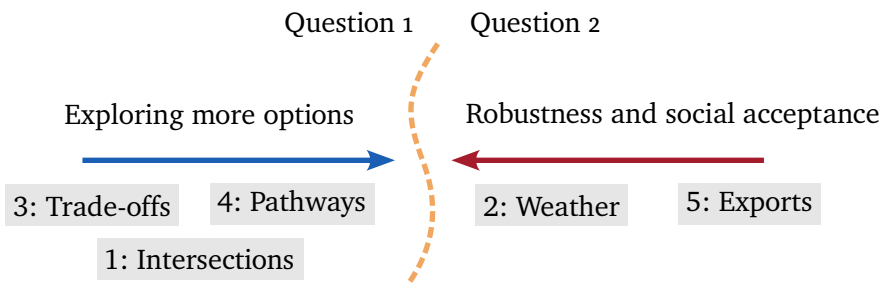

Figure 1.2: Abstact illustration of how the paper position themselves with respect to Questions 1 and 2.

1.4.2 Open modelling and transparency

Openness in energy research is critical for transparency,[41] but open code and data also allow for greatly improved productivity for the research field as a whole. Recent years have seen great leaps in the capabilities of open source energy systems modelling frameworks, and this thesis would not have been possible only a few years earlier for lack of sufficiently capable open source models for the European energy system. While there are currently several alternatives, the work in this thesis has benefited primarily from the PyPSA-Eur model,[11],[42] which itself builds on the PyPSA framework.[43]

All software and data used to produce the results in this thesis have been made available under open licenses; see the individual articles for specific accounts on where to find these resources. Of particular note is the software connected to "1: Intersections", which includes the first adaptation of PyPSA-Eur capable of running with more than a single weather year. Whenever practical, improvements and bug fixes to PyPSA and PyPSA-Eur have been contributed back upstream for the benefit of all users. While each individual change might be small, they add up to a total of +2348/-2433 lines added/removed across 95 commits.

Apart from open source code contributions, work on this thesis has also been the impulse for several dissemination efforts. This includes several popular scientific presentations at events open to the public, as well as a school tour. Of a more persistent nature, three blog entries have been written for `https://blogg.forskning.no/blogg-energiomstillinga` on the topics of nuclear power in Norway, the Longyearbyen energy transition and the results of "2: Weather", respectively.

1.4.3 Research articles not included in this thesis

Two additional works are worth mentioning for completeness even though they are not included in this thesis. The first is a brief exposition[44] of the initial work going into what was then "PyPSA meets Africa" and which has since become the PyPSA-Earth model. This article has been omitted due to my relatively minor contribution towards its publication and in order to preserve the thematic focus of this thesis.

The second is a manuscript in development on stakeholder perspectives on the Longyearbyen energy transition. This collaboration with Oskar Vågerö and Aleksander Grochowicz represents a leap in the practical application of the near-optimal methods developed in this thesis. Building on a model for the isolated Longyearbyen energy system, located on Svalbard, we develop an interactive interface for exploring near-optimal energy alternatives and collect the preferred solutions of about 120 residents (~5% of the total population). The results reveal a wide disparity between residents' visions for their future energy supply, and a surprisingly high willingness to accept higher electricity prices in order to pursue grid resilience and emission reductions, among other objectives. While relevant for this thesis, the manuscript is not included as it is still under development.

1.5 Research philosophy

Research does not spring into the world fully formed as published articles; it is developed over time by human beings. Especially in the field of energy systems modelling, many choices must be made throughout the duration of a research project, from modelling methodology to specific model input parameters. These choices may have both practical and ethical dimensions.[35],[45] Indeed, energy systems research being tightly interwoven with policy and politics means that researchers must balance positivist and normative approaches to their work.[45] In other words, energy systems research can both include dispassionate, objective accounts about how energy systems function and could develop in the future (positivism) as well as prescriptions for energy systems *should* develop (normativism). In this context, personal convictions can easily influence one's work, and it is thus worth discussing the main motivations underpinning this thesis. We follow this up with a brief discussion of the most important principles guiding the choices of methodology and approach to the research questions.

At the foundation of this thesis lies the acknowledgement of the climate crisis being one of the great challenges currently facing humanity. Current policies

put us on track for 2.5–2.9°C of global warming by the end of the century,[46] which would lead to devastating consequences.[1] Keeping global warming well below 2°C and ideally below 1.5°C (as set out in the Paris Agreement[8]) must involve drastic reductions in the use of fossil fuels across the energy, transportation and industrial sectors. The hope is that this thesis will, in a small way, help in the successful execution of this transition for the benefit of humanity.

What this thesis does not aim for is the promotion of any one particular solution or technology over another. As hinted at already, energy transition presents us with many difficult dilemmas such as choices between different low-carbon energy sources (e.g. wind, solar, nuclear, fossil fuels with carbon capture and storage) and means of providing flexibility (e.g. transmission lines, hydrogen storage and transportation, batteries). As this thesis takes a holistic approach (hence the talk of "energy systems", not single sources of energy), it is important to answer our research questions with as little bias as possible, creating a factual basis for democratic decision-making. Each competing sector stands to gain or lose and has its own lobby groups; none of them have influenced the making of this thesis.

An important principle guiding the formation of this thesis, and the choice of research questions and article topics, is that of striving for interdisciplinary work. Straddling the intersection between operations research, engineering, climate science and political economy, the field of energy systems modelling benefits from diverse perspectives, methods and expertise. Indeed, some of the key challenges in energy systems modelling research going forward, such as better integrating climate modelling results[47] and social factors,[48] naturally require interdisciplinary work. Questions 2 and 3 in this thesis are asked in this context.

2

Background

When you are young, they assume you know nothing
— Taylor Swift, cardigan

This chapter gives a more complete overview of the basic theory and techniques used in the field of energy systems modelling than could be given in the included articles. By no means exhaustive, we give an introduction to what energy system models are, and a brief overview of current state-of-the-art understanding of best modelling practices and trade-offs.

In the last part of the chapter, we give an account of near-optimal methods in particular: the technique at the base of "1: Intersections", "3: Trade-offs" and "4: Pathways". We cover both developments in the literature as well as advances made especially in "1: Intersections".

The remainder of this chapter and the next assumes basic familiarity with linear programming; for a reference on this topic see for instance Hillier *et al.*[49] or Smith *et al.*.[13]

2.1 Definitions

Before anything else can be expounded on, we need to resolve a basic question: what is an energy system, and what is an energy system model? Energy systems

modelling takes a rather peculiar role in the field of science. The discipline does not follow the scientific method directly, posing hypotheses about the real world which can be falsified based on observation. Energy system models are not models that aim to describe and predict observed natural processes or the laws of nature. Instead of asking "how do real energy systems behave?", the research questions of interest are usually of a more speculative nature, e.g. "which energy systems are likely to be realised in the future?" (see Question 1). Sometimes, the questions are even of a normative nature, e.g. "what *should* a future energy system look like?".

Given this somewhat ambiguous state of affairs, it is helpful to reflect on what energy systems and energy system models are and are not. Through this philosophical discussion, we see that energy system models often have hypothetical/fictional target systems — a fact it is important to be explicitly aware of when evaluating the usefulness of modelling results. Indeed, the idiom "modelling for insights, not numbers"[50] has become famous for good reason.

2.1.1 Energy systems

One definition of energy systems is given by Kotzur *et al.* in their guide to handling complexity in energy systems modelling.[51] Drawing on general systems studies,[52],[53] they identify a *system* as consisting of a number of elements or components and the interactions between them, with the interactions typically being more complex than the individual elements. Additionally, a system is described as having a *boundary* (i.e. it must be clear which elements are and are not part of the system), but may in turn interact with its environment. As such, one may consider hierarchies of systems, with one system acting as a component in a larger system (see Figure 2 in Kotzur *et al.*[51] for an illustration).

Energy systems in particular can take many forms, that is, there are different types of energy systems with different sets of components, interactions and system boundaries. Still, there are enough commonalities between these large classes of energy systems that they can sensibly be studied (and modelled) in some generality. We define energy systems as follows:

Definition 1. An *energy system* is a system comprising one or more components extracting energy or energy carriers (e.g. electricity, heat, natural gas), one or more consumers of energy (e.g. households, industry, cars) and any number of related components converting, transporting or storing energy.

We may apply the above definition equally to systems that currently exist (i.e. the components and their relations can be found in the real world) and

hypothetical systems that may or may not come to exist in the future.

In simplified terms, we can imagine an energy system having a rather "linear" form where energy is first produced[1], then transported and/or converted, and finally consumed.[48] Left up to interpretation in the above definition are the system boundaries, and this is where individual energy systems diverge widely. Energy system boundaries consist of at least the following facets:

Energy carriers: Which energy carriers are seen to be part of the system? Typically at minimum electricity, but could include heat, natural gas, hydrogen, etc.

Production scope: At which components is energy introduced into the system? Different points include production of primary energy (renewable energy generation, natural gas wells, coal mines), fuel-based electricity generation (natural gas turbines, hydrogen fuel cells) or other sources such as imports or a grid connection.

Consumption scope: At which components is energy consumed? This could be the distribution grid in aggregate, households, industry, consumers of industrial output, etc.

Spatial scope: Spatial location and extent of the system under consideration. In terms of extent, there is room to consider global systems all the way down to individual buildings.

A final dimension which might or might not be considered part of the system boundaries is that of time. Sometimes we consider energy systems as static, time-less entities (a "snapshot" of a past, present or hypothetical energy system), whereas other times we consider energy systems (either real or hypothetical) as evolving over time. One may distinguish between short-term time horizons, where the components of the system stay the same but their operations are considered on a time scale of minutes, hours or days, and long-term horizons where the structure of the system itself changes over the course of years or decades.

Table 2.1 gives an overview of the boundaries of the energy systems studied in the paper included in this thesis, following the above classification. As can be seen from the table, the articles all encompass a large spatial scope, though the spatial resolution is correspondingly low, aggregating all individual components

1. Physically, energy is always conserved and not "produced" from nothing. In keeping with common conventions, we still often refer to extraction of energy as "energy production" in the context of energy systems: the point where energy is introduced into the system.

	Carriers	Production	Consumption	Spatial
"1: Intersections"	Electricity	Renewables, nuclear & natural gas turbines	Fixed load on transmission grid	Europe[2]
"2: Weather"	Electricity	Renewables & nuclear	Fixed load on transmission grid	Europe[2]
"3: Trade-offs"	Elec., heat, others	Renewables, nuclear & fossil fuel extraction/imports	Fixed demands for various energy carriers	Europe[2]
"4: Pathways"	Elec., heat, others	Renewables, nuclear & fossil and green fuel extraction/imports	Fixed demands for various energy carriers	Europe[3]
"5: Exports"	Elec., heat, others	Renewables, nuclear & fossil fuel extraction/imports	Fixed demands for various energy carriers	Norway+[4]

Table 2.1: An overview of the boundaries of the energy systems investigated in the articles included in this thesis. Here, the "others" category in Carriers includes natural and synthetic gas, fossil oil and synthetic fuel, biomass, hydrogen, ammonia and methanol.

and demand to a regional or national level. Some of the articles deal only with the electricity sector directly, while others consider other energy carriers as well.

There are many interactions between energy systems and their environment. One dynamic of particular importance is the entanglement between energy systems and the global carbon cycle. At the most basic level, an energy system can have a one-way interaction with the carbon cycle by emitting CO_2 through the burning of fossil fuels. Energy systems with a larger scope (and especially future energy systems closer to net carbon neutrality) interact with the carbon cycle at more points through carbon capture, utilisation and storage/sequestration[5]. As such, it may at times be useful to consider an "extended energy system" including not only the flow of energy but also the flow of anthropogenic carbon in the same spatial scope. Carbon may enter this system through various means (fossil fuels, biomass, direct air capture) and likewise exit the system through CO_2 emissions to the atmosphere, by sequestering CO_2 underground, etc. See

2. Specifically: the EU in addition to Albania, Bosnia and Herzegovina, Montenegro, North Macedonia, Norway, Serbia, Switzerland and the United Kingdom
3. Specifically: the EU excluding Cyprus, Luxembourg and Malta but including Norway, Switzerland and the United Kingdom
4. Specifically: Denmark, Finland, Germany, Norway, Sweden, the Netherlands and the United Kingdom
5. CO_2 may be stored temporarily, e.g. in pressurised tanks, or may be *sequestered*, that is, pumped underground and stored away almost permanently.

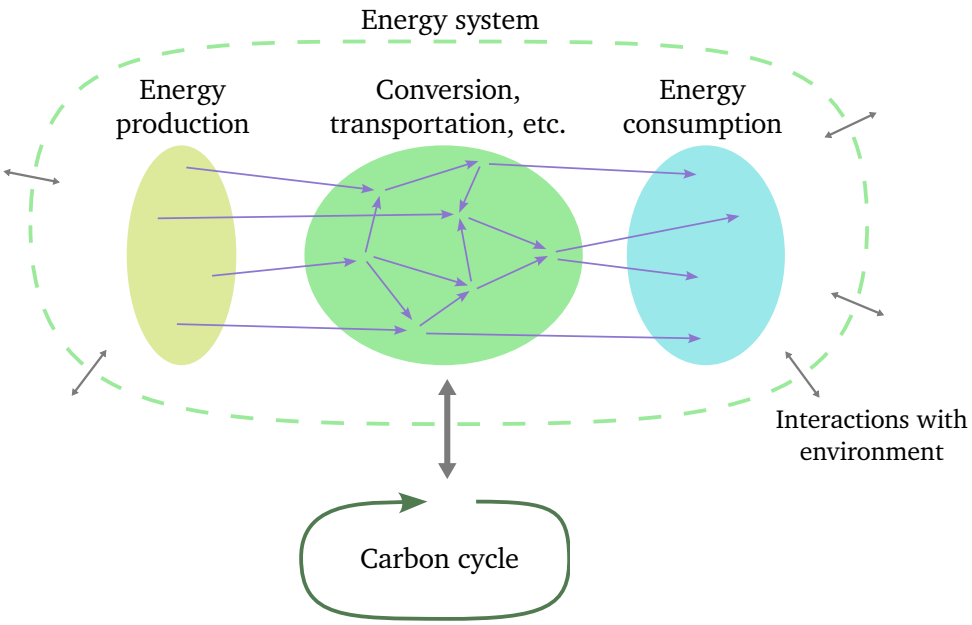

Figure 2.1: An illustration of an energy system, including the interaction with the carbon cycle.

Figure 2.1 for an illustration.

2.1.2 Energy system models

In order to study real and hypothetical energy systems, it is convenient to employ models. Philosophically speaking, it is not easy to define what a model *is*[6]; at a bare minimum, a model is a simplified representation of some aspect of reality or some system or class of systems. In our case, we are interested in models for energy systems, both real and hypothetical. Note that one model typically represents many similar systems (for instance, all possible systems with a specified structure). When a model represents its target system well enough, we can study the model to learn about the target system. In many cases, energy system models are not only used to help understand their target systems, but also as a way of efficiently exploring many different alternatives.

Following Definition 1, a model of an energy system typically consists of a collection of models of the components of the target system(s), together with models for a subset of the interactions between these components, and the interactions with the system environment.

6. See the Stanford Encyclopedia of Philosophy for an excellent discussion of various types of models and how to define them.[54]

A wide variety of different energy system models exist, falling into different categories depending on their purpose and formulation. In the broadest sense, one may distinguish between *operations* and *planning*[7] models, depending on whether the components of the target system are considered to be fixed, or whether one or more is subject to change. This thesis focuses entirely on the latter category. In planning models, there could be one or multiple *planning horizons*, i.e. discrete points in time where the components of the system are changed.

A slightly fuzzier distinction could be made between so-called *top-down* and *bottom-up* models. Herbst *et al.*[55] provide a good overview of this categorisation, and identify several sub-categories. Top-down models generally have highly aggregated representations of the physical components of the target system, while focusing more on the high-level dynamics over time between the components and the system environment. Such models typically employ economic theory to track prices, growth, demographic development, etc., and usually target systems with national to global spatial scope. Bottom-up models, on the other hand, are distinguished by their relatively high level of technological detail (concentrating on more accurate representation of physical infrastructure over time and space), while focusing less on the macroeconomic forces considered in top-down models. Some models may blur the lines between these two categories. The articles in this thesis use a bottom-up model.

Energy system models may be categorised by their mathematical structure[8]. The majority of energy system models in use today are *optimisation models*[56] — also the type used in this thesis. However, other types exist, such as multi-agent models and partial equilibrium models. Several surveys and categorisations have been published on the topic,[56]–[59] and it is outside the scope of this thesis to give a comprehensive account of all possible types of models and their uses in the literature.

Definition 2. An *energy system optimisation model* (ESOM) consists of a set of representations of energy systems (usually called the *feasible space*), as well as an objective function which maps each feasible system to a real number representing some quantity of interest — typically cost.

Strictly speaking, an energy system optimisation model might be considered a set of models together with an objective function. In practice, the individual

7. There is no standard terminology for "planning" models; operations models are sometimes also called "simulation" models.
8. While models can take many forms such as scale models, analogies, and descriptions,[54] energy system models are almost exclusively mathematical in nature, in that some mathematical structure (a collection of mathematical objects and equations describing their relations) is taken to be the simplified reflection of the target system(s).

elements of the feasible space usually follow the same structure, in that each element represents a system with the same set of components, but may differ in the sizing and operations of these components.

In our context, a single instance of an energy system is modelled as a vector $x \in \mathbb{R}^n$, each coordinate representing some physical quantity in the target system, such as the nameplate capacity of a power plant or the amount of electrical current flowing through a transmission line at a particular point in time. The feasible space, then, is simply a subset of $\mathbb{R}^n$, and the objective function is a function $c\colon \mathbb{R}^n \to \mathbb{R}$. Such a model can be *solved* by finding a feasible system minimising or maximising the objective function. The practical difficulty of solving an optimisation model depends on the structure of the feasible space and objective function, as well as the dimensionality n. Sometimes, the ESOM can include multiple objective functions, which leads to the field of multi-objective optimisation.[60]

As defined here, an energy system optimisation model *is* is a set of points $M \subset \mathbb{R}^n$ together with an objective function $c\colon M \to \mathbb{R}$. In practice, models (M, c) are almost always parametrised over certain sets of assumptions (e.g. costs, technological parameters, land use constraints, etc.); the result is sometimes called a *model generator*.[61] For example, PyPSA-Eur[42] can be seen as a model generator; running the data workflow for a particular configuration of parameters produces a concrete model. Some model generators are in turn based on so-called *model frameworks*, which are software packages facilitating the formulation of model generators. Examples include PyPSA[43] and Calliope.[62]

2.2 Basics of energy system optimisation models

The goal of this section is to introduce a simple, explicit example of an energy system optimisation model consisting of variables, constraints and an objective function written out fully. Our example will include energy generation, storage and transmission between different nodes. However, for a much more complete reference on the topic, see e.g. Kirschen *et al.*.[63]

Planning models (as opposed to operations models) are instances of the *capacity expansion problem*. Recall that an optimisation problem in all generality consists of a feasible space $M \subset \mathbb{R}^n$ and an objective function $c\colon M \to \mathbb{R}$. The coordinates of each feasible point $x \in M \subset \mathbb{R}^n$ are called the *decision variables* of the problem. In a capacity expansion problem, there are two types of decision variables: capacity expansion variables, and operational variables. The capacity expansion variables represent components of the target system

that can be expanded, such as new power plants being built or transmission lines reinforced. The operational variables each represent the operational state of a particular component at a particular time, such as the output of a power plant or the state of charge of a battery.

In the simplest form of capacity expansion problems, the feasible space of the optimisation problem is defined by linear constraints and the objective function is also linear in the decision variables, resulting in a linear program (LP). We start by explicitly writing down a simple example, and gradually add more functionality (variables, constraints) to the problem in order to represent more involved energy systems.

ESOMs are defined over a discrete number of time-steps $t \in \{1, \dots, T\}$; these could for instance be the hours in a year. Let a fixed energy demand d_t be given for each time step. Next, assume we have N generators with maximum capacities $g^{\max}$ (in MW) for $i \in \{1, \dots, N\}$. Each generator has a variable cost c_i (€/MWh) of producing energy, and its capacity may be expanded for a cost of C_i (€/MW). This expansion cost is typically annualised. Finally, let u_{it} be the capacity factor of generator i at time t, meaning the fraction of nominal capacity available at that time.

Let the capacity expansion variables be g_i (MW); the optimised size of each power plant. Let x_{it} (MW) be the operational variables, indicating the power output of the ith generator at time step t. Then a complete capacity expansion problem can be formulated as follows:

Minimise:
$\sum_i C_i \cdot g_i + \sum_{i,t} c_i \cdot x_{it}$
Such that:

$$\begin{aligned}
\textstyle\sum_i x_{it} &\geq d_t && \text{for all } t \in \{1, \dots, T\} \\
x_{it} &\leq u_{it} \cdot g_i && \text{for all } t \in \{1, \dots, T\} \text{ and } i \in \{1, \dots, N\} \\
g_i &\leq g_i^{\max} && \text{for all } i \in \{1, \dots, N\} \\
x_{it}, g_i &\geq 0 && \text{for all } t \in \{1, \dots, T\} \text{ and } i \in \{1, \dots, N\}
\end{aligned} \tag{2.1}$$

More abstractly, an LP such as the above can be written as "min $c \cdot x$ s.t. $Ax \leq b$", where c, x and b are vectors and A a matrix; each row of A encodes a constraint and each column a variable.

As a next step, let us incorporate multiple locations (nodes), and a transmission grid connecting them. We can regard the nodes and the transmission lines as forming a directed graph (the orientation of the edges does not matter except as a sign convention). Let n index the nodes in our model so that we now

have demand, production and capacity variables given by d_{tn}, x_{itn} and g_{in}, respectively. Furthermore, let ℓ index the lines/edges in our model. Now, we can let the decision variables $f_{t\ell}$ (MW) denote the active power flow along line ℓ (positive in the direction of ℓ) at time t. Let F_ℓ (MW) denote the maximum capacity of line ℓ. For notational convenience, let $K_{n\ell}$ denote the entries in the incidence matrix of our directed graph. That is, $K_{n\ell} = 1$ if link ℓ ends at node n and $K_{n\ell} = -1$ if link ℓ starts at node n.

A capacity expansion problem with multiple nodes and transmission can then be formulated as follows (omitting the indices for brevity):

$$
\begin{aligned}
&\text{Minimise:} \\
&\textstyle\sum_{i,n} C_{in} \cdot g_{in} + \sum_{i,t,n} c_i \cdot x_{itn} \\
&\text{Such that:} \\
\textstyle\sum_i x_{itn} + \sum_\ell K_{n\ell} \cdot f_{t\ell} &\geq d_{tn} \\
x_{itn} &\leq u_{itn} \cdot g_{in} \\
f_{t\ell} &\leq F_\ell \\
f_{t\ell} &\geq -F_\ell \\
g_{in} &\leq g_{in}^{\max} \\
x_{itn}, g_{in} &\geq 0
\end{aligned}
\tag{2.2}
$$

In the above, we take the capacities F_ℓ to be constant; they might as well be treated as capacity expansion variables in their own right.

The above formulation uses the most simplistic way of modelling electricity transmission; a so-called *transport model*. In reality, active power flow between two nodes is not decided outright by the grid operator, but is a function of the phase angle (voltage angle) between those nodes (as well as the conductance and susceptance, or, equivalently, the resistance and reactance of the line), and the sum of the phase angles over any circuit in the grid must sum up to 0 (Kirchoff's Voltage Law).[64] Under a number of simplifications and linearisations, one can approximate

$$
f_\ell \approx \frac{\theta_n - \theta_m}{x_\ell} \tag{2.3}
$$

where x_ℓ is the reactance of line ℓ and θ_n, θ_m are the phase angles at either end of the line. This constraint can be added directly to Equation 2.2 (adding θ_n as decision variables), but other options are also available in order to implement Kirchoff's Voltage Law. See Neumann *et al.*[65] for an in-depth comparison of various transmission formulations, as well as consideration of transmission losses.

The last major component we have not yet touched on is energy storage. This could be added through capacity expansion variables e_{in} (MWh) and s_{in} (MW)

representing the size and charge/discharge capacity of the ith storage unit at node n. Let $C^{(e)}_{in}$ and $S^{(s)}_{in}$ be their respective capital costs. Let $x^{(i)}_{itn} \geq 0$ and $x^{(o)}_{itn} \geq 0$ be charging and discharge rate in MW, respectively. Let y_{itn} be the state-of-charge of storage unit i at node n and time t. Finally, let η_{in} be discharge efficiency. Then we could reformulate the objective function as

$$\sum_{i,n} \left(C_{in} \cdot g_{in} + C^{(e)} e_{in} + C^{(s)} s_{in} \right) + \sum_{i,t,n} c_i \cdot x_{itn}, \tag{2.4}$$

and the demand constraint as

$$\sum_{i} \left(x_{itn} + \eta_{in} \cdot x^{(o)}_{itn} - x^{(i)}_{itn} \right) + \sum_{\ell} K_{n\ell} \cdot f_{t\ell} \geq d_{tn}. \tag{2.5}$$

We limit $x^{(o)}_{itn}$ and $x^{(i)}_{itn}$ by s_{in}, analogous to generators. The state-of-charge is handled by setting $y_{itn} \leq e_{in}$, and introducing the constraint

$$y_{i,t,n} = y_{i,t-1,n} + x^{(i)}_{itn} - x^{(o)}_{itn} \quad \text{for all } t \in \{2, \ldots, T\}, \tag{2.6}$$

preserving the state-of-charge from one time-step to the next. Optionally, one could also add a standing loss to the above by e.g. substituting $(1 - \delta) y_{i,t-1,n}$ for $y_{i,t-1,n}$ for some percentage loss δ.

Many other types of constraints could be added to the above LP; we do not give an exhaustive overview here. Examples include global constraints to limit certain types of generation, such as in order to limit emissions, global constraints limiting the total build-out of certain types of generators, or constraints enforcing some variation of import/export balance.

While the above LP is designed for a power system (i.e. only electricity generation, transmission, and demand are modelled), LPs with a similar structure can be created to model systems with multiple energy carriers. In such cases, controllable links (similar to transmission lines in the transport model) with conversion factors are typically used to convert from one energy carrier to another.

We restrict our attention to pure linear programs in this thesis, but more complex behaviour can be achieved using, for instance, integer variables, non-linear objective functions or other features making the optimisation non-linear. This naturally impacts solving time.

2.3 Spatial and temporal aggregation

LPs can be solved quite efficiently; they were famously proved to be solvable in polynomial time through the ellipsoid method by Khachiyan in 1979.[9] Modern interior point methods can solve LPs with millions of constraints and variables in a matter of minutes or hours. Still, problem size needs to be kept under control, and the number of variables and constraints can quickly add up. As a simple example, consider a model with 100 nodes, 8760 time steps (one for each hour in a year) and 5 different components at each node. This already results in $100 \cdot 8760 \cdot 5 = 4{,}380{,}000$ operational variables. While still surmountable for good LP solvers, having orders of magnitude more variables quickly becomes impractical.

Moreover, it bears mentioning that LP solvers have not benefited as greatly from hardware improvements as many other applications. This is because increasing hardware capabilities since the mid-2000s has mainly stemmed from larger numbers of processing cores, while CPU frequency has largely flattened.[51] LP solvers spend most of their time on large matrix factorisations, however, and current state-of-the-art solvers are not able to exploit parallelism beyond about 16 threads.[67] While progress has been made on more parallelisable and distributable solving algorithms,[67] such methods are not yet broadly applied in the field of energy systems modelling.

Europe counts more than 7000 power plants.[68] Some aggregation is thus needed in order to produce a model that can be solved effectively. Typically, one uses a combination of spatial aggregation (reducing the number of nodes) and temporal aggregation (reducing the number of time steps). One could consider the study of the most effective aggregation strategies as a research field on its own.[69]–[72] Abstractly speaking, aggregation in the context of LPs means substituting sets of constraints and/or variables (corresponding to sets of rows and columns in the coefficient matrix A, respectively) for a smaller number of representative constraints/variables.[73] A priori, there is no guarantee that such aggregation results in an LP with solutions that are optimal or even feasible in the original LP. The challenge is finding an aggregation scheme which yields results that are close enough to feasible and optimal for practical purposes. Kotzur *et al.* give an excellent overview of aggregation in ESOMs as of 2021,[51] touching on both spatial and temporal aggregation.

There are generally two dimensions of spatial aggregation. The number of generators or other components can be reduced (e.g. grouping generators with similar characteristics that are located at the same model node), and the number of model nodes can be reduced (grouping nodes with similar demand

9. See Grötschel *et al.*[66] for an exposition.

profiles and sets of generators). Frysztacki *et al.*[74] study various combinations of both techniques in the context of the European power system, also providing a brief overview of different clustering algorithms applied to spatial aggregation in ESOMs.

Temporal aggregation has received more attention in the literature; a review[69] by Hoffmann *et al.* lists 129 publications on the topic between 1999 and 2019. In early models it was common to reduce model size by only modelling a few representative hours or days a year. This works well for systems with little temporal interdependence and small spatial scales. The state-of-charge cannot be tracked under naive use of representative periods, however, and over large geographical regions, typical periods become less and less representative. Some progress, however, has been made on various methods to link states-of-charge between chronologically ordered representative periods; see Section 3.2.4 in the above-mentioned review. The alternative is aggregating neighbouring time-steps, either uniformly (e.g. reducing temporal resolution from 1-hourly to 3-hourly) or via some clustering scheme resulting in time-steps of varying lengths. The two approaches may also be combined by first selecting a number of representative periods, and then reducing the time-resolution within each representative period.[75]

After having decided on an overall aggregation strategy (representative periods, merging neighbouring periods, some combination), one needs to decide how to actually construct the reduced set of time-steps. In the case of a uniform time resolution reduction (e.g. 1- to 3-hourly), this is rather trivial. When using representative periods, a common method is to use some clustering algorithm (k-means, hierarchical, etc.) to cluster all available periods, and choose cluster centres (mediods / centroids) as representative periods.[70] This is sometimes combined with the selection of more "extreme" periods in order to better capture the variability in the full set of available periods; see Section 4.1.1 in the aforementioned review.[69]

2.4 Accounting for uncertainty

Energy systems modelling is an exercise in simplification, which necessarily leads to some deviations from the actual energy systems of interest. But simplification is far from the only potential source of error we have to contend with.

As previously explained, planning models have hypothetical target energy systems which are meant to represent plausible realisations of future energy systems; say, a net-zero European energy system in 2050. Such models are

only useful to the extent that their target systems might actually be realised. For example, we *could* model with cheap fusion energy by 2050, but this is so unlikely[76],[77] as to be of little value for decision-making. Oftentimes, it is less clear what is plausible and what is not. For example, how will climate change impact mean wind speeds around the North Sea? Given the unclear magnitude of future climate change as well as an incomplete understanding of its impact on wind speeds,[31],[78],[79] this is an example of *uncertainty* that should be accounted for in energy systems planning.

2.4.1 Uncertainty and sensitivity analysis

In the context of energy systems modelling, uncertainty is usually thought of as influencing the environment and exogenous factors impacting the target energy system. Once those external factors are fixed, however, an energy system optimisation model is deterministic in nature. Thus if the planning horizon is 2050, the modeller needs to make certain choices about parameters such as weather and climate, technology costs, demand patterns and more, and these parameters may be subject to more or less uncertainty. Rather than choosing single values for each parameter (possibly carrying bias), we can also consider ranges or distributions.

Thinking about an ESOM as a feasible space M and objective function c, uncertain parameters may influence both M and c, or both the coefficients A, bounds b and objective c in a linear program. Formally, it is useful to consider choices for all parameters (costs, capacity factors, demand profiles, etc.) as points p in some parameter space $\mathcal{P} \subseteq \mathbb{R}^m$, and the coefficients, bounds and objective function making up a linear ESOM as functions of p, such that the LP is now written as $\min c(p) \cdot x$ s.t. $A(p)x \leq b(p)$. The optimum value of the LP, c^{opt}, is then itself a function $c^{\text{opt}}(p)$ of the parameters p (though by no means a linear function!). LPs do not generally have a unique optimum but rather an optimal facet; letting X^{opt} be the set of optimal solutions to the LP (that is, $X^{\text{opt}} = \{x \in \mathbb{R}^n \mid Ax \leq b \text{ and } c \cdot x = c^{\text{opt}}\}$), this set would also be a function of the parameters: $X^{\text{opt}}(p)$.

The parameter space $\mathcal{P}$ is often implicitly or explicitly equipped with a probability distribution; for the purpose of exposition, it is simplest to consider finite $\mathcal{P}$ with a discrete probability distribution defined in terms of a probability density function $\mathbb{P}(p) \in [0, 1]$ (with $\sum_{p \in \mathcal{P}} \mathbb{P}(p) = 1$). Often, it is difficult to estimate the "true" probability distribution underlying the parameters, and we are left with best guesses. It is now natural to ask about the distribution of the random variable $c^{\text{opt}}(p)$ — what, for instance, is the expected total system cost $\mathbb{E}\left(c^{\text{opt}}(p)\right)$? When the probability distribution on $\mathcal{P}$ represents our best guess at how factors such as climate, costs and demand could develop into the future,

then $\mathbb{E}\left(c^{\text{opt}}(p)\right)$ represents our best guess at the expected minimum cost of a future energy system. The distributions of other properties of ESOMs apart from optimal value c^{opt} may likewise be studied under uncertainty. Usually one cannot hope to calculate such values in closed form (optimal solutions being a non-linear function of p), and we are left estimating their values by means of Monte Carlo simulations or similar techniques.

Commonly, we are not only interested in the distribution of optimal system designs, but also in the relative importance of various parameters. For example, does the cost of solar panels or the cost of natural gas have a greater impact on optimal system design? This can help our understanding of how energy systems interact with their environment, and help identify the most important risk factors for energy systems planning. Analysing the relative importance of parameters is called *sensitivity analysis*, whereas quantifying the distributions of model outputs or characteristics is sometimes called *uncertainty analysis*.[80]

For sensitivity analyses, one usually considers a limited number of individual parameters $(p_1, p_2, \ldots, p_k) = p \in \mathcal{P}$. The general question is then how important each parameter is to the model solution characteristic of interest (such as the optimal system cost $c^{\text{opt}}(p)$). This question can be made more specific in a few different ways. A common approach is to fix the parameters to some baseline value $(p_1, \ldots, p_k) = (b_1, \ldots, b_k)$, and then vary each p_i one at a time. For instance, one could estimate the variance $\mathbb{V}\left(c^{\text{opt}}(p) \mid p_j = b_j \; \forall j \neq i\right)$ for each i by running the model for different values of p_i, keeping the other p_j fixed.

While simple, the one-at-a-time method has a weakness: it may depend strongly on the baseline point b. Generally, sensitivities may be different in different parts of the parameter space $\mathcal{P}$, while a one-at-a-time analysis only explores a small part of $\mathcal{P}$.[81] Various methods exist to assess sensitivities across $\mathcal{P}$, called *global sensitivity analysis*. For instance, one could estimate the variance $\mathbb{V}_{p_i}\left(\mathbb{E}_{p_{\sim i}}\left(c^{\text{opt}}(p) \mid p_i\right)\right)$, where the variance is taken over the ith parameter p_i and the expected value is taken over all other parameters (with p_i fixed). This is in a sense the component of the overall variance of $c^{\text{opt}}(p)$ explained by p_i. An alternative approach, used in "5: Exports", is to perform a multi-variable linear regression to compute coefficients $a_1, \ldots, a_k$ and a constant C such that $c^{\text{opt}}(p) \approx a_1 p_1 + \cdots + a_k p_k + C$; the coefficients are in this case a measure of the sensitivity of c^{opt} to each parameter. Of course, any of the above sensitivity analyses could also be performed on some other model characteristic than optimal system cost c^{opt}. Global sensitivity analysis is an extensive field (with energy systems modelling being far from the only application), and questions abound regarding how best to sample $\mathcal{P}$ in order to produce the most accurate estimates, how to reduce the sample size, etc.; we refer to Saltelli *et al.*[80] for

a reference on this topic.

2.4.2 Stochastic programming

Uncertainty analysis and sensitivity analysis can explain how ESOM results vary with changing parameters. For these analyses, it is not necessary to change anything about the model; it typically just needs to be solved a number of times with different parameters (in a Monte Carlo simulation or similar). Sometimes, it is desirable to include some aspect of uncertainty into the model outright.

In stochastic programming, the premise is to minimise the *expected* objective value of an ESOM over a set of possible parameter combinations (often called *events* in stochastic programming literature). A common starting point is a *two-stage stochastic linear program*,[82] where some decisions are made in stage one, and "recourse" can be taken in the second stage upon the revealing of some previously unknown information. In the case of energy systems modelling, one can naturally take the first-stage decision variables x^{cap} to be the capacity expansion variables, the second-stage decision variables the operational variables x^{op}. Assuming that parameters $p \in \mathcal{P}$ do not affect the capacity expansion variables, we can write a simple two-stage stochastic program as follows:

$$\begin{aligned} &\min_{x^{\text{cap}}} \left(c^{\text{cap}} \cdot x^{\text{cap}} + \mathbb{E}_{p \in \mathcal{P}} \left(\min c^{\text{op}}(p) \cdot x^{\text{op}}(p) \right) \right) \quad \text{s.t.} \\ &\qquad A^{\text{cap}} x^{\text{cap}} \leq b^{\text{cap}} \\ &T(p) x^{\text{cap}} + W x^{\text{op}}(p) \leq b^{\text{op}}(p) \end{aligned} \tag{2.7}$$

Here, the expectation in the objective function is of the objective function of a purely "operational" optimisation problem where the installed capacities x^{cap} have been fixed. The matrices $T(p)$, W define the coefficients in this operational problem; $T(p)$ is called the *transition matrix* determining how

A concrete example would be having to make some investment decisions subject to uncertain future fuel prices, wind conditions or hydro-power reservoir levels; with the above stochastic program it is possible to minimise the expected total system cost over a given probability distribution on $\mathcal{P}$. A stochastic program in the above form can be rewritten as a "plain" linear program whose size increases with the number $|\mathcal{P}|$ of possible parameter realisations under consideration[82] — in this formulation one has a separate set of operational variables $x^{\text{op},p}$ for each $p \in \mathcal{P}$. Since the first-stage capacity variables x^{cap} of a solution to Equation 2.7 are feasible for any scenario $p \in \mathcal{P}$, stochastic programming can help find robust solutions, though the cost for single scenarios may be high as long as the total expected cost across $\mathcal{P}$ is low.

2.5 Near-optimal methods

As laid out in Chapter 1, one of the main aims of this thesis is to take advantage of near-optimal solutions of ESOMs. One of the first techniques used to explore near-optimal solutions systematically is called *modelling to generate alternatives* (MGA), and was originally developed by Brill in the late 70s[17] and applied to problems in land and water management. DeCarolis was the first to apply MGA to the domain of energy systems modelling,[18] while Neumann *et al.*[20] popularised the term *near-optimal feasible space* in the field of energy systems modelling. Recently, Pedersen *et al.*[21] were the first to attempt to fully map out the near-optimal feasible space of an ESOM.

In an ESOM defined as a linear program $\min c \cdot x$ st. $Ax \leq b$ with an optimal value c^{opt}, the *ε-near-optimal space* of the linear program is

$$\mathcal{F}_\varepsilon = \left\{ x \in \mathbb{R}^n \mid Ax \leq b \text{ and } (1+\varepsilon)c \cdot x \leq c^{\text{opt}} \right\}. \tag{2.8}$$

The near-optimal space is obtained from the feasible space of the model (defined as $\{x \in \mathbb{R}^n \mid Ax \leq b\}$) by adding the single constraint $(1+\varepsilon)c \cdot x \leq c^{\text{opt}}$; a bound on total system cost depending on the *cost slack* ε. Each point in $\mathcal{F}_\varepsilon$ is a *near-optimal feasible solution*. The feasible space of an LP is a polyhedron; for energy system models we can safely assume that their feasible spaces are polytopes (i.e. bounded polyhedra; no variables are unbounded). Then, $\mathcal{F}_\varepsilon$ is also a polytope.

In general, large ESOMs may have millions of decision variables, meaning that $\mathcal{F}_\varepsilon$ is a subset of a very high-dimensional space. It is thus helpful to consider projections of $\mathcal{F}_\varepsilon$ onto a smaller number of dimensions. Following the terminology of "1: Intersections", let $\pi\colon (x^{\text{cap}}, x^{\text{op}}) \mapsto x^{\text{cap}}$ be the linear map forgetting about operational variables, and

$$\mathcal{F}'_\varepsilon = \pi(\mathcal{F}_\varepsilon) = \{x^{\text{cap}} \mid (x^{\text{cap}}, x^{\text{op}}) \in \mathcal{F}_\varepsilon\}. \tag{2.9}$$

This is the lower-dimensional polytope of all capacity decision vectors x^{cap} for which there exist operations x^{op} such that the resulting solution is feasible and near-optimal.

Often, $\mathcal{F}'_\varepsilon$ may still be too high-dimensional (i.e. there may be dozens or hundreds of capacity decision variables), and we can further reduce this by a linear map σ, which could, for instance, aggregate all capacity variables of a certain type (say, all wind power capacities). This results in the *reduced ε-near-optimal feasible space* $\mathcal{A}_\varepsilon = \sigma(\mathcal{F}'_\varepsilon)$; again a polytope.

While it is easy to define $\mathcal{A}_\varepsilon$, just formulating an ESOM as a linear program does not automatically give rise to an explicit description of $\mathcal{A}_\varepsilon$ as the convex

hull of a set of vertices. In general, the best we can do is to solve the original LP with various different objective functions and learn one new vertex of $\mathcal{A}_\varepsilon$ for each optimisation. Specifically, for a direction (vector) d in the ambient space of $\mathcal{A}_\varepsilon$ we can solve the LP

$$\max d \cdot y \quad \text{s.t.} \quad \sigma \circ \pi(y) = x \text{ and } x \in \mathcal{F}_\varepsilon. \tag{2.10}$$

A solution y^* to the above is an extreme point of $\mathcal{A}_\varepsilon$ in the direction d; equivalently, in the intersection of $\mathcal{A}_\varepsilon$ and its supporting hyperplane normal to d. Note, however, that the above optimisation problem has as many variables as the original LP, and is no easier to solve. In "1: Intersections", we investigate how to "explore" $\mathcal{A}_\varepsilon$ efficiently using a limited number of optimisations.

In the literature, some reduced space $\mathcal{A}_\varepsilon$ is usually explored primarily in the directions parallel to the axes; for instance, exploring maximum and minimum total installed solar and wind capacities.[20],[83] Another common approach is to find "maximally different" points in $\mathcal{F}'_\varepsilon$ by starting with one point x_1 on the boundary (say, an optimum) and then choosing a direction d_1 pointing "away" from x_1 in some sense, obtaining the point x_2 and repeating this procedure.[18],[19],[84] This is known as the *Hop-Skip-Jump* method.

Near-optimal methods are being developed actively; see Lau *et al.*[85] for a recent review on the topic. Challenges remain in terms of computational complexity, applications and communication; Section 4.2 lists a few open questions and future research directions.

3

Results

Money, money, money
Always sunny
In the rich man's world

— ABBA, Money Money Money

While Subsection 1.4.1 already gives a preview of the research contributions of each article included in this thesis, we revisit the results here from a more technical point of view. The results are organised thematically instead of paper by paper. This chapter is only meant to give an overview of the most important results in each article; see the articles in full for a complete account.

3.1 Near-optimal spaces

Both "1: Intersections", "3: Trade-offs" and "4: Pathways" contribute significantly to the literature on near-optimal spaces in energy systems modelling, helping to answer Question 1. In the first of these articles, we introduce the dimension-reduction framework presented in Section 2.5 in terms of reduced near-optimal spaces, which were only used implicitly in previous publications. Viewing reduced near-optimal spaces as explicit low-dimensional polytopes that can be approximated and subsequently analysed as geometric objects opens up new, previously unexploited opportunities. The headline technique using

this geometric perspective, introduced in "1: Intersections", is the possibility of intersecting reduced near-optimal spaces of variations of the same model, for instance with different parameters (see Subsection 2.4.1). The resulting intersection consists of points that are feasible for each considered model variation — the applications to robustness are discussed in Section 3.2 Moreover, the intersection approach enables the approximate computation of cost-optimal system designs that are feasible for all model variations considered, while such an optimisation with a single combined model might be computationally intractable. This was shown in "1: Intersections" in the case of computing system designs feasible for all weather years from 1980 to 2020.

Suppose that points $y, y' \in \mathcal{A}_\varepsilon$ are obtained via two model optimisations with different objectives. Then it follows from convexity (since $\mathcal{A}_\varepsilon$ is a convex polytope) that any linear interpolation $y'' = ry + (1-r)y'$ is also in $\mathcal{A}_\varepsilon$. The point y'', however, is in the reduced, low-dimensional space $\mathcal{A}_\varepsilon$. It does not give us a full system design in $\mathcal{F}'_\varepsilon$ (or complete solution, including operations, in $\mathcal{F}_\varepsilon$). All we know is that there *exists* some $x'' \in \mathcal{F}_\varepsilon$ such that $\sigma \circ \pi(x'') = y''$. In "1: Intersections", we consider for the first time the problem of finding such an explicit solution x'', including in the case of points in the intersection of several reduced near-optimal spaces. This was applied not in the case of linear interpolations, but with y'' representing a centre point of the intersection of several near-optimal spaces (see Section 3.2).

Another technique that is enabled by the geometric interpretation of near-optimal spaces is that of singling out one variable, and observing how changes in this variable impact the shape of the near-optimal space in terms of the remaining variables. Specifically, let $\mathcal{A} = \mathcal{A}_\varepsilon \subset \mathbb{R}^k$ be a reduced near-optimal space with coordinates $y_1, \ldots, y_k$. Then we can consider the level sets $\mathcal{A}_{y_i=\alpha} = \{(y_1, \ldots, y_k) \in \mathcal{A} \mid y_i = \alpha\}$ for α between $\min_{y\in\mathcal{A}} y_i$ and $\max_{y\in\mathcal{A}} y_i$. For example, we could have y_1, y_2, y_3 represent total installed onshore wind, offshore wind and solar capacities in GW. Then $\mathcal{A}_{y_2=10}$ would represent all points (y_1, y_3) of onshore wind and solar capacity that are near-optimal and feasible together with 10GW of offshore wind. In "3: Trade-offs", we use the *mean width*[1] $\delta(i, \alpha) = \delta(\mathcal{A}_{y_i=\alpha})$ of such level sets to determine the relative impacts of different technologies on design flexibility. For example, when $\delta(i, \alpha)$ increases more rapidly than $\delta(j, \alpha)$ for α between 0 and 10, then technology i contributes more to design flexibility than technology j. Here, we use "design flexibility" to refer to the extent of a near-optimal space; a larger near-optimal space indicates more flexibility in designing a near-optimal feasible system.

The final methodological advance we highlight here is the first application

1. Defined as the mean of the widths $\max_{y\in\mathcal{A}} y_i - \min_{y\in\mathcal{A}} y_i$ for each i.

of near-optimal techniques in combination with myopic foresight pathway optimisations, introduced in "4: Pathways". While terminology is not universally agreed upon, what we mean by "pathway optimisation" here is a sequence of models $M_1, M_2, \ldots$ representing hypothetical energy systems at time horizons $Y = 1, 2, \ldots$, such that the results of M_1 are used as a starting point for M_2, and so forth. Specifically, optimised capacities from M_{i-1} are carried over to M_i while phasing out older capacities; let

$$\min c_i x_i \quad \text{s.t.} \quad A_{i|x_{i-1}} x_i \leq b_{i|x_{i-1}} \tag{3.1}$$

denote the LP for the i time horizon, with capacities x_{i-1} carried over from the previous time horizon. In the context of the next few decades, a decreasing cap on CO_2 emissions may be imposed on successive models. For example, in "4: Pathways" we consider the European energy system at $Y = 2025, 2030, 2035, 2040, 2045, 2050$ with CO_2 limits following the 55%, 90% and 100% reduction targets for 2030, 2040 and 2050 respectively. Let $x_1^*, x_2^*, \ldots$ be cost-optimal solutions at the considered time horizons, and $c_1^{\text{opt}}, c_2^{\text{opt}}, \ldots$ the associated optimal system costs. Then, instead of considering near-optimal spaces for each time horizon in isolation (which would ignore the temporal inter-dependence through the carrying over of optimised capacities), we propose looking instead at a sequence of near-optimal spaces where capacities are carried over and cost bound is determined by $x_1^*, x_2^*, \ldots$:

$$\begin{array}{lccccccc} \text{Cost-optimal:} & x_1^* & \xrightarrow{\text{caps}} & x_2^* & \xrightarrow{\text{caps}} & x_3^* & \longrightarrow & \cdots \\ & \downarrow \text{cost bound} & & \downarrow \text{cost bound} & & \downarrow \text{cost bound} & & \\ \text{Near-optimal:} & \mathcal{F}_\varepsilon^{(1)} & \xrightarrow{\text{caps}} & \mathcal{F}_\varepsilon^{(2)} & \xrightarrow{\text{caps}} & \mathcal{F}_\varepsilon^{(3)} & \longrightarrow & \cdots \end{array} \tag{3.2}$$

To be more specific, we define

$$\mathcal{F}_\varepsilon^{(i)} = \Big\{ x_i \in \mathbb{R}^n \mid \exists x_{i-1} \in \mathcal{F}_\varepsilon^{(i-1)} \text{ s.t. } A_{i|x_{i-1}} x_i \leq b_{i|x_{i-1}} \text{ and } (1+\varepsilon) c_i \cdot x_i \leq c_i^{\text{opt}} \Big\}. \tag{3.3}$$

That is, each point in $\mathcal{F}_\varepsilon^{(i)}$ is near-optimal relative to an LP with capacities carried over from *some* point in $\mathcal{F}_\varepsilon^{(i-1)}$, while the cost bound is determined by the sequence of cost-optimal solutions $x_1^*, x_2^*, \ldots$.

Using this approach, it is possible to study different system evolutions or pathways that are guaranteed to stay within a certain cost slack of the cost-optimal pathway at all time horizons. The technique is applied in "4: Pathways" to map out different trajectories for European green hydrogen production.

3.2 Robustness

The word "robustness" can mean a number of different things in the context of energy systems modelling. Our working definition will be that an energy system is *robust* against a certain *event* if the system is still capable of delivering the specified amount of energy to end-users after the event, possibly with a change in operations at reasonable cost. By "event", we mean specifically a change either to the environment of the system, or to the system itself. A typical example of such an event could be a drought leading to below normal hydro power reservoir levels (external change), a sudden increase in solar panel prices (external change) or the outage of a transmission line (internal change). Of course, many more specific variations of robustness can be studied depending on the type of event and the time scale over which the event and its response play out.

This thesis makes several different contributions on the topic of robustness, addressing Question 2. The first is in "2: Weather", where we introduce a new method for identifying extreme weather events. Energy systems will increasingly rely on variable renewable resources such as wind and solar power, whose energy production depends on the weather at any given time. While the variability can be smoothed out over time and space with the use of energy storage and transmission respectively, there can still be periods with sustained low renewable production over a large area. In Europe, the events of greatest interest are so-called "cold doldrums" or "dunkelflauten"; periods during the winter (meaning low solar power production) with cold temperatures (and thus a high heating demand) and low winds (meaning low wind power production). Such events have previously been identified by analysing country- or continent-wide renewable power production potential or "demand − net renewables" / "net load" (i.e. temperature-dependant demand minus renewable potential).

We show that using a power system model to identify extreme events — thus accounting for energy storage and transmission — makes a difference and leads to a discrepancy in identified events compared to methods using demand − net renewables. In order to identify events, we use shadow prices of electricity. These are the dual variables corresponding to the electricity balance constraints (e.g. the first constraint in Equation 2.2), indicating by how much total system cost would increase if electricity demand were to increase by one unit at the given time and location. "2: Weather" represents the first application of shadow prices to the identification of extreme events in the context of a capacity expansion model; shadow prices are shown to be comparable to the alternative metric of lost load, but easier to obtain. Having obtained a set of extreme periods across the historical weather years 1980–2020, we furthermore compile sets of typical weather patterns (both using near-surface variables and

mid-troposphere variables) to show that the identified events do not conform in a straight-forward way to commonly considered weather regimes. This represents a step towards bridging the gap between energy systems research on one hand and meteorology and climate science on the other.[47]

In "1: Intersections" and "3: Trade-offs", we construct intersections of reduced near-optimal spaces to construct more robust energy system designs. Here, the type of robustness considered is with respect to changes *within* the energy system, and specifically changes to overall investment in renewables. The idea introduced in "1: Intersections" specifically is that points $y \in \mathcal{A}_\varepsilon$ located well into the interior of $\mathcal{A}_\varepsilon$ are robust to changes in the coordinates of the ambient space of $\mathcal{A}_\varepsilon$. For example, suppose that $\mathcal{A}_\varepsilon \subset \mathbb{R}^3$ has coordinates y_1, y_2, y_3 representing total investment in onshore wind, offshore wind and solar power in billion EUR. Let $y \in \mathcal{A}_\varepsilon$ be located at least 5 bn EUR away from the boundary of $\mathcal{A}_\varepsilon$ in any direction. That means that any point y' within a distance of 5 bn EUR of y is still inside of $\mathcal{A}_\varepsilon$; on other words, it represents a set of total investment levels in onshore wind, offshore wind and solar power that are still feasible and near-optimal. Thus, y is robust to perturbations in total investment in renewables of up to 5 bn EUR.

In "1: Intersections", we propose the Chebyshev centre of $\mathcal{A}_\varepsilon$ as the most robust point in $\mathcal{A}_\varepsilon$; it is by definition the point y^* at the centre of the largest radius ball fully contained within $\mathcal{A}_\varepsilon$. Thus, it is the point allowing the largest perturbation in any direction while staying inside of $\mathcal{A}_\varepsilon$. The Chebyshev centre y^* is by definition more costly than the cost-optimal solution, and in the simple electricity-only set-up in "1: Intersections", we show that for a European power system with a high share of renewables, the Chebyshev centre mainly over-invests in onshore wind power and, to a lesser extent, transmission expansion.

In "3: Trade-offs", we consider intersections of near-optimal spaces arising from a number of different scenarios, including scenarios with different land-use limitations and different capital costs for wind and solar power. The points inside the intersection of these spaces thus represent overall investment decisions which are feasible and near-optimal even in the face of changing technology costs.

3.3 Policy implications

Broadly speaking, all papers included in this thesis support the position that a net-zero emissions energy system in Europe is possible, technologically speaking, by 2050 at reasonable cost, as also shown in other studies.[7],[9],[86] Not

only is it possible; near-optimal methods reveal that there are many options for achieving decarbonisation. Other studiesPickering *et al.*, Neumann *et al.* have already shown that many options are available; a common interpretation is that the near-optimal space of most energy systems is quite "flat" around the optimum, meaning that relaxing cost-optimality only a little bit quickly creates lots of space for different options. We show that this holds true in an even wider sense than previously understood.

In "3: Trade-offs", we reveal extensive regional investment flexibility, showing that for instance wind power and hydrogen infrastructure investment can be shifted around in Northern Europe (around the North Sea and Baltic Sea) quite freely. This is despite only considering system designs that are robust to different weather years, restrictive solar land-use constraints and changing capital costs of wind and solar power. The spatial flexibility highlights the need in Europe to coordinate wind power (both onshore and offshore) and hydrogen infrastructure investment, as some minimum wind resources are necessary while there is also some risk of over-investment and stranded assets. On the flip side, we show for the first time how certain technologies in certain places can contribute disproportionately to design flexibility. For example, investment in solar in Germany, the Iberian peninsula and around the Adriatic is seen to be especially important; without this investment, the chances of system inadequacy or cost overruns are increased.

Another dimension where we reveal wide-ranging options that were previously under-explored, is European green hydrogen production ("4: Pathways"). Hydrogen is seen as a promising energy carrier that could play an important role in the energy transition leading up to net-zero emissions. It can be used to store and transport energy, and is useful for satisfying some energy demand directly or as an intermediate product in the production of various e-fuels such as ammonia, methanol and synthetic fuel. It could be produced inside Europe using either electricity (water electrolysis; the product is known as "green" hydrogen) or natural gas (steam-methane reformation; the product is known as "grey" or "blue" hydrogen, depending on whether the resulting CO_2 is captured or not), or imported. We show that wide ranges of green hydrogen production are possible within moderate increases of total system cost, deeply impacting the flow of energy in the entire system. Green hydrogen competes primarily with fossil fuels combined with carbon capture and sequestration technology, and we see that the competition is surprisingly close, meaning that large shifts from one to the other are possible with small changes in total system cost. This makes the balance between green hydrogen and fossil fuels with carbon capture and sequestration a question less of cost and more of other factors such as public acceptance, risk and who stands to gain and lose.

Indeed, the prospects of wide-ranging possibilities for green hydrogen produc-

tion are somewhat tempered by our results in “5: Exports”. Here, we highlight the limitations that potential Norwegian hydrogen exports face in terms of public scepticism around wind power, competition for scarce electricity and distributional justice, even while the technical preconditions are all there. Focusing on overall system impact, it becomes clear that Norways green hydrogen strategy cannot be considered in isolation. If anything, the most significant challenge for Norwegian hydrogen exports is not of a technical nature, but of sourcing electricity in a way that is widely acceptable for the public.

4

Discussion

Strange days have found us
And through their strange hours
We linger alone

— The Doors, Strange Days

Energy systems modelling is moving forward rapidly, with new models, methods and insights appearing ever faster. To a large degree, this is due to the benefits of open science, which in the context of energy systems modelling means open data, open model code and open publications. This is especially important in fields touching on policy and decision-making, where transparency is crucial.[41] Starting with pioneering open source models such as BALMOREL[87] (2000) and OSeMOSYS[88] (2008), there is now a wide selection of general purpose open source energy system models available.[16] In particular, European-wide models such as PyPSA-Eur[42],[89] and Euro-Calliope[90] covering the electricity, heating, gas and other energy sectors at the high spatial and temporal resolution needed to capture renewable variability now enable research that would have been painstaking in the past. Increasingly, PyPSA-Earth[91] is bringing these benefits to a global coverage.

These crucial improvements in "modelling infrastructure" are leading to fruitful new insights regarding the possible design and operations of the renewables-based energy systems of the future, showing how the variability of wind- and solar power can be compensated for by flexibility in storage, transmission, sector-coupling and demand response. Several of the works in this thesis

("1: Intersections", "3: Trade-offs", "4: Pathways") have helped to show that in powering Europe with renewables, there is ample room for different choices. Wherever we look (total renewable investment by technology, regional renewable investment, green hydrogen production), near-optimal methods reveal many more choices than would be visible from a cost-optimal perspective alone.

High-resolution technology-rich modelling studies are also encountering fundamental limitations regarding what can and cannot easily be represented in optimisation models. Increasingly, we see that the plausibility of modelled solutions for the energy transition is less a question of technological feasibility, and more contingent on factors such as social acceptance, equity, geopolitics ("5: Exports") and compatibility with accepted visions for the future.[92] To point out just one specific incongruence, optimisation models typically take the perspective of a "central planner", missing the intricacies of how decision-making works in reality. A large-scale analysis of publications in energy research between 1999 and 2013 found that only 12.6% of the articles used any qualitative methods;[93] the risks of over-quantification, meanwhile, are real.[94] This prompts more interdisciplinary work incorporating elements from social science and qualitative methods.[95]–[98] The present work also pushes for more interdisciplinarity by including collaborations across meteorology ("2: Weather") and the social sciences ("5: Exports").

One of the central themes of this thesis in addressing the pitfalls of over-quantification and modelling blind-spots is to map out the options relevant for particular questions as fully as possible. With a good overview of what is *technically* feasible, it is possible to explore non-technological questions and trade-offs systematically. That is, near-optimal methods create room for public and academic debate around the different options for the energy transition, without making too many assumptions or choices in advance.

4.1 Limitations

While limitations are discussed in each individual article included in this thesis, we list here a few elements relevant to most or all of the modelling results throughout the papers. We focus here on limitations of a "technical" nature, i.e., over-simplifications or blind spots of the models in accurately representing the intended target system. The account in this section is not meant to be exhaustive, but rather point out only the most significant recurring limitations.

The evolution and path-dependence of energy infrastructure is only taken into

account in "4: Pathways", whereas the other included publication are based on single-horizon optimisation models only accounting for a single planning horizon (2050, except for "5: Exports", which uses 2030 as the planning horizon). It could be argued that most energy infrastructure that exists today will be (nearly) phased out by 2050, justifying a "clean slate" approach to what the energy system might look like by 2050. This, however, ignores potential challenges in scaling up nascent technologies such carbon capture and storage as well as green hydrogen production, distribution and processing. More significantly, even "4: Pathways" does not adequately represent technological learning dynamics over time. Technological learning is the cost reduction observed with increasing adoption of technologies such as solar panels, wind turbines, batteries and hydrogen technology, and is often modelled as a percentage cost decrease per global doubling of production of the given technology or product. It is a fundamentally non-linear dynamic, and thus difficult to include in large-scale ESOMs. However, a study on technological learning in the European energy sector using integer linear programming and multi-horizon perfect-foresight optimisations has found very large effects.[99] With perfect foresight and technological learning it becomes much more attractive to invest heavily and early in key technologies in order to drive down costs; such dynamics are not captured in the studies included in this thesis.

Another dynamic that is ignored (except for in rudimentary form in "4: Pathways") is that of most types of energy imports. Except for constant-price imports of fossil fuels (which are, however, limited due to assumed decarbonisation), the included publications except for "4: Pathways" do not include the possibility of importing electricity or green fuels such as hydrogen, ammonia or methanol from outside of Europe. Such imports, however, can have a large effect on both optimal and near-optimal system design, as explored in "4: Pathways" and investigated in much more detail a recent preprint on the topic.[100] The EU imported 62.5% of its energy in 2022;[101] the transition to greater shares of renewable energy presents an opportunity to achieve complete energy self-sufficiency ("3: Trade-offs"). On the other hand, the EU has already set a target for imports of 10Mt (~330 TWh in lower heating value) of green hydrogen by 2030.[102] Exactly which fraction of energy will be imported by 2050 is a wide-open question.

The climate impact even of green hydrogen is also a potential challenge not accounted for in the present work. While hydrogen is not itself a greenhouse gas, but reacts with OH in the atmosphere, forming water on one hand and prolonging the life-time of methane on the other (which is also broken down by OH). Recently hydrogen was estimated to have a 100-year global warming potential of 11.6,[103] meaning that 1 kg of hydrogen has the same warming potential as 11.6 kg of CO_2 over 100 years. The emerging hydrogen economy will therefore need to be exceedingly cautious about potential leaks. And

while a decarbonised energy system needs some combination of green hydrogen production or fossil fuel use combined with carbon capture and storage ("4: Pathways"), the latter is not free of leakage concerns either.[104] The risk of hydrogen-, methane or CO_2-leaks has not been accounted for in the included publications.

The works in this thesis mostly use the goal of a net-zero emissions energy system by 2050 as a baseline. However, several complicating factors are not taken into account. While "3: Trade-offs" and "4: Pathways" consider the possibility for negative emissions through the use of biomass with carbon capture and storage (often known as "BECCS"), the overall net emission/absorption of CO_2 from land-use and other sources not related to energy are not very well accounted for. Indeed, land use, land use change and forestry removed a net 230 Mt CO_2-equivalent from the atmosphere in in the EU in 2021,[105] equivalent to 7% of EU CO_2-emissions that year. At the same time, it is likely for global warming to "overshoot" the 1.5°C target, necessitating sustained negative emissions.[1] Thus, the target level of positive or negative net CO_2-emissions from energy systems in 2050 and beyond and subject to uncertainty; this uncertainty is not taken into account in the present work.

Future energy demand is possibly subject to even more uncertainty; still, demand is mostly held fixed in the studies included in this thesis. Energy demand may change with changing population sizes and economic development, as well as behavioural patterns, efficiency gains and infrastructure changes (e.g. increased use of public transportation). The fact that drastic changes in demand are possible was recently demonstrated by a 19% reduction in natural gas demand in the EU between August 2022 and January 2023 as a response to the Russian invasion of Ukraine and the resulting energy crisis.[106] In a sustainable society, humanity's physical footprint must not exceed planetary boundaries,[107] and it has been debated[108]–[111] whether continued economic growth (and rising or even constant energy demand) is possible within these boundaries over the next decades.

4.2 Future directions

Any of the limitations above give rise to new avenues of research. In this section, we take a broader perspective on promising directions for future work.

There is most likely potential for further development of methods for exploring and exploiting near-optimal spaces of ESOMs. Some immediate improvements might be made to the procedures for selecting directions in which to explore a near-optimal feasible space, developed in "1: Intersections". Moreover, it seems

plausible that there might be more efficient ways of approximating the intersection of a number of near-optimal spaces than first fully approximating each component space and then intersecting them. Rather, a "running" approximation of the intersection could be kept track of, the the optimisation directions for exploring component near-optimal spaces could be selected based on this running approximation. This could help avoid the unnecessary exploration of parts of the component near-optimal spaces which don't determine the intersection.

Approximating near-optimal spaces is computationally expensive, typically requiring hundreds of optimisations of the same model with different objective functions. The computational expense needed to produce works such as "1: Intersections" and "3: Trade-offs" is in the tens of thousands of processor-hours. Reducing the computational burden would make near-optimal research significantly easier to conduct, and lower the barrier of entry for researchers and others. Exciting advances have been demonstrated using "surrogate modelling",[83] which involves training a specialised statistical model to "scale up" the results of low-resolution models to results mimicking those of high-resolution models. Surrogate modelling has been applied in one study on near-optimal alternatives,[83] but not in the context of fully mapping our reduced near-optimal spaces such as in "1: Intersections" and "3: Trade-offs". A radical further step could be to train a statistical model (e.g. a neural network) to predict key solution characteristics based on objective function for a single model, or possibly for a parametrised set of models. This may help in exploring high-dimensional reduced near-optimal spaces (e.g. for $n \geq 10$) where conventional convex hull computations become impractical; the question is whether generating a sufficiently large training dataset is computationally feasible.

Major advances could also be made in research on the presentation, dissemination and communication of results from near-optimal studies. It's impossible to draw a 5-dimensional polytope intelligibly, and generally near-optimal spaces present the risk of creating an overload of information, both for researchers and others. One research article that is in development but not included in this thesis (see Subsection 1.4.3) builds on data collected using a purpose-built interactive user interface made for exploring the near-optimal space of a model for the Longyearbyen energy system. Another example worth mentioning is the interactive interface accompanying a recent work by Pickering *et al.*,[19] found at `https://explore.callio.pe`. More work in this direction could prove fruitful.

In terms of robustness, "2: Weather" presents advances in terms of understanding extreme weather events, but leaves other questions open. The single most expensive week in each year between 1980 and 2020 explains between 18%

and 77% of total system cost in the model employed in “2: Weather”, and we have an understanding of what kind of weather causes these short/medium-duration events. But what, exactly, makes a weather year generally difficult is still an open question. That is, which combination of extreme events, seasonal variations and annual means determine system cost and design for energy systems with a high share of renewables?

“3: Trade-offs” showcased a new method for finding (approximate) system designs that are robust against both different weather years, changes in technology costs and different land-use limitations. Further development of this technique could be useful. As presented, the method guarantees robustness against every single scenario under consideration; relaxing or refining this assumption would be more realistic (not assuming simultaneous worst outcomes in many independent factors). This might also enable the inclusion of more varied scenarios still, including different supply shocks, climate change scenarios and social acceptance scenarios.

4.3 Conclusion

The world is hurtling towards an uncertain future; it is claimed that today’s state of affairs already qualifies as a “polycrisis”.[112] The climate crisis will only worsen.[1] Our energy systems play a central role — the energy transition is crucial for cutting emissions, and climate change in turn will impact energy systems through supply, demand and infrastructure damage.

While the energy transition is technically feasible, it is fraught with difficult trade-offs and compromises. Moreover, a successful transition will require both domestic and international cooperation on a large scale. This thesis contributes to the factual basis supporting the transition. We highlight the large ranges of options that near-optimal methods reveal, as well as make advances in developing more robust options. In a small way, this helps create space for debate around different alternatives, making it easier to agree on and swiftly execute the drastic measures needed to prevent climate disaster.

Bibliography

[1] IPCC, «Climate Change 2023: Synthesis Report. Contribution of Working Groups I, II and III to the Sixth Assessment Report of the Intergovernmental Panel on Climate Change [Core Writing Team, H. Lee and J. Romero (eds.)],» Geneva, Switzerland, AR6, 2023.

[2] M. Kotz, A. Levermann, and L. Wenz, «The economic commitment of climate change,» *Nature*, vol. 628, no. 8008. 2024, ISSN: 1476-4687. DOI: 10.1038/s41586-024-07219-0.

[3] A. Bilal and D. R. Känzig. «The Macroeconomic Impact of Climate Change: Global vs. Local Temperature.» National Bureau of Economic Research: 32450. (2024), pre-published.

[4] K. Rennert, F. Errickson, B. C. Prest, L. Rennels, R. G. Newell, W. Pizer, C. Kingdon, J. Wingenroth, R. Cooke, B. Parthum, D. Smith, K. Cromar, D. Diaz, F. C. Moore, U. K. Müller, R. J. Plevin, A. E. Raftery, H. Ševčíková, H. Sheets, J. H. Stock, T. Tan, M. Watson, T. E. Wong, and D. Anthoff, «Comprehensive evidence implies a higher social cost of CO2,» *Nature*, vol. 610, no. 7933. 2022, ISSN: 1476-4687. DOI: 10.1038/s41586-022-05224-9.

[5] K. Ricke, L. Drouet, K. Caldeira, and M. Tavoni, «Country-level social cost of carbon,» *Nature Climate Change*, vol. 8, no. 10. 2018, ISSN: 1758-6798. DOI: 10.1038/s41558-018-0282-y.

[6] EEX, *Emission Spot Primary Market Auction Report 2023*, 2023.

[7] M. Victoria, E. Zeyen, and T. Brown, «Speed of technological transformations required in Europe to achieve different climate goals,» *Joule*, vol. 6, no. 5. 2022, ISSN: 2542-4785, 2542-4351. DOI: 10.1016/j.joule.2022.04.016.

[8] UNFCCC, *Paris Agreement*, 2016.

[9] T. Brown, T. Bischof-Niemz, K. Blok, C. Breyer, H. Lund, and B. Mathiesen, «Response to 'Burden of proof: A comprehensive review of the feasibility of 100% renewable-electricity systems',» *Renewable and Sustainable Energy Reviews*, vol. 92. 2018, ISSN: 13640321. DOI: 10.1016/j.rser.2018.04.113.

[10] IEA, «Net Zero by 2050,» IEA, Paris, 2021.

[11] T. Brown, D. Schlachtberger, A. Kies, S. Schramm, and M. Greiner, «Synergies of sector coupling and transmission reinforcement in a cost-

optimised, highly renewable European energy system,» *Energy*, vol. 160. 2018, ISSN: 0360-5442. DOI: 10.1016/j.energy.2018.06.222.

[12] M. Tanenbaum, S. Eilon, W. K. Holstein, and R. L. Ackoff, «Operations research,» *Encyclopedia Britannica*. 2024.

[13] D. K. Smith and A. Schrijver, «Theory of Linear and Integer Programming.,» *The Journal of the Operational Research Society*, vol. 38, 1987. DOI: 10.2307/2582770. JSTOR: 2582770.

[14] L. G. Fishbone and H. Abilock, «Markal, a linear-programming model for energy systems analysis: Technical description of the bnl version,» *International Journal of Energy Research*, vol. 5, no. 4. 1981, ISSN: 0363907X, 1099114X. DOI: 10.1002/er.4440050406.

[15] IEA-ETSAP, Antti-L, and Ggiannakidis, *Etsap-TIMES/TIMES_model: TIMES Version 4.5.3*, version v4.5.3, Zenodo, 2021. DOI: 10.5281/ZENODO.3865460.

[16] H.-K. Ringkjøb, P. M. Haugan, and I. M. Solbrekke, «A review of modelling tools for energy and electricity systems with large shares of variable renewables,» *Renewable and Sustainable Energy Reviews*, vol. 96. 2018, ISSN: 1364-0321. DOI: 10.1016/j.rser.2018.08.002.

[17] E. D. Brill, «The Use of Optimization Models in Public-Sector Planning,» *Management Science*, vol. 25, no. 5. 1979, ISSN: 0025-1909. DOI: 10.1287/mnsc.25.5.413.

[18] J. F. DeCarolis, «Using modeling to generate alternatives (MGA) to expand our thinking on energy futures,» *Energy Economics*, vol. 33, no. 2. 2011, ISSN: 01409883. DOI: 10.1016/j.eneco.2010.05.002.

[19] B. Pickering, F. Lombardi, and S. Pfenninger, «Diversity of options to eliminate fossil fuels and reach carbon neutrality across the entire European energy system,» *Joule*, vol. 6, no. 6. 2022, ISSN: 25424351. DOI: 10.1016/j.joule.2022.05.009.

[20] F. Neumann and T. Brown, «The near-optimal feasible space of a renewable power system model,» *Electric Power Systems Research*, vol. 190. 2021, ISSN: 0378-7796. DOI: 10.1016/j.epsr.2020.106690.

[21] T. T. Pedersen, M. Victoria, M. G. Rasmussen, and G. B. Andresen, «Modeling all alternative solutions for highly renewable energy systems,» *Energy*, vol. 234. 2021, ISSN: 03605442. DOI: 10.1016/j.energy.2021.121294.

[22] E. Bini, G. Garavini, and F. Romero, *Oil Shock: The 1973 Crisis and Its Economic Legacy*. Bloomsbury Publishing, 2016, 281 pp., ISBN: 978-0-85772-755-8. Google Books: SBKMDwAAQBAJ.

[23] European Commission, «State of the Energy Union Report 2023,» European Union, Brussels, COM/2023/650, 2023.

[24] J. W. Busby, K. Baker, M. D. Bazilian, A. Q. Gilbert, E. Grubert, V. Rai, J. D. Rhodes, S. Shidore, C. A. Smith, and M. E. Webber, «Cascading risks: Understanding the 2021 winter blackout in Texas,» *Energy Research*

& Social Science, vol. 77. 2021, ISSN: 22146296. DOI: 10.1016/j.erss.2021.102106.

[25] F. Mockert, C. M. Grams, T. Brown, and F. Neumann, «Meteorological conditions during periods of low wind speed and insolation in Germany: The role of weather regimes,» *Meteorological Applications*, vol. 30, no. 4. 2023, ISSN: 1469-8080. DOI: 10.1002/met.2141.

[26] H. C. Bloomfield, D. J. Brayshaw, L. C. Shaffrey, P. J. Coker, and H. E. Thornton, «The changing sensitivity of power systems to meteorological drivers: A case study of Great Britain,» *Environmental Research Letters*, vol. 13, no. 5. 2018, ISSN: 1748-9326. DOI: 10.1088/1748-9326/aabff9.

[27] H. C. Bloomfield, D. J. Brayshaw, L. C. Shaffrey, P. J. Coker, and H. E. Thornton, «Quantifying the increasing sensitivity of power systems to climate variability,» *Environmental Research Letters*, vol. 11, no. 12. 2016, ISSN: 1748-9326. DOI: 10.1088/1748-9326/11/12/124025.

[28] J. A. Dowling, K. Z. Rinaldi, T. H. Ruggles, S. J. Davis, M. Yuan, F. Tong, N. S. Lewis, and K. Caldeira, «Role of Long-Duration Energy Storage in Variable Renewable Electricity Systems,» *Joule*, vol. 4, no. 9. 2020, ISSN: 2542-4351. DOI: 10.1016/j.joule.2020.07.007.

[29] C. Neubacher, D. Witthaut, and J. Wohland, «Multi-decadal offshore wind power variability can be mitigated through optimized European allocation,» *Advances in Geosciences*, vol. 54, Copernicus GmbH, 2021. DOI: 10.5194/adgeo-54-205-2021.

[30] M. T. Craig, P. Jaramillo, B.-M. Hodge, B. Nijssen, and C. Brancucci, «Compounding climate change impacts during high stress periods for a high wind and solar power system in Texas,» *Environmental Research Letters*, vol. 15, no. 2. 2020, ISSN: 1748-9326. DOI: 10.1088/1748-9326/ab6615.

[31] J. Wohland, M. Reyers, J. Weber, and D. Witthaut, «More homogeneous wind conditions under strong climate change decrease the potential for inter-state balancing of electricity in Europe,» *Earth System Dynamics*, vol. 8, no. 4. 2017, ISSN: 2190-4987. DOI: 10.5194/esd-8-1047-2017.

[32] I. Tobin, S. Jerez, R. Vautard, F. Thais, E. Van Meijgaard, A. Prein, M. Déqué, S. Kotlarski, C. F. Maule, G. Nikulin, T. Noël, and C. Teichmann, «Climate change impacts on the power generation potential of a European mid-century wind farms scenario,» *Environmental Research Letters*, vol. 11, no. 3. 2016, ISSN: 1748-9326. DOI: 10.1088/1748-9326/11/3/034013.

[33] I. Tobin, W. Greuell, S. Jerez, F. Ludwig, R. Vautard, M. T. H. Van Vliet, and F.-M. Bréon, «Vulnerabilities and resilience of European power generation to 1.5 °C, 2 °C and 3 °C warming,» *Environmental Research Letters*, vol. 13, no. 4. 2018, ISSN: 1748-9326. DOI: 10.1088/1748-9326/aab211.

[34] J. Krupa and C. Jones, «Black Swan Theory: Applications to energy market histories and technologies,» *Energy Strategy Reviews*, Nuclear

Energy Today & Strategies for Tomorrow, vol. 1, no. 4. 2013, ISSN: 2211-467X. DOI: 10.1016/j.esr.2013.02.004.

[35] A. Silvast, E. Laes, S. Abram, and G. Bombaerts, «What do energy modellers know? An ethnography of epistemic values and knowledge models,» *Energy Research & Social Science*, vol. 66. 2020, ISSN: 22146296. DOI: 10.1016/j.erss.2020.101495.

[36] A. Grochowicz, K. van Greevenbroek, F. E. Benth, and M. Zeyringer, «Intersecting near-optimal spaces: European power systems with more resilience to weather variability,» *Energy Economics*, vol. 118. 2023, ISSN: 0140-9883. DOI: 10.1016/j.eneco.2022.106496.

[37] A. Grochowicz, K. Van Greevenbroek, and H. C. Bloomfield, «Using power system modelling outputs to identify weather-induced extreme events in highly renewable systems,» *Environmental Research Letters*, vol. 19, no. 5. 2024, ISSN: 1748-9326. DOI: 10.1088/1748-9326/ad374a.

[38] K. van Greevenbroek, A. Grochowicz, M. Zeyringer, and F. E. Benth. «Enabling agency: Trade-offs between regional and integrated energy systems design flexibility.» arXiv: 2312.11264 [cs, eess, math]. (2023), pre-published.

[39] K. van Greevenbroek, J. Schmidt, and M. Zeyringer. «Diverse pathways for green hydrogen production in Europe.» (2024), pre-published.

[40] C. Cheng, K. van Greevenbroek, and I. Viole, «The competitive edge of Norway's hydrogen by 2030: Socio-environmental considerations,» *International Journal of Hydrogen Energy*, vol. 85. 2024, ISSN: 0360-3199. DOI: 10.1016/j.ijhydene.2024.08.377.

[41] S. Pfenninger, L. Hirth, I. Schlecht, E. Schmid, F. Wiese, T. Brown, C. Davis, M. Gidden, H. Heinrichs, C. Heuberger, S. Hilpert, U. Krien, C. Matke, A. Nebel, R. Morrison, B. Müller, G. Pleßmann, M. Reeg, J. C. Richstein, A. Shivakumar, I. Staffell, T. Tröndle, and C. Wingenbach, «Opening the black box of energy modelling: Strategies and lessons learned,» *Energy Strategy Reviews*, vol. 19. 2018, ISSN: 2211-467X. DOI: 10.1016/j.esr.2017.12.002.

[42] J. Hörsch, F. Hofmann, D. Schlachtberger, and T. Brown, «PyPSA-Eur: An open optimisation model of the European transmission system,» *Energy Strategy Reviews*, vol. 22. 2018, ISSN: 2211-467X. DOI: 10.1016/j.esr.2018.08.012.

[43] T. Brown, J. Hörsch, and D. Schlachtberger, «PyPSA: Python for Power System Analysis,» *Journal of Open Research Software*, vol. 6, no. 1. 1 2018, ISSN: 2049-9647. DOI: 10.5334/jors.188.

[44] D. Kirli, J. Hampp, K. Van Greevenbroek, R. Grant, M. Mahmood, M. Parzen, and A. Kiprakis, «PyPSA meets Africa: Developing an open source electricity network model of the African continent,» *2021 IEEE AFRICON*, Arusha, Tanzania, United Republic of: IEEE, 2021, ISBN: 978-1-66541-984-0. DOI: 10.1109/AFRICON51333.2021.9570911.

[45] A. Silvast, S. Abram, and C. Copeland, «Energy systems integration as research practice,» *Technology Analysis & Strategic Management*, vol. 35, no. 3. 2023, ISSN: 0953-7325, 1465-3990. DOI: 10.1080/09537325.2021.1974376.

[46] P. Arora, «COP28: Ambitions, realities, and future,» *Environmental Sustainability*, vol. 7, no. 1. 2024, ISSN: 2523-8922. DOI: 10.1007/s42398-024-00304-0.

[47] M. T. Craig, J. Wohland, L. P. Stoop, A. Kies, B. Pickering, H. C. Bloomfield, J. Browell, M. De Felice, C. J. Dent, A. Deroubaix, F. Frischmuth, P. L. M. Gonzalez, A. Grochowicz, K. Gruber, P. Härtel, M. Kittel, L. Kotzur, I. Labuhn, J. K. Lundquist, N. Pflugradt, K. van der Wiel, M. Zeyringer, and D. J. Brayshaw, «Overcoming the disconnect between energy system and climate modeling,» *Joule*, vol. 6, no. 7. 2022, ISSN: 2542-4351. DOI: 10.1016/j.joule.2022.05.010.

[48] S. Pfenninger, A. Hawkes, and J. Keirstead, «Energy systems modeling for twenty-first century energy challenges,» *Renewable and Sustainable Energy Reviews*, vol. 33. 2014, ISSN: 1364-0321. DOI: 10.1016/j.rser.2014.02.003.

[49] F. S. Hillier and G. J. Lieberman, *Introduction to Operations Research*. McGraw-Hill Higher Education, 2010, 1047 pp., ISBN: 978-0-07-337629-5. Google Books: fRRCPgAACAAJ.

[50] H. G. Huntington, J. P. Weyant, and J. L. Sweeney, «Modeling for insights, not numbers: The experiences of the energy modeling forum,» *Omega*, vol. 10, no. 5. 1982, ISSN: 0305-0483. DOI: 10.1016/0305-0483(82)90002-0.

[51] L. Kotzur, L. Nolting, M. Hoffmann, T. Groß, A. Smolenko, J. Priesmann, H. Büsing, R. Beer, F. Kullmann, B. Singh, A. Praktiknjo, D. Stolten, and M. Robinius, «A modeler's guide to handle complexity in energy systems optimization,» *Advances in Applied Energy*, vol. 4. 2021, ISSN: 2666-7924. DOI: 10.1016/j.adapen.2021.100063.

[52] L. Skyttner, *General Systems Theory*. London: Macmillan Education UK, 1996, ISBN: 978-0-333-61833-2. DOI: 10.1007/978-1-349-13532-5.

[53] D. H. Meadows, *Thinking in Systems: A Primer*. Chelsea Green Publishing, 2008, 242 pp., ISBN: 978-1-60358-055-7. Google Books: CpbLAgAAQBAJ.

[54] R. Frigg and S. Hartmann, «Models in Science,» *The Stanford Encyclopedia of Philosophy*, E. N. Zalta, Ed., Spring 2020, Metaphysics Research Lab, Stanford University, 2020.

[55] A. Herbst, F. Toro, F. Reitze, and E. Jochem, «Introduction to Energy Systems Modelling,» *Swiss Journal of Economics and Statistics*, vol. 148, no. 2. 2012, ISSN: 2235-6282. DOI: 10.1007/BF03399363.

[56] M. Chang, J. Z. Thellufsen, B. Zakeri, B. Pickering, S. Pfenninger, H. Lund, and P. A. Østergaard, «Trends in tools and approaches for modelling the energy transition,» *Applied Energy*, vol. 290. 2021, ISSN: 0306-2619. DOI: 10.1016/j.apenergy.2021.116731.

[57] G. Savvidis, K. Siala, C. Weissbart, L. Schmidt, F. Borggrefe, S. Kumar, K. Pittel, R. Madlener, and K. Hufendiek, «The gap between energy policy challenges and model capabilities,» *Energy Policy*, vol. 125. 2019, ISSN: 0301-4215. DOI: 10.1016/j.enpol.2018.10.033.

[58] B. Müller, F. Gardumi, and L. Hülk, «Comprehensive representation of models for energy system analyses: Insights from the Energy Modelling Platform for Europe (EMP-E) 2017,» *Energy Strategy Reviews*, vol. 21. 2018, ISSN: 2211-467X. DOI: 10.1016/j.esr.2018.03.006.

[59] T. Horschig and D. Thrän, «Are decisions well supported for the energy transition? A review on modeling approaches for renewable energy policy evaluation,» *Energy, Sustainability and Society*, vol. 7, no. 1. 2017, ISSN: 2192-0567. DOI: 10.1186/s13705-017-0107-2.

[60] Y. Collette and P. Siarry, *Multiobjective Optimization* (Decision Engineering), R. Roy, red. Berlin, Heidelberg: Springer, 2004, ISBN: 978-3-642-07283-3. DOI: 10.1007/978-3-662-08883-8.

[61] S. Hilpert, C. Kaldemeyer, U. Krien, S. Günther, C. Wingenbach, and G. Plessmann, «The Open Energy Modelling Framework (oemof) - A new approach to facilitate open science in energy system modelling,» *Energy Strategy Reviews*, vol. 22. 2018, ISSN: 2211-467X. DOI: 10.1016/j.esr.2018.07.001.

[62] S. Pfenninger and B. Pickering, «Calliope: A multi-scale energy systems modelling framework,» *Journal of Open Source Software*, vol. 3, no. 29. 2018, ISSN: 2475-9066. DOI: 10.21105/joss.00825.

[63] D. S. Kirschen and G. Strbac, *Fundamentals of Power System Economics*. Chichester, West Sussex, England ; Hoboken, NJ: John Wiley & Sons, 2004, 284 pp., ISBN: 978-0-470-84572-1.

[64] J. A. Taylor, *Convex Optimization of Power Systems*, 1st ed. Cambridge University Press, 2015, ISBN: 978-1-107-07687-7. DOI: 10.1017/CBO9781139924672.

[65] F. Neumann, V. Hagenmeyer, and T. Brown, «Assessments of linear power flow and transmission loss approximations in coordinated capacity expansion problems,» *Applied Energy*, vol. 314. 2022, ISSN: 0306-2619. DOI: 10.1016/j.apenergy.2022.118859.

[66] M. Grötschel, L. Lovász, and A. Schrijver, «The Ellipsoid Method,» *Geometric Algorithms and Combinatorial Optimization*, M. Grötschel, L. Lovász, and A. Schrijver, Eds., Berlin, Heidelberg: Springer, 1993, ISBN: 978-3-642-78240-4. DOI: 10.1007/978-3-642-78240-4_4.

[67] D. Rehfeldt, H. Hobbie, D. Schönheit, T. Koch, D. Möst, and A. Gleixner, «A massively parallel interior-point solver for LPs with generalized arrowhead structure, and applications to energy system models,» *European Journal of Operational Research*, vol. 296, no. 1. 2022, ISSN: 0377-2217. DOI: 10.1016/j.ejor.2021.06.063.

[68] K. K, H. G. I, M. H, and Z. A, «The joint research centre power plant database (JRC-PPDB): A european power plant database for energy

modelling. »KJ-NA-28549-EN-N 2017, ISSN: 1831-9424. DOI: 10.2760/329310.

[69] M. Hoffmann, L. Kotzur, D. Stolten, and M. Robinius, «A Review on Time Series Aggregation Methods for Energy System Models,» *Energies*, vol. 13, no. 3. 3 2020. DOI: 10.3390/en13030641.

[70] L. Kotzur, P. Markewitz, M. Robinius, and D. Stolten, «Impact of different time series aggregation methods on optimal energy system design,» *Renewable Energy*, vol. 117. 2018, ISSN: 0960-1481. DOI: 10.1016/j.renene.2017.10.017.

[71] H. Teichgraeber and A. R. Brandt, «Time-series aggregation for the optimization of energy systems: Goals, challenges, approaches, and opportunities,» *Renewable and Sustainable Energy Reviews*, vol. 157. 2022, ISSN: 1364-0321. DOI: 10.1016/j.rser.2021.111984.

[72] M. Hoffmann, J. Priesmann, L. Nolting, A. Praktiknjo, L. Kotzur, and D. Stolten, «Typical periods or typical time steps? A multi-model analysis to determine the optimal temporal aggregation for energy system models,» *Applied Energy*, vol. 304. 2021, ISSN: 0306-2619. DOI: 10.1016/j.apenergy.2021.117825.

[73] D. F. Rogers, R. D. Plante, R. T. Wong, and J. R. Evans, «Aggregation and Disaggregation Techniques and Methodology in Optimization,» *Operations Research*, vol. 39, no. 4. 1991, ISSN: 0030-364X. DOI: 10.1287/opre.39.4.553.

[74] M. M. Frysztacki, J. Hörsch, V. Hagenmeyer, and T. Brown, «The strong effect of network resolution on electricity system models with high shares of wind and solar,» *Applied Energy*, vol. 291. 2021, ISSN: 0306-2619. DOI: 10.1016/j.apenergy.2021.116726.

[75] M. Hoffmann, L. Kotzur, and D. Stolten, «The Pareto-optimal temporal aggregation of energy system models,» *Applied Energy*, vol. 315. 2022, ISSN: 0306-2619. DOI: 10.1016/j.apenergy.2022.119029.

[76] T. E. G. Nicholas, T. P. Davis, F. Federici, J. Leland, B. S. Patel, C. Vincent, and S. H. Ward, «Re-examining the role of nuclear fusion in a renewables-based energy mix,» *Energy Policy*, vol. 149. 2021, ISSN: 0301-4215. DOI: 10.1016/j.enpol.2020.112043.

[77] S. Entler, J. Horacek, T. Dlouhy, and V. Dostal, «Approximation of the economy of fusion energy,» *Energy*, vol. 152. 2018, ISSN: 03605442. DOI: 10.1016/j.energy.2018.03.130.

[78] S. C. Pryor, R. J. Barthelmie, M. S. Bukovsky, L. R. Leung, and K. Sakaguchi, «Climate change impacts on wind power generation,» *Nature Reviews Earth & Environment*, vol. 1, no. 12. 2020, ISSN: 2662-138X. DOI: 10.1038/s43017-020-0101-7.

[79] J. Wohland, «Process-based climate change assessment for European winds using EURO-CORDEX and global models,» *Environmental Research Letters*, vol. 17, no. 12. 2022, ISSN: 1748-9326. DOI: 10.1088/1748-9326/aca77f.

[80] A. Saltelli, M. Ratto, T. Andres, F. Campolongo, J. Cariboni, D. Gatelli, M. Saisana, and S. Tarantola, *Global Sensitivity Analysis: The Primer*. John Wiley & Sons, 2008, 307 pp., ISBN: 978-0-470-72517-7. Google Books: wAssmt2vumgC.

[81] A. Saltelli and P. Annoni, «How to avoid a perfunctory sensitivity analysis,» *Environmental Modelling & Software*, vol. 25, no. 12. 2010, ISSN: 1364-8152. DOI: 10.1016/j.envsoft.2010.04.012.

[82] J. R. Birge and F. Louveaux, *Introduction to Stochastic Programming* (Springer Series in Operations Research and Financial Engineering). New York, NY: Springer New York, 2011, ISBN: 978-1-4614-0236-7. DOI: 10.1007/978-1-4614-0237-4.

[83] F. Neumann and T. Brown, «Broad Ranges of Investment Configurations for Renewable Power Systems, Robust to Cost Uncertainty and Near-Optimality,» *iScience*. 2023, ISSN: 25890042. DOI: 10.1016/j.isci.2023.106702.

[84] F. Lombardi, B. Pickering, E. Colombo, and S. Pfenninger, «Policy Decision Support for Renewables Deployment through Spatially Explicit Practically Optimal Alternatives,» *Joule*, vol. 4, no. 10. 2020, ISSN: 2542-4785, 2542-4351. DOI: 10.1016/j.joule.2020.08.002.

[85] M. Lau, N. Patankar, and J. D. Jenkins. «Measuring Exploration: Review and Systematic Evaluation of Modelling to Generate Alternatives Methods in Macro-Energy Systems Planning Models.» arXiv: 2405.17342 [cs, eess, math]. (2024), pre-published.

[86] M. Millinger, F. Hedenus, L. Reichenberg, E. Zeyen, F. Neumann, and G. Berndes. «Diversity of biomass usage pathways to achieve emissions targets in the European energy system.» (2023), pre-published.

[87] F. Wiese, R. Bramstoft, H. Koduvere, A. Pizarro Alonso, O. Balyk, J. G. Kirkerud, Å. G. Tveten, T. F. Bolkesjø, M. Münster, and H. Ravn, «Balmorel open source energy system model,» *Energy Strategy Reviews*, vol. 20. 2018, ISSN: 2211467X. DOI: 10.1016/j.esr.2018.01.003.

[88] M. Howells, H. Rogner, N. Strachan, C. Heaps, H. Huntington, S. Kypreos, A. Hughes, S. Silveira, J. DeCarolis, M. Bazillian, and A. Roehrl, «OSeMOSYS: The Open Source Energy Modeling System: An introduction to its ethos, structure and development,» *Energy Policy*, Sustainability of Biofuels, vol. 39, no. 10. 2011, ISSN: 0301-4215. DOI: 10.1016/j.enpol.2011.06.033.

[89] T. Brown, Martavp, Lisazeyen, M. Maria, Leon, and F. Neumann, *PyPSA/pypsa-eur-sec: PyPSA-Eur-Sec Version 0.4.0*, version v0.4.0, Zenodo, 2020. DOI: 10.5281/ZENODO.3938042.

[90] T. Tröndle, J. Lilliestam, S. Marelli, and S. Pfenninger, «Trade-Offs between Geographic Scale, Cost, and Infrastructure Requirements for Fully Renewable Electricity in Europe,» *Joule*, vol. 4, no. 9. 2020, ISSN: 25424351. DOI: 10.1016/j.joule.2020.07.018.

[91] M. Parzen, H. Abdel-Khalek, E. Fedotova, M. Mahmood, M. M. Frysztacki, J. Hampp, L. Franken, L. Schumm, F. Neumann, D. Poli, A. Kiprakis, and D. Fioriti, «PyPSA-Earth. A new global open energy system optimization model demonstrated in Africa,» *Applied Energy*, vol. 341. 2023, ISSN: 0306-2619. DOI: 10.1016/j.apenergy.2023.121096.

[92] S. Sgouridis, C. Kimmich, J. Solé, M. Černý, M.-H. Ehlers, and C. Kerschner, «Visions before models: The ethos of energy modeling in an era of transition,» *Energy Research & Social Science*, vol. 88. 2022, ISSN: 2214-6296. DOI: 10.1016/j.erss.2022.102497.

[93] B. K. Sovacool, «What are we doing here? Analyzing fifteen years of energy scholarship and proposing a social science research agenda,» *Energy Research & Social Science*, vol. 1. 2014, ISSN: 2214-6296. DOI: 10.1016/j.erss.2014.02.003.

[94] A. Saltelli, «Ethics of quantification or quantification of ethics?» *Futures*, vol. 116. 2020, ISSN: 0016-3287. DOI: 10.1016/j.futures.2019.102509.

[95] O. Vågerö and M. Zeyringer, «Can we optimise for justice? Reviewing the inclusion of energy justice in energy system optimisation models,» *Energy Research & Social Science*, vol. 95. 2023, ISSN: 2214-6296. DOI: 10.1016/j.erss.2022.102913.

[96] C. S. W. Cheng, «Does time matter? A multi-level assessment of delayed energy transitions and hydrogen pathways in Norway,» *Energy Research & Social Science*, vol. 100. 2023, ISSN: 2214-6296. DOI: 10.1016/j.erss.2023.103069.

[97] E. Trutnevyte, L. F. Hirt, N. Bauer, A. Cherp, A. Hawkes, O. Y. Edelenbosch, S. Pedde, and D. P. Van Vuuren, «Societal Transformations in Models for Energy and Climate Policy: The Ambitious Next Step,» *One Earth*, vol. 1, no. 4. 2019, ISSN: 25903322. DOI: 10.1016/j.oneear.2019.12.002.

[98] S. E. Bell, C. Daggett, and C. Labuski, «Toward feminist energy systems: Why adding women and solar panels is not enough,» *Energy Research & Social Science*, vol. 68. 2020, ISSN: 2214-6296. DOI: 10.1016/j.erss.2020.101557.

[99] E. Zeyen, M. Victoria, and T. Brown, «Endogenous learning for green hydrogen in a sector-coupled energy model for Europe,» *Nature Communications*, vol. 14, no. 1. 1 2023, ISSN: 2041-1723. DOI: 10.1038/s41467-023-39397-2.

[100] F. Neumann, J. Hampp, and T. Brown. «Energy Imports and Infrastructure in a Carbon-Neutral European Energy System.» arXiv: 2404.03927 [physics]. (2024), pre-published.

[101] Eurostat, *Energy import dependency by products*, sdg_07_50, 2024. DOI: 10.2908/SDG_07_50.

[102] European Commission, *Commission staff working document implementing the REPowerEU action plan: Investment needs, hydrogen accelerator and achieving the bio-methane targets [SWD/2022/230 final]*, 2022.

[103] M. Sand, R. B. Skeie, M. Sandstad, S. Krishnan, G. Myhre, H. Bryant, R. Derwent, D. Hauglustaine, F. Paulot, M. Prather, and D. Stevenson, «A multi-model assessment of the Global Warming Potential of hydrogen,» *Communications Earth & Environment*, vol. 4, no. 1. 2023, ISSN: 2662-4435. DOI: 10.1038/s43247-023-00857-8.

[104] J. Burger, J. Nöhl, J. Seiler, P. Gabrielli, P. Oeuvray, V. Becattini, A. Reyes-Lúa, L. Riboldi, G. Sansavini, and A. Bardow, «Environmental impacts of carbon capture, transport, and storage supply chains: Status and the way forward,» *International Journal of Greenhouse Gas Control*, vol. 132. 2024, ISSN: 1750-5836. DOI: 10.1016/j.ijggc.2023.104039.

[105] European Environment Agency, «Greenhouse gas emissions from land use, land use change and forestry in Europe,» 2023.

[106] European Council, *Gas demand reduction in the EU*, 2024.

[107] J. Rockström, W. Steffen, K. Noone, Å. Persson, F. S. Chapin, E. F. Lambin, T. M. Lenton, M. Scheffer, C. Folke, H. J. Schellnhuber, B. Nykvist, C. A. de Wit, T. Hughes, S. van der Leeuw, H. Rodhe, S. Sörlin, P. K. Snyder, R. Costanza, U. Svedin, M. Falkenmark, L. Karlberg, R. W. Corell, V. J. Fabry, J. Hansen, B. Walker, D. Liverman, K. Richardson, P. Crutzen, and J. A. Foley, «A safe operating space for humanity,» *Nature*, vol. 461, no. 7263. 2009, ISSN: 1476-4687. DOI: 10.1038/461472a.

[108] J. Hickel, «Is it possible to achieve a good life for all within planetary boundaries?» *Third World Quarterly*, vol. 40, no. 1. 2019, ISSN: 0143-6597, 1360-2241. DOI: 10.1080/01436597.2018.1535895.

[109] J. Hickel, P. Brockway, G. Kallis, L. Keyßer, M. Lenzen, A. Slameršak, J. Steinberger, and D. Ürge-Vorsatz, «Urgent need for post-growth climate mitigation scenarios,» *Nature Energy*, vol. 6, no. 8. 2021, ISSN: 2058-7546. DOI: 10.1038/s41560-021-00884-9.

[110] H. Schlesier, M. Schäfer, and H. Desing, «Measuring the Doughnut: A good life for all is possible within planetary boundaries,» *Journal of Cleaner Production*, vol. 448. 2024, ISSN: 0959-6526. DOI: 10.1016/j.jclepro.2024.141447.

[111] J. Priewe, «Growth in the ecological transition: Green, zero or degrowth?» *European Journal of Economics and Economic Policies*, vol. 19, no. 1. 2022, ISSN: 2052-7764, 2052-7772. DOI: 10.4337/ejeep.2022.01.04.

[112] M. Lawrence, T. Homer-Dixon, S. Janzwood, J. Rockstöm, O. Renn, and J. F. Donges, «Global polycrisis: The causal mechanisms of crisis entanglement,» *Global Sustainability*, vol. 7. 2024, ISSN: 2059-4798. DOI: 10.1017/sus.2024.1.

Notes on included articles

First, a note on the publication status of the attached articles as of writing:

- "1: Intersections" is published in *Energy Economics* (2023).
- "2: Weather" is published in *Environmental Research Letters* (2024).
- "3: Trade-offs" is under review at *Nature Sustainability* at the time of writing but is not published yet.
- "4: Pathways" is a manuscript in the final stages of preparation before submission to an academic journal. The results are complete and fully represented.
- "5: Exports" is published in the *International Journal of Hydrogen Energy* (2024).

Second, a note on authorship of the attached articles. I have main authorship (shared or sole) in all five articles. As noted where relevant, main authorship is shared based on equal contribution as follows:

- "1: Intersections": Koen van Greevenbroek & Aleksander Grochowicz.
- "2: Weather": Koen van Greevenbroek & Aleksander Grochowicz.
- "3: Trade-offs": Koen van Greevenbroek & Aleksander Grochowicz.
- "4: Pathways": Koen van Greevenbroek (sole main author).
- "5: Exports": Koen van Greevenbroek, Claudia Cheng & Isabelle Viole.

The listed order of main authors in each article was decided by a coin toss or is alphabetical ("5: Exports"), and does not reflect differing levels of contribution.

Article 1: “Intersections”

A. Grochowicz *et al.*, «Intersecting near-optimal spaces: European power systems with more resilience to weather variability,» *Energy Economics*, vol. 118, p. 106 496. Feb. 1, 2023, ISSN: 0140-9883. DOI: 10.1016/j.eneco.2022.106496

Energy Economics 118 (2023) 106496

Contents lists available at ScienceDirect

Energy Economics

journal homepage: www.elsevier.com/locate/eneeco

Intersecting near-optimal spaces: European power systems with more resilience to weather variability

Aleksander Grochowicz [a,*,1], Koen van Greevenbroek [b,1], Fred Espen Benth [a], Marianne Zeyringer [c]

[a] Department of Mathematics, University of Oslo, P.O. Box 1053 Blindern, Oslo, 0316, Norway
[b] Department of Computer Science, UiT The Arctic University of Norway, Postboks 6050 Langnes, 9037, Tromsø, Norway
[c] Department of Technology Systems, University of Oslo, P.O. Box 70, 2027, Kjeller, Norway

ARTICLE INFO

JEL classification:
C61
C63
D81
L94
Q48
Q54

Keywords:
Climate-resilient energy systems
Energy system optimisation model
Weather uncertainty
Near-optimal solutions
Robust energy systems
Modelling to generate alternatives

ABSTRACT

We suggest a new methodology for designing robust energy systems. For this, we investigate so-called near-optimal solutions to energy system optimisation models; solutions whose objective values deviate only marginally from the optimum. Using a refined method for obtaining explicit geometric descriptions of these near-optimal feasible spaces, we find designs that are as robust as possible to perturbations. This contributes to the ongoing debate on how to define and work with robustness in energy systems modelling.

We apply our methods in an investigation using multiple decades of weather data. For the first time, we run a capacity expansion model of the European power system (one node per country) with a three-hourly temporal resolution and 41 years of weather data. While an optimisation with 41 weather years is at the limits of computational feasibility, we use the near-optimal feasible spaces of single years to gain an understanding of the design space over the full time period. Specifically, we intersect all near-optimal feasible spaces for the individual years in order to get designs that are likely to be feasible over the entire time period. We find significant potential for investment flexibility, and verify the feasibility of these designs by simulating the resulting dispatch problem with four decades of weather data. They are characterised by a shift towards more onshore wind and solar power, while emitting more than 50% less CO_2 than a cost-optimal solution over that period.

Our work builds on recent developments in the field, including techniques such as Modelling to Generate Alternatives (MGA) and Modelling All Alternatives (MAA), and provides new insights into the geometry of near-optimal feasible spaces and the importance of multi-decade weather variability for energy systems design. We also provide an effective way of working with a multi-decade time frame in a highly parallelised manner. Our implementation is open-sourced, adaptable and is based on PyPSA-Eur.

1. Introduction

The climate crisis and tumbling prices for renewable technologies in the last decade are leading to an unprecedented shift to variable renewable and other low-carbon energy sources. The pace and extent at which this transition is projected to take place often corresponds to a complete overhaul of currently existing energy systems within a few decades. This necessitates a renewed understanding of the workings and planning of energy systems, taking into account future unknowns including weather, climate, costs, and politics.

In the domain of energy system modelling, grappling with these unknowns is an open research problem which has prompted many different approaches. In particular, weather variability has been identified to have a large impact on model solutions: cost-optimal solutions are often fragile in the sense that modelling with one weather year can produce solutions that are infeasible for other weather years. At the same time, recent work involving the relaxation of cost-optimality has revealed the opportunities and insights provided by the near-optimal feasible space of energy system optimisation models. Still, existing methods only map out near-optimal solutions partially or heuristically, and a complete understanding of the theoretical and computational trade-offs has not yet been developed.

In this paper, we introduce a methodology to study robustness of energy systems against uncertainties in inputs and apply it to inter-annual weather variability. To start with, we investigate methods for

* Corresponding author.
E-mail address: aleksgro@math.uio.no (A. Grochowicz).
[1] Equal contribution.

https://doi.org/10.1016/j.eneco.2022.106496
Received 24 June 2022; Received in revised form 21 October 2022; Accepted 23 December 2022
Available online 3 January 2023

approximating projections of near-optimal feasible spaces of energy system models. We then intersect these spaces for varying input data to produce solutions which are feasible in all scenarios. Finally, we propose to consider points well in the *interior* of this intersection as candidate robust solutions. This geometric approach lends itself to building increased resilience against uncertainties and perturbation in a systematic way and generating greater flexibility for policymakers.

We are interested in the problem of long-term planning of the European power system with a large share of renewable production capacity in order to meet emission targets. Capacity expansion models are often used for this purpose, in which capacities of generation technologies, storage, and transmission are optimised. The model at the same time ensures feasibility by simultaneously solving the corresponding optimal dispatch problem over a certain time period, "simulating" the operations of the network. Such models are vital exploratory tools used to shape high-level European energy policy.

In this study, we use the open-source, bottom-up energy system optimisation model (ESOM) called PyPSA-Eur (Hörsch et al., 2018) for our implementation. PyPSA-Eur consists of a model-building routine based on the PyPSA (Python for Power System Analysis) framework (Brown et al., 2018), collecting and processing the required input data from various sources. It assembles a faithful representation of the European high-voltage transmission grid and existing generation capacities, and uses Atlite (Hofmann et al., 2021) to compute capacity factor time series for renewable energy sources (PV, wind, hydro), based on historical ERA5 reanalysis weather data. We use PyPSA-Eur with a partial greenfield approach under perfect foresight, including existing transmission (expandable), hydropower and nuclear capacities (both non-extendable), but optimising renewables (onshore & offshore wind power, solar power), gas turbines and storage from zero. For the purpose of demonstrating and validating our methodology, we use a spatial resolution of one node per country, and a 3-hourly temporal resolution (without time aggregation). However, our techniques can be applied also when using a significantly higher resolution and including more technologies and energy sectors.

Usually, these types of energy system models are optimised using one or a few historical weather years (Ringkjøb et al., 2018), or different weather years are used for sensitivity analyses (Lombardi et al., 2020). The issue of weather year variability has been addressed in the literature (Pfenninger and Staffell, 2016; Pfenninger, 2017; Collins et al., 2018; Staffell and Pfenninger, 2018; Hilbers et al., 2020; Craig et al., 2022; Ruhnau and Qvist, 2022) and has been identified as an important factor for ESOM outcomes (Zeyringer et al., 2018). In particular, using only a single weather year as input data for ESOMs can produce design solutions which are over-fitted to that year, and are not feasible in general (Bloomfield et al., 2016; Zeyringer et al., 2018). However, most previous studies running ESOMs with decades of weather data have either focused on a single country such as Germany (Ruhnau and Qvist, 2022), the UK (Pfenninger, 2017; Zeyringer et al., 2018), and the US (Dowling et al., 2020) (a single-node model), or used only a European dispatch model to solve for operations, not capacity expansion (Collins et al., 2018). One study on the impact of different climate scenarios applied a TIMES model for the European power system with a decades-long modelling horizon (Simoes et al., 2021) in which the usage of representative time slices limited the ability to model storage and capture medium- and long-term effects. Pickering, Lombardi and Pfenninger have recently used the sector-coupled Euro-Calliope model in a study of the European energy system at a 96-node two-hourly resolution (Pickering et al., 2022); the main results were generated over a single weather year but validated using 8 additional weather years.

To the authors' knowledge, this is the first paper to run a spatially resolved ESOM for the European power sector with multiple decades of weather data, without aggregating to time slices. For this analysis, we use 41 years of ERA5 reanalysis data (Hersbach et al., 2018) for the European continent (from 1980 until 2020 inclusive). While we aim to find system designs which are feasible for all weather years under consideration, we base our methods on optimisations with single weather years in order to reduce the computational burden. However, we are still able to optimise our model with all 41 weather years in order to validate our approach.

The robust solutions that we are interested in are near-optimal feasible solutions, meaning that their costs do not go beyond a previously defined threshold. These solutions are "close to cost-optimal" and leave room for alternative objectives and desirable qualities; the additional costs we accept lie below the 9%–23% deviation from cost optimality (due to political, social, or technical reasons) that have been observed in recent years in the UK (Trutnevyte, 2016). Following the works by Neumann and Brown (2021) and Pedersen et al. (2021) we exploit the geometric shape and properties of the near-optimal space defined by the ESOM. Instead of studying the full-dimensional near-optimal feasible space, we study a projection onto 5 relevant dimensions representing total investments in certain technologies.

By varying the weather years as inputs, we then construct one (reduced) near-optimal feasible space for each year. When we intersect these near-optimal feasible spaces, we obtain a space of solutions in which each point represents a set of total investment decisions which are feasible for every year under consideration.

As the most robust candidate in the intersection, we choose the point which lays in the middle, being as far away from being infeasible as possible. This means that changes in total investment decisions (up to a certain point) still leave us in the near-optimal feasible space for every weather year. We then map the total investments back to a full system design, and verify its feasibility by simulating its operations over the entire time period. Note that our form of "robustness" is a geometric concept (laying in the middle of a near-optimal feasible space) and is only loosely connected to robust optimisation.

Apart from contributing to the discussion on energy system robustness, our methods also have implications for ESOM parallelisation. The difficulty in parallelising linear program (LP) solvers has been highlighted as the main barrier preventing ESOMs in taking advantage of increasing computational power (Kotzur et al., 2021). While there are efforts to address this problem at the level of LP solvers (Rehfeldt et al., 2022), we work at the level of model formulation. Finding solutions which are feasible for many weather years by studying the intersection of their respective near-optimal spaces can be an alternative to solving ESOMs with many weather years outright, which is computationally prohibitive. Thus, our methods constitute a way of heuristically replacing one large (difficult to parallelise) optimisation by many optimisations with single weather years.

Finally, we formalise and significantly deepen the understanding of the geometry and approximation of near-optimal feasible spaces of ESOMs. Previously, Pedersen et al. proposed a methodology for approximating near-optimal feasible spaces of ESOMs (Pedersen et al., 2021), and used the results to study the density of certain system design properties under projections of the near-optimal feasible space. Furthermore, Lombardi et al. mapped out the utilisation of renewable capacity, transmission capacity, and storage capacity of chosen near-optimal solutions, depending on different uncertainties, indicating overlaps between these (Lombardi et al., 2020). We detail the dimension reductions involved in working with near-optimal feasible spaces, and how to map back and forth between the different stages. We then propose several variations on a general algorithm for approximating reduced near-optimal feasible spaces, and analyse their convergence characteristics. The application of geometric descriptions of near-optimal spaces to studying different weather years is also novel.

In summary, our paper contributes to the literature on ESOMs in several ways. We formalise a general framework for working with and intersecting near-optimal feasible spaces, which allows us to study uncertainties of different kinds. We apply this framework to a first-of-its-kind study of robustness of highly renewable scenarios for the

European power system to decades of weather data. Beyond robustness, the methods also contribute to parallelisation of energy system optimisation models.

In Section 2 we formalise the methodology and introduce the necessary steps to define "robust" energy system designs. Afterwards, in Section 3, we describe the adapted PyPSA-Eur model we use and our modelling set-up to obtain power systems resilient to 41 years of weather data. In Section 4 we present our main findings on using intersections of near-optimal feasible spaces, features of robust solutions, and performance. We discuss ramifications of our approach in Section 5, before we conclude with Section 6.

2. Methodology and formal definitions

We introduce the methodology used in this paper and describe how we apply this to obtain energy system designs robust to weather variability: in Section 2.1 we revisit the concept of near-optimality. In Section 2.2 we discuss how dimension reduction is necessary to describe the near-optimal feasible space in a computationally tractable manner, and we elaborate on how we approximate near-optimal feasible spaces. Afterwards we introduce robustness as the geometric property of lying in the intersection of different near-optimal feasible spaces (Section 2.3). In Section 2.4 we then justify our choice of the Chebyshev centre as our robust solution of choice, as its location implies maximal stability to perturbations. Finally, in Section 2.5 we suggest different allocations that can translate a point in the low-dimensional intersection of the near-optimal feasible spaces to a spatially resolved (full-dimensional) energy system design.

2.1. Near-optimality

Let a capacity expansion problem be given as the linear program

$$\min c \cdot x \quad \text{such that} \quad Ax \leq b. \tag{1}$$

Here, $x \in \mathbb{R}^N$ is a vector of decision variables, $c \in \mathbb{R}^N$ the coefficients of the objective function, and $A \in \mathbb{R}^M \times \mathbb{R}^N$ and $b \in \mathbb{R}^M$ give the set of M linear constraints. Let $\mathcal{F}$ be the feasible space of the linear program Eq. (1), defined as

$$\mathcal{F} := \{x \mid Ax \leq b\}. \tag{2}$$

Letting $x^* \in \mathcal{F}$ be an optimal solution with objective value $c \cdot x^* = c_{\text{opt}} \in \mathbb{R}$, and $\varepsilon > 0$ a chosen slack level, we define the *ε-near-optimal feasible space* as

$$\mathcal{F}_\varepsilon := \{x \in \mathcal{F} \mid c \cdot x \leq (1+\varepsilon) \cdot c_{\text{opt}}\}. \tag{3}$$

When ε is clear from the context, we simply refer to $\mathcal{F}_\varepsilon$ as the *near-optimal* space. For general linear programs, $\mathcal{F}_\varepsilon$ is a convex polyhedron, and when x is bounded (as is the case for energy system models), $\mathcal{F}_\varepsilon$ is a convex polytope. To work with $\mathcal{F}_\varepsilon$ geometrically, we can solve the optimisation problem $\min d \cdot x$ s.t. $Ax \leq b$ and $c \cdot x \leq (1+\varepsilon) \cdot c_{\text{opt}}$ for some objective d in order to find a vertex or boundary point of $\mathcal{F}_\varepsilon$. In the context of ESOMs, this amounts to solving the energy system model once with an alternative objective function.

The definition of a near-optimal space is not new in the context of ESOMs, and previous work has explored the near-optimal space either through uniform sampling as Pedersen et al. (2021), maximally different solutions as DeCarolis (2011) and Price and Keppo (2017), or extreme points of the space (Neumann and Brown, 2021).

2.2. Dimension reduction

The near-optimal space $\mathcal{F}_\varepsilon$ is high-dimensional and complex; large-scale ESOMs typically involve millions of variables (dimensions) and constraints (hyperplanes defining the polytope). In this section we reduce to a much lower-dimensional space in two steps; see Fig. 1 for an overview of the maps and spaces involved.

In the case of capacity expansion models, we are most interested in *investment decision variables* of the linear program, as opposed to all other (operational) decision variables. Specifically, let $x = (x^I, x^O)^T \in \mathbb{R}^N$ be split into investment decision variables $x^I \in \mathbb{R}^{N_{\text{inv}}}$ and operational decision variables $x^O \in \mathbb{R}^{N_{\text{op}}}$, where $N = N_{\text{inv}} + N_{\text{op}}$. Then we define the projection map $\pi : \mathbb{R}^N \to \mathbb{R}^{N_{\text{inv}}}$ by simply forgetting about the operational decision variables. The image

$$\mathcal{F}'_\varepsilon = \pi(\mathcal{F}_\varepsilon) = \{x^I \in \mathbb{R}^{N_{\text{inv}}} \mid x = (x^I, x^O)^T \in \mathcal{F}_\varepsilon\} \tag{4}$$

of $\mathcal{F}_\varepsilon$ under π is the N_{inv}-dimensional ε-near-optimal feasible space of investment variables.

The convex polytope $\mathcal{F}'_\varepsilon$ consists of all points x^I such that an energy system with capacity investments given by x^I is feasible and whose total system cost (including operations) is at most $(1+\varepsilon) \cdot c_{\text{opt}}$. In short, it is the space of all near-optimal feasible investment decisions. This makes an explicit description of $\mathcal{F}'_\varepsilon$ interesting for decision-makers in order to explore different kinds of near-optimal investments.

However, in a model with a high spatial resolution, the number of investment decision variables N_{inv} is typically still in the hundreds or more (with multiple investment decisions at each node, and transmission expansion). This makes the polytope $\mathcal{F}'_\varepsilon \subseteq \mathbb{R}^{N_{\text{inv}}}$ difficult to work with, visually and mathematically. Specifically, in order to work with $\mathcal{F}'_\varepsilon$ we would want to find a set of points P such that $\mathcal{F}'_\varepsilon$ is the convex hull of P. However, the number of vertices of an N_{inv}-dimensional polytope defined by M hyperplanes is in $O(M^{\lfloor N_{\text{inv}}/2 \rfloor})$ — see Tóth et al. (2017), Chapter 26. This puts a precise description of $\mathcal{F}'_\varepsilon$ in terms of vertices out of reach.

One solution is to map down to a much lower-dimensional space where we group and aggregate investment decision variables. Let $x^I = (x_1, \ldots, x_{N_{\text{inv}}})$ be the individual investment decision variables. Let $T_1, \ldots, T_k$ be a collection of sets of indices with $T_i \subseteq \{1, \ldots, N_{\text{inv}}\}$ and $T_i \cap T_j = \emptyset$. For each index j in one of these sets, we also choose a coefficient/weight c_j. Then we define a linear map $\sigma : \mathcal{F}'_\varepsilon \to \mathbb{R}^k$ as:

$$\sigma(x) = \left(\sum_{j \in T_i} c_j x_j\right)_{i=1}^{k}. \tag{5}$$

In our case, we take each T_i to be the set of indices identifying decision variables that belong to a specific technology. We weight these decision variables x_j (for $j \in T_i$) by their respective capital costs c_j. Specifically, throughout this paper we consider $k = 5$, with $T_1, \ldots, T_5$ corresponding to transmission expansion, PV expansion, onshore wind expansion, offshore wind expansion and gas turbine expansion respectively. In effect, σ maps a vector x^I of investment decisions to a summary of selected total investment costs.

Let

$$\mathcal{A}_\varepsilon = \sigma(\mathcal{F}'_\varepsilon) = \{\sigma(x^I) \mid x^I \in \mathcal{F}'_\varepsilon\} \subseteq \mathbb{R}^k \tag{6}$$

be the image of $\mathcal{F}'_\varepsilon$ under σ. Then $\mathcal{A}_\varepsilon$ is a k-dimensional convex polytope (since convex polytopes are preserved by linear maps). Note that in our specific choice of $T_1, \ldots, T_5$ we have not included *all* investment decision variables in σ, only those we deemed most important for the particular model instances we work with. Of course, different dimension reductions can be achieved by other choices of aggregation (groups of indices T_i and coefficients c_j). While we have taken the coefficients c_j to be capital costs (making investment in different technologies easier to compare), the coefficients could, for example, also be set to 1 in order to consider only capacities.

The utility of the reduced near-optimal space $\mathcal{A}_\varepsilon$ is as a proxy for system feasibility. If we can describe $\mathcal{A}_\varepsilon$ well, we can quickly assess whether any given set of total investments $y \in \mathcal{A}_\varepsilon$ can result in a feasible system design. However, by aggregating investment decision variables, we lose information on the specific feasible system designs $\sigma^{-1}(y) \subseteq \mathcal{F}'_\varepsilon$ realising the total investments y. The trade-off is that the fewer dimensions k we aggregate to, the easier $\mathcal{A}_\varepsilon$ is to work with, but the less information it gives us. Each point $y \in \mathcal{A}_\varepsilon$ can have a large preimage under σ and π, meaning there may be many near-optimal

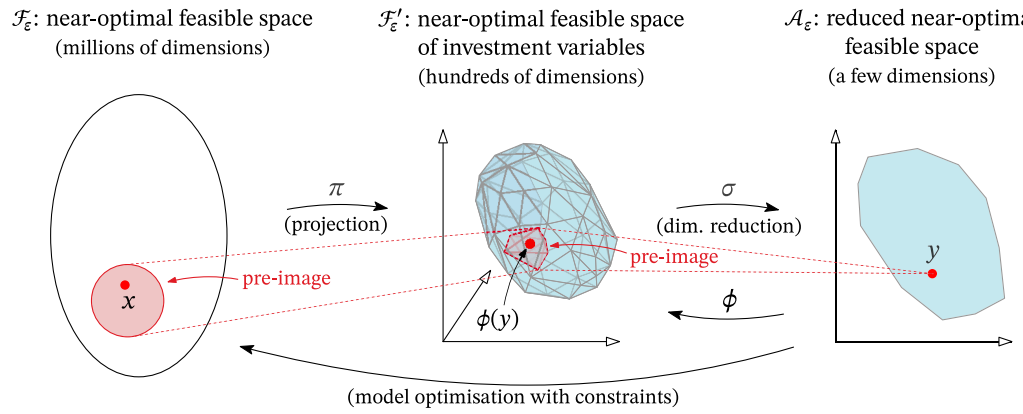

Fig. 1. Illustration of how the spaces $\mathcal{F}_\varepsilon$, $\mathcal{F}'_\varepsilon$ and $\mathcal{A}_\varepsilon$ are connected. The map ϕ can be seen as a composition of a model optimisation "$\min c \cdot x$ s.t. $Ax \leq b$ and $\sigma\circ\pi(x) = y$" composed with the projection π. It gives an explicit model design based on chosen coordinates y in the reduced near-optimal feasible space $\mathcal{A}_\varepsilon$.

feasible solutions $x \in \mathcal{F}_\varepsilon$ with the given total investments y (see Fig. 1). As we discuss in more detail in Section 2.5, to find a specific solution $x \in (\sigma\circ\pi)^{-1}(y) \subseteq \mathcal{F}_\varepsilon$, we must solve a version of the original model Eq. (1) in $\mathbb{R}^N$.

Similarly to Pedersen et al. (2021), we attempt to describe the low-dimensional space $\mathcal{A}_\varepsilon$ explicitly. Again, in order to find an explicit description of the polytope $\mathcal{A}_\varepsilon$, we would like to find (a large subset of) its vertices. We can do this by optimising over $\mathcal{A}_\varepsilon$ with different objective functions or *directions* in $\mathbb{R}^k$. For each direction $d \in \mathbb{R}^k$, the solution to the linear program

$$\max d \cdot y \quad \text{such that} \quad y = \sigma(\pi(x)) \text{ and } Ax \leq b \text{ and } x \in \mathcal{F}_\varepsilon \tag{7}$$

is an extreme point of $\mathcal{A}_\varepsilon$ in the direction d. The above linear program can be solved by solving the original problem in Eq. (1) with the new objective function $-d \cdot \sigma(\pi(x))$ (which is linear), and mapping the solution to $\mathcal{A}_\varepsilon$ by $\sigma\circ\pi$. In effect, for each extreme point of $\mathcal{A}_\varepsilon$ that we want to find, we need to solve the original capacity expansion problem once with an adapted objective function.

While we cannot expect to find all vertices of $\mathcal{A}_\varepsilon$ (quadratic in the number of model constraints when $k = 4, 5$ Tóth et al., 2017), we want to find a set of extreme points P such that their convex hull approximates $\mathcal{A}_\varepsilon$ well. Given a "budget" of n optimisations (and hence n extreme points), the natural question is: how do we choose the directions $d_1, \ldots, d_n$ to optimise in, in order to get a set of points P whose convex hull approximates $\mathcal{A}_\varepsilon$ the best possible?

We use an iterative approach to approximate $\mathcal{A}_\varepsilon$ while filtering on already used (or similar) directions. At each step we optimise in a different direction: depending on which property of the near-optimal feasible space is of interest, there can be many different ways to choose these directions. In our case we are interested in the largest ball within the near-optimal feasible space, the Chebyshev ball (see Section 2.4). Thus, we optimise at each iteration in the normal direction to a facet tangential to the Chebyshev ball of the current approximated polytope. If these have been exhausted, we choose the normal direction to the largest facet by volume. For other approaches to choosing directions, caveats and performance comparisons, see Appendix A. An illustration of one step in this process is shown in Fig. 2. A simplified version of the algorithm (based only on normals to large facets) is given in pseudo-code in Algorithm 1.

Once in the low-dimensional space $\mathbb{R}^k$ (with $k = 5$ in our case), the complexity of the geometric objects of interest is low enough that we can do efficient exact computations on them. In particular, recall that a polytope with n vertices can only have $O(n^2)$ facets for $k = 4, 5$, so computing the convex hull of the vertices, its volume, etc. has a time complexity of $O(n^2)$. We use the qhull software (Barber et al., 1996) for computational geometry related to polytopes. Since the number of vertices n which we can compute (by solving Eq. (7) for each vertex) is limited, the complexity of $O(n^2)$ is acceptable for our purposes. In particular, note that for our application, the complexity of Algorithm 1 is dominated by the model optimisations, not the computational geometry.

Algorithm 1: Outline of algorithm for approximating $\mathcal{A}_\varepsilon$

```
P := ∅;
for d ∈ {e_1, −e_1, e_2, −e_2, …, e_k, −e_k} do
    Let y be extreme point on A_ε in direction d (optimisation);
    Add y to P;
end
for i ∈ {1, …, n} do
    Let H be the convex hull of P;
    Let F_1, F_2, … be the facets of H, sorted by decreasing
      volume;
    Let d_i be the normal of facet F_i;
    Let d be the first of d_1, d_2, … which is not within a small
      angle θ of any previously used direction;
    Let y be extreme point on A_ε in direction d (optimisation);
    Add y to P;
end
Return convex hull of P;
```

2.3. Intersections and robust solutions

One of the new ideas we propose is to investigate the intersections of the near-optimal spaces of related capacity expansion problems, or different instances of the same abstract model. Of course, if $\mathcal{F}^{(a)}, \mathcal{F}^{(b)} \subseteq \mathbb{R}^N$ are the feasible spaces of two linear programs A and B, then $\mathcal{F}^{(a)} \cap \mathcal{F}^{(b)}$ is simply the space of all solutions x which are feasible for both problems. More interestingly for capacity expansion problems, consider $\mathcal{F}'^{(a)}_\varepsilon \cap \mathcal{F}'^{(b)}_\varepsilon$: the space of all investment allocations which are both feasible and near-optimal for both A and B.

In our case, we consider the near-optimal spaces for optimisation problems defined with different weather years. Specifically, we use 41 years of reanalysis weather data (1980–2020) in order to compute capacity factors and load time series as input for our model (Section 3.2 and Appendix B). This gives 41 model instances, each defined with the input data from a different weather year. For brevity, let $\mathcal{Y} := \{1980, \ldots, 2020\}$ denote the set of weather years. Then for $i \in \mathcal{Y}$ write

$$\min c^{(i)} \cdot x^{(i)} \quad \text{such that} \quad A^{(i)}x^{(i)} \leq b^{(i)} \tag{8}$$

for the LP in Eq. (1) defined with weather year i. Let $\mathcal{F}^{(i)}$ be the feasible space of the above LP. From these feasible spaces, we want to recover investment allocations which are feasible for each of the weather years.

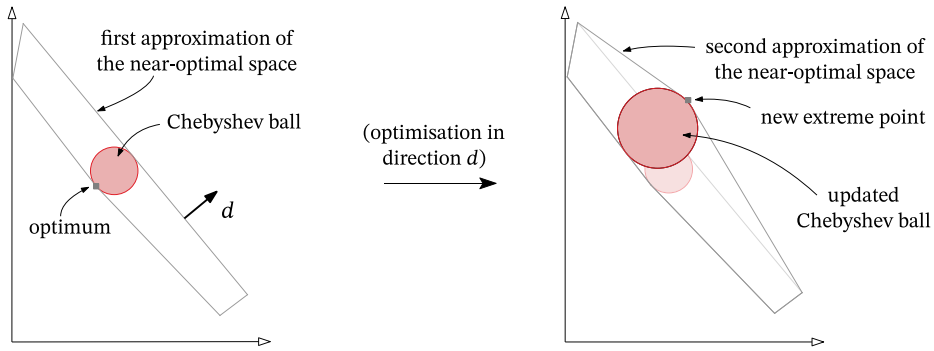

Fig. 2. Illustration of a single step of Algorithm 1. Additionally, the Chebyshev ball (see Section 2.4) is shown at each stage.

Since total system costs vary considerably between cost optimisations with different weather years, we define a uniform system cost bound across all weather years. Specifically, letting $c^{(i)}_{\text{opt}}$ be the optimal objective value (total system cost) for weather year i, we take

$$c^* = \max_{i \in \mathcal{Y}} c^{(i)}_{\text{opt}} \tag{9}$$

to be the highest optimal system cost across all weather years under investigation. In defining near-optimal spaces with the different weather years, we then set the slack relative to c^* instead of relative to each $c^{(i)}_{\text{opt}}$ for each weather year individually:

$$\mathcal{F}_\varepsilon^{(i)} = \{x \in \mathcal{F}^{(i)} \mid c \cdot x \le (1+\varepsilon) \cdot c^*\}. \tag{10}$$

We define $\mathcal{F}'^{(i)}_\varepsilon$ and $\mathcal{A}^{(i)}_\varepsilon$ similarly to $\mathcal{F}'_\varepsilon$ and $\mathcal{A}_\varepsilon$ (Eqs. (4) and (6)).

Now, the intersection $\bigcap_{i \in \mathcal{Y}} \mathcal{F}'^{(i)}_\varepsilon$ is the space of investment decisions which are feasible for all weather years under consideration and near-optimal (relative to the most expensive year).[2] We are interested in the intersection of the reduced near-optimal space $\mathcal{A}^{(i)}_\varepsilon$. Repurposing our notation slightly, we write $\mathcal{A}_\varepsilon := \bigcap_i \mathcal{A}^{(i)}_\varepsilon$. Note that $\mathcal{A}_\varepsilon = \bigcap_i \sigma(\mathcal{F}'^{(i)}_\varepsilon) = \sigma\left(\bigcap_i \mathcal{F}'^{(i)}_\varepsilon\right)$. However, while we cannot easily find explicit descriptions of the spaces $\mathcal{F}'^{(i)}_\varepsilon$, we *can* approximate each (low-dimensional) $\mathcal{A}^{(i)}_\varepsilon$ as explained above. This, in turn, enables us to find an explicit (approximate) description of $\mathcal{A}_\varepsilon = \bigcap_i \mathcal{A}^{(i)}_\varepsilon$.

We call a set of total investments $y \in \mathbb{R}^k$ *robust* when $y \in \mathcal{A}_\varepsilon$. This means that for each weather year i, there exists some near-optimal feasible model solution $x^{(i)} \in \mathcal{F}^{(i)}_\varepsilon$ (including investment and operation decisions) such that $\sigma \circ \pi(x^{(i)}) = y$. Note that the same total investment for each technology, $y \in \mathcal{A}_\varepsilon$, may be spread differently onto the different nodes of the model for each $x^{(i)}, i \in \mathcal{Y}$. Formally speaking, it is plausible that $\bigcap_i \mathcal{F}'^{(i)}_\varepsilon = \emptyset$ even if we find some robust point $y \in \mathcal{A}_\varepsilon$. In Section 2.5, however, we propose different methods for finding robust allocations $x^I \in \bigcap_i \mathcal{F}'^{(i)}_\varepsilon$ such that $\sigma(x^I) = y$ if they exist, and in Section 4.1 we show that this works well in practice.

2.4. Chebyshev centre

Among the total investment decisions in the intersection $\mathcal{A}_\varepsilon = \bigcap_i \mathcal{A}^{(i)}_\varepsilon$, we want to find choices that are not only feasible for all years considered. We want to find the most resilient choice among all the alternatives. We therefore select the point $y_{\text{ch}} \in \mathcal{A}_\varepsilon$ maximally removed in all directions from the boundary of $\mathcal{A}_\varepsilon$, meaning y_{ch} is as far away from being infeasible as possible. This is realised if we pick y_{ch} to be the Chebyshev centre (see Boyd and Vandenberghe (2004), Section 8.5.1), i.e.

$$y_{\text{ch}} = \operatorname*{argmax}_{y \in \mathcal{A}_\varepsilon}(r) \text{ s.t. } B_r(y) \subseteq \mathcal{A}_\varepsilon, \tag{11}$$

where $B_r(y)$ is the ball of radius r around y. Figs. 2 and 3(b) show examples of Chebyshev balls. The point y_{ch} can be found efficiently using a linear program. Specifically, let a_j be the normal vectors of the hyperplanes supporting $\mathcal{A}_\varepsilon$ and b_j the associated offsets, so that each $y \in \mathcal{A}_\varepsilon$ satisfies $a_j \cdot y \le b_j$ for all j. Then y_{ch} is given by

$$\max r \quad \text{such that} \quad a_j \cdot y + r\|a_j\| \le b_j \quad \forall j \quad \text{and} \quad r \ge 0. \tag{12}$$

2.5. Disaggregating robust solutions

The previous steps leading to the Chebyshev centre, one chosen robust point, have all been performed in the reduced ε-near-optimal feasible spaces and their intersection, $\mathcal{A}_\varepsilon$. The designs that are of ultimate interest to us, however, are elements in $\mathcal{F}'_\varepsilon$, including *all* investment decision variables. Thus, we would like to define a function $\phi : \mathcal{A}_\varepsilon \to \mathcal{F}'_\varepsilon$ mapping robust total investments to complete system designs realising those total investments. Being more precise, we need to specify over which weather years the space we map back to is defined — we want a map

$$\phi : \mathcal{A}_\varepsilon \to \mathcal{F}'^{\mathcal{Y}}_\varepsilon, \tag{13}$$

recalling the notation $\mathcal{Y} = \{1980, \dots, 2020\}$. From this map, we want to obtain a robust near-optimal energy system design $x_{\text{rob}} = \phi(y_{\text{ch}})$ at the Chebyshev centre of $\mathcal{A}_\varepsilon$.

We can write our ESOM as in Eq. (8) but instead define it with all 41 weather years as $\min c^{\mathcal{Y}} \cdot x^{\mathcal{Y}}$ such that $A^{\mathcal{Y}} x^{\mathcal{Y}} \le b^{\mathcal{Y}}$; its ε-near-optimal feasible space of investment variables is $\mathcal{F}'^{\mathcal{Y}}_\varepsilon$. Then we define the map ϕ (which we call $\phi^{\mathcal{Y}}$ for clarity) by adding constraints to the above LP to ensure that the solution has total investments given by $y \in \mathcal{A}_\varepsilon$:

$$\phi^{\mathcal{Y}}(y) = \pi(\operatorname{argmin} c^{\mathcal{Y}} \cdot x^{\mathcal{Y}}) \text{ such that } A^{\mathcal{Y}} x^{\mathcal{Y}} \le b^{\mathcal{Y}} \text{ and } \sigma \circ \pi(x^{\mathcal{Y}}) = y. \tag{14}$$

Given that π and σ are linear, the above is still a linear program. Note that $\phi^{\mathcal{Y}}$ may not be well-defined for all y if the corresponding linear program has no solutions; this can happen if some total investments y are realisable for each individual weather year, but not realisable by any one complete system design over all 41 years.

Solving Eq. (14) amounts to solving an ESOM defined with 41 weather years, which is computationally challenging. Indeed, one of the motivations for working with the intersection $\mathcal{A}_\varepsilon$ is that it can be computed on the basis of model optimisations with single weather years.

Thus, we propose two alternatives to the "exact" map $\phi^{\mathcal{Y}}$. We call the exact map and its alternatives *allocations* since they map total investments $y \in \mathcal{A}_\varepsilon$ to a spatially resolved allocation of investments $\phi(y) \in \mathcal{F}'^{\mathcal{Y}}_\varepsilon$. The alternative allocations are heuristics in the sense that they map to designs that are not strictly speaking guaranteed to be feasible. Formally, they map $\mathcal{A}_\varepsilon \to \mathbb{R}^{N_{\text{inv}}}$ but may map some points of $\mathcal{A}_\varepsilon$ outside of $\mathcal{F}'^{\mathcal{Y}}_\varepsilon$ (whereas $\phi^{\mathcal{Y}}(\mathcal{A}_\varepsilon) \subseteq \mathcal{F}'^{\mathcal{Y}}_\varepsilon$). For the first

[2] In fact, this resembles the near-optimal feasible space of a robust optimisation program defined over the weather years $\mathcal{Y}$. Strictly speaking, however, the different operational variables for different weather years make this a loose generalisation of classical robust optimisation.

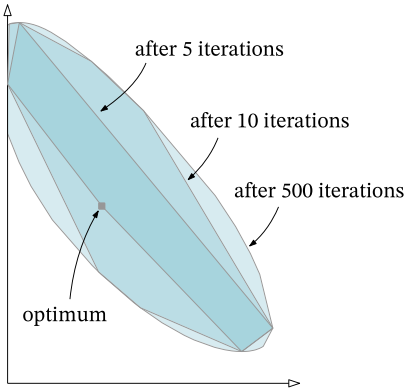

(a) The approximation of a reduced near-optimal feasible space after 5, 10, and 500 iterations (with decreasing opaqueness).

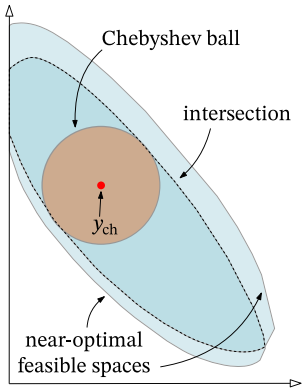

(b) The Chebyshev centre y_{ch} of the intersection of two reduced near-optimal feasible spaces. The radius of the Chebyshev ball around the centre can give us an idea of how much flexibility we might expect around this point.

Fig. 3. Near-optimal space approximation, intersection and Chebyshev centre.

Table 1
Overview over three different allocations to obtain "robust" solutions.

Map	Short name	Description	Computation
$\phi^{\mathcal{Y}}$	exact	Fix the investment costs in y_{ch} as additional constraints. Then solve Eq. (1) jointly over all years.	Optimisation over 41 years (134 GB RAM, 35 h)
$\phi^{(i^*)}$	conservative	Fix the investment costs in y_{ch} as additional constraints. Then solve Eq. (1) for the year with the highest optimal cost, c^*.	1 single-year optimisations (ca. 3 GB RAM, 0.25 h)
ϕ^{mean}	mean	Fix the investment costs in y_{ch} as additional constraints. Then solve Eq. (1) for all single years and take the mean over all capacities.	41 single-year optimisations (parallelisable, each ca. 3 GB RAM, 0.25 h)

alternative, which we call the "conservative" allocation, let i^* be the most expensive year, for which $c_{\text{opt}}^{(i^*)} = c^*$. Then we simply take $\phi^{(i^*)}$ as an alternative to $\phi^{\mathcal{Y}}$. That is, for the conservative allocation we take the solution of the ESOM defined with weather year i^*, with the added constraints that $\sigma \circ \pi(x^{(i^*)}) = y_{ch}$. Computing $\phi^{(i^*)}$ involves only one model optimisation with a single weather year.

For the second alternative, which we call the "mean" allocation, we follow the idea of the conservative allocation $\phi^{(i^*)}$, but involve the other weather years more. Indeed, we define ϕ^{mean} as

$$\phi^{\text{mean}} = \frac{1}{|\mathcal{Y}|} \sum_{i \in \mathcal{Y}} \phi^{(i)}. \tag{15}$$

Computing ϕ^{mean} involves $|\mathcal{Y}|$ model optimisations with single weather years. In our case, $|\mathcal{Y}| = 41$. The exact and alternative allocations are summarised in Table 1.

For comparison, we also define a "baseline" point in $\mathbb{R}^{N_{\text{inv}}}$ which is obtained by scaling up investments uniformly in the optimal solution for the most expensive weather year. This is explained in more detail in Section 4.3.

3. Implementation

3.1. Modelling set-up

We base our implementation on the PyPSA-Eur 0.4 model (Hörsch et al., 2018), which is itself based on the general PyPSA framework (version 0.18) (Brown et al., 2018). While we have modified PyPSA-Eur for our purposes (as described in Appendix B), especially in order to support multiple weather years, we have kept the model set-up relatively close to the defaults as described in Hörsch et al. (2018). We use the model in a partial greenfield configuration, where existing transmission, nuclear[3] and hydro capacities at current (2020) capacities are included in the model from the start, but all other technologies start at zero capacity.[4] The extendable technologies included in the model are transmission (both AC and relevant DC connections), battery and hydrogen storage, onshore and offshore wind power, solar power and open-cycle gas turbines. The model is run with a single investment period and perfect foresight. We limit annual CO_2 emissions to 95% of 1990 levels.[5] A one-node-per-country[6] spatial resolution and a 3-hourly temporal resolution is chosen. Note, however, that the spatial and temporal resolution can be increased easily (as in PyPSA-Eur); the resolution is limited in this paper in order to allow extensive validation of our methods. We model the year 2030 with 41 distinct historical weather years (1980–2020) driving renewable capacity factors and electricity demand based on the default PyPSA-Eur cost assumptions[7] (given in 2013 EUR) for the year 2030. Thus all weather years are viewed as different potential realisations of 2030, and we can compare investment and operational costs of multi-year optimisations to single-year optimisations by taking annual averages.

Using enough weather data to accurately represent long- and short-term dynamics and extreme events is difficult in ESOMs, considering the resulting model size and increased solving complexity. However limited the lessons of historical weather data are on future weather (van der Wiel et al., 2019), further driven more and more by climate change, the extreme events and variability represented here will still likely offer insights for future designs. We capture historical climate change implicitly here, whereas incoming trends and changes through climate change are hard to predict and an active field of research in itself (Wohland et al., 2017; Schlott et al., 2018; Kozarcanin et al., 2019; Bloomfield et al., 2021).

[3] Nuclear power in Germany is removed from the model.

[4] PyPSA-Eur can also include existing biomass capacities in the model. Due to their limited capacities, they do not lead to significant deviations in results compared to the scenario we considered, so we choose to omit biomass for simplicity of the setup.

[5] We present additional results with a 100% emission reduction in Appendix C.

[6] Except for countries in multiple synchronous zones (Denmark, Spain, Italy, UK), which are represented through two nodes.

[7] https://github.com/PyPSA/pypsa-eur/blob/v0.4.0/data/costs.csv (accessed 06/10/2022).

3.2. Data

The data we use as input for our model lean heavily on the data and sources used in PyPSA-Eur. For instance, we use cost data based on the default costs considered in PyPSA-Eur, which are estimates for 2030[7] (in 2013 EUR). However, time series input data have been extended to 41 weather years.

We use reanalysis data to generate capacity factors for the renewable energy sources; our source is the hourly ERA5 dataset (Hersbach et al., 2018) for the time period from 1980 up to and including 2020. The open-source tool Atlite (Hofmann et al., 2021) translates weather data to hourly capacity factors for solar PV, on- and offshore wind. The inflow profiles for hydropower are generated similarly, however they are corrected to fit production data given by Administration (2022). We describe in detail how we process the data in Appendix B.

The load input data are generated using a regression model on 1980–2020 ERA5 temperature data. The regression is based on hourly country-level ENTSO-E load data from 2010 to 2014 (ENTSO-E, 2022), as well as the temperature data. We conduct a two-staged regression with a similar approach to that used in Bloomfield et al. (2020). This allows us to generate 41 years of country-level temperature-dependent load data matching the weather data we use. Finally, we scale the demand by a factor of 1.13 according to load projections for 2030 by the European Commission.[8] More details on the generated load data can be found in Appendix B.

3.3. Modeller's decisions

In this section, we discuss various details and choices regarding the implementation of the methods described in Section 2. For the exact code, including configuration options and installation and running instructions, we refer to the GitHub repository.[9]

One of the first decisions we have to make is choosing a suitable slack level ε. For small ε the intersection $\mathcal{A}_\varepsilon$ may be empty; a priori it is not clear how large ε has to be for $\mathcal{A}_\varepsilon$ to be nonempty. In our case, we choose $\varepsilon = 5\%$ on top of the most expensive weather year, but found that $\mathcal{A}_\varepsilon$ is even nonempty with $\varepsilon = 2.5\%$; this may change with a different modelling set-up. For comparison, Trutnevyte found in Trutnevyte (2016) that the transition in the UK energy system from 1990 to 2014 deviated between 9 and 23% from the cost optimum.

Given that the dimension reduction map σ is our main tool in working with near-optimal spaces (see Section 2.2), we need to define it carefully. Both the number of dimensions k that σ maps to and which investment decision variables are mapped to each dimension must be considered. We have investigated the convergence of Algorithm 1 with $k = 2, 3, \ldots, 7$ (Appendix A) and we find that it is tractable to work with this number of dimensions. The decision variables that are mapped to each dimension (the sets $T_1, \ldots, T_k$ in the notation of Section 2.2, here abbreviated to "dimensions") should be chosen meaningfully. On one hand, including as a dimension a technology which is not utilised in cost-optimal solutions may be detrimental, as much computational effort will be expended on potentially irrelevant solutions including this technology. Moreover, the Chebyshev centre of the resulting space must include at least a Chebyshev radius worth of that technology, which may be sub-optimal. On the other hand, *not* including as a dimension a technology which plays a significant role in any near-optimal solution can limit the usefulness of the results. In our case, we choose to map investment decision variables for transmission expansion, solar, onshore wind, offshore wind and gas to 5 respective dimensions.

Lastly, we choose the coefficients c_j in the definition of σ to be the investment cost associated with the investment decision variable x_j; this has the advantage of mapping to the single unit of EUR in every dimension, making different dimensions easily comparable. In contrast, for example, comparing renewable capacity expansion in MW and storage capacity expansion in MWh directly is more difficult and not as useful for the purpose of working with a Chebyshev ball. For some applications one might consider scaling the weights c_j for certain dimensions, for example, when robustness to changes in investment in one technology are more important than for other technologies.

A key driver of the computational demands of our approach is the desired quality of approximation of near-optimal spaces. How many iterations of Algorithm 1 are needed, depends on the number of dimensions k, the mode of finding new directions to explore (see Fig. A.1) and the intended use-case. A fixed number of iterations can be chosen, or the algorithm can be ended once some convergence criteria is satisfied. Either way, we refer to Appendix A for a discussion of the various trade-offs involved.

The other factor influencing the computational effort is how much time and computing power every single optimisation takes. This is typically driven by the number of technologies, inter-temporal relations between different variables (e.g. through storage), temporal resolution (Hoffmann et al., 2020) and spatial resolution (Tröndle et al., 2020; Frysztacki et al., 2021). Deciding on the model complexity must be done in light of the research question at hand. For our application with weather years, we do assume that each individual model is defined over a time period of one calendar year.

4. Results

We first present the main results pertaining to system design with 41 weather years, and the use of near-optimal spaces in this context (Section 4.1). This is followed by a more detailed description of the characteristics of our proposed robust solutions (Section 4.2). The subsequent subsection focuses on validation results and a comparison of the different robust design allocations (Section 4.3). Finally, we touch on computational results and parallelisability (Section 4.4).

4.1. Weather years and intersection

First of all, optimising our model with each of the 41 considered weather years individually shows large discrepancies in the respective optimal solutions, re-affirming the importance of considering a large set of different weather years. Optimal total system costs range from 121 billion EUR for 2020 to 152 billion EUR in 1985.[10] The composition of investment by technology also differs significantly between weather years, with especially the onshore- and offshore wind investment varying by up to around 20 and 25 billion EUR between years (corresponding to variations up to 243 GW for onshore wind and 82 GW for offshore wind), respectively. The inter-year variability in optimal investments is illustrated in Fig. 5, where the investments are compared to the robust solution x_{rob}.

Meanwhile, for this study we also conduct the first capacity expansion optimisations of a spatially resolved model for the European power system with 41 weather years directly (one node per country, 3-hourly resolution). These optimisations took in the order of 1–2 days (using two threads) and up to 134 GB of memory. The optimal annualised total system cost for the 41-year model is 137 billion EUR; only slightly higher than the average of the total system costs of optimisations with single weather years at 134 billion EUR. See also Fig. 7 for a breakdown into investment (for extendable technologies)- and variable costs and comparison with the optimisations with single weather years. Apart

[8] https://ec.europa.eu/clima/document/download/ec1acac9-10fe-4eeb-915f-cad388990e0f_en, Fig. 44 (accessed 23/06/2022).

[9] https://github.com/aleks-g/intersecting-near-opt-spaces/tree/v1.0.1.

[10] These and all the following total system costs are annualised and include investment in new capacities as well as variable costs (in 2013 EUR), but not existing capacities. See Section 3.1 for details on which existing technologies are included in the model.

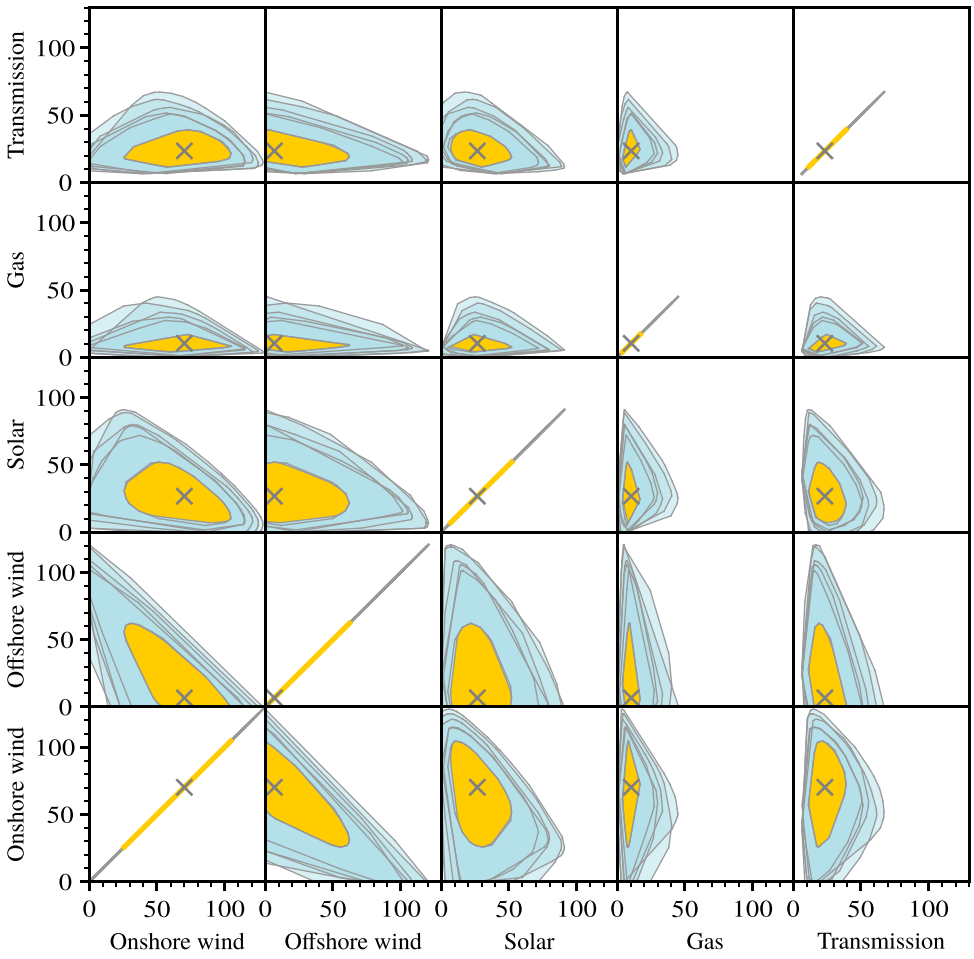

Fig. 4. Projections of the near-optimal spaces for different weather years and their intersection. All values are annualised total investment costs per technology. For illustrative purposes, we only plot the near-optimal spaces for 6 out of 41 weather years (in different hues of blue). The intersection of all 41 near-optimal spaces is filled in yellow and the Chebyshev centre is marked with a cross.

from providing a basis of comparison, optimising the model with 41 weather years also allows us to compute the exact robust map $\phi^{\mathcal{Y}}$ in order to validate the alternative mean and conservative allocations (Section 4.3).

We implement (as in Section 3) the methodology of intersecting near-optimal spaces (laid out in Section 2) using PyPSA-Eur. With a slack level of $\epsilon = 0.05$ as in Eq. (9), we obtain a nonempty intersection $\mathcal{A}_\epsilon$ and a robust allocation x_{rob} that is fully feasible using all the weather data of 41 years. Thus we show that there are robust solutions with less than 5% additional costs (on top of the most expensive year). We even find robust solutions which are less than 5% more expensive than a system optimised with the entire period of 41 years (see Fig. 7). Furthermore, the space $\mathcal{A}_\epsilon$ offers significant flexibility for policymakers beyond our point of reference x_{rob}, and beyond what flexibility is shown by previous MGA approaches.

Fig. 4 shows projections of a selection of near-optimal spaces $\mathcal{A}_\epsilon^{(i)}$ for weather years $i \in \{1985, 1989, 1996, 2006, 2014, 2020\}$ in addition to the intersection $\mathcal{A}_\epsilon = \bigcap_{i\in\mathcal{Y}} \mathcal{A}_\epsilon^{(i)}$ over all weather years. While the spaces are 5-dimensional (with the dimensions being investment in onshore wind, offshore wind, solar, gas and transmission expansion), they have been projected down to all possible pairs of technologies considered. The Chebyshev centre, marked by a cross, is located within the intersection which consists of the robust solutions. The figure reveals that there is significant flexibility in these dimensions; while a certain amount of investment in renewables is needed, the investment can be shifted between different technologies while staying feasible and near-optimal. Note also that the near-optimal spaces for different years resemble each other in shape and location in space, but mainly differ in size. This indicates that the effect of "difficult" weather years on modelling is mainly that they restrict the size of the feasible design space.

We find that the Chebyshev radius of $\mathcal{A}_\epsilon$ is 3.43 billion EUR, coming near to the theoretical maximum possible radius of 3.80 billion EUR given by the chosen slack level. Indeed, note that the distance between cost-optimal solutions and the near-optimal cost constraint is $c^*_{\text{opt}} \cdot \epsilon$, meaning that any near-optimal space can have a Chebyshev radius of at most $c^*_{\text{opt}} \cdot \epsilon/2 \approx 3.80$ billion EUR. The result means that the total investments in technologies that make up the dimensions of $\mathcal{A}_\epsilon$ can change by up to 3.43 billion EUR (corresponding to 2.35% of the total cost of the robust system) in any direction, starting at the robust point y_{ch}. The resulting (potentially reduced) total investments can still result in a feasible design for every weather year.

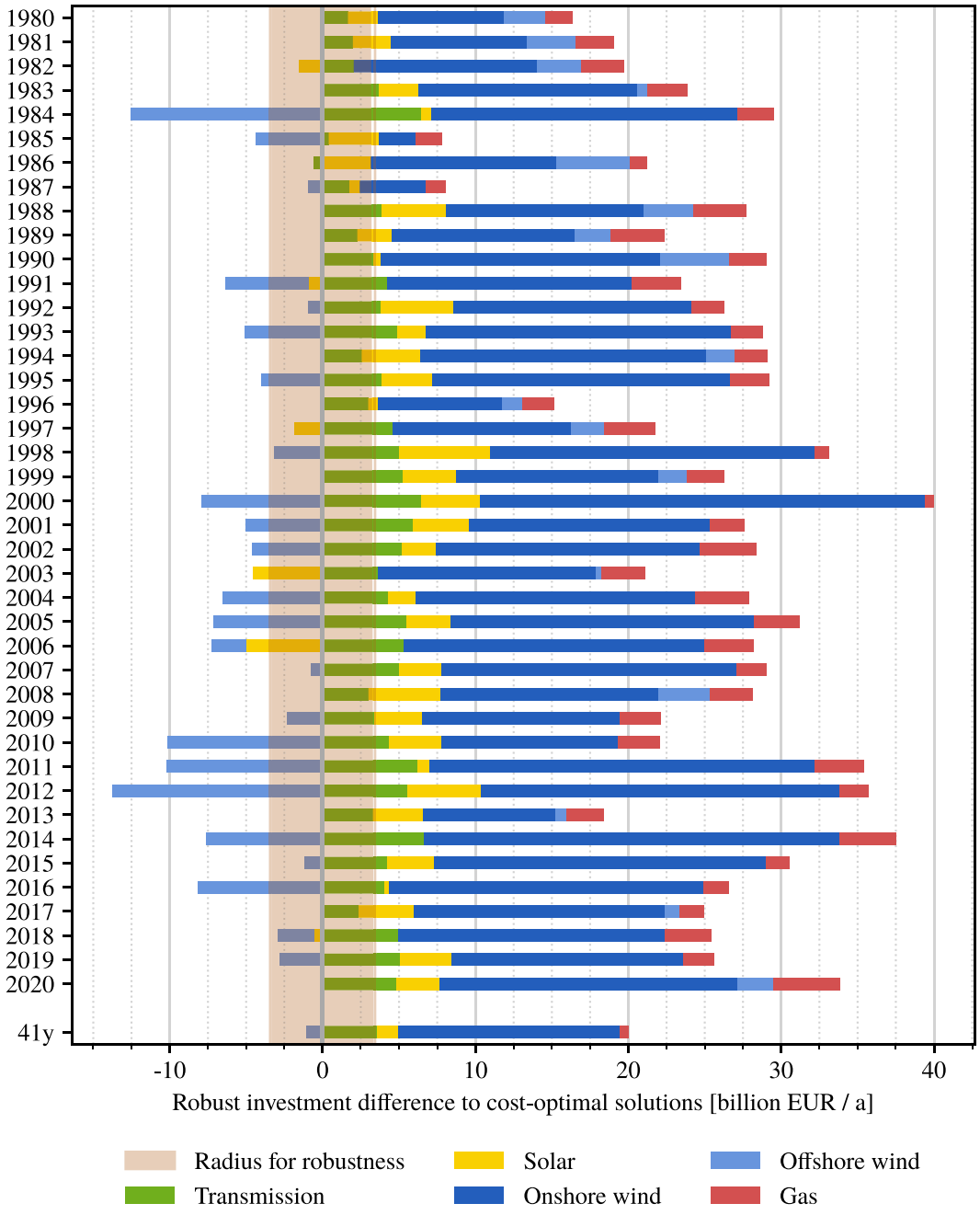

Fig. 5. Comparison of total investments for selected technologies in the optimal solutions for each weather year and the optimal solution with all weather years ("41y") to the robust point y_{ch}. Positive values mean greater investment in the given technology by the robust solution.

Given that we work with an absolute objective bound (1.05 times the cost of the most expensive year) for all near-optimal spaces, we find that the smallest and largest near-optimal spaces differ in volume by a factor of about 79. This means that some weather years by themselves allow for many more different near-optimal feasible solutions than others. Put differently, some weather years restrict the system design much more than others. The smallest and largest near-optimal spaces come from the weather years 1985 and 2020 respectively, and the difference in volume corresponds to an average scaling factor of $79^{1/5} \approx 2.4$ in every dimension. Meanwhile, the intersection of the near-optimal spaces has a volume that is 79% and 36% of the volumes of the near-optimal space for years 1985 and 1987, respectively, and is between 1% and 10% of the volume of all other near-optimal spaces. This means that except for 1985 and 1987, 10% or less of near-optimal solutions for any particular weather year are feasible for all other weather years under consideration.

In fact, we find that the optimal solutions with the years 1985 and 1987 actually have total investments that lie within the intersection $\mathcal{A}_\varepsilon$. When operated over the entire weather year dataset, these designs are practically feasible, with negligible load shedding. These results can inform the choice of weather year to model with — if only a single (or few) years can be chosen.

We note, however, that while there are weather years to which our model does not "over-fit" in a single-year optimisation (1985 being

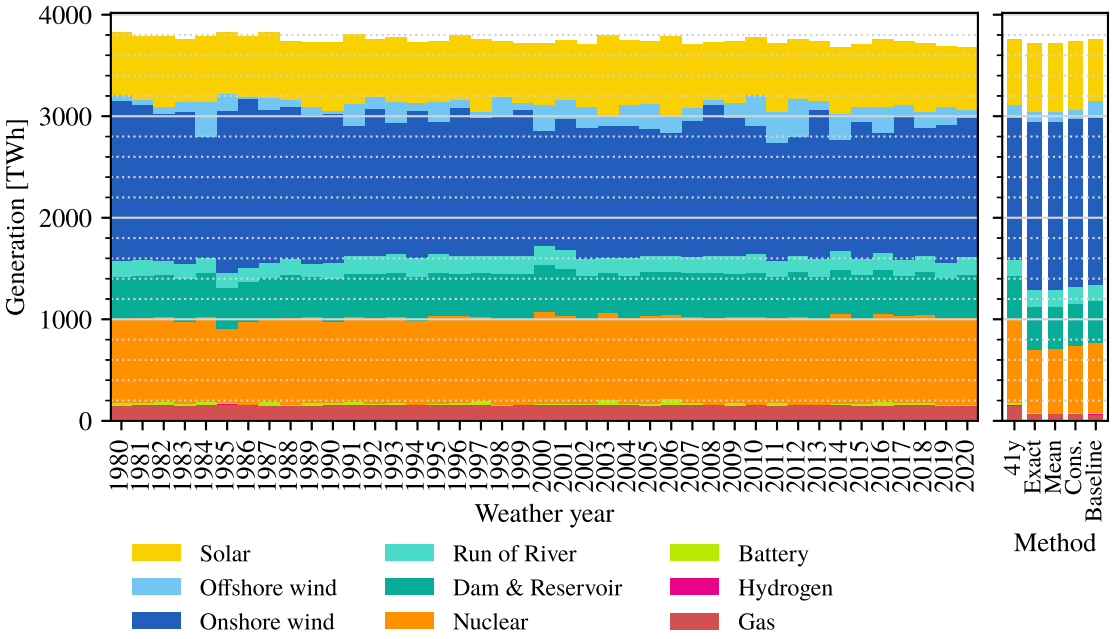

Fig. 6. Annual average generation mixes for the optimal solutions for each single weather year, the optimal solution with all weather years ("41y") and the robust allocations as well as the baseline design. The baseline design is used for comparison in validation (Section 4.3).

such a year resulting in a generally applicable design), this result could be particular to our modelling set-up.

4.2. Robust design characteristics

The robust solutions we compute, coming from the Chebyshev centre of the intersection $\mathcal{A}_\varepsilon$, have several interesting properties. First, we compare the investment composition of the robust point y_{ch} to that of optimisations using just a single year of weather data. We then analyse total investment and operational costs. Finally, we present results related to the CO_2 limit.

Fig. 5 shows the differences in investment per technology between the robust point and each of the optimal designs for individual years. The robust point is characterised by more investment in onshore wind, solar, transmission, and gas (sorted by decreasing additional investments). Meanwhile, most optima from single weather years over-invest significantly in offshore wind power compared to the robust allocation due to higher relative costs. In this particular set-up where gas can smooth the electricity production, the cost benefits of additional onshore wind capacities outweigh the potential of offshore wind power in the most favourable years. We conclude that here onshore wind power contributes more than other technologies to robustness, followed by solar power and transmission capacity.[11] This holds as well when one compares the investments in the robust ("exact") allocation to the optimal solution using all weather years (see the "41y" row in Fig. 5).

Fig. 6 shows the annual (for the optimisations with more weather years, average) total electricity generation per technology. This shows the increased importance of onshore wind and solar for the robust system. Meanwhile, the figure also shows that although solutions for individual years typically under-invest in gas turbines relative to the robust ones, the robust solutions actually generate less power with gas (and nuclear) in total. This reflects the fact that while additional gas capacity is needed for robustness, the additional investment in renewables leads to a reduced dependence on gas for "day-to-day" operations.

On that topic, Fig. 7 shows the variable and total system costs of systems optimised with single weather years, as well as the robust system and a system optimised with the full dataset of 41 weather years. It illustrates that the robust design has a higher total investment cost than designs for individual years, while the (average) operating costs are lower due to the reduced use of gas and nuclear as mentioned above. Recall that while we set the slack ε to 5%, we see that the investment costs in fact lie only 0.4% above what would have to be invested based on the most expensive year. With the (average) variable costs of the robust system being lower due to a strengthening of renewables, the total (annualised) system cost of the robust solution is about 146 billion EUR and actually lower than the system costs for some optimal solutions with single weather years. This is because the total system cost for the robust solution is averaged over all 41 weather years, with some being more expensive than others.

We also see that robust system designs emit less CO_2 in our tests compared to the single-year optimisations, and use 48% of the given CO_2 limit.[12] This is again because robust designs direct more of the total system cost into capital investment of renewables and less into variable costs including gas, the only source of emissions in our model. However, we should note that when we operate the design obtained from e.g. a system optimisation with the single weather year 1985 over the entire time period (over which it is practically feasible), it also does not use up the whole CO_2 limit. Although capacity expansion optimisations with single weather years always use up the CO_2 limit, the designs which are adapted to difficult years such as 1985 have enough renewable capacities that they do not use up the CO_2 limit in a typical year.

Finally, Fig. 8 shows the geographical differences in investment between the exact robust allocation and the cost-optimal solution with 41 weather years. We see that the majority of additional onshore wind power in the robust system is allocated to the UK, followed by Poland, France, Estonia and Sweden. The transmission capacity to the UK also receives more investment in the robust allocation. Meanwhile, although

[11] The conclusions can change with different assumptions — see Appendix C.

[12] The optimal solution with all 41 weather years uses the whole CO_2 limit as well.

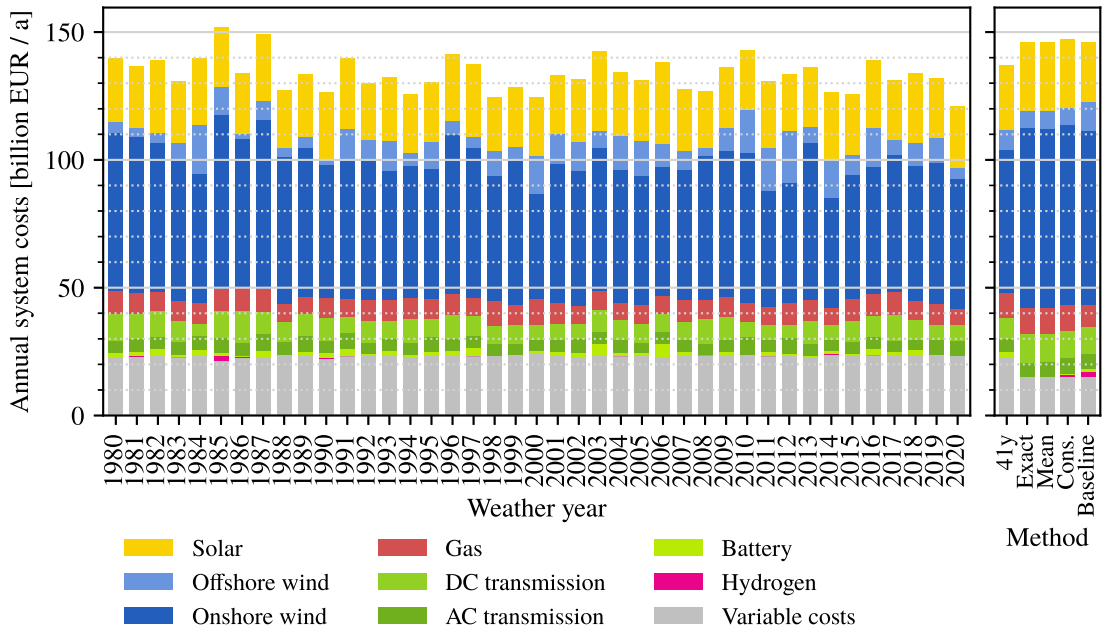

Fig. 7. Comparison of cost-minimal designs based on optimisations over individual years to the annualised costs of robust designs (exact, mean and conservative, respectively), an optimisation with all 41 years ("41y") and the baseline design.

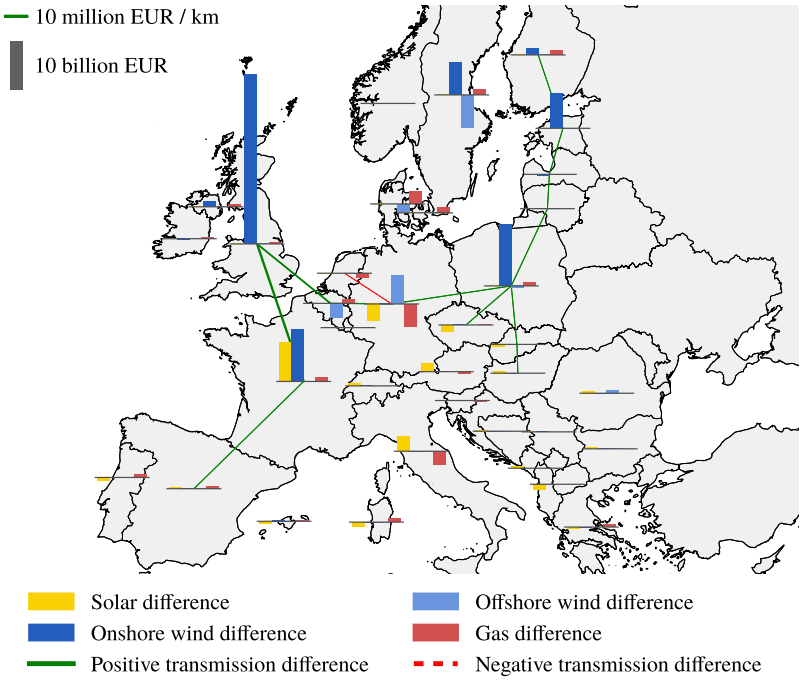

Fig. 8. Difference in investment between the exact robust allocation and the optimum solution with 41 weather years. Bars above the baselines mean that there is more investment for that technology in the robust solution. For transmission there are only positive differences (negative differences are too small to appear on this scale), and AC and DC transmission have been combined. For both bars and transmission lines, the same area means the same investment difference in EUR. All costs are annualised.

the system invests less in offshore wind in total, more offshore wind investment is shifted to Denmark.

4.3. Validation of robust allocations

Recall from Section 2 that we can use a (large) number of optimisations with single weather years to find a robust point of *total* capacity allocations $y_{\text{ch}} \in \mathcal{A}_\varepsilon$ — the Chebyshev centre in the intersection of near-optimal spaces of model instances using different weather years. However, in order to find *specific* (per-node) investment allocations fitting the given robust totals and being feasible for every weather year, we have to map y_{ch} back to $\mathcal{F}_\varepsilon'^{\mathcal{Y}}$. The exact allocation $\phi^{\mathcal{Y}}$ does this by solving the original ESOM (with the additional constraint that $\sigma \circ \pi(x) = y_{\text{ch}}$) with 41 weather years. Section 2.5 gives two alternatives for allocating the robust capacities to individual nodes: the "mean" and "conservative" allocations, both based only on a number of optimisations with one single weather year at a time (see Table 1). Recall that both the mean and conservative allocations have the same coordinates

Table 2
Performance of the different allocation methods and the baseline for comparison. Note that total load shedding (over 41 years) here includes technical infeasibility and over-budget operations as explained earlier. The relative load shedding is with respect to the total load of all 41 weather years.

Allocation method	Total load shedding [TWh]	Relative load shedding [%]
Exact	0.0	0.000
Conservative	46.7	0.032
Mean	119.0	0.081
Baseline	132.3	0.090

in $\mathcal{A}_\varepsilon$ as the exact allocation, namely y_{ch}, but are not guaranteed to be feasible for all 41 weather years.

In this section, we investigate the quality of these heuristic allocations. The basis for comparison is two-fold: the exact robust allocation on the one hand, and a "naïve" baseline allocation based solely on the most expensive weather year on the other hand. Specifically, in order to make the designs more comparable, the baseline allocation is obtained by taking the allocation from the single most expensive weather year (1985 in our case) and uniformly scaling all expandable capacities up by such a factor that the total capital cost of the whole network equals that of the exact robust design. This way, the only difference between the exact, mean, conservative, and baseline designs is how investment is allocated (by technology and spatially), not the total investment volume.

The validation of the robust allocations consists of a "stress test" where we operate the systems over the entire dataset of weather years (i.e. only optimise the dispatch and not the investments). This dispatch optimisation includes the 95% CO_2 reduction constraint as in the capacity optimisation. Similarly to how we ensure that the total investment cost is equal between the four different allocations, we also ensure that all designs keep to the same operational budget; namely the total operational costs of the exact robust design. By allowing costly load shedding (with variable costs of 7 300 EUR/MWh, as in Price and Zeyringer (2022)), we make sure that the models are solvable. The quality of the allocations is then measured in the amount of load shedding; 0 load shedding means complete feasibility. In the presence of a hard operational budget constraint, it should be understood that total unmet demand combines actual unmet demand due to technical infeasibility and over-budget operations. Without the operations budget constraint, a number of designs – including all robust allocations and also some optimal solutions for single years – are practically feasible with all weather years (see Section 4.1), but simply have higher operational costs. In general, however, optimal solutions from single years fail to serve the entire time period reliably.

Table 2 shows that the exact allocation has 0 load shedding as expected, and is followed by the conservative allocation in quality. The mean and baseline designs perform slightly worse, but still only up to about 0.1% of the total load is shed or produced over budget. This shows that the conservative and mean heuristics produce results that are practically feasible.

4.4. Performance and computational effort

Our work demonstrates methods for working with decades of weather and demand data in a parallelised setting. Namely, the mean and conservative allocations produce robust system designs with decades of weather data while only requiring model optimisations with single weather years which can be parallelised effectively. This is done by using the centre point of the intersection of near-optimal spaces for different weather years to obtain a robust set of total capacities per technology. From these we then compute specific per-node capacity allocations adhering to the robust totals for each individual weather year, and average the resulting capacities.

This is particularly relevant because solving ESOMs is usually memory-constrained: a single large model may take more memory to solve than is available on common systems. While effort is being spent on splitting up and parallelising the solving process (Rehfeldt et al., 2022), this is not yet practical. With our methods we avoid solving models defined over a period of decades, and instead obtain results based on many smaller runs — a process which is easily parallelised. The workflow is now constrained by the number of available processors, which is better suited to current computational developments which are in the direction of more, not faster processing cores.

While computational time often varies significantly based on a multitude of factors (exact modelling set-up, model size, nature of objective and constraints, numerical issues among others) and is difficult to predict, the memory requirements are easier to derive directly from model size (number of technologies, temporal and spatial resolution). With our modelling set-up (see Section 3.1), a capacity expansion optimisation with a single weather year takes 3.5–4 GB of memory using the commercial optimisation software Gurobi (Gurobi Optimization, 2022). Thus, our methods put optimal energy system design with decades of weather data within reach of typical desktop computers for the first time. For comparison, optimising with 41 years of weather data in one model takes approximately 41 times as much memory, around 134 GB. For models with a higher spatial and temporal resolution, our methods may currently be the only viable method of designing a system with decades of weather data; we estimate that optimising a typical PyPSA-Eur model with an hourly resolution and 181 nodes (as suggested in Frysztacki et al. (2021)) with 41 weather years could take around 1.7TB of memory, while this can be split into single-year optimisations taking around 45 GB of memory each using our methods.

With our modelling set-up, a model optimisation with one weather year takes 23 min of CPU time[13] on average using Gurobi with 2 threads. Spending 10 initial optimisations along unit vectors in positive and negative direction, 150 for the algorithm to approximate the near-optimal space for each year and finally 1 optimisation per year to compute per-node allocation of robust allocations, the mean allocation takes approximately $41 \cdot (10 + 150 + 1) \cdot 23 = 151\,823$ min ≈ 2530 h of CPU time to compute. On a cloud computing platform with 64 CPU cores (and around $4 \cdot 64 = 256$ GB of memory), this equates to around 40 h of wall time.[13] This is actually comparable to the wall time it typically takes to solve a single capacity expansion optimisation with 41 weather years of the same model on the same platform, which is in the range of 1–2 days.

We also investigate different methods for approximating near-optimal spaces of ESOMs, focusing on how optimisation directions are chosen, and how many optimisations are needed for a good approximation (for a different number of dimensions or projection variables). The results presented in Appendix A support the configurations we choose as default options.

5. Discussion

The urgent transition to energy systems based on intermittent renewable generation comes at a time with increasing computational power and availability of extensive climate data. However, while using ever larger models is helping us to understand the detailed functioning of future energy systems, it does not necessarily improve the understanding of uncertainties and resilience. In this paper, we propose a framework for producing energy system designs that are robust to uncertainty, taking advantage of the geometry of near-optimal spaces. We apply the framework to a study involving 41 weather years; the importance of using as much weather data as possible has been shown in the literature and is confirmed by our findings. Our framework can

[13] We make a distinction between the *CPU time* of a process, which is the sum of time spent on the process by all CPUs, and the *wall time* of a process, which is the elapsed real time between process start and finish. Thus CPU time may be larger than wall time for a parallelised process.

help policymakers to investigate different alternatives (similarly to the predecessors of this methodology, MGA and MAA) and overcome the fallacy of single solutions that can become infeasible through marginal perturbations.

Our choice of using the Chebyshev centre as a robust point is motivated by it being maximally tolerant to changes in investment in any direction. This is one of the distinctions to robust optimisation, where the optimum solution (with respect to the worst-case scenario) lies at the boundary of the intersection of feasible spaces, thus becoming infeasible with just marginal perturbations. At the same time, we see that even a naïve over-investment starting at the cost-optimal solution with a difficult weather year results in a system design which is practically feasible for all considered weather years. The choice of the Chebyshev centre can be seen as an attempt to find the most advantageous over-investment for robustness. In other words, while all additional investment contributes to robustness to some extent, our methods are aimed at finding the most efficient additional investments for robustness.

The first runs of a spatially resolved European power system optimisation model with four decades of weather data build on advances in open data accessibility and computational resources. Our results show that robust solutions stand out from standard cost-optimal solutions by a relatively higher investment in onshore wind and solar power. Furthermore, the increased investment in renewables reduces the usage of gas and nuclear, which lowers the CO_2 emissions of the system by more than 50% (in comparison to optimising the system with 41 weather years). By adjusting the slack level ε, our methods allow for a trade-off between robustness and additional costs.

Beyond looking at how weather years influence total system cost or investment composition, we see the effects of the choice of the weather year on the entire near-optimal space. Whereas the shapes and locations are fairly uniform, we see that near-optimal spaces for different weather years vary significantly in size. We still find a significant amount of flexibility within their intersection, mainly limited by a small number of most difficult weather years.

In previous studies utilising MGA techniques, dimension reduction has been used somewhat implicitly in order to make a systematic exploration of reduced near-optimal spaces feasible. Mapping down to a lower-dimensional space was seen as a way of summarising a few key properties of model solutions. However, the *geometry* of reduced near-optimal spaces has been largely unexploited, a gap we aimed to fill with this paper. Moreover, we investigate and propose practical methods for going back to spatially explicit investment decisions from points in the reduced near-optimal space. Mapping the Chebyshev centre of an intersection of near-optimal spaces back to a robust system design is just one application of this idea.

At the same time, approximating and intersecting near-optimal spaces as a way of designing systems which are feasible for many weather years is a reasonable alternative to optimising with many weather years directly from a computational perspective. Having split the problem into many smaller optimisations with single weather years, our methods are easily parallelised. This represents a new approach to optimisation problems which previously have been considered intractable or at least very impractical. In particular, an application of our methods to larger models (including sectoral coupling, higher spatial or temporal resolution) would be interesting and computationally feasible. While we expect the heuristic allocations to work at higher spatial resolutions (see also Frysztacki et al., 2022 for related work), their quality should be investigated under such conditions.

We highlight that we study just one out of many definitions of robustness (Moret et al., 2016; Maggioni et al., 2017); note also that our techniques do not directly follow the concept of *robust optimisation*. In all generality, robustness is a relative concept and is directed towards some uncertainty. Although these uncertainties can be well understood, some of them may be hard to quantify (e.g. political, societal changes), other could be epistemic (e.g. extreme weather events, changes in costs, or misspecifications of the model), or even aleatoric (as the actual future weather conditions). For instance, Stirling (2010) locates robustness in the overlap of problematic levels of knowledge about possibilities and probabilities. All in all, our approach contributes to a wide academic debate about how to deal with uncertainty and robustness in energy systems modelling.

6. Conclusion

In this article we find that studying the near-optimal feasible space is a helpful tool to achieve more robust solutions against uncertainties for energy systems. When investigating weather variability, this enables us to quantify the variations and to find alternative designs that allow some flexibility for policymakers.

Since we utilised historical climate reanalysis data, we have not incorporated the consequences of climate change that an energy system in transition will face, nor the possibility of unseen extreme events. It would be interesting to understand which developments will limit flexibility and what events are defining for the design of a future (climate-)robust energy system. Moreover, we see that a small number of weather years including 1985 and 1987 constrain our system design the most, having relatively small near-optimal feasible spaces. These results call for a deeper understanding of which meteorological properties of these weather years, including extreme and compound events, are determining for energy system design.

While we have applied a notion of robustness in the reduced near-optimal space $\mathcal{A}_\varepsilon$, we have not considered robustness at lower levels of the network. So although the point $y_{\text{ch}} \in \mathcal{A}_\varepsilon$ is robust to a shift in investments of 3.4 billion EUR, the system $x_{\text{rob}} \in \mathcal{F}'_\varepsilon$ is not robust to such a shift at any one particular node in the network. There may also be many system designs with very different per-node capacities mapping to the same point y_{ch}. Another interplay with the spatial dimension is whether different regions contribute differently to the robustness of the whole system, as hinted at by Fig. 8. Thus, spatial aspects of robustness form an interesting avenue for future research.

More generally speaking, our methods leave a lot of room for different choices of dimension reduction: choosing which variables to aggregate and how. The choice leading to the most suitable reduced near-optimal space should be considered application-specific, depending on the technologies of interest, their relative importance and use-case for the reduced near-optimal space. Mapping to a space of investment costs as we did is a neutral choice, but which reduction is the most efficient for more specific purposes is still an open question.

The results we present here may depend on our particular modelling set-up. To which extent specific technologies contribute to robustness and flexibility may change if other technologies are included (e.g. through sector coupling), additional restrictions are introduced (e.g. on transmission) or the spatial and temporal resolutions of the model are improved. And whereas our model has a single investment period, it would be interesting to apply our methods with a model considering transition pathways through multiple investment periods. As our implementation is open-source and customisable, it should be adaptable to this setting.

Last but not least, our methodology can also be used to investigate other uncertainties besides weather variability. As near-optimal spaces strongly depend on cost assumptions, future applications of the present framework can contribute to an improved understanding of robustness in the face of uncertain costs.

CRediT authorship contribution statement

Aleksander Grochowicz: Conceptualisation, Data curation, Formal analysis, Investigation, Methodology, Software, Validation, Visualisation, Original draft & editing. **Koen van Greevenbroek:** Conceptualisation, Data curation, Formal analysis, Investigation, Methodology, Software, Validation, Visualisation, Original draft & editing. **Fred Espen Benth:** Conceptualisation, Methodology, Supervision, Review & editing. **Marianne Zeyringer:** Conceptualisation, Methodology, Supervision, Review & editing.

Declaration of competing interest

The authors declare that they have no known competing financial interests or personal relationships that could have appeared to influence the work reported in this paper.

Acknowledgements

We would like to thank the anonymous reviewers for their helpful comments and suggestions.

The computations were partly performed on the Norwegian Research and Education Cloud (NREC), using resources provided by the University of Bergen and the University of Oslo. http://www.nrec.no/.

A.G., F.E.B. and M.Z. acknowledge funding by UiO:Energy (SPATUS).

Code & data availability

The code for our approach and its documentation can be found at https://github.com/aleks-g/intersecting-near-opt-spaces/tree/v1.0.1, and is made available under the GPL 3.0 license. Some of the data included in the above repository (load and hydropower capacity factors) were generated using the workflow available at https://github.com/aleks-g/multidecade-data/tree/v1.0 (code licensed GPL 3.0, data licensed CC-BY-4.0).

The reanalysis data we used for this study (for renewable capacity factors and temperature-dependent load data) were downloaded from the Copernicus Climate Change Service (C3S) Climate Data Store (Hersbach et al., 2018) using the Atlite software (Hofmann et al., 2021) as documented in the main repository. We have additionally made these weather data more easily available at https://doi.org/10.11582/2022.00034[14]; they are shared under the "License to use Copernicus Products",[15] which is comparable to the CC-BY license. Neither the European Commission nor the European Centre for Medium-Range Weather Forecasts is responsible for any use that may be made of the Copernicus information or data it contains.

Given the substantial size of the weather data needed for this study, we generated a number of PyPSA networks which can be used to reproduce our results without having to download and process the ERA5 data. They are available at https://doi.org/10.5281/zenodo.6683829 under the CC-BY-4.0 license.

All other data used in our model is directly inherited from PyPSA-Eur and also openly available as described in Hörsch et al. (2018).

Appendix A. Direction generation

We give a more detailed overview on how to explore the near-optimal space $\mathcal{A}_\epsilon$ (here in the original sense as a reduced near-optimal space and not the intersection), using the notation from Section 2. Recall that we can compute an approximation of $\mathcal{A}_\epsilon$ by finding a number of its vertices (or rather, extreme points), and each such point is obtained by solving the linear program in Eq. (7) with some different objective (*direction*) d. As described in Algorithm 1, we first optimise over $\mathcal{A}_\epsilon \subseteq \mathbb{R}^k$ in each of the cardinal directions (positive and negative) in order to obtain a first full k-dimensional approximation. Each of these optimisations can be performed in parallel. Thereafter, in which direction d we choose to optimise over $\mathcal{A}_\epsilon$ has a significant effect on how well $\mathcal{A}_\epsilon$ can be approximated in a limited number of optimisations.

We investigate and compare three methods that generate directions in which to optimise over $\mathcal{A}_\epsilon$. The first method is the simplest and consists of choosing directions uniformly at random. For the remaining two methods, the idea is to compute the convex hull of the points obtained so far after every optimisation, say H_i, and use the geometric properties of H_i in some way to generate the "next" direction d_{i+1}. The convex hull is computed using the program qhull (Barber et al., 1996). The three methods are as follows:

1. "random-uniform": Choose a random vector from the uniform distribution on the sphere in $\mathbb{R}^k$.
2. "facets": Choose the normal vector to the facet of H_i with the largest volume.
3. "maximal-centre-then-facets": Compute the Chebyshev centre y_{ch} of H_i and the ball of maximal radius around it by solving Eq. (12). Of all facets of H_i tangential to this ball, choose the one with the largest associated dual variable in Eq. (12) and take its normal vector. If already used, take the normal vector to the facet of H_i with the largest volume.

With all these methods, we also use a filtering procedure: we discard vectors that have already been used. For each method, it is clear how to generate another direction if the first was discarded: for example for the "facets" method we choose the normal of the facet with the second-largest volume if the first direction was discarded. For the "maximal-centre-then-facets" methods we fall back on the "facets" method when all normals to facets tangential to the Chebyshev ball have already been used.

In the filtering procedure, we employ an angle threshold θ such that a potential direction d is discarded if it is within θ degrees of any previously used direction. If the filter discards all possible directions, we reduce the angle threshold θ by 20%. This is repeated every time a method "runs out of directions", until θ falls below a pre-defined minimum angle θ_{min}, at which point the whole algorithm is terminated.

Note that the approximation of $\mathcal{A}_\epsilon$ can be parallelised effectively for any of the three direction generation methods, in the sense that multiple optimisations in different directions can be run in parallel. For the latter two methods, this means that the convex hull H_{i-P} must be used in the calculation of the ith direction when there are P parallel optimisations. When P is large, this means some of the generated direction could be slightly inferior (being generated with an older hull H_{i-P}).

We compare the performance of different methods in Fig. A.1. The plots show that the three different direction generation methods have different characteristics, but also that their performance varies substantially between different spaces (different weather years). Generally speaking, we see that the "random-uniform" method attains the largest volume in the long term, while the "facets" and "maximal-centre-then-facets" methods attain similar volumes and have a stronger performance initially. In terms of radius, the "random-uniform" method performs worse, while the "maximal-centre-then-facets' method converges the quickest initially.

We see that a large number of iterations is needed to converge in terms of volume, with the "random-uniform" attaining the highest volume, but still not converging after 2000 iterations. Meanwhile, the other two methods based on facet normals make large strides initially, but display a false convergence below the actual volume after about 1000 iterations. Convergence in terms of the radius is better (especially for the "maximal-centre-then-facets" method), but can be more erratic than the convergence of volume. 150 iterations with the "maximal-centre-then-facest" method were chosen as a compromise between accuracy and computational demand for this paper.

In Fig. A.2 we compare convergence of volume between different numbers of dimensions k of the spaces $\mathcal{A}_\epsilon \subseteq \mathbb{R}^k$. For this plot, we use the "maximal-centre-then-facets" direction generation method and approximated the near-optimal spaces for the weather year 2020, but use different dimension reduction maps σ. The final approximated volumes are all normalised to 1. We see that 3- and especially 2-dimensional spaces are quickly approximated, while the convergence

[14] See instructions at https://github.com/aleks-g/intersecting-near-opt-spaces/tree/v1.0.1.

[15] https://cds.climate.copernicus.eu/api/v2/terms/static/licence-to-use-copernicus-products.pdf (accessed 23/06/2022).

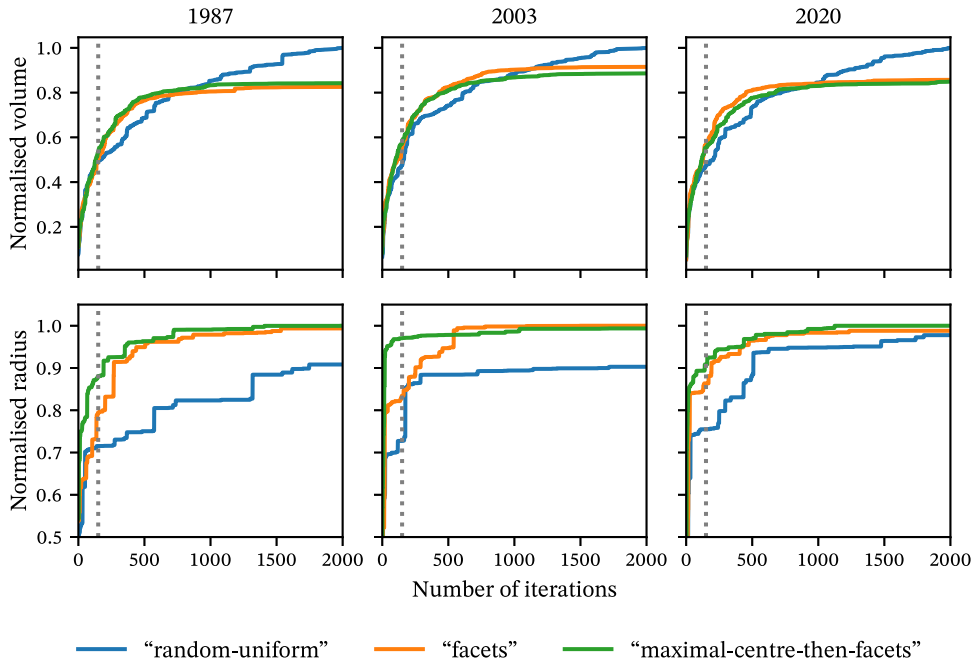

Fig. A.1. Performance of the different direction generation methods in terms of volume and Chebyshev radius convergence. We selected three years (among those, the years with the highest and lowest optimal costs) and approximated their near-optimal spaces with 2000 iterations. For each of the years the plotted volumes and radii have been normalised by the largest volume and radius obtained by any method for that year. The dotted lines mark 150 iterations.

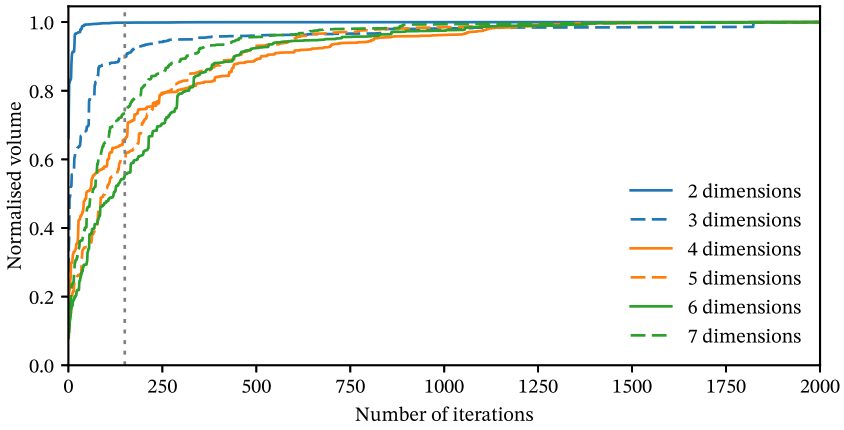

Fig. A.2. The convergence of volume in approximating the near-optimal space for the weather year 2020, reduced to different numbers of dimensions. The direction generation method is "maximal-centre-then-facets". The vertical dotted lines marks 150 iterations. The volume is normalised for each of the dimensions individually.

is slower for higher dimensional spaces. However, we do not find a significant difference in convergence between 4, 5, 6 or 7 dimensions.

The results in this section can be used to inform a termination criterion for Algorithm 1. The simplest option is to terminate the algorithm after a fixed number of iterations. Alternatively, the algorithm may be terminated after the volume or Chebyshev radius of H_i have not changed more than δ percent between successive iterations for the last N_{conv} iterations. In this case, we advise that N_{conv} be chosen as large as possible, since we can see from Fig. A.1 that the convergence on volume and especially radius is often somewhat erratic.

Appendix B. Data

B.1. Load data

In this article we use load data based on two regressions that were trained on hourly country-level ENTSO-E data from 2010 to 2014 from ENTSO-E (2022).[16] The aim is to infer country-level synthetic load data for each weather year between 1980 and 2020, whose profiles relate to weather patterns but are otherwise directly comparable. In other words, we disregard long-term changes in demand due to demographic and technological developments.

First we infer weekly load profiles (at an hourly resolution) for each country; for the purpose of this regression we treat holidays for each country as Sundays (using the Python package `python-holidays` Montel, 2022). Specifically, for each country c, we first divide the hourly demand values by the daily average value. On these normalised values, we conduct a regression based on the following model formulation:

$$D_c^{\text{norm}}(t) = \alpha_c \cdot t + \alpha_{c,\, t \bmod 168}, \tag{B.1}$$

[16] Due to inconsistencies for Swiss ENTSO-E data, we additionally used data from the Swiss transmission operator (Swissgrid, 2022).

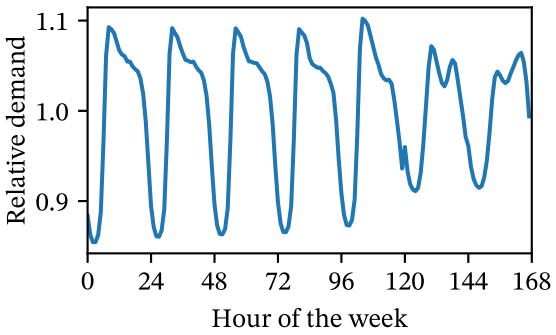

Fig. B.1. Weekly load profile for Norway, based on the regression described in Eq. (B.1).

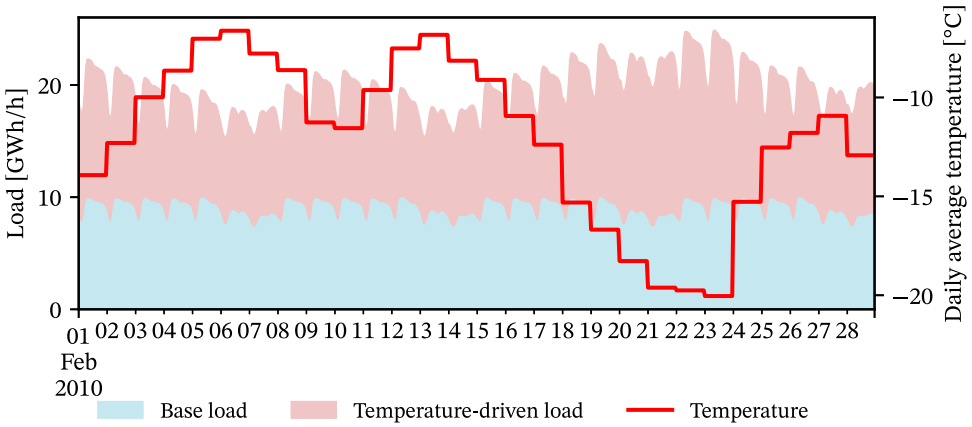

Fig. B.2. Load data (here for Norway in February 2010) split into base load and temperature-driven load. The underlying temperature data are daily, country-wide averages from ERA5 reanalysis. Base load and temperature-driven load are derived from the regression described in Appendix B.

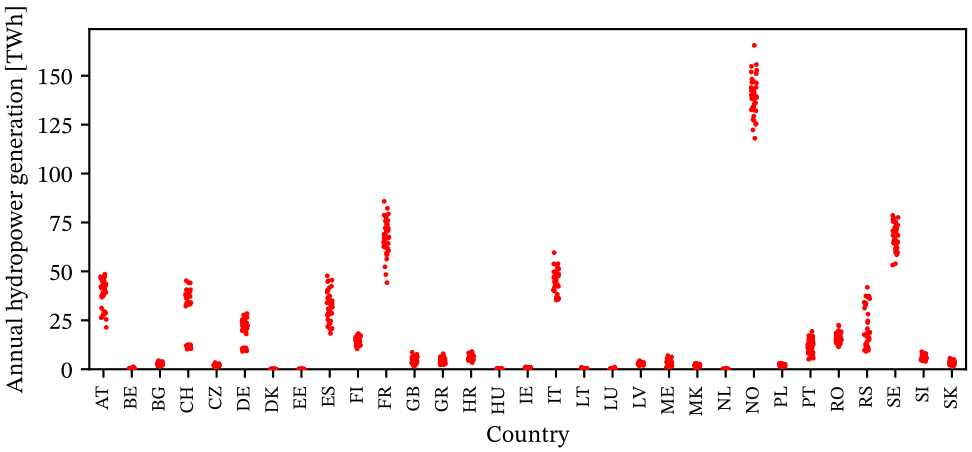

Fig. B.3. Variability of annual hydropower generation (1980–2020) based on EIA data (Administration, 2022), normalised by the reported hydropower capacities from 2020.

where α_c is an annual linear trend component, and the parameters $\alpha_{c,t \bmod 168}$ describe the weekly profile (see an example of this in Fig. B.1).

Afterwards we use the concept of heating and cooling degree days (HDD and CDD resp.) as in Benth et al. (2008) to find temperature-independent daily demand and demand driven by heating or cooling demand. For simplicity we only use one threshold for both HDD and CDD, which we set to be 15.5 °C as (Spinoni et al., 2015) use for HDD:

$$\mathrm{CDD}_c(d) = \max\{T_c(d) - 15.5, 0\},$$
$$\mathrm{HDD}_c(d) = \max\{15.5 - T_c(d), 0\},$$

where $T_c(d)$ is daily average temperature in country c during day d. Note that by using the daily averages we represent smoothing effects of thermal inertia on heating and cooling demand (compare Fig. B.2). The country-wide temperatures are computed from ERA5 reanalysis data (Hersbach et al., 2018) via the open-source tool Atlite (Hofmann et al., 2021). We now conduct a regression on the daily average load, $D_c(d)$, with dummy variables for each weekday (where national holidays are classified as Sundays), and exogenous variables given by heating degrees and cooling degrees:

$$D_c(d) = \beta_{c,\mathrm{weekday}(d)} + \beta_c^{\mathrm{cooling}} \cdot \mathrm{CDD}_c(d) + \beta_c^{\mathrm{heating}} \cdot \mathrm{HDD}_c(d). \tag{B.2}$$

For both regressions, we test the parameters for statistical significance; in some cases we thus set the trend parameter α_c and the cooling parameter $\beta_c^{\mathrm{cooling}}$ to 0.

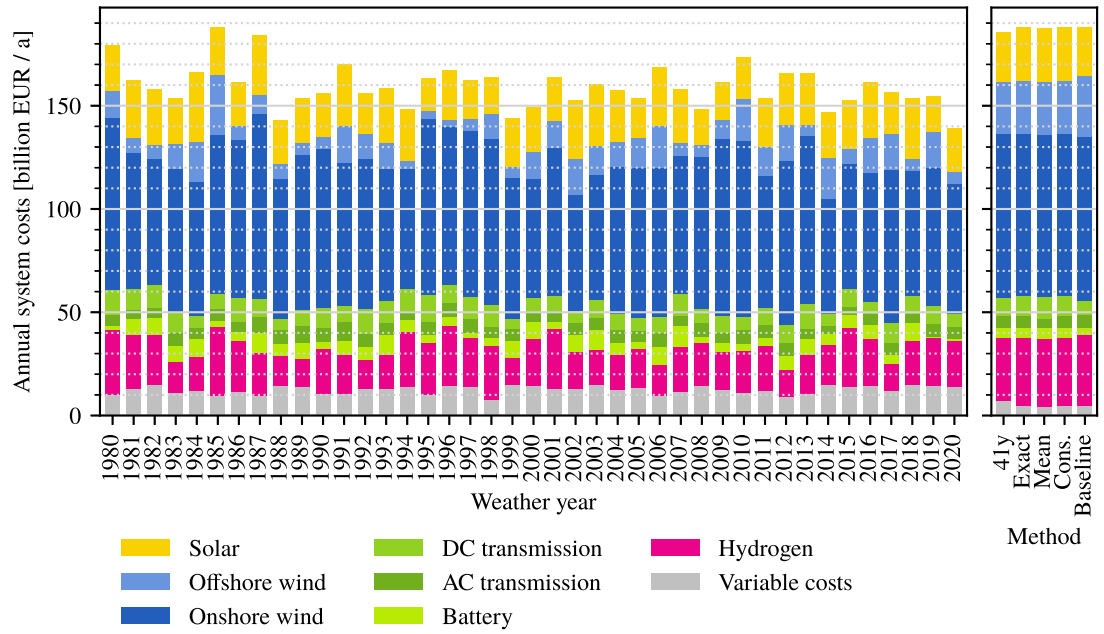

Fig. C.1. Comparison of cost-minimal designs under a 100% emission reduction based on optimisations over individual years compared to the annualised costs of robust designs (exact, mean, conservative and baseline, respectively) and an optimisation with all 41 years ("41y").

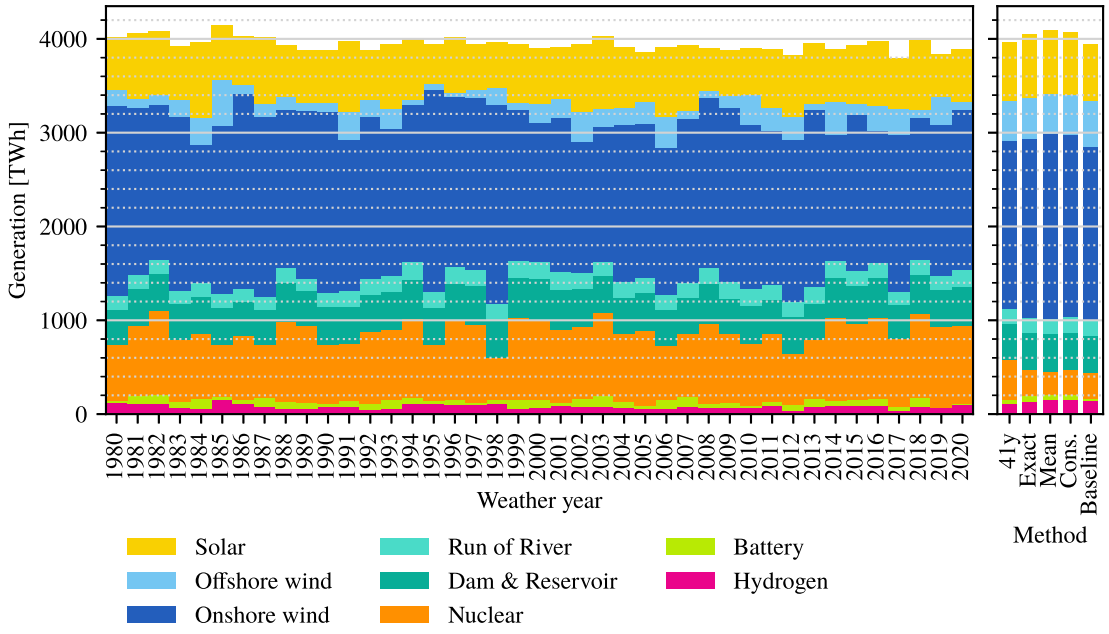

Fig. C.2. For 100% emission reduction, annual average generation mixes for the optimal solutions for each single weather year, the optimal solution with all weather years ("41y") and the robust allocations.

With these regressions and the temperatures for 1980–2020 from ERA5, we can compute the artificial load for each hour as follows:

$$\widetilde{D}_c(t) = \alpha_{c,t \bmod 168} \cdot \Big[\alpha_c \cdot (t \bmod 8760) + \beta_{c,\text{weekday}(t)} + \beta_c^{\text{cooling}} \cdot \text{CDD}_c(t) + \beta_c^{\text{heating}} \cdot \text{HDD}_c(t)\Big], \tag{B.3}$$

where the index c is over countries, t is the time in hours, $\alpha_{c,i}$ the regression parameter for the ith hour of the week, α_c is the annual trend component, $\beta_{c,j}$ the regression parameter for weekday j, and β_c^{cooling}, β_c^{heating} are the regression parameters for one degree of cooling/heating demand for country c. We abuse notation slightly by writing $\text{CDD}_c(t)$ to mean $\text{CDD}_c(d)$ where d is the day containing t (and likewise for HDD). For an example, see Fig. B.2.

We validate the regression on hourly ENTSO-E load data on the country level for 2015, and show it to be a good fit — more information about this can be found in the GitHub repository.[17]

[17] https://github.com/aleks-g/multidecade-data/tree/v1.0.

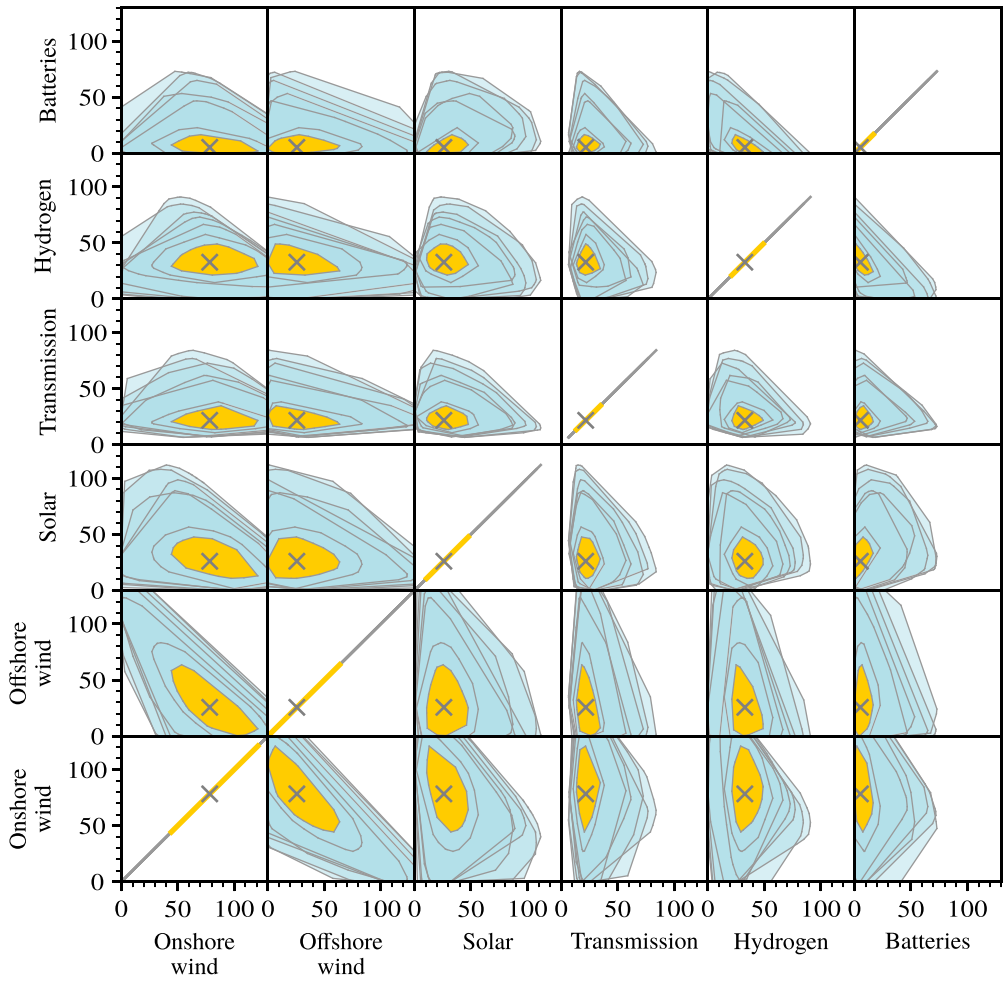

Fig. C.3. Projections of the near-optimal spaces for different weather years and their intersection under 100% emission reduction. All values are annualised total investment costs per technology. For illustrative purposes, we only plot the near-optimal spaces for 6 out of 41 weather years (in different hues of blue). The intersection of all 41 near-optimal spaces is filled in yellow and the Chebyshev centre is marked with a cross.

In accordance with load projections for 2030 by the European commission[18] we increased the demand in each country by 13%.

B.2. Hydropower data

For hydropower data we follow the approach in PyPSA-Eur which uses ERA5 reanalysis data to generate inflow profiles (using Atlite) that are then scaled by historical country-level hydro generation data from the US Energy Information Administration (EIA) (Administration, 2022). We have extended the default dataset in PyPSA-Eur to cover the entire period of 1980 to 2020, and we have also normalised EIA's production data to EIA's capacity levels of 2020[17]:

$$\text{gen}_c(y) = \text{nom\_gen}(y) \cdot \frac{\text{cap}_c(2020)}{\text{cap}_c(y)},$$

where $\text{gen}_c(y)$ and $\text{nom\_gen}_c(y)$ are the normalised and reported hydropower generation for country c in year y respectively, and $\text{cap}_c(y)$ is the reported hydropower capacity for country c in year y.

This allows a comparison throughout different years without any trends in infrastructure development. To avoid anachronisms, we have distributed generation and capacities of former countries onto the current states (based on the first year of current borders, e.g. 1993 for Czechia and Slovakia, or the sum of West and East Germany)[17].

The historical generation data ensure that the inflow profiles are scaled to reasonable values (see the general approach in Schlachtberger et al. (2017) and in particular Fig. 4 in Liu et al. (2019)); we are interested in variability and not trends, therefore we want fixed capacities to have comparable weather years (see Fig. B.3).

Appendix C. Additional results of a 100% emission reduction

We showcase the impact of a 100% emission reduction (as opposed to the 95% reduction studied in the main text) on the results we present in this paper. As the other assumptions remain unchanged and gas turbines are the only sources of CO_2 emissions in our model, this

[18] https://ec.europa.eu/clima/document/download/ec1acac9-10fe-4eeb-915f-cad388990e0f_en, Fig. 44 (accessed 23/06/2022).

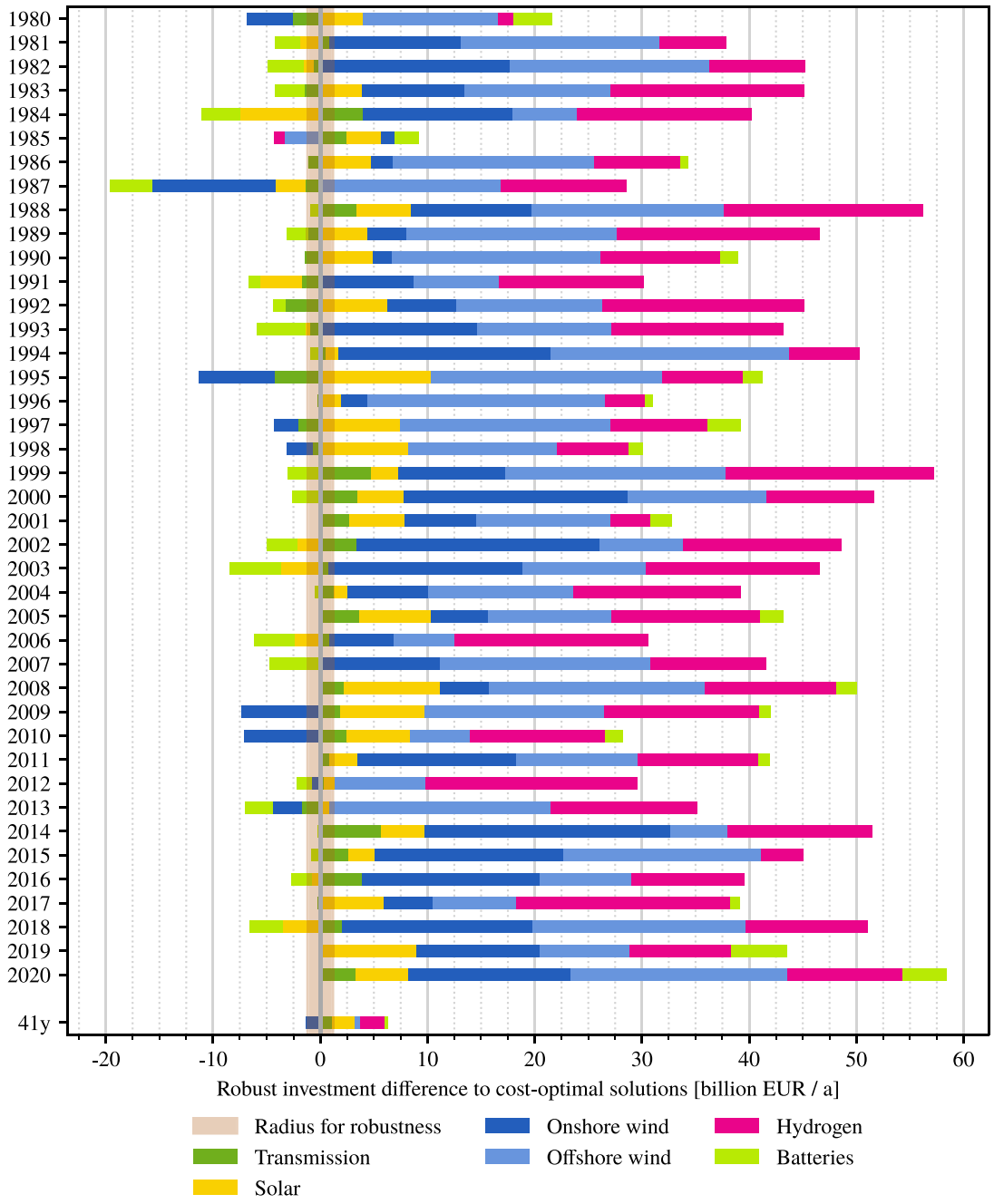

Fig. C.4. For 100% emission reduction, a comparison of total investments for selected technologies in the optimal solutions for each weather year and the optimal solution with all weather years ("41y") to the robust point y_{ch}. Positive values mean greater investment in the given technology by the robust solution.

corresponds to replacing gas as a generation technology with carbon-neutral alternatives. The results sharpen the uncertainty that weather variability introduces to renewable power systems. We investigate a different reduced near-optimal feasible space than before (replacing the gas investment dimension by two new dimensions, investment in battery and hydrogen storage). This means that the Chebyshev centre under this new reduction is additionally robust to changes in investment in battery and hydrogen storage, which is not the case for the results in the main text.

Without gas as a dispatchable generation technology, the costs of the now carbon-neutral power systems increase by 15 to 40 billion EUR/a, depending on the weather year. The last percentage points of emission reductions are thus overproportionally costly (as also shown in Neumann and Brown (2021)), in particular in "more difficult" years. Wind power in combination with storage technologies see an increase in investment (see Fig. C.1), most pronounced in the 1985, the year with the highest optimal costs.

Fig. C.2 shows that the different optimal power systems are also mostly driven by (onshore) wind power, as in the 95% reduction case. Additionally, it depicts a strengthening of battery and hydrogen storage, which previously did not appear in the optimal solutions, although their shares of generation vary throughout the years. Similarly, the optimal share of nuclear generation becomes more volatile and decreases not only in the robust allocations (which are characterised by higher renewable investment by design), but also in the 41-year optimisation. As nuclear power has higher variable costs than renewable generators, the existing capacities are not fully used, indicating the competitiveness of newly installed renewable capacities.

As with the 95% emission reduction, significant investment in both onshore wind power and solar power is necessary for a power system

that can withstand weather variability. Figs. C.1 and C.3 show additionally the need for investment in hydrogen storage and additional transmission capacities. In comparison to optimal solutions for different weather years, additional investment in wind power and hydrogen strengthens robustness against weather variability (see Fig. C.4). The full decarbonisation increases the value of offshore wind power which did not feature prominently in the robust solution under 95% emission reduction (see Fig. 5). Finally, it should be noted that there is a significant amount of investment flexibility for onshore wind, offshore wind and solar among the robust solutions for all 41 weather years.

References

Administration, U.E.I., 2022. International - U.S. energy information administration (EIA). https://www.eia.gov/international/data/world/electricity.

Barber, B.C., Dobkin, D.P., Huhdanpaa, H., 1996. The quickhull algorithm for convex hulls. ACM Trans. Math. Software 22 (4), 469–483. http://dx.doi.org/10.1145/235815.235821.

Benth, F.E., Benth, J.Š., Koekebakker, S., 2008. Stochastic Modeling of Electricity and Related Markets. In: Advanced Series on Statistical Science & Applied Probability, 11, World Scientific, http://dx.doi.org/10.1142/6811.

Bloomfield, H., Brayshaw, D., Charlton-Perez, A., 2020. ERA5 derived time series of European country-aggregate electricity demand, wind power generation and solar power generation: Hourly data from 1979–2019. http://dx.doi.org/10.17864/1947.272.

Bloomfield, H.C., Brayshaw, D.J., Shaffrey, L.C., Coker, P.J., Thornton, H.E., 2016. Quantifying the increasing sensitivity of power systems to climate variability. Environ. Res. Lett. 11 (12), 124025. http://dx.doi.org/10.1088/1748-9326/11/12/124025.

Bloomfield, H.C., Brayshaw, D.J., Troccoli, A., Goodess, C.M., De Felice, M., Dubus, L., Bett, P.E., Saint-Drenan, Y.M., 2021. Quantifying the sensitivity of European power systems to energy scenarios and climate change projections. Renew. Energy 164, 1062–1075. http://dx.doi.org/10.1016/j.renene.2020.09.125.

Boyd, S.P., Vandenberghe, L., 2004. Convex Optimization. Cambridge University Press, Cambridge, UK.

Brown, T., Hörsch, J., Schlachtberger, D., 2018. PyPSA: Python for power system analysis. J. Open Res. Softw. 6 (1), 4. http://dx.doi.org/10.5334/jors.188.

Collins, S., Deane, P., Ó Gallachóir, B., Pfenninger, S., Staffell, I., 2018. Impacts of inter-annual wind and solar variations on the European power system. Joule 2 (10), 2076–2090. http://dx.doi.org/10.1016/j.joule.2018.06.020.

Craig, M.T., Wohland, J., Stoop, L.P., Kies, A., Pickering, B., Bloomfield, H.C., Browell, J., De Felice, M., Dent, C.J., Deroubaix, A., Frischmuth, F., Gonzalez, P.L.M., Grochowicz, A., Gruber, K., Härtel, P., Kittel, M., Kotzur, L., Labuhn, I., Lundquist, J.K., Pflugradt, N., van der Wiel, K., Zeyringer, M., Brayshaw, D.J., 2022. Overcoming the disconnect between energy system and climate modeling. Joule http://dx.doi.org/10.1016/j.joule.2022.05.010.

DeCarolis, J.F., 2011. Using modeling to generate alternatives (MGA) to expand our thinking on energy futures. Energy Econ. 33 (2), 145–152. http://dx.doi.org/10.1016/j.eneco.2010.05.002.

Dowling, J.A., Rinaldi, K.Z., Ruggles, T.H., Davis, S.J., Yuan, M., Tong, F., Lewis, N.S., Caldeira, K., 2020. Role of long-duration energy storage in variable renewable electricity systems. Joule 4 (9), 1907–1928. http://dx.doi.org/10.1016/j.joule.2020.07.007.

ENTSO-E, 2022. Power statistics. https://www.entsoe.eu/data/power-stats/.

Frysztacki, M.M., Hagenmeyer, V., Brown, T., 2022. Inverse methods: How feasible are spatially low-resolved capacity expansion modeling results when dis-aggregated at high resolution?. http://dx.doi.org/10.48550/arXiv.2209.02364, arXiv:2209.02364, URL http://arxiv.org/abs/2209.02364.

Frysztacki, M.M., Hörsch, J., Hagenmeyer, V., Brown, T., 2021. The strong effect of network resolution on electricity system models with high shares of wind and solar. Appl. Energy 291, 116726. http://dx.doi.org/10.1016/j.apenergy.2021.116726.

Gurobi Optimization, L., 2022. Gurobi optimizer reference manual.

Hersbach, H., Bell, B., Berrisford, P., Biavati, G., Horányi, A., Muñoz Sabater, J., Nicolas, J., Peubey, C., Radu, R., Rozum, I., Schepers, D., Simmons, A., Soci, C., Dee, D., Thépaut, J.-N., 2018. ERA5 hourly data on single levels from 1959 to present. http://dx.doi.org/10.24381/cds.adbb2d47.

Hilbers, A.P., Brayshaw, D.J., Gandy, A., 2020. Importance subsampling for power system planning under multi-year demand and weather uncertainty. In: 2020 International Conference on Probabilistic Methods Applied To Power Systems (PMAPS). IEEE, Liege, Belgium, pp. 1–6. http://dx.doi.org/10.1109/PMAPS47429.2020.9183591.

Hoffmann, M., Kotzur, L., Stolten, D., Robinius, M., 2020. A review on time series aggregation methods for energy system models. Energies 13 (3), 641. http://dx.doi.org/10.3390/en13030641.

Hofmann, F., Hampp, J., Neumann, F., Brown, T., Hörsch, J., 2021. Atlite: A lightweight python package for calculating renewable power potentials and time series. J. Open Source Softw. 6 (62), 3294. http://dx.doi.org/10.21105/joss.03294.

Hörsch, J., Hofmann, F., Schlachtberger, D., Brown, T., 2018. PyPSA-Eur: An open optimisation model of the European transmission system. Energy Strategy Rev. 22, 207–215. http://dx.doi.org/10.1016/j.esr.2018.08.012.

Kotzur, L., Nolting, L., Hoffmann, M., Groß, T., Smolenko, A., Priesmann, J., Büsing, H., Beer, R., Kullmann, F., Singh, B., Praktiknjo, A., Stolten, D., Robinius, M., 2021. A modeler's guide to handle complexity in energy systems optimization. Adv. Appl. Energy 4, 100063. http://dx.doi.org/10.1016/j.adapen.2021.100063.

Kozarcanin, S., Liu, H., Andresen, G.B., 2019. 21St century climate change impacts on key properties of a large-scale renewable-based electricity system. Joule 3 (4), 992–1005. http://dx.doi.org/10.1016/j.joule.2019.02.001.

Liu, H., Andresen, G.B., Brown, T., Greiner, M., 2019. A high-resolution hydro power time-series model for energy systems analysis: Validated with Chinese hydro reservoirs. MethodsX 6, 1370–1378. http://dx.doi.org/10.1016/j.mex.2019.05.024.

Lombardi, F., Pickering, B., Colombo, E., Pfenninger, S., 2020. Policy decision support for renewables deployment through spatially explicit practically optimal alternatives. Joule 4 (10), 2185–2207. http://dx.doi.org/10.1016/j.joule.2020.08.002.

Maggioni, F., Potra, F.A., Bertocchi, M., 2017. A scenario-based framework for supply planning under uncertainty: Stochastic programming versus robust optimization approaches. Comput. Manag. Sci. 14 (1), 5–44. http://dx.doi.org/10.1007/s10287-016-0272-3.

Montel, M., 2022. Python-Holidays 0.12. https://github.com/dr-prodigy/python-holidays.

Moret, S., Bierlaire, M., Maréchal, F., 2016. Robust optimization for strategic energy planning. Informatica 27 (3), 625–648. http://dx.doi.org/10.15388/Informatica.2016.103.

Neumann, F., Brown, T., 2021. The near-optimal feasible space of a renewable power system model. Electr. Power Syst. Res. 190, 106690. http://dx.doi.org/10.1016/j.epsr.2020.106690.

Pedersen, T.T., Victoria, M., Rasmussen, M.G., Andresen, G.B., 2021. Modeling all alternative solutions for highly renewable energy systems. Energy 234, 121294. http://dx.doi.org/10.1016/j.energy.2021.121294.

Pfenninger, S., 2017. Dealing with multiple decades of hourly wind and PV time series in energy models: A comparison of methods to reduce time resolution and the planning implications of inter-annual variability. Appl. Energy 197, 1–13. http://dx.doi.org/10.1016/j.apenergy.2017.03.051.

Pfenninger, S., Staffell, I., 2016. Long-term patterns of European PV output using 30 years of validated hourly reanalysis and satellite data. Energy 114, 1251–1265. http://dx.doi.org/10.1016/j.energy.2016.08.060.

Pickering, B., Lombardi, F., Pfenninger, S., 2022. Diversity of options to eliminate fossil fuels and reach carbon neutrality across the entire European energy system. Joule 6 (6), 1253–1276. http://dx.doi.org/10.1016/j.joule.2022.05.009.

Price, J., Keppo, I., 2017. Modelling to generate alternatives: A technique to explore uncertainty in energy-environment-economy models. Appl. Energy 195, 356–369. http://dx.doi.org/10.1016/j.apenergy.2017.03.065.

Price, J., Zeyringer, M., 2022. highRES-Europe: The high spatial and temporal resolution electricity system model for Europe. SoftwareX 17, 101003. http://dx.doi.org/10.1016/j.softx.2022.101003.

Rehfeldt, D., Hobbie, H., Schönheit, D., Koch, T., Möst, D., Gleixner, A., 2022. A massively parallel interior-point solver for LPs with generalized arrowhead structure, and applications to energy system models. European J. Oper. Res. 296 (1), 60–71. http://dx.doi.org/10.1016/j.ejor.2021.06.063.

Ringkjøb, H.-K., Haugan, P.M., Solbrekke, I.M., 2018. A review of modelling tools for energy and electricity systems with large shares of variable renewables. Renew. Sustain. Energy Rev. 96, 440–459. http://dx.doi.org/10.1016/j.rser.2018.08.002.

Ruhnau, O., Qvist, S., 2022. Storage requirements in a 100% renewable electricity system: Extreme events and inter-annual variability. Environ. Res. Lett. http://dx.doi.org/10.1088/1748-9326/ac4dc8.

Schlachtberger, D.P., Brown, T., Schramm, S., Greiner, M., 2017. The benefits of cooperation in a highly renewable European electricity network. Energy 134, 469–481. http://dx.doi.org/10.1016/j.energy.2017.06.004.

Schlott, M., Kies, A., Brown, T., Schramm, S., Greiner, M., 2018. The impact of climate change on a cost-optimal highly renewable European electricity network. Appl. Energy 230, 1645–1659. http://dx.doi.org/10.1016/j.apenergy.2018.09.084.

Simoes, S.G., Amorim, F., Siggini, G., Sessa, V., Saint-Drenan, Y.-M., Carvalho, S., Mraihi, H., Assoumou, E., 2021. Climate proofing the renewable electricity deployment in Europe - Introducing climate variability in large energy systems models. Energy Strategy Rev. 35, 100657. http://dx.doi.org/10.1016/j.esr.2021.100657.

Spinoni, J., Vogt, J., Barbosa, P., 2015. European degree-day climatologies and trends for the period 1951–2011. Int. J. Climatol. 35 (1), 25–36. http://dx.doi.org/10.1002/joc.3959.

Staffell, I., Pfenninger, S., 2018. The increasing impact of weather on electricity supply and demand. Energy 145, 65–78. http://dx.doi.org/10.1016/j.energy.2017.12.051.

Stirling, A., 2010. Keep it complex. Nature 468 (7327), 1029–1031. http://dx.doi.org/10.1038/4681029a.

Swissgrid, 2022. Production and consumption. https://www.swissgrid.ch/en/home/operation/grid-data/generation.html.

Tóth, C.D., Goodman, J.E., O'Rourke, J., 2017. Handbook of Discrete and Computational Geometry. CRC Press, http://dx.doi.org/10.1201/9781315119601.

Tröndle, T., Lilliestam, J., Marelli, S., Pfenninger, S., 2020. Trade-offs between geographic scale, cost, and infrastructure requirements for fully renewable electricity in Europe. Joule 4 (9), 1929–1948. http://dx.doi.org/10.1016/j.joule.2020.07.018.

Trutnevyte, E., 2016. Does cost optimization approximate the real-world energy transition? Energy 106, 182–193. http://dx.doi.org/10.1016/j.energy.2016.03.038.

van der Wiel, K., Stoop, L.P., van Zuijlen, B.R.H., Blackport, R., van den Broek, M.A., Selten, F.M., 2019. Meteorological conditions leading to extreme low variable renewable energy production and extreme high energy shortfall. Renew. Sustain. Energy Rev. 111, 261–275. http://dx.doi.org/10.1016/j.rser.2019.04.065.

Wohland, J., Reyers, M., Weber, J., Witthaut, D., 2017. More homogeneous wind conditions under strong climate change decrease the potential for inter-state balancing of electricity in Europe. Earth Syst. Dyn. 8 (4), 1047–1060. http://dx.doi.org/10.5194/esd-8-1047-2017.

Zeyringer, M., Price, J., Fais, B., Li, P.-H., Sharp, E., 2018. Designing low-carbon power systems for great britain in 2050 that are robust to the spatiotemporal and inter-annual variability of weather. Nat. Energy 3 (5), 395–403. http://dx.doi.org/10.1038/s41560-018-0128-x.

Supplementary material

A Direction generation

We give a more detailed overview on how to explore the near-optimal space $\mathcal{A}_\varepsilon$ (here in the original sense as a reduced near-optimal space and not the intersection), using the notation from Section 2. Recall that we can compute an approximation of $\mathcal{A}_\varepsilon$ by finding a number of its vertices (or rather, extreme points), and each such point is obtained by solving the linear program in Equation (7) with some different objective (*direction*) d. As described in Algorithm 1, we first optimise over $\mathcal{A}_\varepsilon \subseteq \mathbb{R}^k$ in each of the cardinal directions (positive and negative) in order to obtain a first full k-dimensional approximation. Each of these optimisations can be performed in parallel. Thereafter, in which direction d we choose to optimise over $\mathcal{A}_\varepsilon$ has a significant effect on how well $\mathcal{A}_\varepsilon$ can be approximated in a limited number of optimisations.

We investigate and compare three methods that generate directions in which to optimise over $\mathcal{A}_\varepsilon$. The first method is the simplest and consists of choosing directions uniformly at random. For the remaining two methods, the idea is to compute the convex hull of the points obtained so far after every optimisation, say H_i, and use the geometric properties of H_i in some way to generate the "next" direction d_{i+1}. The convex hull is computed using the program qhull [BDH96]. The three methods are as follows:

1. "random-uniform": Choose a random vector from the uniform distribution on the sphere in $\mathbb{R}^k$.
2. "facets": Choose the normal vector to the facet of H_i with the largest volume.
3. "maximal-centre-then-facets": Compute the Chebyshev centre y_{ch} of H_i and the ball of maximal radius around it by solving Equation (12). Of all facets of H_i tangential to this ball, choose the one with the largest associated dual variable in Equation (12) and take its normal vector. If already used, take the normal vector to the facet of H_i with the largest volume.

With all these methods, we also use a filtering procedure: we discard vectors that have already been used. For each method, it is clear how to generate another direction if the first was discarded: for example for the "facets" method we choose the normal of the facet with the second-largest volume if the first direction was discarded. For the "maximal-centre-then-facets" methods we fall back on the "facets" method when all normals to facets tangantial to the Chebyshev ball have already been used.

In the filtering procedure, we employ an angle threshold θ such that a potential direction d is discarded if it is within θ degrees of any previously used direction. If the filter discards all possible directions, we reduce the angle threshold θ by 20%. This is repeated every time a method "runs out of directions", until θ falls below a pre-defined minimum angle θ_{min}, at which point the whole algorithm is terminated.

Note that the approximation of $\mathcal{A}_\varepsilon$ can be parallelised effectively for any of the three direction generation methods, in the sense that multiple optimisations in different directions can be run

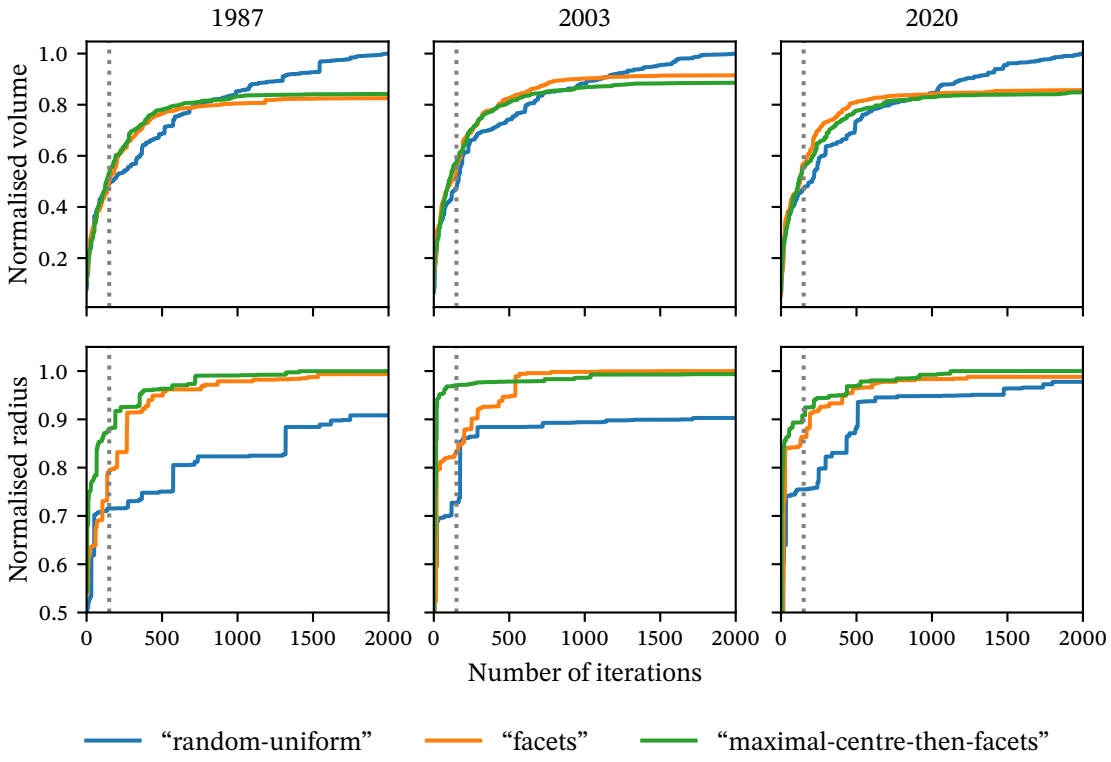

Figure A.1: Performance of the different direction generation methods in terms of volume and Chebyshev radius convergence. We selected three years (among those, the years with the highest and lowest optimal costs) and approximated their near-optimal spaces with 2000 iterations. For each of the years the plotted volumes and radii have been normalised by the largest volume and radius obtained by any method for that year. The dotted lines mark 150 iterations.

in parallel. For the latter two methods, this means that the convex hull H_{i-P} must be used in the calculation of the i-th direction when there are P parallel optimisations. When P is large, this means some of the generated direction could be slightly inferior (being generated with an older hull H_{i-P}).

We compare the performance of different methods in Figure A.1. The plots show that the three different direction generation methods have different characteristics, but also that their performance varies substantially between different spaces (different weather years). Generally speaking, we see that the "random-uniform" method attains the largest volume in the long term, while the "facets" and "maximal-centre-then-facets" methods attain similar volumes and have a stronger performance initially. In terms of radius, the "random-uniform" method performs worse, while the "maximal-centre-then-facets' method converges the quickest initially.

We see that a large number of iterations is needed to converge in terms of volume, with the

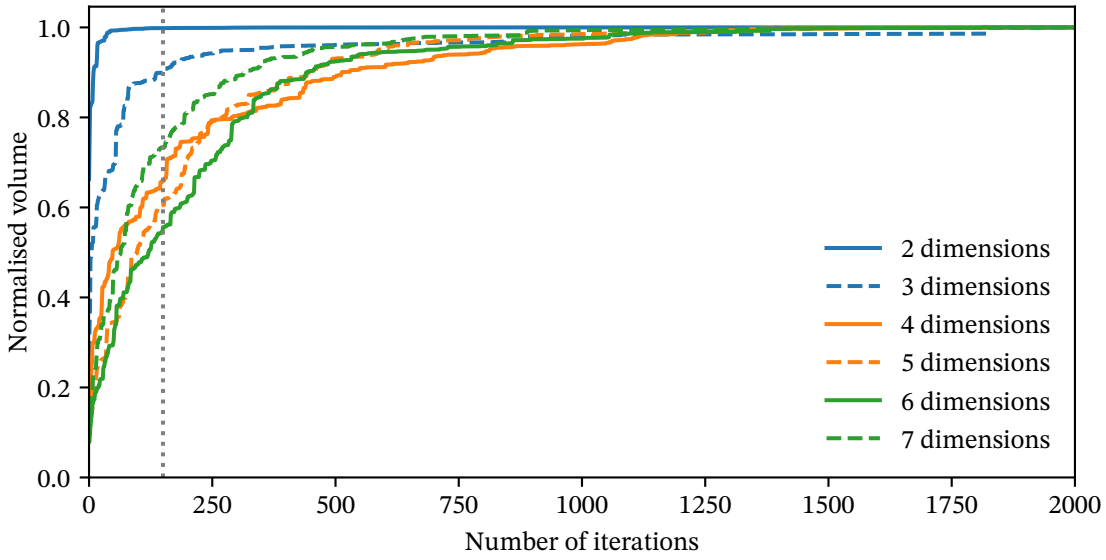

Figure A.2: The convergence of volume in approximating the near-optimal space for the weather year 2020, reduced to different numbers of dimensions. The direction generation method is "maximal-centre-then-facets". The vertical dotted lines marks 150 iterations. The volume is normalised for each of the dimensions individually.

"random-uniform" attaining the highest volume, but still not converging after 2000 iterations. Meanwhile, the other two methods based on facet normals make large strides initially, but display a false convergence below the actual volume after about 1000 iterations. Convergence in terms of the radius is better (especially for the "maximal-centre-then-facets" method), but can be more erratic than the convergence of volume. 150 iterations with the "maximal-centre-then-facest" method were chosen as a compromise between accuracy and computational demand for this paper.

In Figure A.2 we compare convergence of volume between different numbers of dimensions k of the spaces $\mathcal{A}_\varepsilon \subseteq \mathbb{R}^k$. For this plot, we use the "maximal-centre-then-facets" direction generation method and approximated the near-optimal spaces for the weather year 2020, but use different dimension reduction maps σ. The final approximated volumes are all normalised to 1. We see that 3- and especially 2-dimensional spaces are quickly approximated, while the convergence is slower for higher dimensional spaces. However, we do not find a significant difference in convergence between 4, 5, 6 or 7 dimensions.

The results in this section can be used to inform a termination criterion for Algorithm 1. The simplest option is to terminate the algorithm after a fixed number of iterations. Alternatively, the algorithm may be terminated after the volume or Chebyshev radius of H_i have not changed more than δ percent between successive iterations for the last N_{conv} iterations. In this case, we advise that N_{conv} be chosen as large as possible, since we can see from Figure A.1 that the convergence on volume and especially radius is often somewhat erratic.

B Data

B.1 Load data

In this article we use load data based on two regressions that were trained on hourly country-level ENTSO-E data from 2010 to 2014 from [ENT22][15]. The aim is to infer country-level synthetic load data for each weather year between 1980 and 2020, whose profiles relate to weather patterns but are otherwise directly comparable. In other words, we disregard long-term changes in demand due to demographic and technological developments.

First we infer weekly load profiles (at an hourly resolution) for each country; for the purpose of this regression we treat holidays for each country as Sundays (using the Python package `python-holidays` [Mon22]). Specifically, for each country c, we first divide the hourly demand values by the daily average value. On these normalised values, we conduct a regression based on the following model formulation:

$$D_c^{\text{norm}}(t) = \alpha_c \cdot t + \alpha_{c,\, t \bmod 168}, \tag{16}$$

where α_c is an annual linear trend component, and the parameters $\alpha_{c,t \bmod 168}$ describe the weekly profile (see an example of this in Figure B.1).

Afterwards we use the concept of heating and cooling degree days (HDD and CDD resp.) as in [BBK08] to find temperature-independent daily demand and demand driven by heating or cooling demand. For simplicity we only use one threshold for both HDD and CDD, which we set to be 15.5°C as [SVB15] use for HDD:

$$\begin{aligned} \text{CDD}_c(d) &= \max\{T_c(d) - 15.5, 0\}, \\ \text{HDD}_c(d) &= \max\{15.5 - T_c(d), 0\}, \end{aligned}$$

where $T_c(d)$ is daily average temperature in country c during day d. Note that by using the daily averages we represent smoothing effects of thermal inertia on heating and cooling demand (compare Figure B.2). The country-wide temperatures are computed from ERA5 reanalysis data [**era5-data**] via the open-source tool Atlite [Hof+21]. We now conduct a regression on the daily average load, $D_c(d)$, with dummy variables for each weekday (where national holidays are classified as Sundays), and exogenous variables given by heating degrees and cooling degrees:

$$D_c(d) = \beta_{c,\text{weekday}(d)} + \beta_c^{\text{cooling}} \cdot \text{CDD}_c(d) + \beta_c^{\text{heating}} \cdot \text{HDD}_c(d). \tag{17}$$

For both regressions, we test the parameters for statistical significance; in some cases we thus set the trend parameter α_c and the cooling parameter β_c^{cooling} to 0.

With these regressions and the temperatures for 1980–2020 from ERA5, we can compute the artificial load for each hour as follows:

$$\widetilde{D}_c(t) = \alpha_{c,t \bmod 168} \cdot \Big[\alpha_c \cdot (t \bmod 8760) + \beta_{c,\text{weekday}(t)} + \beta_c^{\text{cooling}} \cdot \text{CDD}_c(t) + \beta_c^{\text{heating}} \cdot \text{HDD}_c(t)\Big], \tag{18}$$

[15] Due to inconsistencies for Swiss ENTSO-E data, we additionally used data from the Swiss transmission operator [Swi22].

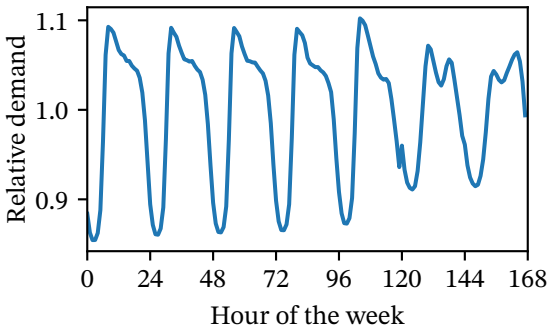

Figure B.1: Weekly load profile for Norway, based on the regression described in Equation (16).

where the index c is over countries, t is the time in hours, $\alpha_{c,i}$ the regression parameter for the i-th hour of the week, α_c is the annual trend component, $\beta_{c,j}$ the regression parameter for weekday j, and β_c^{cooling}, β_c^{heating} are the regression parameters for one degree of cooling/heating demand for country c. We abuse notation slightly by writing $\text{CDD}_c(t)$ to mean $\text{CDD}_c(d)$ where d is the day containing t (and likewise for HDD). For an example, see Figure B.2.

We validate the regression on hourly ENTSO-E load data on the country level for 2015, and show it to be a good fit — more information about this can be found in the GitHub repository[16].

In accordance with load projections for 2030 by the European commission[17] we increased the demand in each country by 13%.

B.2 Hydropower data

For hydropower data we follow the approach in PyPSA-Eur which uses ERA5 reanalysis data to generate inflow profiles (using Atlite) that are then scaled by historical country-level hydro generation data from the US Energy Information Administration (EIA) [Adm22]. We have extended the default dataset in PyPSA-Eur to cover the entire period of 1980 to 2020, and we have also normalised EIA's production data to EIA's capacity levels of 2020[16]:

$$\text{gen}_c(y) = \text{nom\_gen}(y) \cdot \frac{\text{cap}_c(2020)}{\text{cap}_c(y)},$$

where $\text{gen}_c(y)$ and $\text{nom\_gen}_c(y)$ are the normalised and reported hydropower generation for country c in year y respectively, and $\text{cap}_c(y)$ is the reported hydropower capacity for country c in year y.

This allows a comparison throughout different years without any trends in infrastructure development. To avoid anachronisms, we have distributed generation and capacities of former

[16] https://github.com/aleks-g/multidecade-data/tree/v1.0

[17] https://ec.europa.eu/clima/document/download/ec1acac9-10fe-4eeb-915f-cad388990e0f_en, Fig. 44 (accessed 23/06/2022)

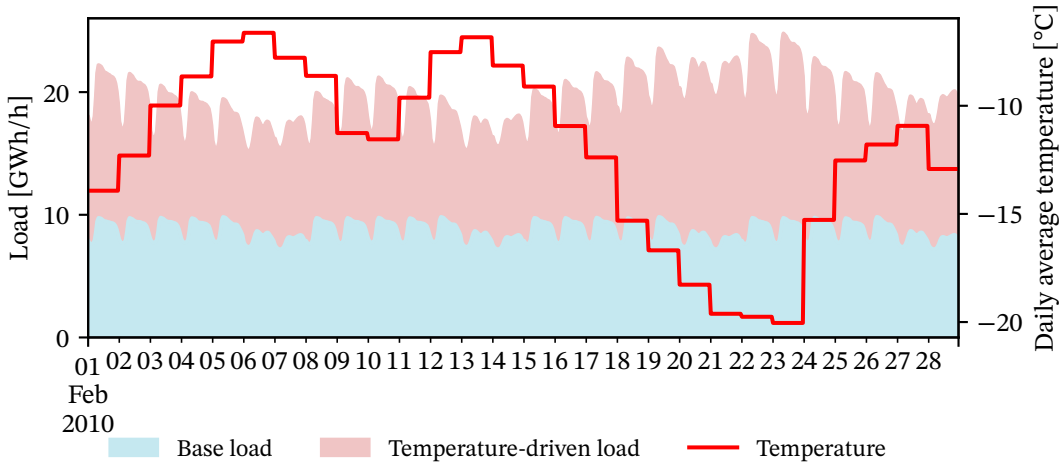

Figure B.2: Load data (here for Norway in February 2010) split into base load and temperature-driven load. The underlying temperature data are daily, country-wide averages from ERA5 reanalysis. Base load and temperature-driven load are derived from the regression described in Appendix B.

countries onto the current states (based on the first year of current borders, e.g. 1993 for Czechia and Slovakia, or the sum of West and East Germany)[16].

The historical generation data ensure that the inflow profiles are scaled to reasonable values (see the general approach in [Sch+17] and in particular Fig. 4 in [Liu+19]); we are interested in variability and not trends, therefore we want fixed capacities to have comparable weather years.

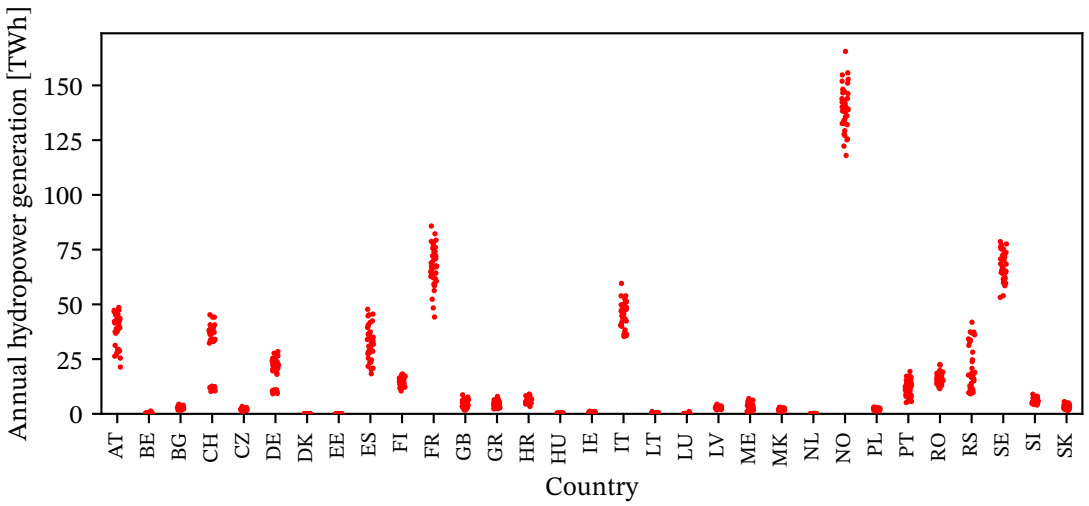

Figure B.3: Variability of annual hydropower generation (1980–2020) based on EIA data [Adm22], normalised by the reported hydropower capacities from 2020.

C Additional results of a 100% emission reduction

We showcase the impact of a 100% emission reduction (as opposed to the 95% reduction studied in the main text) on the results we present in this paper. As the other assumptions remain unchanged and gas turbines are the only sources of CO_2 emissions in our model, this corresponds to replacing gas as a generation technology with carbon-neutral alternatives. The results sharpen the uncertainty that weather variability introduces to renewable power systems. We investigate a different reduced near-optimal feasible space than before (replacing the gas investment dimension by two new dimensions, investment in battery and hydrogen storage). This means that the Chebyshev centre under this new reduction is additionally robust to changes in investment in battery and hydrogen storage, which is not the case for the results in the main text.

Without gas as a dispatchable generation technology, the costs of the now carbon-neutral power systems increase by 15 to 40 billion EUR/a, depending on the weather year. The last percentage points of emission reductions are thus overproportionally costly (as also shown in [NB21]), in particular in “more difficult” years. Wind power in combination with storage technologies see an increase in investment (see Figure C.1), most pronounced in the 1985, the year with the highest optimal costs.

Figure C.2 shows that the different optimal power systems are also mostly driven by (onshore) wind power, as in the 95% reduction case. Additionally, it depicts a strengthening of battery and hydrogen storage, which previously did not appear in the optimal solutions, although their shares of generation vary throughout the years. Similarly, the optimal share of nuclear generation becomes more volatile and decreases not only in the robust allocations (which are

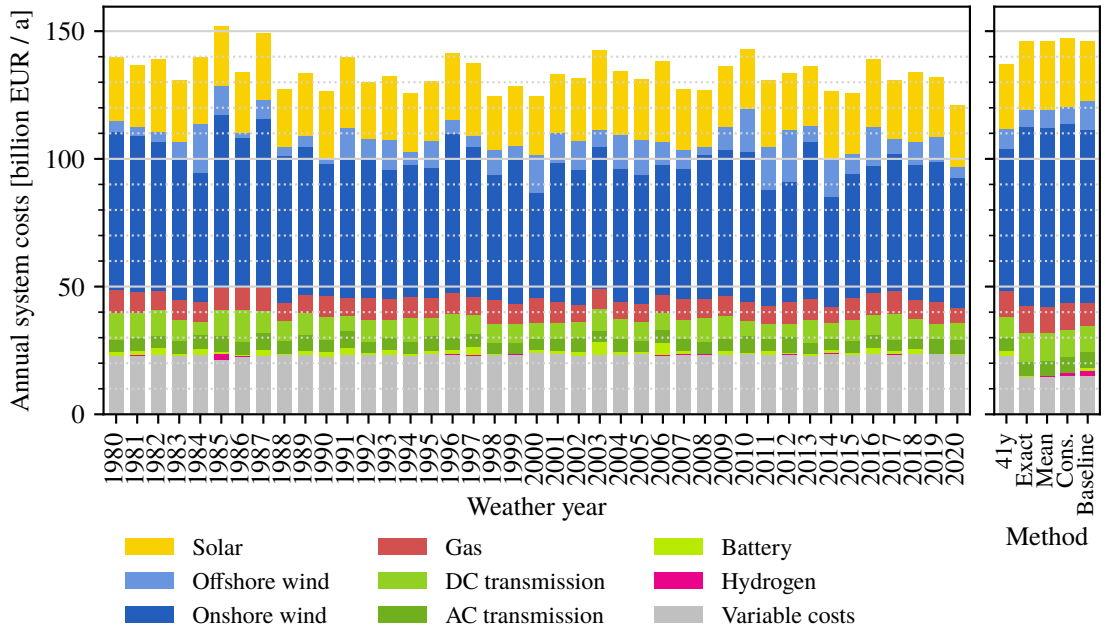

Figure C.1: Comparison of cost-minimal designs under a 100% emission reduction based on optimisations over individual years compared to the annualised costs of robust designs (exact, mean, conservative and baseline, respectively) and an optimisation with all 41 years ("41y").

characterised by higher renewable investment by design), but also in the 41-year optimisation. As nuclear power has higher variable costs than renewable generators, the existing capacities are not fully used, indicating the competitiveness of newly installed renewable capacities.

As with the 95% emission reduction, significant investment in both onshore wind power and solar power is necessary for a power system that can withstand weather variability. Figures C.1 and C.3 show additionally the need for investment in hydrogen storage and additional transmission capacities. In comparison to optimal solutions for different weather years, additional investment in wind power and hydrogen strengthens robustness against weather variability (see Figure C.4). The full decarbonisation increases the value of offshore wind power which did not feature prominently in the robust solution under 95% emission reduction (see Figure 5). Finally, it should be noted that there is a significant amount of investment flexibility for onshore wind, offshore wind and solar among the robust solutions for all 41 weather years.

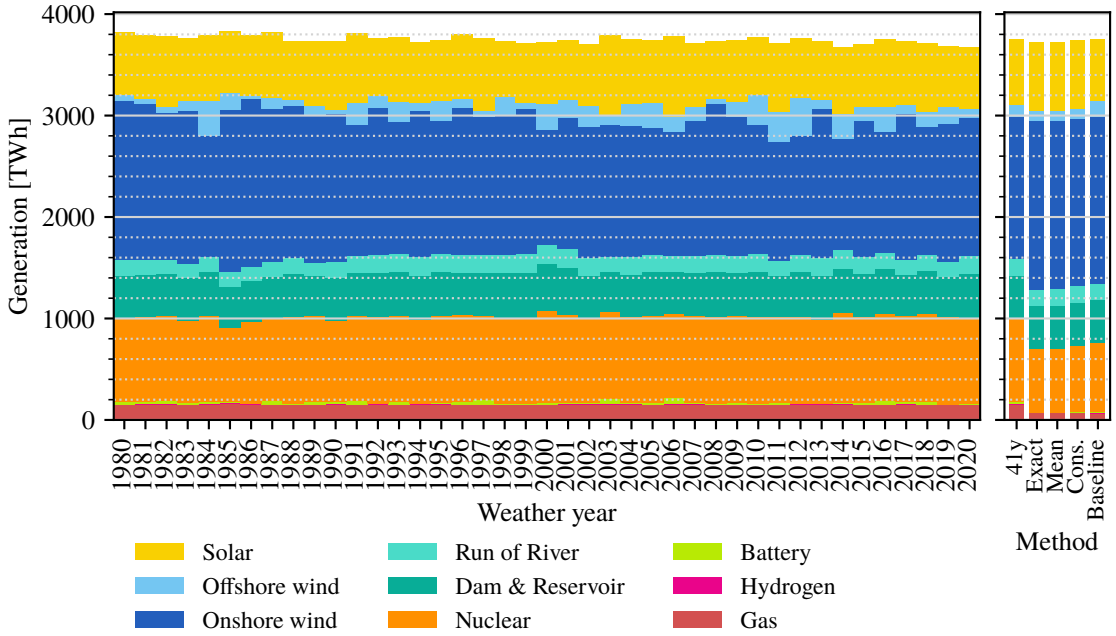

Figure C.2: For 100% emission reduction, annual average generation mixes for the optimal solutions for each single weather year, the optimal solution with all weather years (“41y”) and the robust allocations.

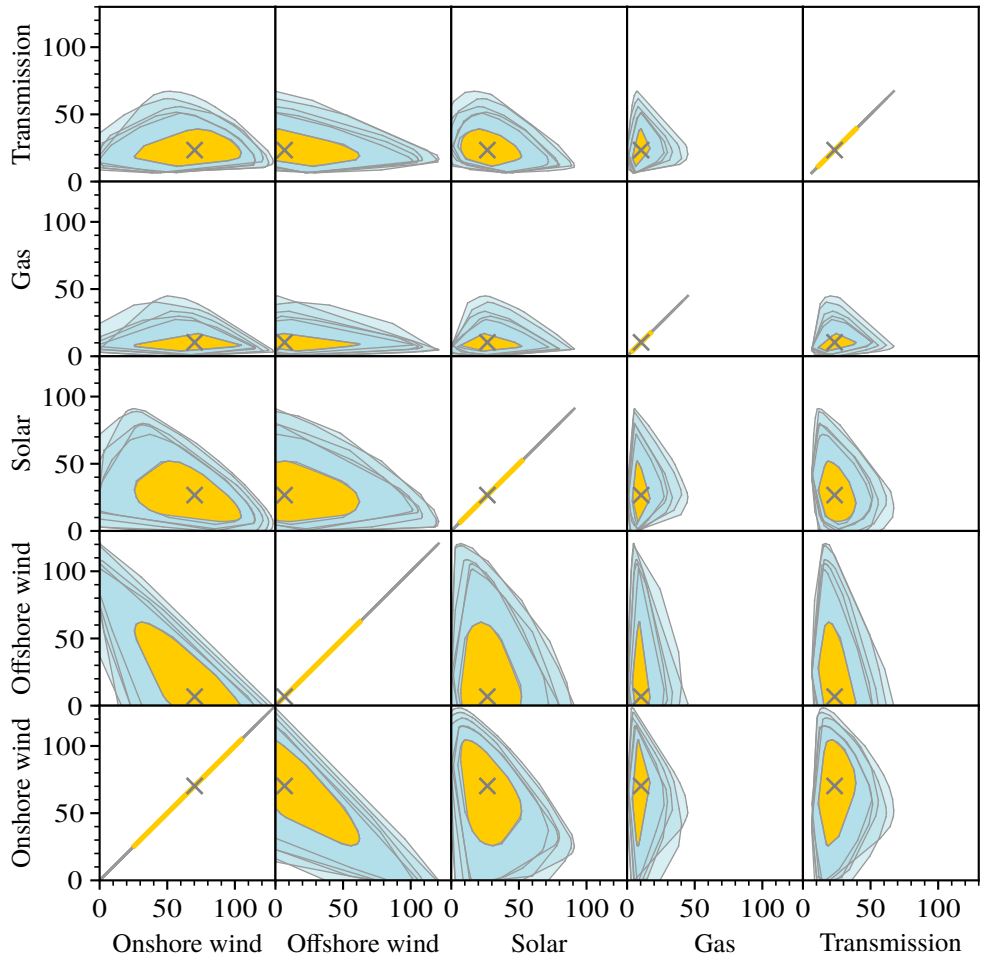

Figure C.3: Projections of the near-optimal spaces for different weather years and their intersection under 100% emission reduction. All values are annualised total investment costs per technology. For illustrative purposes, we only plot the near-optimal spaces for 6 out of 41 weather years (in different hues of blue). The intersection of all 41 near-optimal spaces is filled in yellow and the Chebyshev centre is marked with a cross.

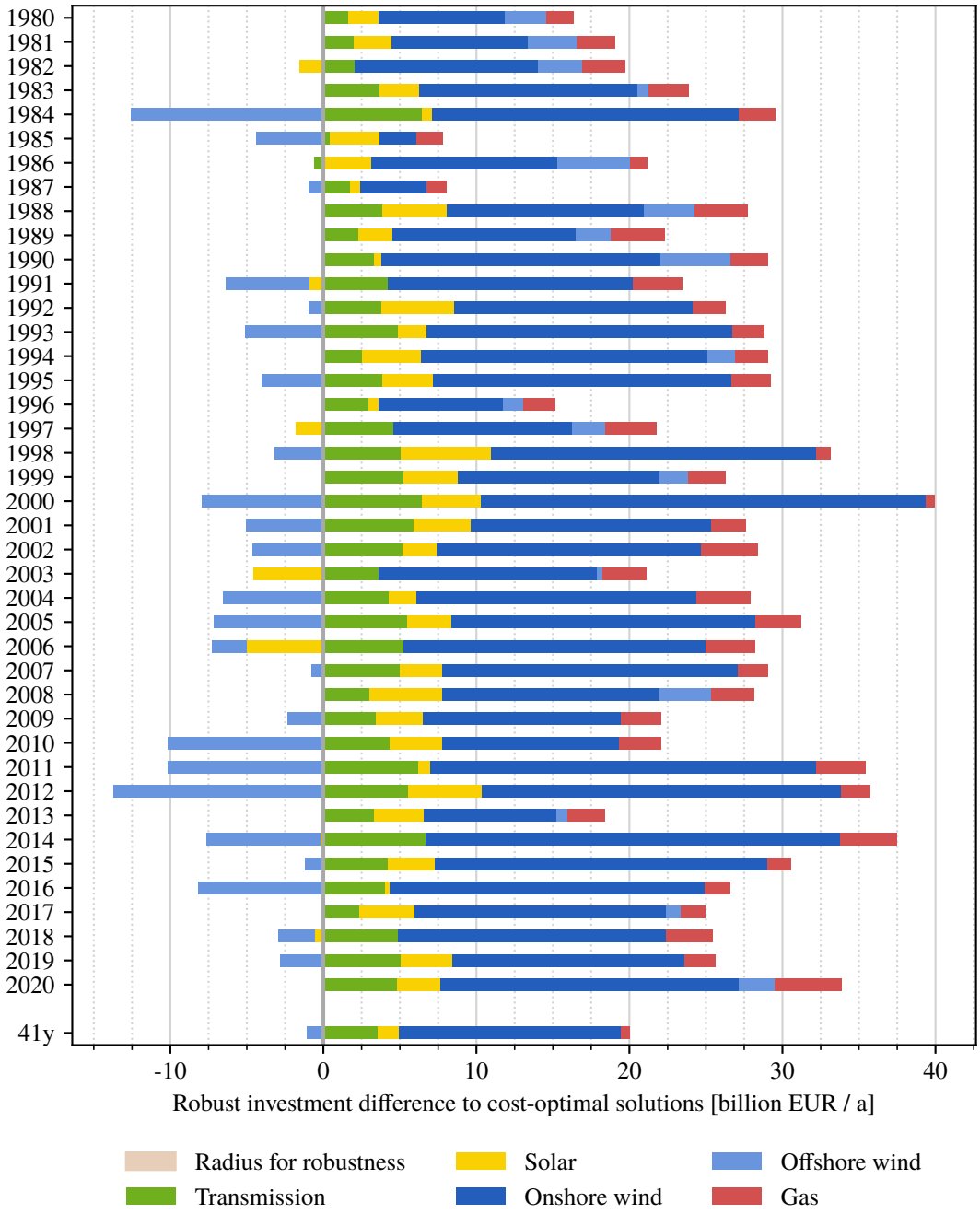

Figure C.4: For 100% emission reduction, a comparison of total investments for selected technologies in the optimal solutions for each weather year and the optimal solution with all weather years ("41y") to the robust point y_{ch}. Positive values mean greater investment in the given technology by the robust solution.

Article 2: “Weather”

A. Grochowicz *et al.*, «Using power system modelling outputs to identify weather-induced extreme events in highly renewable systems,» *Environmental Research Letters*, vol. 19, no. 5, p. 054 038. May 1, 2024, ISSN: 1748-9326. DOI: 10.1088/1748-9326/ad374a

ENVIRONMENTAL RESEARCH
LETTERS

CrossMark

OPEN ACCESS

RECEIVED
17 October 2023

REVISED
11 March 2024

ACCEPTED FOR PUBLICATION
20 March 2024

PUBLISHED
26 April 2024

LETTER

Using power system modelling outputs to identify weather-induced extreme events in highly renewable systems

Aleksander Grochowicz[1,5,*], **Koen van Greevenbroek**[2,5] **and Hannah C Bloomfield**[3,4]

[1] Department of Mathematics, University of Oslo, PO Box 1053, Blindern 0316 Oslo, Norway
[2] Department of Computer Science, UiT The Arctic University of Norway, Postboks 6050, Langnes 9037 Tromsø, Norway
[3] School of Geographical Sciences, University of Bristol, University Road, Clifton, Bristol BS8 1SS, United Kingdom
[4] School of Engineering, Newcastle University, Newcastle upon Tyne NE1 7RU, United Kingdom
[5] Contributed equally, order decided by coin toss.
[*] Author to whom any correspondence should be addressed.

E-mail: aleksgro@math.uio.no

Keywords: extreme weather, power system modelling, PyPSA-Eur, weather variability, shadow prices, energy meteorology, energy drought

Supplementary material for this article is available online

Abstract

In highly renewable power systems the increased weather dependence can result in new resilience challenges, such as renewable energy droughts, or a lack of sufficient renewable generation at times of high demand. The weather conditions responsible for these challenges have been well-studied in the literature. However, in reality multi-day resilience challenges are triggered by complex interactions between high demand, low renewable availability, electricity transmission constraints and storage dynamics. We show these challenges cannot be rigorously understood from an exclusively power systems, or meteorological, perspective. We propose a new method that uses electricity shadow prices—obtained by a European power system model based on 40 years of reanalysis data—to identify the most difficult periods driving system investments. Such difficult periods are driven by large-scale weather conditions such as low wind and cold temperature periods of various lengths associated with stationary high pressure over Europe. However, purely meteorological approaches fail to identify which events lead to the largest system stress over the multi-decadal study period due to the influence of subtle transmission bottlenecks and storage issues across multiple regions. These extreme events also do not relate strongly to traditional weather patterns (such as Euro-Atlantic weather regimes or the North Atlantic Oscillation index). We therefore compile a new set of weather patterns to define energy system stress events which include the impacts of electricity storage and large-scale interconnection. Without interdisciplinary studies combining state-of-the-art energy meteorology and modelling, further strive for adequate renewable power systems will be hampered.

1. Introduction

As electricity grids reach ever higher levels of renewable penetration to meet net-zero emissions targets, their weather dependence increases. Weather and climate variability therefore become increasingly important for power system operations and planning [1, 2]. However, traditional power system modelling has relied on a 'typical meteorological year' which may only include a few hourly time slices to represent demand and renewable variability. There has been a large effort over recent years to incorporate the impacts of climate variability into power system modelling, and running multi-year hourly simulations is becoming more common [3–11] with climate scientists now producing demand, wind and solar inputs for national and continental-scale modelling [12–16]. Particularly in systems containing large amounts of wind power generation, the choice of simulation years can significantly impact the operational adequacy of a system [3–5] and not considering year-to-year climate variability can also lead to failure to meet long-term decarbonisation objectives [4].

Multi-decadal climate simulations are also important for characterising the most challenging days for power system operation (e.g. days that might lead to blackouts). These *energy system stress events* can be investigated without a full power system modelling approach by looking at time series of demand or demand–net-renewables ('net load') [17–21]. Although these events are commonly periods of peak demand, they may include times of wind droughts (prolonged low wind speeds) [22], solar droughts or dunkelflauten ('dark doldrums').

In a renewables-based power system both electricity demand and generation are driven by weather and cannot be considered independently; it is thus becoming common practice to consider times of energy system stress as compound events involving a combination of near-surface temperatures, wind speeds, irradiance and hydrological variables across large geographic and temporal scales [10, 23, 24]. For example, high pressure systems can cause compound events [17, 25], affecting multiple countries simultaneously. While the basic mechanics of periods with energy scarcity in Europe revolve around extremely low near-surface temperatures (for demand) and low near-surface wind speeds (for wind power production), we still lack a detailed understanding of the power system dynamics during these weather-driven extremes, including electricity transmission and storage.

The complicating factors of transmission and storage motivate the use of a high-resolution power system optimisation model to identify periods of power system stress. Such models output *shadow prices*, a proxy for nodal electricity prices, which have been used successfully as a metric for strained supply situations in studies using dispatch optimisation models [24, 26, 27]. With the shift towards power systems dominated by variable renewable generation, where capital expenditure represents the majority of total system costs instead of operational and fuel costs, we propose using a capacity expansion model instead. Thus, we co-optimise infrastructure investments and dispatch decisions simultaneously in order to generate cost-optimal, fully decarbonised power system designs for Europe. In this setting, high shadow prices primarily indicate *system-defining events* triggering large investments. For the present study, we use PyPSA-Eur [28, 29], an open optimisation model for the European power system.

The central question we address is that of identifying energy system stress events for decarbonised systems, and classifying the weather regimes leading to such events. We investigate events using three different approaches over four decades of weather variability. Approach 1 is a baseline method rooted in energy meteorology and assesses the difficulty of a period by net load as is commonly done [17–19]. The main novelty lays in approach 2, where we filter system-defining events whose total electricity costs explain large investments, based on the shadow prices obtained by the capacity expansion model. Approach 3 is a validation using dispatch optimisations with out-of-sample weather years and lost load as an alternative metric to shadow prices.

Identifying the large-scale weather patterns leading to system-defining events is of central importance for systems planning, operations and forecasting. Whereas previous studies have compiled weather patterns leading to high net load or compound events [17, 18, 25], an analysis informed by the operation of power systems including transmission and storage into account is missing. We show that this additional consideration can impact results significantly. While both approach 2 & 3 take power system dynamics into account, we find that approach 2 is the more practical and computationally less demanding of the two (as approach 3 requires many additional optimisations), while the outcomes of approach 2 & 3 are similar.

To summarise, the key aims of this paper are to:

- Filter out and delineate system-defining events using shadow price outputs from a power system optimisation model.
- Classify these events based on the prevailing weather conditions, and determine the main factors leading to continent-wide system stress.
- Construct a new set of weather patterns that define European power system stress from both a climate and power systems modelling perspective.

Section 2 describes the meteorological and modelling set-up and introduces the definition of system-defining events. In section 3 we combine the insights from the power system model and meteorology to lay out weather patterns underlying power system stress. We put the results into context of the expansion of renewables and conclude with section 4.

2. Data and methods

In the spirit of Craig *et al* [2] we apply a transdisciplinary approach to identifying challenging weather for power systems. First, we use outputs from a power system optimisation model to filter out system-defining events that drive investment in additional generator capacities. For these time periods, we cluster the meteorological conditions into groups such that we can identify weather patterns that drive weather stress events. Then we analyse the effects in the power system (model) during these time periods to determine which components lead to difficulties and are under stress.

2.1. Datasets and tools

The weather inputs to the meteorological analyses and to the power system optimisation model are based on ERA5 reanalysis data [30] and are described in the following section. We represent the European

power system by using the open-source energy system optimisation model (ESOM) PyPSA-Eur (github.com/PyPSA/PyPSA-Eur) [31] (version 0.6.1) with small modifications; the modelling setup follows thereafter.

2.1.1. Meteorological inputs and energy variables

We use gridded weather variables from the ERA5 reanalysis [30] from 1980 until 2021. 2 m temperature, 10 m wind speed and surface air pressure over the region 34°–72° N, 15°–35° E) are used to investigate the meteorological conditions at times of power system stress. We use 500 hPa geopotential height anomalies over the Euro-Atlantic region (90° W–30° E, 20°–80° N) to create European weather regimes (see section 2.4).

Weather-dependent power systems time series are mainly generated using the open-source software Atlite [15]. In Atlite, 100 m wind speeds from ERA5 are first extrapolated to turbine hub height using a logarithm law and passed through a reference power curve to obtain capacity factors (fraction of rated power output that can be produced at the given wind speed); we use the Vestas 112 V 3MW turbine for our calculations. PV capacity factors are computed from ERA5 direct and diffuse shortwave radiation influx data using a reference solar panel model, assuming no tracking and a fixed 35° panel slope. Weather-dependent electricity demand is generated based on historical ENTSO-E data and adjusted for heating or cooling demand using a heating/cooling degree days approach as in [9, 23, 32].

2.1.2. Power system modelling set-up

PyPSA-Eur is configured with high spatial (181 generation and 90 network nodes [33]) and temporal resolution (1-hourly), making it well-suited to investigating a highly renewable European electricity network [9, 34–40]. The model is solved for forty individual weather years (July 1980 – June 2020, preserving winters). Although capable of a sector-coupled representation of the European energy system (e.g. including the heat and transport sectors), we restrict PyPSA-Eur to the optimisation of the power sector alone for clarity. We minimise total system costs of the European power system by optimising investment and dispatch of electricity generation, storage, and transmission to meet prescribed hourly national demand over a year. The model performs a partial greenfield optimisation, i.e. with existing transmission network (2019) and capacities of hydropower and nuclear power (2022), but without existing renewable capacities (see figure S1 for a break-down of total system costs for the forty different weather years). Our cost assumptions are based on a modelling horizon of 2030 and we assume a fully decarbonised power system; the available generation technologies are thus nuclear and renewables: hydropower and biomass (non-expandable), solar, onshore and offshore wind power (all expandable). Transmission can be expanded (overnight) by 25% compared to current levels (figure 6 in Hörsch and Brown [28]), and electricity can be stored through hydro reservoirs (non-expandable), battery storage and hydrogen storage. This can be thought of as modelling an ambitious, early decarbonisation of the European electricity sector using current or near-future technologies. The focus on the power system enables a study of weather dependence providing more evidence on transmission and storage before the impacts of long-term climate change emerge.

We run capacity expansion optimisations for each of the 40 weather years (July–June) separately, arriving at 40 different cost-optimal system designs. The overall make-up the resulting designs is similar for all weather years with total system costs being dominated by wind, then solar investment expenditure. However, there are significant variations in the magnitudes of installed capacities, as well as in the investment in hydrogen and battery storage; see figure S1. Running separate optimisations allows for the identification of system-defining events in each weather year, as opposed to only a smaller number of events that are defining over the entire 40 year period. The single-year optimisations also allow for a high spatial and temporal resolution, whereas 40 year optimisations have only been accomplished at a moderate resolution [9]. While basing the results on 40 different system designs is a potential limitation (is a period identified as challenging for one design also challenging for other designs?), cross-validation using load shedding (Approach 3) shows that there is very good alignment between system-defining events in one year and load shedding events for other designs operated on the same year (see also section 2.6).

2.2. Dual variables and shadow prices

PyPSA-Eur is formulated as a linear program in order to find investment- and operational decisions which minimise the objective (total system costs) with linear constraints ensuring feasibility of the model result. An optimal solution to a linear program consists of an optimal value for each decision variable, as well as an optimal *dual value* for each linear constraint. These dual values indicate how much the objective function would decrease if the corresponding constraint was relaxed by one unit, quantifying the 'difficulty' of satisfying the given constraint.

The dual variables corresponding to the constraints ensuring that a fixed demand is met at each network node n and timestep t are denoted $\lambda_{n,t}$ following [31]. These dual variables—also called shadow prices of electricity—can be interpreted as the modelled price of electricity (in EUR / MWh) at the given node and time (see e.g. [26, 27] in the context of dispatch optimisation). Note, however, that despite this economic interpretation the shadow prices are not comparable to electricity prices in the current European market, as the shadow prices are largely

driven by the need for renewable expansion in the model, not marginal operating costs.

Apart from these, other hourly and locational dual variables corresponding to constraints on transmission and storage can be used to reveal transmission congestion rents and values of stored energy in the model, respectively (see supplementary materials A.2). Since transmission expansion costs are recovered through congestion rents in the model, the congestion rent time series can reveal which times primarily triggered investment in transmission; the same goes for storage.

2.3. Identifying system-defining events

In this paper a *system-defining event* is a period where the incurred electricity costs surpass a specified threshold within a limited time frame. We restrict the duration of a system-defining event to a maximum of two weeks, and set the minimum cost threshold to 100 bn EUR.

An event starting at t_0 and lasting for T hours is considered system-defining if

$$\sum_{n} \sum_{t=t_0}^{t_0+T-1} d_{n,t} \cdot \lambda_{n,t} \geqslant C \tag{1}$$

for $C = 100$ bn EUR and $T \leqslant 336$ (the number of hours in two weeks), where $d_{n,t}$ is the electricity demand at node n and time step t, in MWh. *A priori*, many overlapping events of various lengths meet the above criteria. For the purposes of this study, we thus filter out overlapping events until only a non-overlapping set of system-defining events remains; see the supplementary materials for an exact description of the filtering procedure.

By definition, relaxing either the length or cost threshold can only lead to additional events being classified as system-defining; we have chosen the threshold values used in this study so as to produce approximately one system-defining event per year. The relative values of the thresholds *can* affect the average duration of identified events; we chose the cost threshold so as to obtain events averaging around 7 days—the discharge duration of hydrogen storage included in our model. See also figure S2 for an overview of most costly periods of varying times across the studied weather years. It should be stressed that the thresholds can be freely adjusted in future studies to fit the research questions at hand.

2.4. Traditional meteorological weather regimes

To understand the weather conditions present during system-defining events we use a weather regimes approach. Weather regimes are recurring large-scale atmospheric circulation patterns that can be linked to surface weather, and energy system impacts [14]. Previous work has shown weather regimes have predictability for energy applications out to a few weeks ahead [41], which is beneficial for energy system planning. Weather regimes are calculated from daily-mean October–March 500 hPa geopotential height (Z500) anomalies over the Euro-Atlantic region (90° W–30° E, 20°–80° N) following the classification method of [42]. The first 14 empirical orthogonal functions (EOFs) of the Z500 data are computed [43], which capture 89% of total data variance. The associated Principal Component time series (PCs) are used as inputs for the k-means clustering algorithm, with four clusters (which has previously been found to be the optimal number over the region [42]). Using the PCs of the Z500 data makes the problem significantly quicker to compute without losing useful information about the large-scale weather conditions. The four cluster centroids are: the positive and negative phases of the North Atlantic Oscillation (NAO), the Atlantic Ridge and Scandinavian Blocking (see figures 6(c)–(f) for visualisation of these). We then find the weather regime present during each system-defining event. Previous work has shown that although these patterns have some useful sub-seasonal predictability for energy applications, extreme events are not necessarily represented well by the cluster centroids [18]. Therefore, apart from finding the regime number during each extreme event, the pattern correlation between the days' Z500 anomaly, and the days' cluster centroid is also calculated.

2.5. K-means clustering of system-defining events

In addition to weather regimes defined in terms of 500 hPa geopotential height anomaly representing mid-troposphere dynamics, we also study near-surface weather data during extreme events. These near-surface data better represent the weather conditions present near the power system impacts. For each system-defining event hourly gridded 2 m temperature and 10 m wind speeds are taken for the region described in section 2.1.1. This gives 5615 hours (∼233 days) of data. We then perform another k-means clustering, similar to the method of [42] and applied above to Z500 data (see section 2.4). Temperatures and wind speeds are first normalised by their 1980–2021 daily climatologies (by both mean and standard deviation, to allow both fields to be comparable). The data are then converted into principal components (the first 14 are kept, explaining 56% of the total variance). These principal components are then grouped into four clusters using the k-means algorithm. Four was identified as the optimal number of clusters using the silhouette score (commonly used to determine optimal cluster number for k-means algorithms). There was no obvious elbow present when using the elbow method (not shown). The cluster centroids can then be analysed and compared to more traditional methods as in section 2.4.

2.6. Validation using load shedding as indicator for difficulty

An alternative approach to capture the adequacy of the power system is to measure load shedding (unmet demand) in a fixed power system design. In the context of net-zero scenarios, we can first obtain a power system design from a capacity expansion model, and then subject that design to a dispatch optimisation with *different* inputs in order to measure potential load shedding. In our case, we run a capacity expansion model with one weather year y_1, and perform a dispatch optimisation over a different weather year y_2. Periods of system stress in weather year y_2 can then be recognised by high load shedding in this dispatch optimisation. We perform this cross-year dispatch optimisation for all 1600 combinations of $y_1, y_2 \in \{1980/81, \ldots, 2019/20\}$ and average the load shedding profiles for each weather year to obtain time series comparable to those derived from electricity shadow prices. Calculating the average load shedding based on the out-of-sample weather years relies on the optimal networks (or some other network assumptions) and is computationally more expensive than section 2.3.

3. Results

Traditionally, power grids and generation stock have been designed around fossil fuels which could act as dispatchable generators, especially during peak demand. With increased reliance on variable renewables and balancing via transmission and energy storage, this paradigm breaks down. In particular, the most critical events to system design extend beyond a single hour or day, and identifying such periods no longer depends only on weather data but also power system parameters including storage and transmission [7, 20, 44, 45].

We propose a re-orientation to studying power system stress through system-defining weather events (see table 1 and figure 1). Electricity shadow prices reveal which time periods cause additional infrastructure investments (section 2.3) and determine an hourly total electricity cost (figure 2) whose yearly sum is the total annual value of electricity in the model. The total annual value of electricity is closely linked to the total system cost (differing only because of existing infrastructure), which is dominated in this model by investment costs (especially as renewables are optimised from scratch—see figure S1).

3.1. Characteristics of periods driving system design

We find that on average across 40 weather years, the single most expensive day in each year accounts for 12.4% (6.6%–31.3%) of total yearly electricity cost, whereas 19 weather years contain a three-week period accruing more than 50% of total electricity cost (figure S2). This heterogeneity of events calls into question the use of representative periods or time slices in energy systems modelling. Moreover, we find large variations between different weather years, with the single most expensive week explaining between 18% and 77% of total respective electricity costs. For context, the total yearly electricity costs (that also include the value of existing infrastructure) range from 216 to 330 billion EUR depending on the weather year.

Table 1. An overview over the three approaches we compare in this study. Approach 1 is commonly used in the literature. We introduce approach 2 in this study (also see sections 2.2 and 2.3) and validate it with approach 3 (see section 2.6). Also see figure 1 for a visualisation of the workflow.

	Approach	Underlying method	Description
1	Net load	Energy meteorology inputs	Periods of mismatch of load and renewable production.
2	Shadow prices	Capacity expansion	Periods that are defining for system design.
3	Load shedding	Dispatch optimisation	Periods of failure to meet demand.

As introduced in section 2.3, we define a system-defining event as accumulating costs exceeding 100 billion EUR in less than two weeks. We identify 32 such events which all happen between November and February (see figure 2 and table S1). The events vary in length considerably (2–13 days), being 7 days long on average.

We find that meteorologically extreme single days [18, 19, 46] do not reliably identify system-defining events in individual weather years (figure S3). While such extreme days almost always lead to high shadow prices, these are not necessarily surrounded by a challenging enough period to have a large impact on system design (e.g. see the events in 1997/98, 2011/12 and 2012/13 from Bloomfield *et al* [19], figures S3 and S4); the same also holds for week-long events (figures 2 and S5–S8).

As opposed to methods considering only peak load or net load, (i.e. peak mismatch between renewable generation and load) [17–20, 23], using power system optimisation outputs to identify system-defining events takes the complex interactions between storage and transmission into account. Moreover, we need not make assumptions about the availability of storage and transmission in any particular region.

3.2. Origins of power systems stress events

In line with previous research, we find that power system stress occurs in the winter months when temperatures, wind and solar production are low in Europe

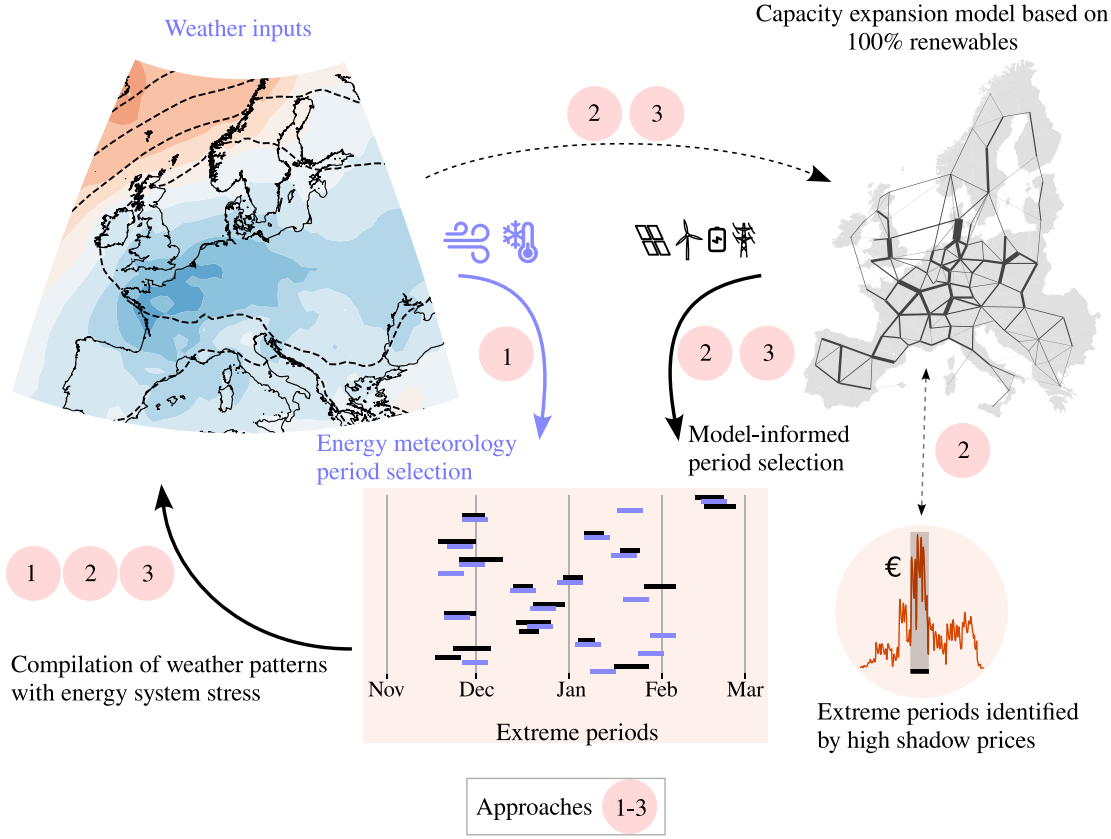

Figure 1. An overview over the workflow and the three approaches we compare in this study. For a definition of the approaches, see table 1.

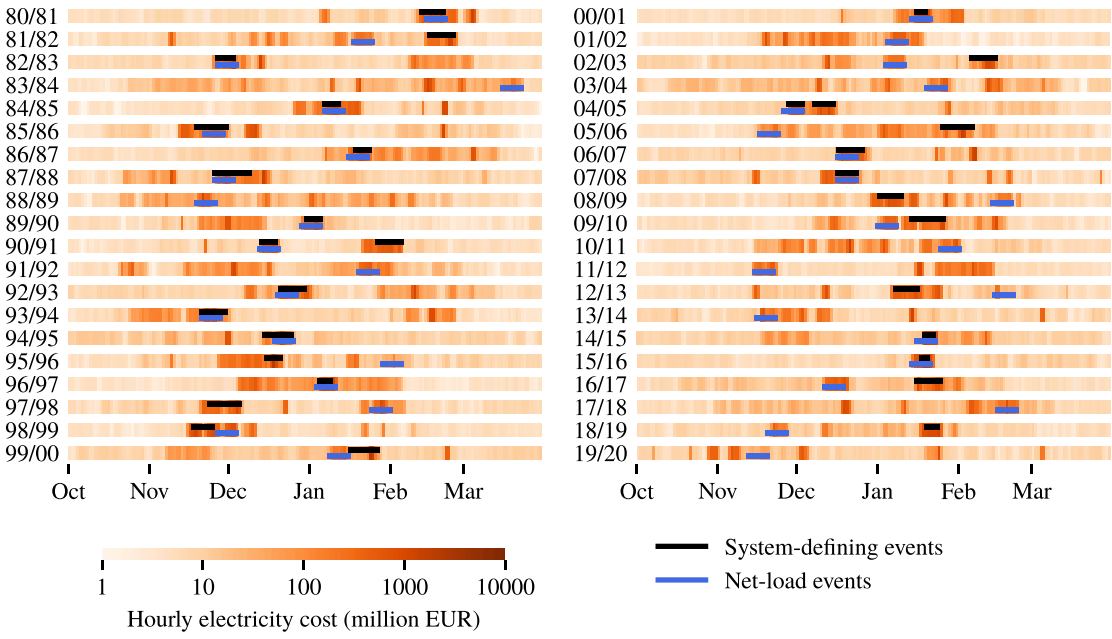

Figure 2. An overview of all identified system-defining events in the context of daily system cost. Additionally the week with the highest net load for each year is marked (approach 1 in table 1). Only winter months are shown as shadow prices are consistently low during the summer. All costs are in 2013 EUR, but derive from model shadow prices, not actual market prices.

[19, 40, 45]. Power systems based on renewables are primarily wind-dependent in the winter, especially in the northern latitudes [47], making them prone to 'wind droughts'. Using standard cost projections, we see annualised investments of 60.9 bn EUR in wind power (onshore and offshore), 28.4 bn EUR in solar power, 15.2 and 13.3 bn EUR in batteries and hydrogen storage respectively, and 18.4 bn EUR

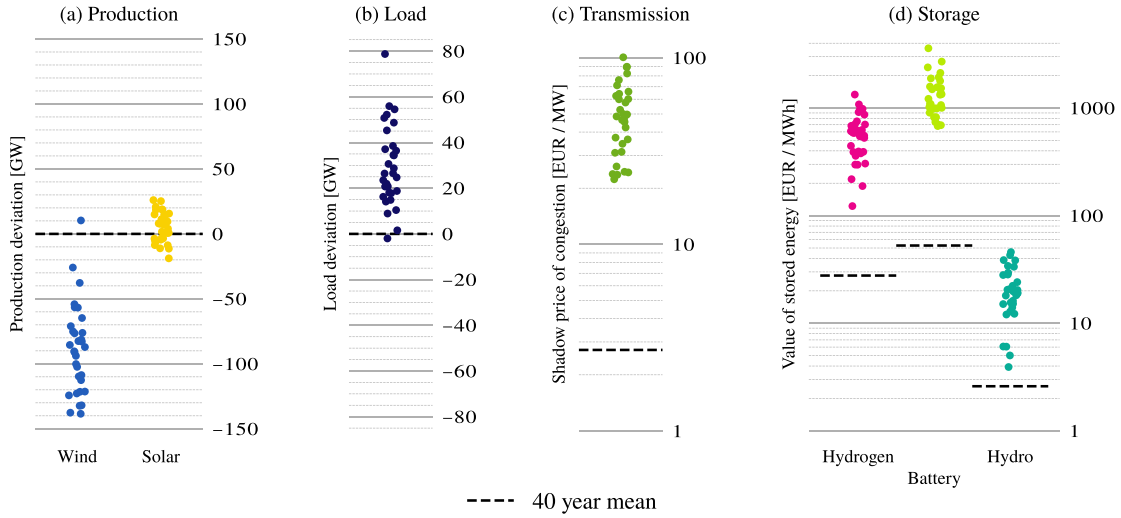

Figure 3. A summary of key metrics compared to 40 year means. Each dot represents the mean value of the metric in question over one system-defining event. From left to right: (a) renewable production deviation from 40 year mean at the time of each event, (b) load deviation from 40 year mean at the time of each event, (c) mean shadow price of transmission congestion during each event, (d) mean value of stored energy for each event. An overview over all events can be found in table S1.

in transmission expansion (mean over 40 individual weather year optimisations—figure S1).

We find significant variations in the magnitude and location of stress triggers over Europe across the 32 system-defining events (e.g. figures S9 and S10). Still, all but one identified events are consistently driven by low wind power *and* high load anomalies (figures 3(a) and (b)) when aggregating over the whole system. Moreover, we find that even though the low wind and high load anomalies during system-defining events are concentrated over certain regions, high shadow prices typically spread to the whole continent (figure 4). This is despite a modest maximum allowed transmission investment of 25% compared to the current-day grid value in the model. Only peripheral regions (northern Scandinavia and, to a lesser extent, the Iberian peninsula) have significantly lower shadow prices during some of the events; even then they are much higher than average.

3.3. Role of transmission and storage during system-defining events

While system-defining events can be caused by various meteorological conditions, the most severe events almost always impact the sizing of *all* power system components. Figure 4 shows a representative example of a week-long system-defining event during December 2007. This period was caused by a high pressure system over central Europe causing a period of prolonged low wind as well as high heating load (figures 4(a) and (b)). The event is identified as difficult by the spiking electricity shadow prices (shown by region in figure 4(c) and over time in (d)).

To discern the roles of transmission and storage during this event, we consider the dual variables of the line capacity constraints and inter-hour storage energy level linking constraints respectively (see section 2.2 and supplementary materials for details). While we see in figure 3 that the 40 year mean shadow price of congestion $\mu_{l,t}$ across the network is just below 2 EUR / MW, figure 4(c) shows that $\mu_{l,t}$ reaches event-average values above 1000 EUR / MW for individual lines. This demonstrates that the event in question is a major factor in driving transmission expansion—in fact some 39% of the total annual network congestion rent for the 2007/08 network was gained during the week in figure 4. There is significant congestion between continental Europe on one hand and Scandinavia and the British Isles on the other hand, with significant wind- and hydropower supplied from these regions. The transmission grid is well-connected enough to avoid extreme price spikes in the affected regions.

The value of stored hydrogen energy around the December 2007 event in figure 4(d) reaches a maximum during the event, but as the marginal electricity prices are higher still, the entire hydrogen storage reserves in the network are discharged. This particular system-defining event was preceded by a week of already high prices and high values of stored energy, during which not all hydrogen storage was able to fill up in anticipation of the main event. Other weather years contain meteorologically distinct system-defining periods up to several weeks apart that are nonetheless connected by sustained high values of storage in the interim. This underlines the temporal interdependence of power system dynamics when storage is included, meaning that periods of system stress cannot be studied as isolated events.

3.4. Comparison to the traditional relationship between climate and power systems

Composites of the normalised surface weather conditions observed during each of the 32 events from

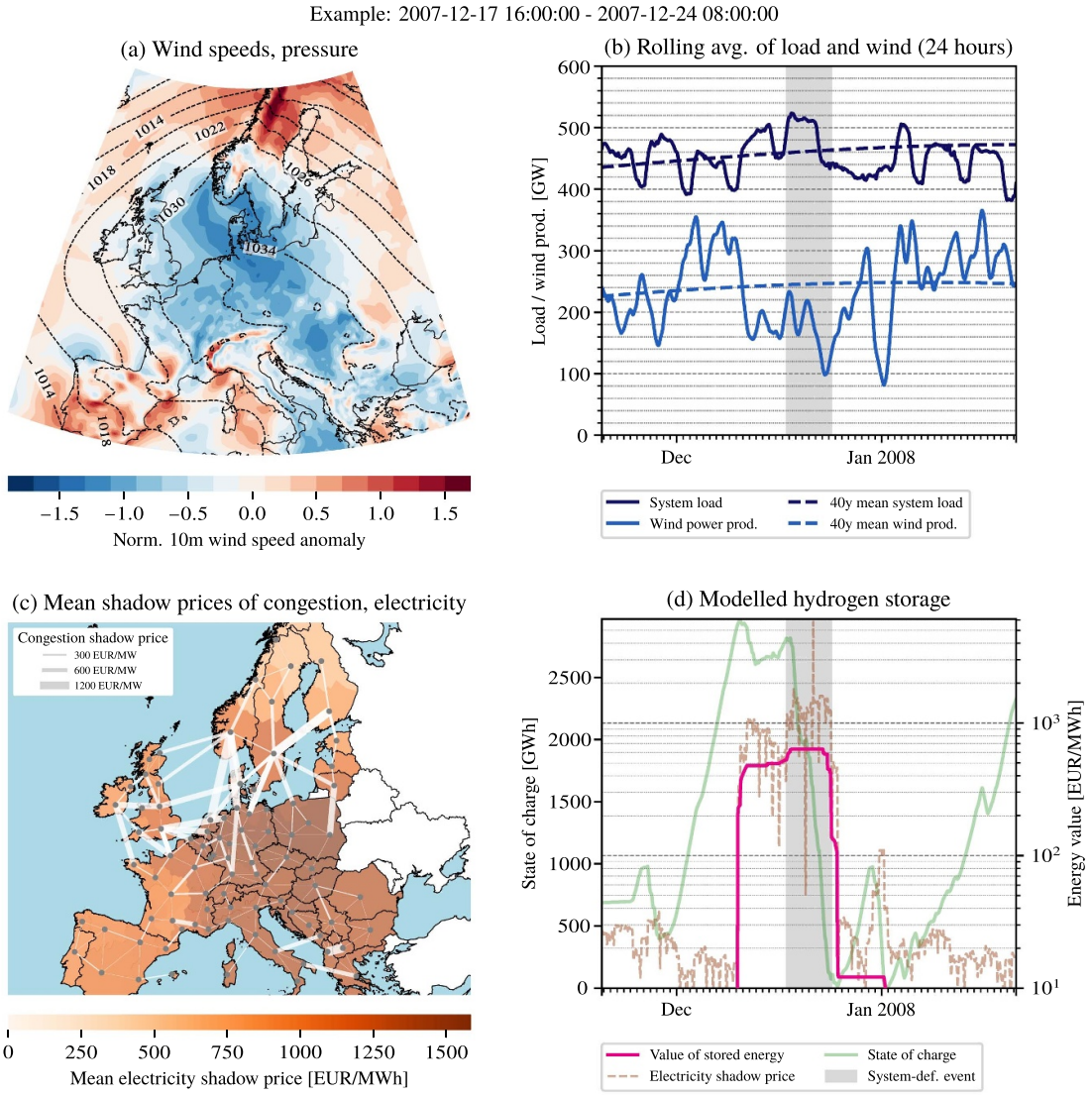

Figure 4. System-defining events are the result of an interplay of low renewable availability, high load, storage constraints and transmission congestion. Inputs in the top row, comparable to a usual meteorological approach (approach 1). System variables in the bottom row. (a) Average weather in Europe over the example event. Note the wind speed anomalies over the North Sea region and the temperature anomalies in Central Europe in figure S11. (b) Time series of wind power production and electricity load around the highlighted event (smoothed with rolling averages of 24 hours). The dashed lines show seasonality deduced from the period 1980–2020. (c) Network map of the European power system with the edge widths showing shadow prices of congestion and the regions shaded with the average electricity price during the event. (d) Time series of electricity prices, value of hydrogen storage (with logarithmic scales), and the hydrogen storage level around the highlighted event (all network averages). All costs are in 2013 EUR.

approach 2 (table 1) are shown in figures 5(a) and (b). The events are defined by high pressure systems over Central Europe and the North Sea region (where the capacity expansion model mainly builds wind power), resulting in cold temperatures and low wind speeds. This is similar to the synoptic situations [17, 18, 25] seen using approach 1.

Within figures 5(a) and (b) multiple surface weather conditions are present. Performing K-means clustering on the normalised hourly near-surface temperature and wind speed fields over the 32 events to isolate key weather patterns of interest (see section 2.5) gives the four clusters shown in figures 5(c)–(j). All include high pressure centres over parts of Europe and low winds over the North Sea. However, each cluster has very different spatial patterns of surface temperature anomalies, which are not seen in studies neglecting transmission and storage constraints [18, 19]. Future work will investigate if these conditions are unique to system-defining events, or if it is possible to also have these anomalous weather conditions at times of low power system stress.

If instead each day is assigned to a more traditional Euro-Atlantic weather regimes framework from Cassou [42], we see a high frequency of Scandinavian blocking (54%) which is over double the 25% seen climatologically. We also see over four times fewer instances of NAO+ (figure 6). Generally the pattern correlation between each day's weather

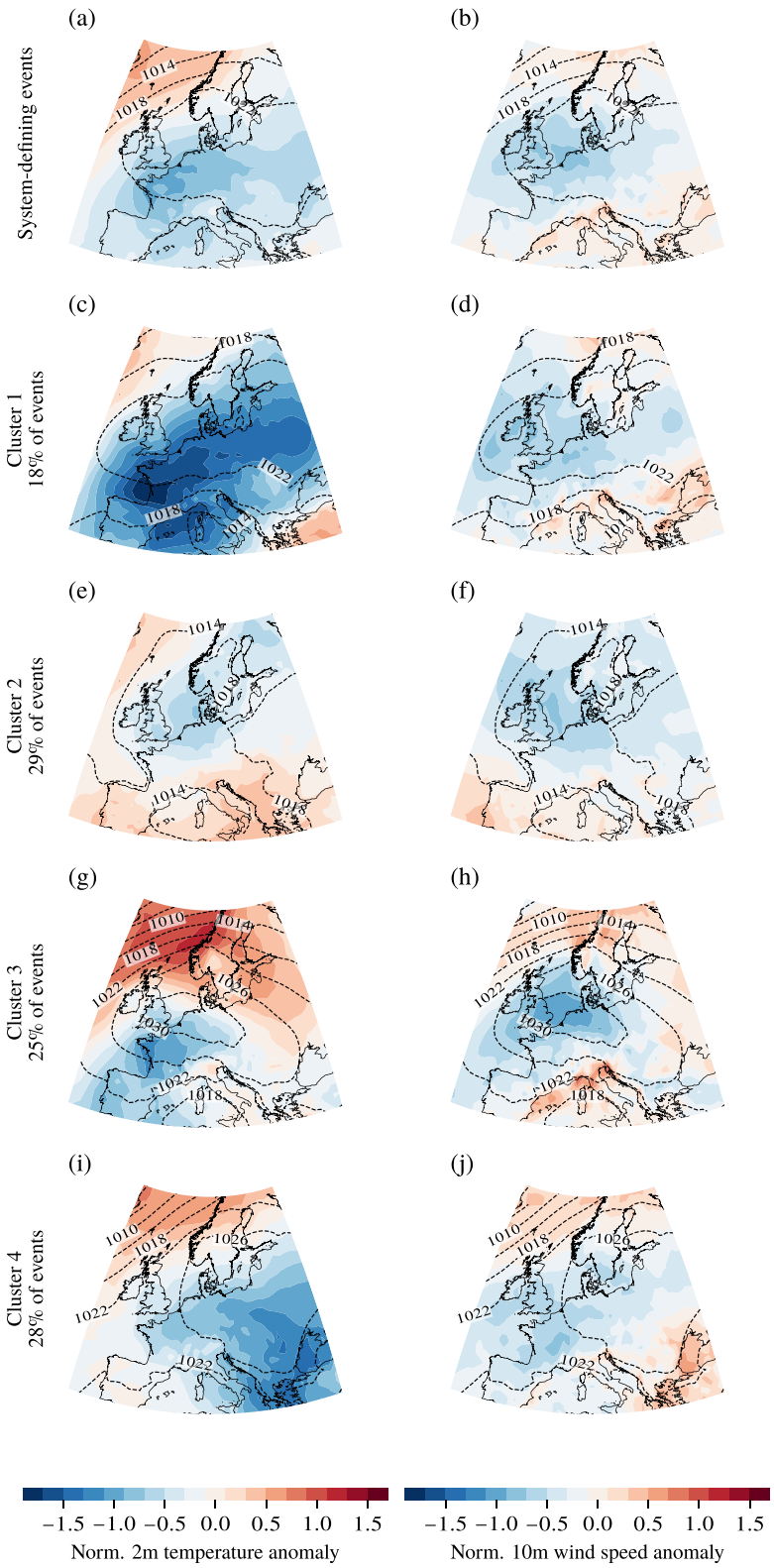

Figure 5. Meteorological conditions during system-defining events (a) and (b). For all 32 events, (c)–(j) are the four extracted clusters of events.

and the assigned cluster is low (figure 6), particularly when a day is assigned to NAO+ or the Atlantic ridge. Figure 6(g) shows the 500 hPa geopotential height composite for all of the system defining events. This explains the higher prevalence of Scandinavian blocking events (figure 6(d)) but importantly, the system defining events resemble a fusion between the high pressure centre from the Scandinavian blocking pattern, and low pressure region from the NAO− pattern.

Figure 7 shows the temporal evolution of the weather regime categorisation from figure 6 over each

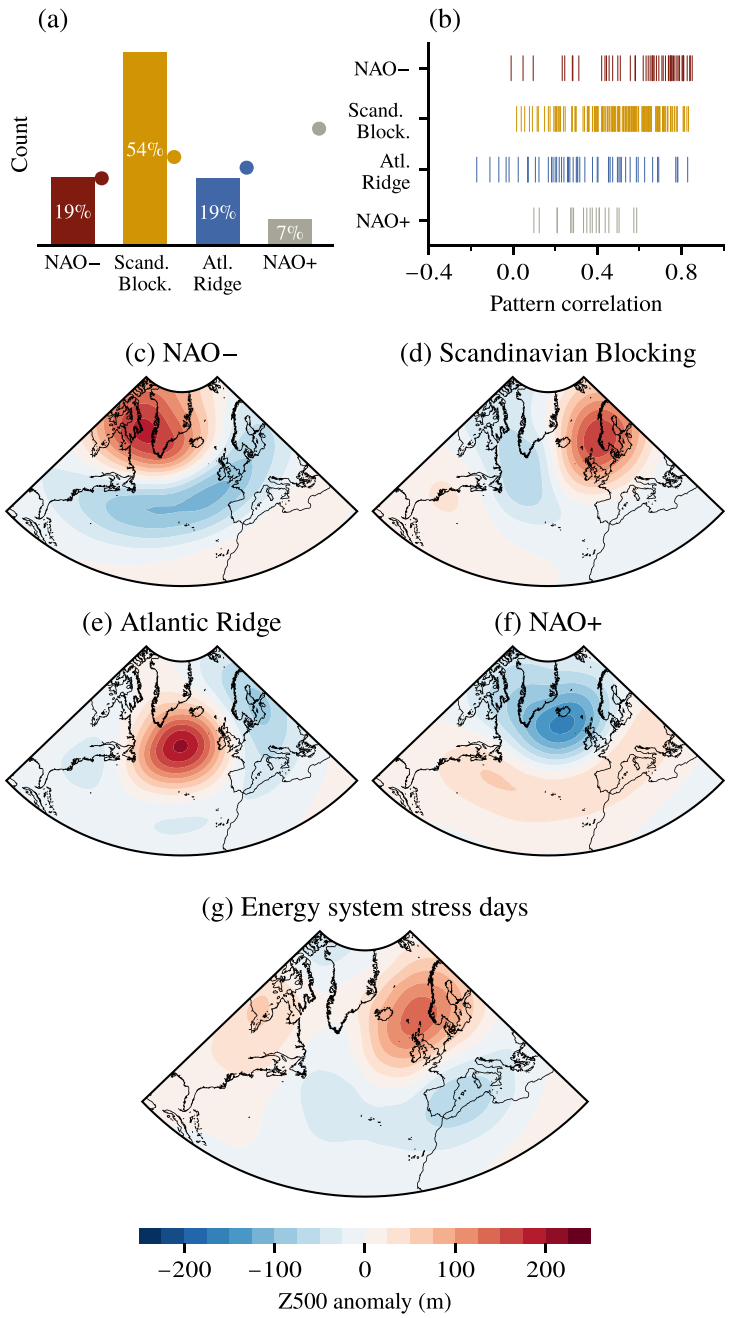

Figure 6. (a) Frequency of occurrence of Euro-Atlantic weather regimes as defined in [42] during system-defining events (with the solid dot marking the overall 40 year relative frequency of each regime), (b) pattern correlation between the daily 500 hPa geopotential height anomaly from the 32 system-defining events and the four Euro-Atlantic weather regimes, (c)–(f) 500 hPa geopotential height (Z500) anomaly composites for the Euro-Atlantic weather regime cluster centroids, (g) Z500 anomaly composite during the 32 system-defining events.

event. The figure is centred around the *peak day* of each event, which is the day containing the single most expensive hour of the event. It is interesting to note that the peak day can be at any point during the extreme event, and that the weather regime present during an extreme event is often quite persistent. Both of these are interesting points for future work. The results in this section motivate the need for more bespoke approaches to extreme energy days [48, 49].

When considering seasonal extremes, previous studies have shown strong correlations between the NAO and national demand and wind power generation [17, 50–52]. Winters with a negative NAO index have weaker surface pressure gradients across Europe, leading to colder, stiller conditions and higher seasonal demands. Figure 8(a) shows positive correlation between the October-March NAO index and European mean wind capacity factor ($R = 0.52$), with similarly strong negative correlations seen for NAO index and European mean load (Figure 8(b)). Significant correlation is also found when costs of electricity (between October and March) are considered ($R = -0.42$). Winters with a negative NAO index generally exhibit higher costs (figure 8(c)).

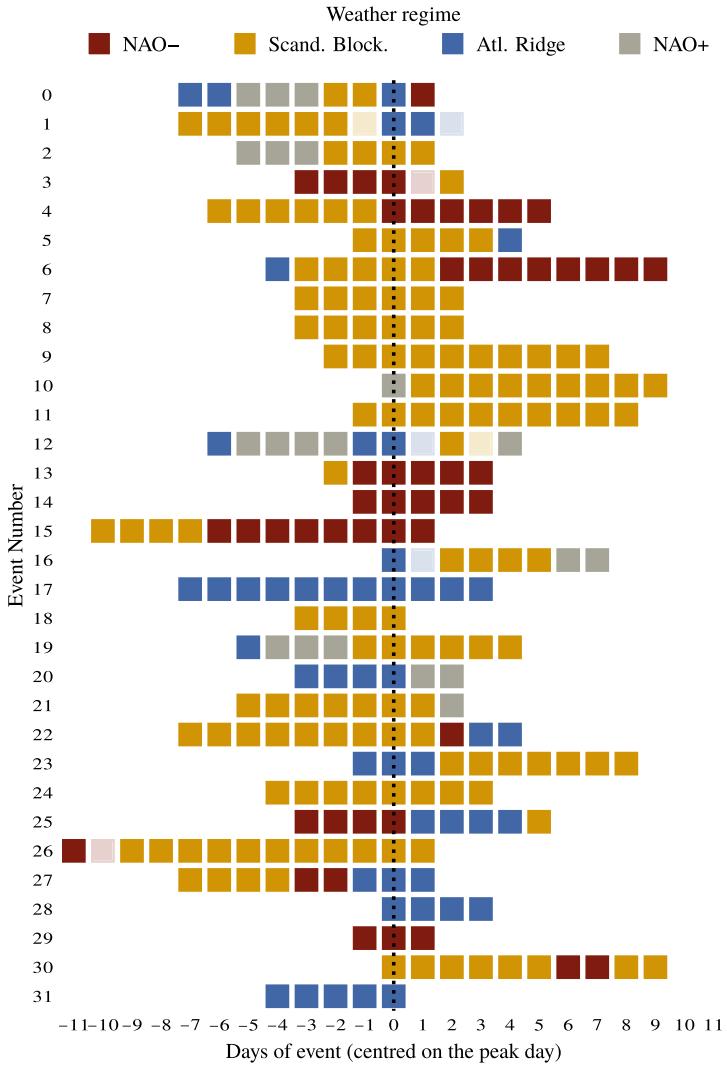

Figure 7. Daily evolution of the predominant weather regime during each system-defining event (see table S1). The events are centred around the peak day, which is the day containing the single most expensive hour of the event. If the association of a day to a weather regime is not statistically significant, it is shown with high transparency.

However, there are times where a high cost can happen in a mild winter. For instance, January 1997 (figures S12 and S13) experienced a low-wind-cold-snap driving high system costs; a very anomalous event compared to the rest of the season.

Fully modelling transmission and storage constraints can lead to a different characterisation of the most challenging winters for power system operation than seen in studies entirely based on meteorological input variables. This is particularly important when considering the sub-seasonal to seasonal prediction of extreme energy events.

3.5. Validation of system-defining events

We validate our approach through load shedding (or lost load) which is a commonly used tool to measure power system adequacy [9, 49, 53, 54]. Load shedding can be measured in dispatch optimisations of fixed power system designs, whereas capacity expansion models avoid any load shedding by design.

To validate whether system-defining events align with periods of high load shedding, we calculate for each weather year y_i the hourly average load shedding in the dispatch optimisations of the power system designs obtained from weather years $y_j, j \in \{1980/81, \ldots, 2019/20\}$ operating over year y_i (a total of 40 dispatch optimisations per weather year). See section 2.6 and supplementary materials for details. We find that all but one system-defining events overlap with the week-long periods of highest load shedding in the weather year they occurred in.

In any year, system-defining events tend to be those with high load shedding; either method can be used to identify power system stress. Crucially, both shadow prices and load shedding agree on extreme events that are different than those from approach 1 (table 1) based only on net load (figures S14–S17). This highlights yet again the importance of detailed power systems modelling (also required for computing load shedding) in identifying weather stress events.

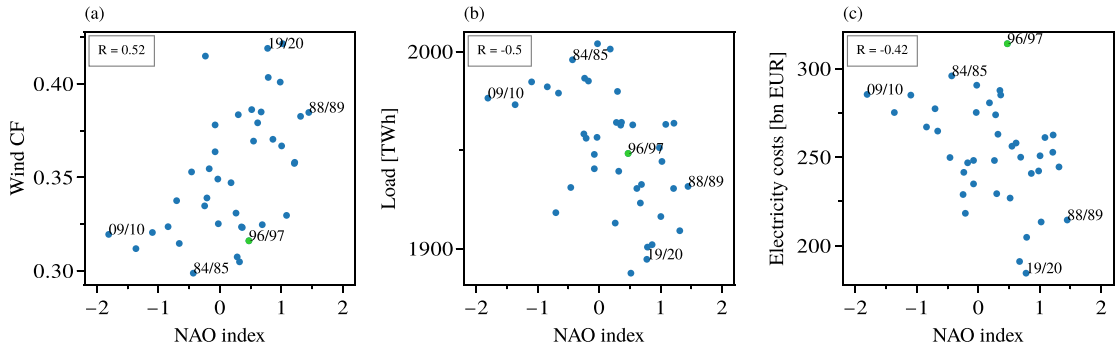

Figure 8. The relationship between October–March mean North Atlantic Oscillation (NAO) index and October–March (a) European mean onshore wind capacity factor, (b) total European net load, and (c) total costs of electricity (all between October and March). The year with the highest costs accrued between October and March (1996/97) is marked with green in (a)–(c). R values show the Pearson correlation coefficient between variables. Similar results are seen for individual countries (not shown).

Arriving at load shedding data takes an additional step (possibly on top of approach 2): first obtaining one or several system designs and *then* running them in dispatch mode to reveal load shedding. The latter approach also entails additional assumptions: one has to choose which input scenarios to use for capacity expansion steps and dispatch steps respectively.

4. Discussion & conclusions

In this study we investigate difficult weather events for power systems through an integrated approach combining meteorology with power systems modelling. To improve resilience against weather extremes, we show that it is not enough to look at meteorological variables alone (Approach 1), but we also need to include a detailed representation of future, to-be-designed energy systems (Approaches 2 and 3). We propose identifying system-defining weather periods as those being the main drivers of investments; such periods are defined by high electricity shadow prices in a power systems model. As this approach builds directly on modelling outputs, it is free of assumptions on specific characteristics of extreme events.

We find that risk factors like persistent low temperatures and low wind align well with previous literature [21, 22, 55], however, conventional meteorological analysis does not reliably identify the most severe difficult periods for future power systems. In particular, challenging periods for the integrated European network vary in duration and are characterised by transmission and storage interactions over time, not only extreme weather. We see that isolated regional studies are not good enough, as the vast majority of the continent experiences uniformly high shadow prices during all system-defining events. To reliably predict future energy system stress events traditional meteorological classifications [18, 42, 55] are not enough, and more detailed knowledge on surface weather impacts on power systems is needed [14, 49].

Since our approach is based on single-year optimisations resulting in different system designs for different weather years, electricity shadow prices and thus severity of events are not directly comparable across weather years. This limitation can be addressed by using load shedding (approach 3 in table 1) instead of electricity shadow prices to identify extreme events. However, our validation shows that the load shedding and shadow price approaches agree on the most severe events in each individual weather year. Computing load shedding is also more computationally expensive and involves more assumptions, requiring a two-step process.

Restricting our analysis to events shorter than two weeks, we capture significant fractions of total electricity cost, but do not capture the full chain of cascading compound events. A complete understanding of how seasonal weather relates to total annual system cost (beyond the partial correlation with the NAO index) is still elusive. Perfect foresight also limits the ability of our model to react realistically to multi-week or longer events. On the other hand, our analysis also does not focus on very brief events. Further analysis over a variety of event length, both longer and shorter, would be beneficial.

An interesting extension of this study would be the inclusion of sector coupling: electrification of heating strengthens the impacts of heating load and the inclusion of more sectors could lead to different dynamics than in the power sector alone. Still, low wind generation will be key in years to come due to higher penetration of renewable technologies. With ever-improving climate models, these methods could be applied to climate model projections, as system insights based on weather from the 1980s might not necessarily be transferable to mid-century systems under climate change.

The question of pinning down what makes certain weather years difficult (in terms of system costs) remains complicated and computationally expensive; the main part of investments throughout the years is driven by a few short-lived and severe events. Our classification can help meteorologists, transmission system operators and long-term system planners

to develop early warning systems and resilience strategies for these events. It is worth remembering that current systems usually struggle with high load, but that these risks and coping mechanisms will shift towards supply issues when renewable production dominates. A good understanding of the anatomy of such events will help in risk assessments including frequency and severity under climate change, crucial for ensuring system adequacy.

Our flexible approach can be applied to other contexts beyond this European case study and shows that rigid assumption-based analyses within one discipline do not suffice for challenges the world is facing. Our approach exploits inherent information from existing models and unites perspectives from linear optimisation, energy modelling, and meteorology to enhance the understanding on how more resilient future energy systems can be planned. Without interdisciplinary studies with state-of-the-art power system models and meteorological data, progress in researching and implementing renewable energy systems cannot be made.

Data availability statement

The data and the code that support the findings of this study are openly available at the following URL/DOI: https://github.com/koen-vg/stressful-weather/tree/v0. All code is open source (licensed under GPL v3.0 and MIT), and all data used are open (various licenses).

Acknowledgments

We would like to thank the anonymous reviewers for their helpful comments and suggestions.

HB is grateful for support via a Newcastle University Academic Track (NUAcT) Fellowship.

ERA5 reanalysis data [30] were downloaded from the Copernicus Climate Change Service (C3S) [56].

The results contain modified Copernicus Climate Change Service information 2020. Neither the European Commission nor ECMWF is responsible for any use that may be made of the Copernicus information or data it contains.

The computations were partly performed on the Norwegian Research and Education Cloud (NREC), using resources provided by the University of Bergen and the University of Oslo. http://www.nrec.no/.

Conflicts of interests

The authors declare no competing interests.

ORCID iDs

Aleksander Grochowicz https://orcid.org/0000-0002-1029-2858
Koen van Greevenbroek https://orcid.org/0000-0002-6105-2846
Hannah C Bloomfield https://orcid.org/0000-0002-5616-1503

References

[1] Bloomfield H C *et al* 2021 The importance of weather and climate to energy systems: a workshop on next generation challenges in energy–climate modeling *Bull. Am. Meteorol. Soc.* **102** E159–67
[2] Craig M T *et al* 2022 Overcoming the disconnect between energy system and climate modeling *Joule* **6** 1405–17
[3] Pfenninger S 2017 Dealing with multiple decades of hourly wind and PV time series in energy models: a comparison of methods to reduce time resolution and the planning implications of inter-annual variability *Appl. Energy* **197** 1–13
[4] Zeyringer M, Price J, Fais B, Li P-H and Sharp E 2018 Designing low-carbon power systems for Great Britain in 2050 that are robust to the spatiotemporal and inter-annual variability of weather *Nat. Energy* **3** 395–403
[5] Collins S, Deane P, Gallachóir B O, Pfenninger S and Staffell I 2018 Impacts of inter-annual wind and solar variations on the European power system *Joule* **2** 2076–90
[6] Schlott M, Kies A, Brown T, Schramm S and Greiner M 2018 The impact of climate change on a cost-optimal highly renewable European electricity network *Appl. Energy* **230** 1645–59
[7] Kaspar F, Borsche M, Pfeifroth U, Trentmann J, Drücke J and Becker P 2019 A climatological assessment of balancing effects and shortfall risks of photovoltaics and wind energy in Germany and Europe *Adv. Sci. Res.* **16** 119–28
[8] Hill J, Kern J, Rupp D E, Voisin N and Characklis G 2021 The effects of climate change on interregional electricity market dynamics on the U.S. West Coast *Earth's Future* **9** e2021EF002400
[9] Grochowicz A, van Greevenbroek K, Benth F E and Zeyringer M 2023 Intersecting near-optimal spaces: European power systems with more resilience to weather variability *Energy Econ.* **118** 106496
[10] Richardson D, Pitman A J and Ridder N N 2023 Climate influence on compound solar and wind droughts in Australia *npj Clim. Atmos. Sci.* **6** 184
[11] Gunn A, Dargaville R, Jakob C and McGregor S 2023 Spatial optimality and temporal variability in Australia's wind resource *Environ. Res. Lett.* **18** 114048
[12] Pfenninger S and Staffell I 2016 Long-term patterns of European PV output using 30 years of validated hourly reanalysis and satellite data *Energy* **114** 1251–65
[13] Staffell I and Pfenninger S 2016 Using bias-corrected reanalysis to simulate current and future wind power output *Energy* **114** 1224–39
[14] Bloomfield H, Brayshaw D and Charlton-Perez A 2020 ERA5 derived time series of European country-aggregate electricity demand, wind power generation and solar power generation: hourly data from 1979–2019 *IEEE Dataport* (available at: https://doi.org/10.21227/f7pt-2823)
[15] Hofmann F, Hampp J, Neumann F, Brown T and Hörsch J 2021 Atlite: a lightweight python package for calculating renewable power potentials and time series *J. Open Source Softw.* **6** 3294
[16] Staffell I, Pfenninger S and Johnson N 2023 A global model of hourly space heating and cooling demand at multiple spatial scales *Nat. Energy* **8** 1–17
[17] Bloomfield H C, Brayshaw D J, Shaffrey L C, Coker P J and Thornton H E 2018 The changing sensitivity of power systems to meteorological drivers: a case study of Great Britain *Environ. Res. Lett.* **13** 054028
[18] van der Wiel K, Stoop L P, van Zuijlen B R H, Blackport R, van den Broek M A and Selten F M 2019 Meteorological

conditions leading to extreme low variable renewable energy production and extreme high energy shortfall *Renew. Sustain. Energy Rev.* **111** 261–75
[19] Bloomfield H C, Suitters C C and Drew D R 2020 Meteorological drivers of European power system stress *J. Renew. Energy* **2020** e5481010
[20] Ruhnau O and Qvist S 2022 Storage requirements in a 100% renewable electricity system: extreme events and inter-annual variability *Environ. Res. Lett.* **17** 044018
[21] Tedesco P, Lenkoski A, Bloomfield H C and Sillmann J 2023 Gaussian copula modeling of extreme cold and weak-wind events over Europe conditioned on winter weather regimes *Environ. Res. Lett.* **18** 034008
[22] Kay G, Dunstone N J, Maidens A, Scaife A A, Smith D M, Thornton H E, Dawkins L and Belcher S E 2023 Variability in North Sea wind energy and the potential for prolonged winter wind drought *Atmos. Sci. Lett.* **24** e1158
[23] van der Most L, van der Wiel K, Benders R M J, Gerbens-Leenes P W, Kerkmans P and Bintanja R 2022 Extreme events in the European renewable power system: validation of a modeling framework to estimate renewable electricity production and demand from meteorological data *Renew. Sustain. Energy Rev.* **170** 112987
[24] Su Y, Kern J D, Reed P M and Characklis G W 2020 Compound hydrometeorological extremes across multiple timescales drive volatility in California electricity market prices and emissions *Appl. Energy* **276** 115541
[25] Otero N, Martius O, Allen S, Bloomfield H and Schaefli B 2022 Characterizing renewable energy compound events across Europe using a logistic regression-based approach *Meteorol. Appl.* **29** e2089
[26] Ziya Akdemir K Z, Kern J D and Lamontagne J 2022 Assessing risks for New England's wholesale electricity market from wind power losses during extreme winter storms *Energy* **251** 123886
[27] Wessel J, Kern J D, Voisin N, Oikonomou K and Haas J 2022 Technology pathways could help drive the U.S. West Coast Grid's exposure to hydrometeorological uncertainty *Earth's Future* **10** e2021EF002187
[28] Hörsch J and Brown T 2017 The role of spatial scale in joint optimisations of generation and transmission for European highly renewable scenarios *2017 14th Int. Conf. on the European Energy Market* (*EEM*) (*Dresden, Germany*) (IEEE) pp 1–7
[29] Schlachtberger D P, Brown T, Schramm S and Greiner M 2017 The benefits of cooperation in a highly renewable European electricity network *Energy* **134** 469–81
[30] Hersbach H *et al* 2018 ERA5 hourly data on single levels from 1940 to present (available at: https://doi.org/10.24381/cds.adbb2d47)
[31] Brown T, Hörsch J and Schlachtberger D 2018 PyPSA: Python for power system analysis *J. Open Res. Softw.* **6** 4
[32] Frysztacki M, van der Most L and Neumann F 2022 Interannual electricity demand calculator (Version 0.1.0) (Zenodo) (available at: https://doi.org/10.5281/ZENODO.7070438)
[33] Frysztacki M M, Hörsch J, Hagenmeyer V and Brown T 2021 The strong effect of network resolution on electricity system models with high shares of wind and solar *Appl. Energy* **291** 116726
[34] Victoria M, Zhu K, Brown T, Andresen G B and Greiner M 2019 The role of storage technologies throughout the decarbonisation of the sector-coupled European energy system *Energy Convers. Manage.* **201** 111977
[35] Sasse J-P and Trutnevyte E 2020 Regional impacts of electricity system transition in Central Europe until 2035 *Nat. Commun.* **11** 4972
[36] Schyska B U, Kies A, Schlott M, Von Bremen L and Medjroubi W 2021 The sensitivity of power system expansion models *Joule* **5** 2606–24
[37] Victoria M, Zhu K, Brown T, Andresen G B and Greiner M 2020 Early decarbonisation of the European energy system pays off *Nat. Commun.* **11** 6223
[38] Brown T and Reichenberg L 2021 Decreasing market value of variable renewables can be avoided by policy action *Energy Econ.* **100** 105354
[39] Victoria M, Zeyen E and Brown T 2022 Speed of technological transformations required in Europe to achieve different climate goals *Joule* **6** 1066–86
[40] Neumann F, Zeyen E, Victoria M and Brown T 2023 The potential role of a hydrogen network in Europe *Joule* **7** 1793–817
[41] Bloomfield H C, Brayshaw D J, Gonzalez P L M and Charlton-Perez A 2021 Pattern-based conditioning enhances sub-seasonal prediction skill of european national energy variables *Meteorol. Appl.* **28** e2018
[42] Cassou C 2008 Intraseasonal interaction between the Madden–Julian Oscillation and the North Atlantic Oscillation *Nature* **455** 523–7
[43] Dawson A 2016 Eofs: a library for EOF analysis of meteorological, oceanographic and climate data *J. Open Res. Softw.* **4** e14
[44] Drücke J, Borsche M, James P, Kaspar F, Pfeifroth U, Ahrens B and Trentmann J 2021 Climatological analysis of solar and wind energy in Germany using the Grosswetterlagen classification *Renew. Energy* **164** 1254–66
[45] Mockert F, Grams C M, Brown T and Neumann F 2023 Meteorological conditions during periods of low wind speed and insolation in Germany: the role of weather regimes *Meteorol. Appl.* **30** e2141
[46] van der Wiel K, Bloomfield H C, Lee R W, Stoop L P, Blackport R, Screen J A and Selten F M 2019 The influence of weather regimes on European renewable energy production and demand *Environ. Res. Lett.* **14** 094010
[47] Dvorak A J and Victoria M 2023 Key determinants of solar share in solar- and wind-driven grids *IEEE J. Photovolt.* **13** 476–83
[48] Bloomfield H C, Brayshaw D J, Troccoli A, Goodess C M, De Felice M, Dubus L, Bett P E and Saint-Drenan Y-M 2021 Quantifying the sensitivity of european power systems to energy scenarios and climate change projections *Renew. Energy* **164** 1062–75
[49] Sundar S, Craig M T, Payne A E, Brayshaw D J and Lehner F 2023 Meteorological drivers of resource adequacy failures in current and high renewable Western U.S. power systems *Nat. Commun.* **14** 6379
[50] Ely C R, Brayshaw D J, Methven J, Cox J and Pearce O 2013 Implications of the North Atlantic oscillation for a UK–Norway renewable power system *Energy Policy* **62** 1420–7
[51] Cradden L C, McDermott F, Zubiate L, Sweeney C and O'Malley M 2017 A 34 year simulation of wind generation potential for Ireland and the impact of large-scale atmospheric pressure patterns *Renew. Energy* **106** 165–76
[52] Thornton H E, Scaife A A, Hoskins B J, Brayshaw D J, Smith D M, Dunstone N, Stringer N and Bett P E 2019 Skilful seasonal prediction of winter gas demand *Environ. Res. Lett.* **14** 024009
[53] Schröder T and Kuckshinrichs W 2015 Value of lost load: an efficient economic indicator for power supply security? A literature review *Front. Energy Res.* **3** 55
[54] Antonini E G A, Ruggles T H, Farnham D J and Caldeira K 2022 The quantity-quality transition in the value of expanding wind and solar power generation *iScience* **25** 104140
[55] Grams C M, Beerli R, Pfenninger S, Staffell I and Wernli H 2017 Balancing Europe's wind-power output through spatial deployment informed by weather regimes *Nat. Clim. Change* **7** 557–62
[56] Copernicus Climate Change Service (C3S) 2023 ERA5 hourly data on single levels from 1940 to present (available at: https://doi.org/10.24381/cds.adbb2d47)

A Additional methodological details

A.1 Energy system optimisation models and dual variables

Many energy system optimisation models (such as PyPSA-Eur) are formulated as a linear program, which means they have a linear objective and linear constraints:

$$\min_{x \in \mathbb{R}^N} c^T \cdot x \text{ s.t. } Ax \leq b, x \geq 0$$
$$A \in \mathbb{R}^{M \times N}, b \in \mathbb{R}^M, c \in \mathbb{R}^N, \text{for } M, N \in \mathbb{N}.$$

This formulation gives rise to a dual problem

$$\max_{y \in \mathbb{R}^M} b^T \cdot y \text{ s.t. } A^T y \geq c, y \geq 0$$
$$A \in \mathbb{R}^{M \times N}, b \in \mathbb{R}^M, c \in \mathbb{R}^N, \text{for } M, N \in \mathbb{N}.$$

We are interested in the dual variables that stem from the nodal energy balance constraints for every time step t and node n; equation (12) in Brown et al. [1]. These constraints ensure that supply meets a given inelastic electricity demand at each hour and node, and following Brown et al. [1] we denote their respective dual variables $\lambda_{n,t}$ (also known as marginal or shadow prices). By definition, $\lambda_{n,t}$ is the rate of change of the objective function, here total system costs, with respect to demand at node n and time t. More usefully, $\lambda_{n,t}$ (given in EUR / MWh) can be interpreted as the marginal electricity price at each node and time step. Letting $d_{n,t}$ be electricity demand, $d_{n,t} \cdot \lambda_{n,t}$ is the cost of satisfying electricity load at node n and hour t. It follows that $\sum_{n,t} d_{n,t} \cdot \lambda_{n,t}$ is the total cost of electricity over the entire modelling horizon.

It should be noted that the marginal prices $\lambda_{n,t}$ typically do not follow the same profile as real electricity market prices; this is due to the inclusion of capacity expansion in our model. This leads $\lambda_{n,t}$ to not only be driven by marginal operating costs of power plants, as in free electricity markets, but mainly by conditions triggering investments. Thus, the shadow prices $\lambda_{n,t}$ typically stay very low most of the type, and increase drastically during periods necessitating additional investment in generation, storage and transmission capacity. Nonetheless, $\sum_{n,t} d_{n,t}\lambda_{n,t} / \sum_{n,t} d_{n,t}$ gives a good indication of the system-average electricity price resulting from the model.

In a simple greenfield capacity expansion model, with no included existing infrastructure, the total cost of electricity $\sum_{n,t} d_{n,t}\lambda_{n,t}$ (plus the shadow cost of emissions in case of a global emission constraint) is equal to the objective value of the optimisation problem; this following from strong duality for linear programs. Since our model includes existing transmission, hydropower, nuclear and biomass generation infrastructure whose costs are not included in the objective function, the objective value is lower than the total electricity cost. Still, $\sum_{n,t} d_{n,t}$ is a good indicator for total system cost.

A.2 Transmission congestion and value of stored energy

For each transmission line l, the electricity flow $f_{l,t}$ over that line at time t is subject to the constraints $f_{l,t} \geq -F_l$ and $f_{l,t} \leq F_l$ where F_l is the capacity of the line in MW and the sign determines the direction of the flow. The dual variables $\mu_{l,t}^{\text{lower}}$ and $\mu_{l,t}^{\text{upper}}$ to these constraints are called the shadow prices of congestion. The capacity-weighted sum $\sum_l (\mu_{l,t}^{\text{lower}} + \mu_{l,t}^{\text{upper}}) F_l$ is the congestion rent of the network, and equal to the surplus gained by the transmission grid at time t [2]. This way we can judge whether certain periods are determining in the transmission expansion decisions.

Similarly, constraints preserving the state of charge from one hour to the next give rise to dual variables which can be interpreted as the marginal value of stored energy, with each storage unit discharging if and only if its value of stored energy is below the marginal price of electricity at the network node it is connected to [3, 4]. It should be noted that these considerations can be a useful indicator for locating crucial regions.

A.3 Selection of system-defining events

Recall that an event starting at t_0 and lasting for T hours is considered system-defining if

$$\sum_n \sum_{t=t_0}^{t_0+T-1} d_{n,t} \cdot \lambda_{n,t} \geq C \tag{1}$$

for $C = 100$ bn EUR and $T \leq 336$ (the number of hours in two weeks).

A priori, many overlapping time periods of the same or different lengths can attain the above thresholds. For example, if the period $[t_0, t_1]$ is system-defining and strictly shorter than two weeks, then $[t_0, t_1 + 1]$ is also system-defining. For the purposes of this study, we select a disjoint subset of all system-defining events. In particular, we build up the subset iteratively by going through system-defining events from shorter to longer events (and in decreasing order of total electricity cost for events of the same length), and only adding each event to the selected subset if it does not overlap with previously

selected events. This corresponds to imposing a partial order on all system-defining events by defining $e_1 < e_2$ if and only if e_1 and e_2 overlap and e_1 is shorter than e_2 or, if of the same length, is more expensive; our selected subset consists of the minimal elements of the resulting partially ordered set.

As a final step, we extend the selected events on either side as long as this does not decrease event-average hourly electricity cost. Thus, for the left side of each event, we extend from $[t_0, t_1]$ to $[t_0 - 1, t_1]$ as long as

$$\frac{1}{t_1 - t_0} \sum_n \sum_{t=t_0}^{t_1} d_{n,t} \cdot \lambda_{n,t} \leq \frac{1}{t_1 - (t_0 - 1)} \sum_n \sum_{t=t_0-1}^{t_1} d_{n,t} \cdot \lambda_{n,t}. \tag{2}$$

The right side of the events is extended similarly.

A.4 Validation using load shedding

To compute load shedding profiles to compare to shadow prices, we fix system designs D_j, each obtained by a capacity expansion based on a weather year y_j, $j \in \{1980/81, \ldots, 2019/20\}$ (preserving winters from July – June), and optimise the dispatch of D_j year-by-year with all weather years $y_i, i \in \{1980/81, \ldots, 2019/20\}$. The forty initial optimisations lead to different electricity networks with large discrepancies in total system costs (as in Grochowicz et al. [5]) and are often inadequate for weather conditions that are not represented in the inputs. Keeping the capacities of D_j fixed, we add an artificial generator at each node n which can supply electricity at very high variable (and no capital) costs if demand cannot be met any other way. The power supplied by this artificial generator, $g^j_{n,t}$ can be interpreted as load shedding and quantifies the extent and times during which the system fails to meet demand.

For each weather year y_i, we compute the average load shedding $\bar{\ell}_t$ across all 40 system designs D_j (although D_i cannot have any load shedding for y_i by the model formulation), thus obtaining values for each time step between July 1980 and June 2020:

$$\bar{\ell}_t = \frac{1}{40} \sum_j \sum_n g^j_{n,t}, \tag{3}$$

where $g^j_{n,t}$ is the load shedding at node n when the system design D_j is operated at time t.

One advantage of using load shedding over electricity shadow prices is that latter may suffer from "overshadowing" effects. Since shadow prices indicate events triggering investment, one event might overshadow another in the same weather year if one is slightly more severe than the other but similar otherwise, thus triggering investments (leading to high shadow prices) that render the second event benign. We see limited evidence of this in Fig. S16 (comparing electricity shadow prices and load shedding), but shadow prices and load shedding match well for the most severe events (Figs. S12–15).

B Additional figures

B.1 Inter-annual variability of investment decisions

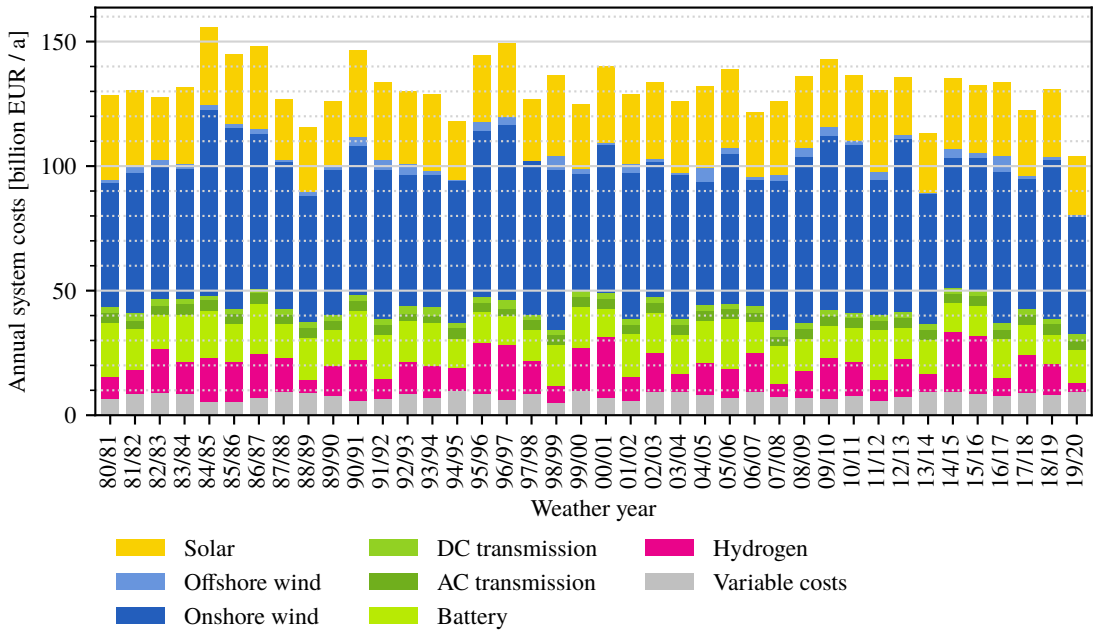

Figure S1: Annualised total system costs of optimal system designs across 40 different weather years after [5]. All costs are in 2013 EUR.

B.2 Duration and cost of system-defining events

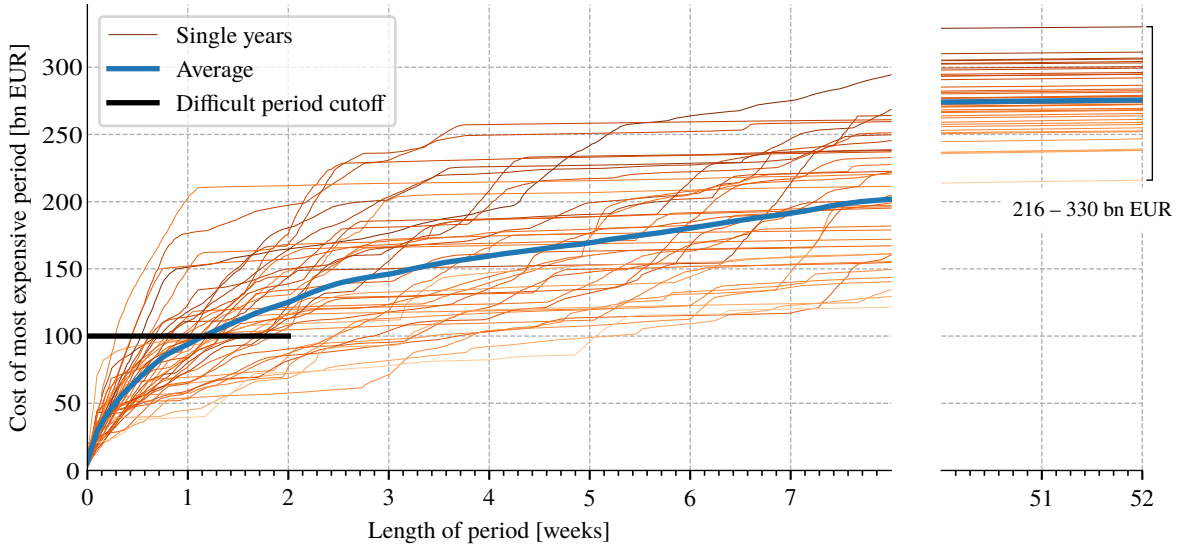

Figure S2: Total electricity costs of most expensive contiguous periods as a function of period length across different weather years. For instance, the vertical slice of the graph at $x = 1$ week shows that the single most expensive week ranges in cost between about 40 and 200 bn EUR. The thick black line segment shows the cutoff that was used to identify system-defining events: periods of at most 2 weeks having a total electricity cost of at least 100 bn EUR. The weather years without system-defining events correspond to the curves that do not intersect the cutoff line. Note that the cutoff line on this graph cannot be used to identify multiple system-defining events in the same weather year.

B.3 System-defining events across different years

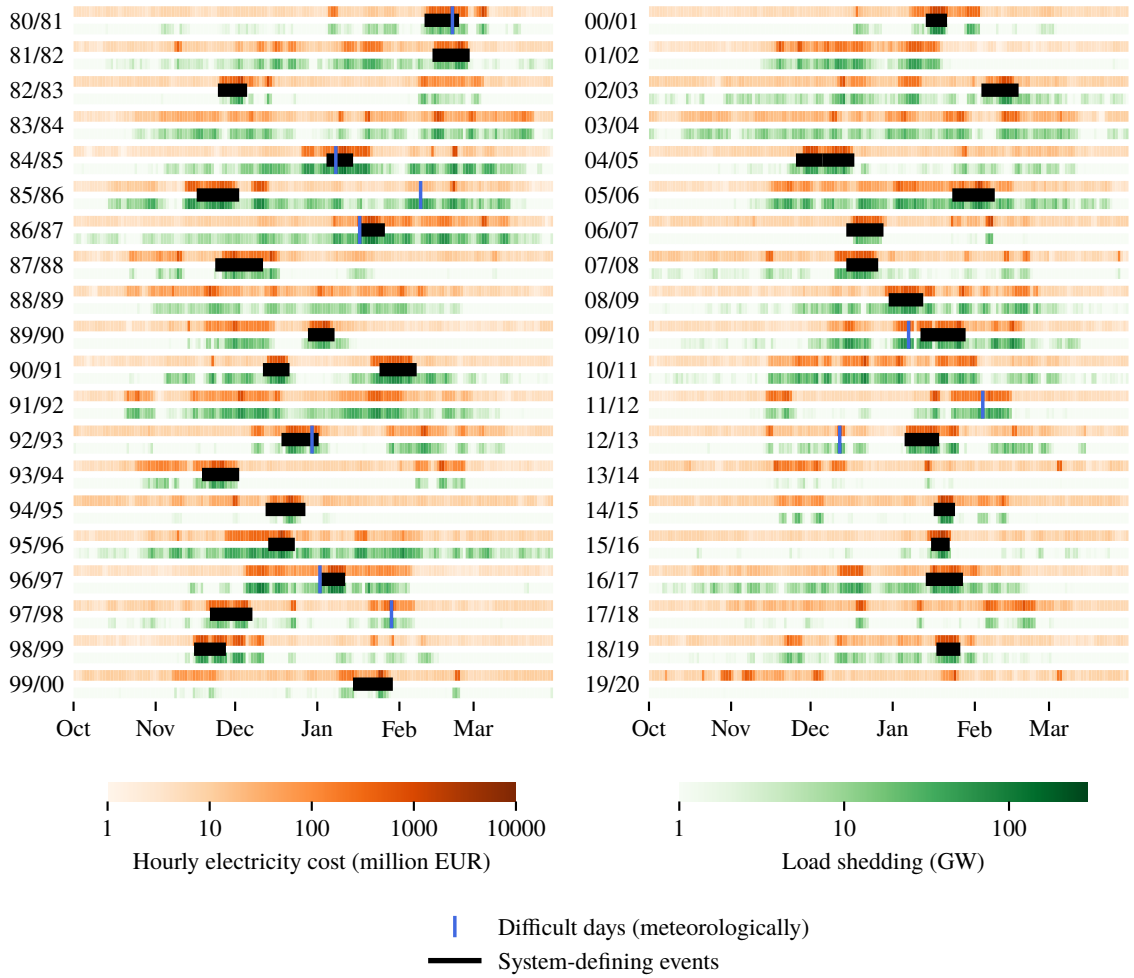

Figure S3: An overview over all identified system-defining events in the context of daily system cost. Apart from the costs we also plot average load shedding (as in Methods). The marked "difficult days" are from [6]. Only winter months are shown as shadow prices are consistently low during the summer. All costs are in 2013 EUR.

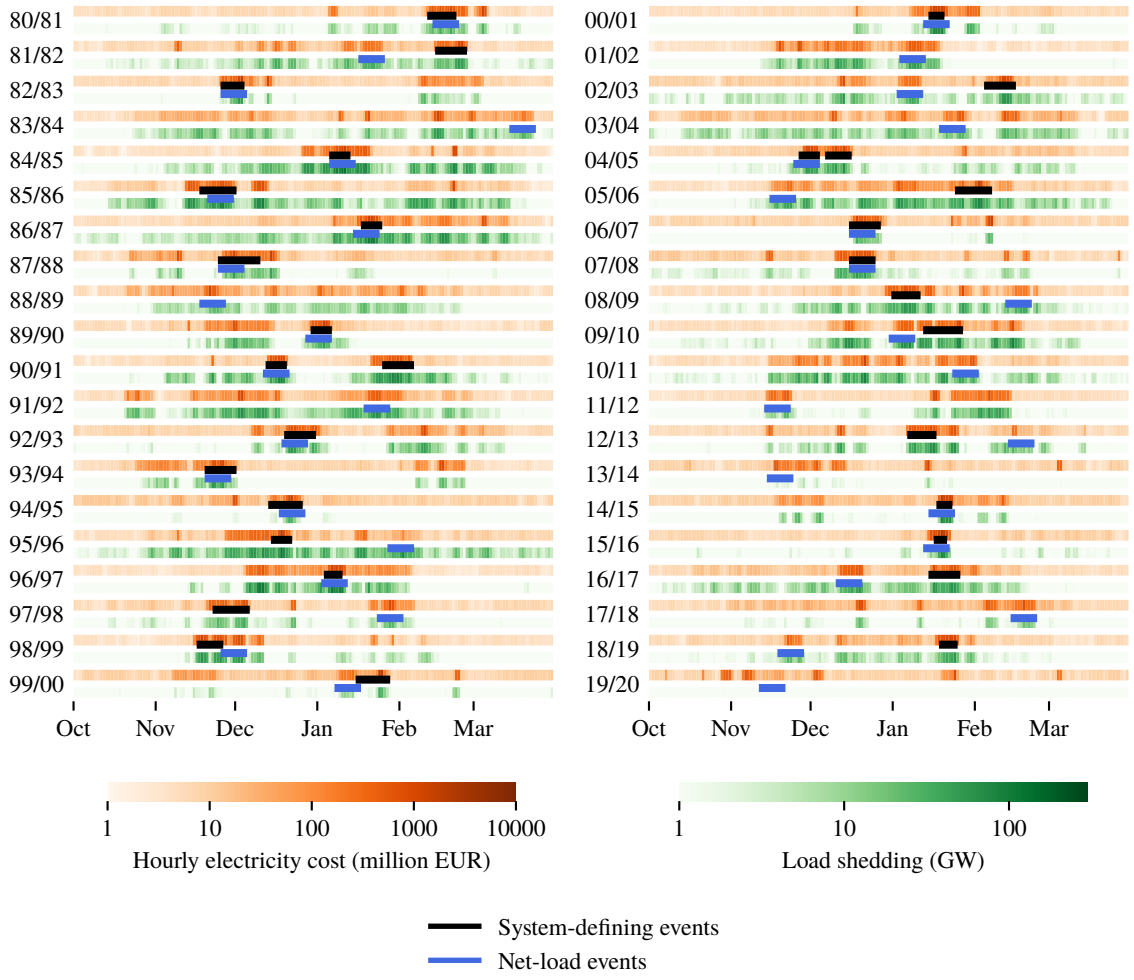

Figure S4: An overview over all identified system-defining events in the context of daily system cost. Apart from the costs we also plot average load shedding (as in Methods). Additionally the week with the highest net load for each year is marked (Approach 1 in Table 1). Only winter months are shown as shadow prices are consistently low during the summer. All costs are in 2013 EUR.

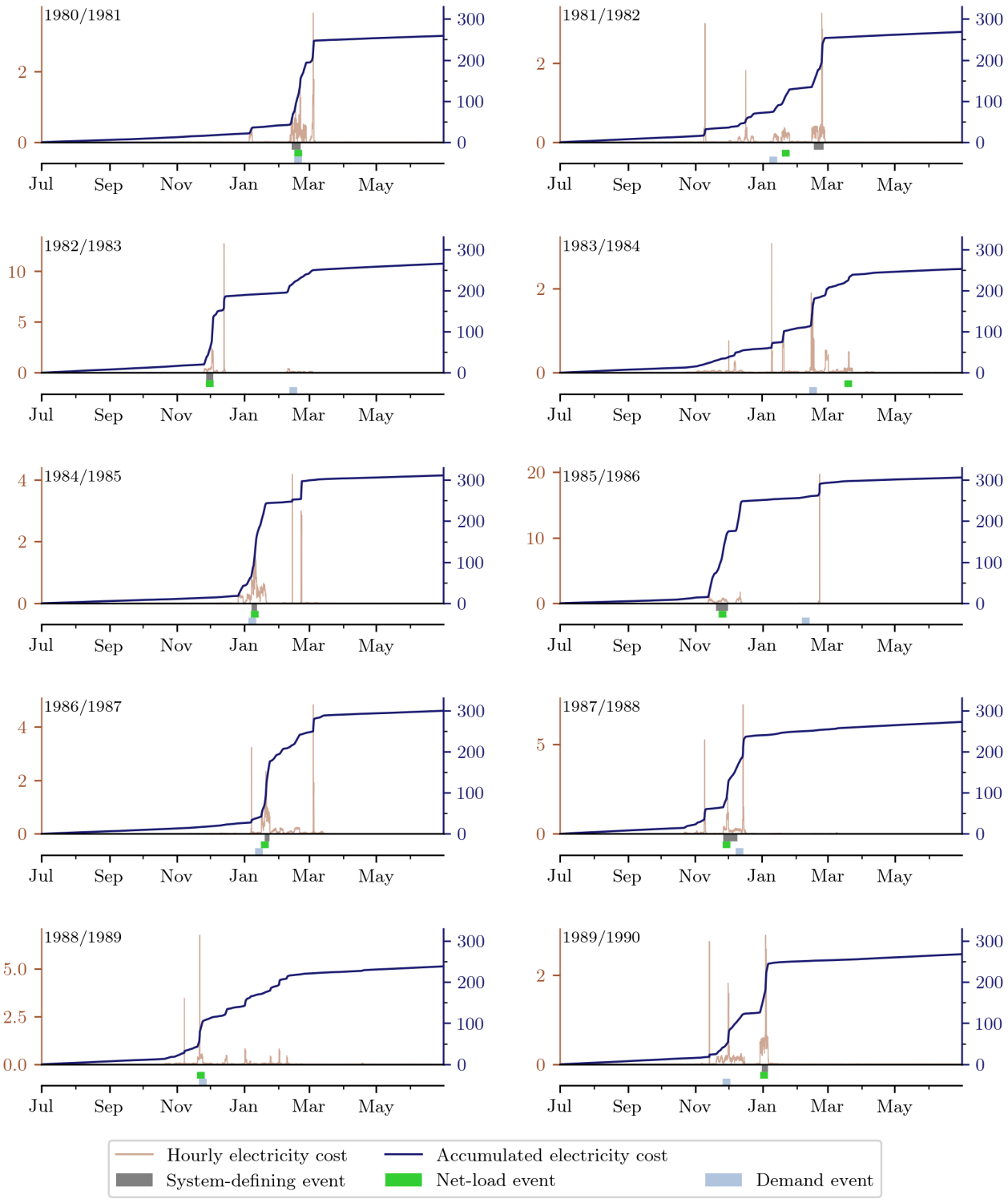

Figure S5: Hourly and accumulated electricity costs across the weather years 1980–1990. System-defining events are marked along with two weather input-based filters: for each year the week with the highest electricity load ("Demand") and the week with the largest mismatch between electricity load and renewable production ("net load"). All values in bn EUR (2013).

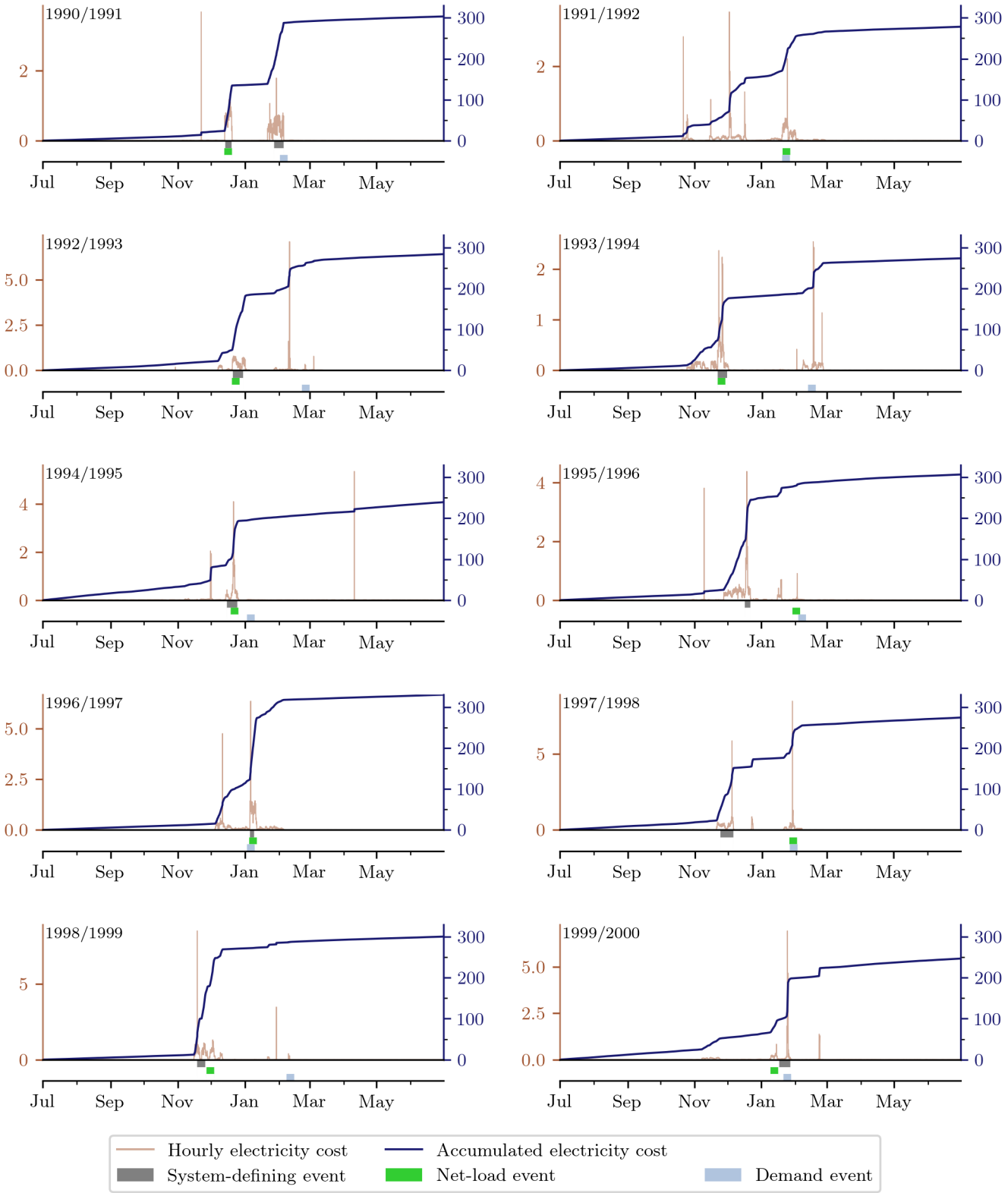

Figure S6: Hourly and accumulated electricity costs across the weather years 1990–2000. System-defining events are marked along with two weather input-based filters: for each year the week with the highest electricity load ("Demand") and the week with the largest mismatch between electricity load and renewable production ("net load"). All values in bn EUR (2013).

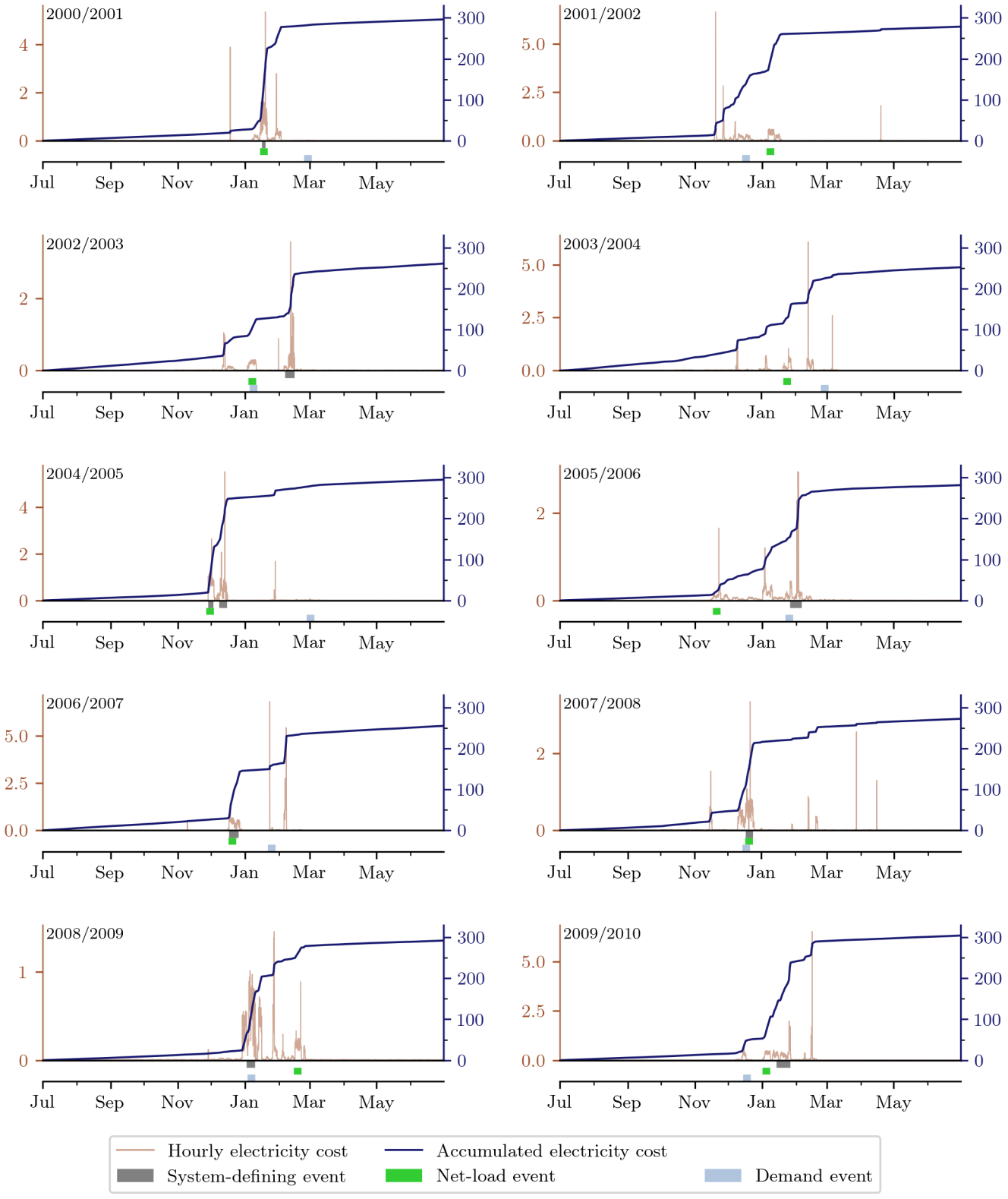

Figure S7: Hourly and accumulated electricity costs across the weather years 2000–2010. System-defining events are marked along with two weather input-based filters: for each year the week with the highest electricity load ("Demand") and the week with the largest mismatch between electricity load and renewable production ("net load"). All values in bn EUR (2013).

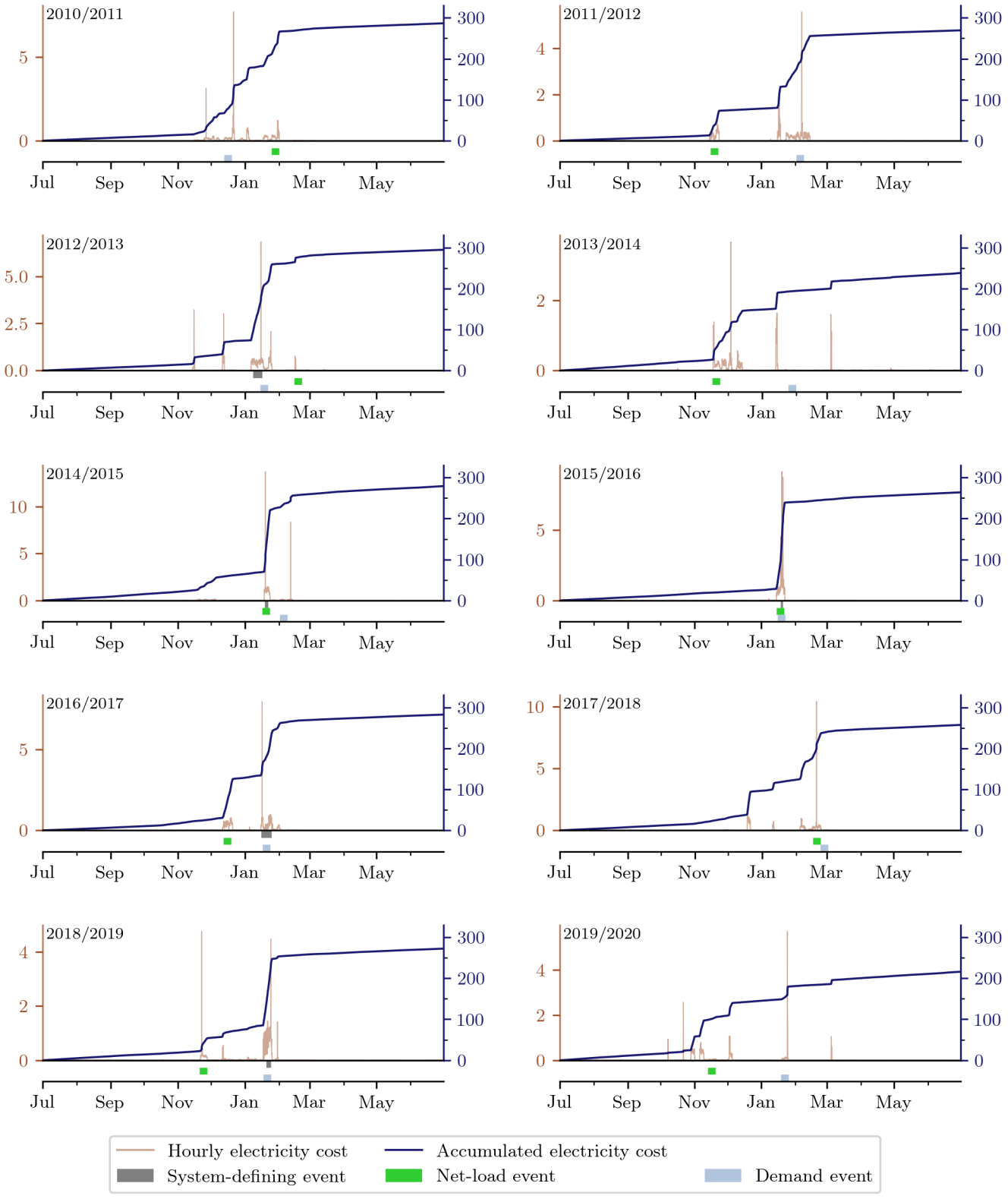

Figure S8: Hourly and accumulated electricity costs across the weather years 2010–2020. System-defining events are marked along with two weather input-based filters: for each year the week with the highest electricity load ("Demand") and the week with the largest mismatch between electricity load and renewable production ("net load"). All values in bn EUR (2013).

B.4 Key metrics for the system-defining events

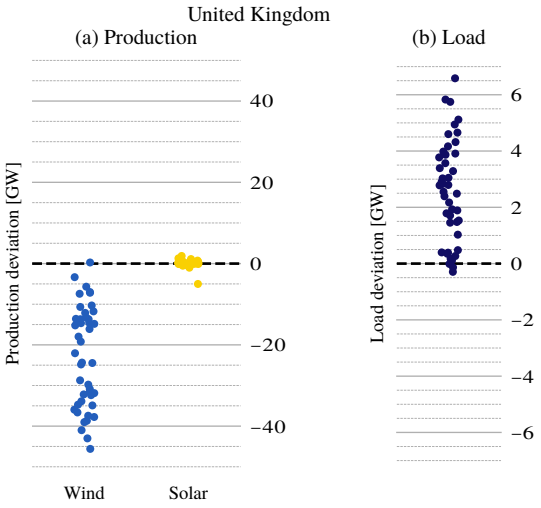

Figure S9: A summary of key metrics for the United Kingdom compared to 40-year means. Each dot represents the mean value of the metric in question over one system-defining event. From left to right: (a) renewable production deviation from 40-year mean at the time of each event, (b) load deviation from 40-year mean at the time of each event.

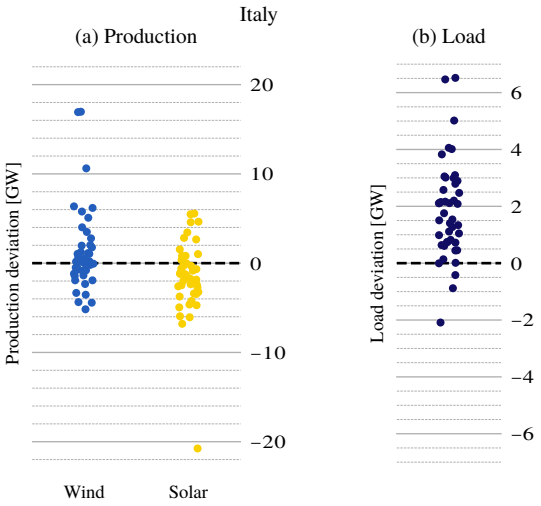

Figure S10: A summary of key metrics for Italy compared to 40-year means. Each dot represents the mean value of the metric in question over one system-defining event. From left to right: (a) renewable production deviation from 40-year mean at the time of each event, (b) load deviation from 40-year mean at the time of each event.

Start	End	Wind anom. [GW]	Solar anom. [GW]	Load anom. [GW]	Transmission [EUR/MW]	Hydrogen [EUR/MWh]	Battery [EUR/MWh]	Hydro [EUR/MWh]
1981-02-13 04:00	1981-02-21 08:00	-93.9	14.8	34.4	22.3	587.2	1102.1	18.2
1982-02-16 12:00	1982-02-25 10:00	-81.4	-3.5	26.5	31.3	359.5	983.0	15.6
1982-11-27 12:00	1982-12-03 23:00	-87.1	-5.1	21.9	36.5	390.1	1329.8	18.1
1985-01-07 16:00	1985-01-12 17:00	-138.4	25.2	78.7	48.5	610.0	1582.3	19.8
1985-11-19 16:00	1985-11-30 15:00	-100.2	-3.1	48.7	23.8	553.5	799.5	6.1
1987-01-19 16:00	1987-01-24 01:00	-137.6	9.6	52.2	49.7	707.4	1885.4	38.6
1987-11-26 15:00	1987-12-09 13:00	-54.1	-4.4	20.7	24.3	297.3	692.5	12.2
1989-12-31 06:00	1990-01-05 21:00	-109.7	18.9	8.9	52.7	545.9	1561.2	20.4
1990-12-14 04:00	1990-12-19 22:00	-132.3	11.3	28.7	48.9	702.5	1493.6	6.1
1991-01-27 16:00	1991-02-05 08:00	-121.3	18.6	36.4	23.6	597.3	1020.7	20.5
1992-12-21 02:00	1992-12-30 10:00	-76.5	7.3	-2.0	34.6	625.2	1003.7	28.3
1993-11-21 16:00	1993-11-30 06:00	-37.7	8.0	50.8	46.5	297.9	992.7	14.0
1994-12-15 16:00	1994-12-25 03:00	-25.9	1.7	10.4	65.9	218.1	822.4	15.2
1995-12-16 20:00	1995-12-21 21:00	-121.5	-8.6	17.8	62.5	391.6	1527.4	24.1
1997-01-05 16:00	1997-01-09 10:00	-122.8	-11.4	45.3	64.1	982.9	2121.7	19.1
1997-11-24 04:00	1997-12-05 23:00	-56.5	-8.7	20.8	45.3	444.8	689.2	15.1
1998-11-18 13:00	1998-11-25 23:00	-56.7	20.9	54.5	46.0	752.4	1083.4	16.2
2000-01-17 06:00	2000-01-27 09:00	10.3	10.5	23.5	37.4	122.6	706.4	5.0
2001-01-16 15:00	2001-01-19 20:00	-124.3	7.8	38.5	76.0	1333.8	2702.0	45.8
2003-02-06 17:00	2003-02-15 07:00	-91.1	9.5	18.8	24.5	304.5	991.8	3.9
2004-11-28 16:00	2004-12-03 09:00	-90.4	-18.8	20.9	60.1	868.4	1785.0	34.1
2004-12-08 16:00	2004-12-15 20:00	-71.0	26.0	14.9	71.2	683.1	1343.6	28.1
2006-01-26 15:00	2006-02-06 06:00	-112.6	8.2	18.0	26.2	188.2	740.4	33.5
2006-12-17 15:00	2006-12-26 09:00	-64.7	4.0	1.6	42.3	527.5	1065.7	18.8
2007-12-17 16:00	2007-12-24 08:00	-75.1	15.6	24.7	82.4	622.4	1383.0	29.5
2009-01-02 15:00	2009-01-10 08:00	-82.9	0.8	34.5	59.9	588.2	1217.3	20.7
2010-01-14 06:00	2010-01-26 21:00	-82.5	-3.6	14.1	31.0	379.0	680.3	12.8
2013-01-08 14:00	2013-01-16 23:00	-102.3	-6.3	16.3	50.0	562.6	905.4	19.5
2015-01-19 06:00	2015-01-22 09:00	-108.7	-11.1	30.6	89.2	1080.6	2386.3	42.9
2016-01-18 16:00	2016-01-20 17:00	-131.9	15.0	55.9	89.6	916.2	3591.0	12.1
2017-01-16 01:00	2017-01-25 10:00	-76.2	18.7	26.4	57.6	394.7	822.4	22.3
2019-01-20 15:00	2019-01-24 21:00	-85.5	0.6	37.1	100.7	970.2	1929.0	38.4

Table S1: Key metrics for all identified system-defining events. The anomalies (to the mean for 1980–2020) for wind power production, solar production, and load are hourly averages in GW, and the values for transmission and the different storage technologies are hourly averages for shadow prices of congestion (in EUR/MW) and value of stored energy (in EUR/MWh).

B.5 Examples of a system-defining event

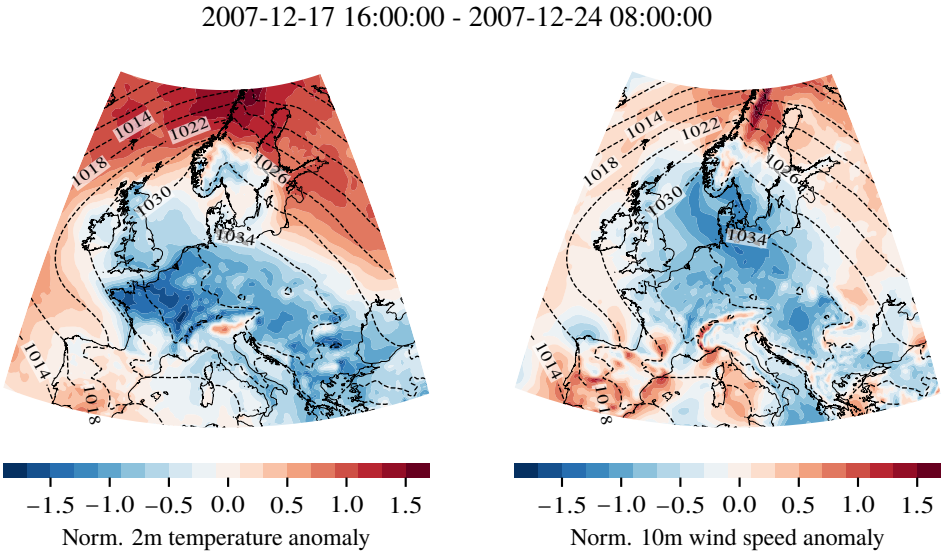

Figure S11: Average weather in Europe over the example event in 2007. Note the temperature anomalies in Central Europe and in particular wind speed anomalies over the North Sea region.

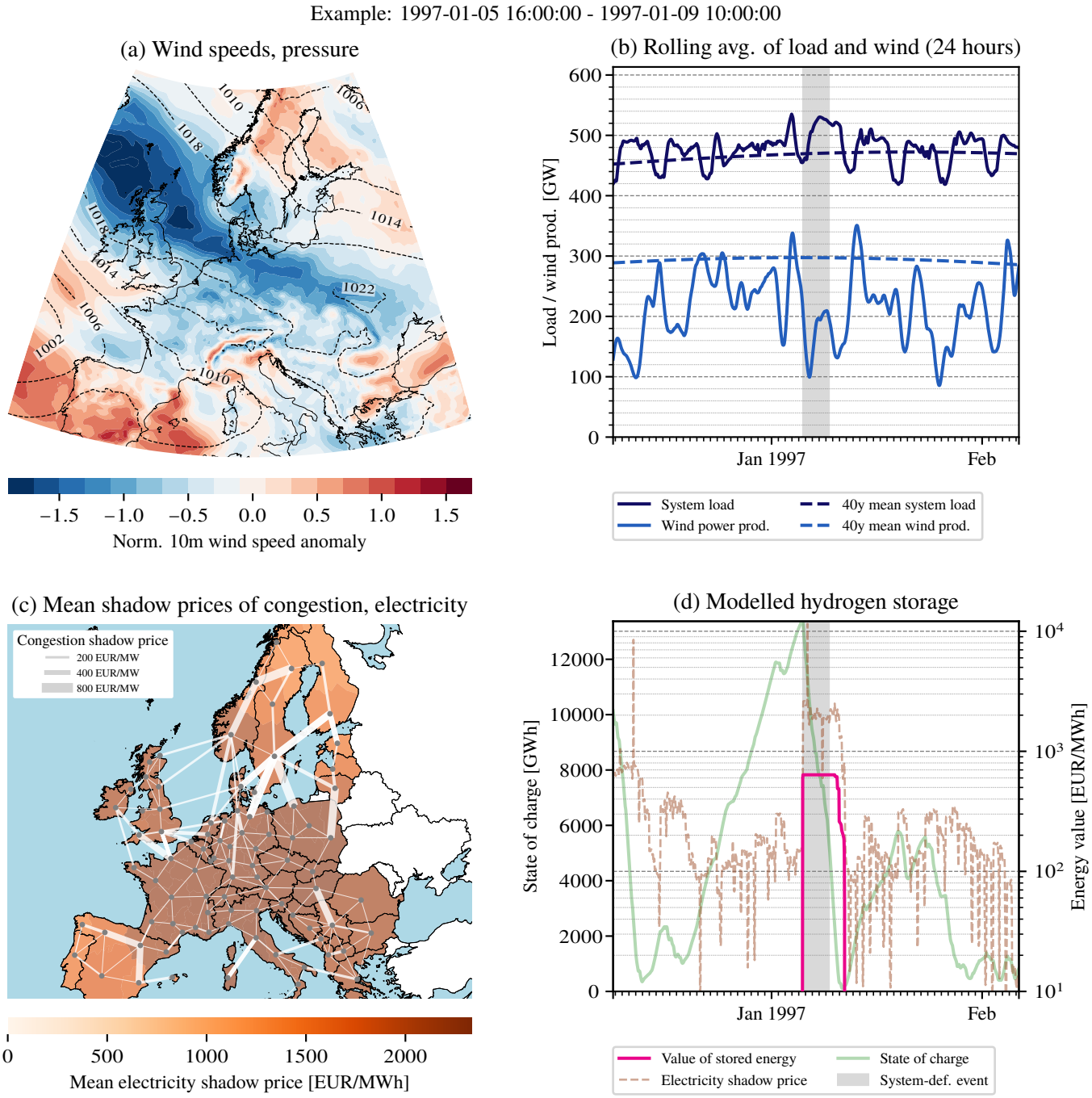

Figure S12: Inputs in the top row, comparable to a usual meteorological approach. System variables in the bottom row. (a) Average weather in Europe over the example event. Note the wind speed anomalies over the North Sea region and the temperature anomalies in Central Europe in Figure S11. (b) Time series of wind power production and electricity load around the highlighted system-defining event (smoothed with rolling averages of 24 hours). The dashed lines show seasonality deduced from the period 1980–2020. (c) Network map of the European power system with the edge widths showing shadow prices of congestion and the regions shaded with the average electricity price during the event. (d) Time series of electricity prices, value of hydrogen storage (with logarithmic scales), and the hydrogen storage level around the highlighted system-defining event.

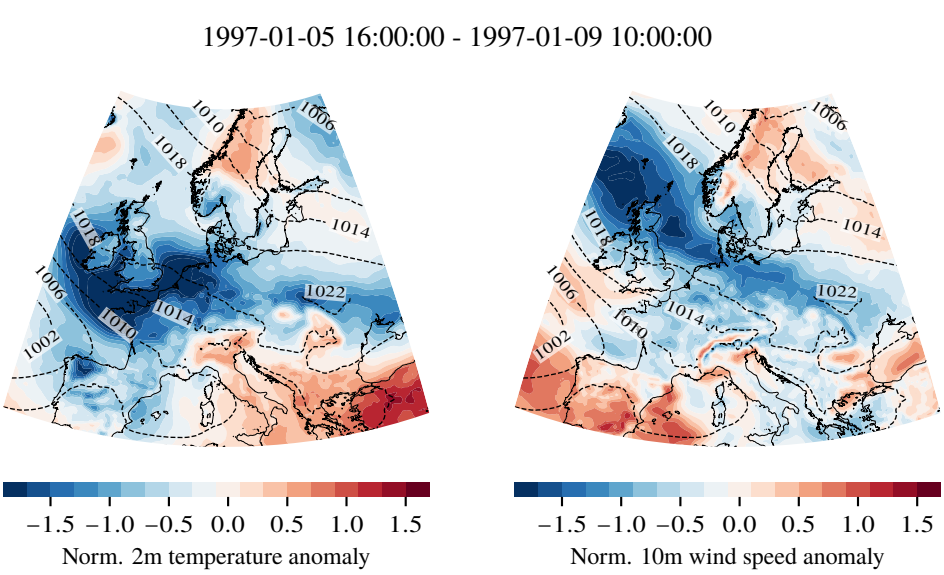

Figure S13: Average weather in Europe over the example event in January 1997.

B.6 Load shedding provides an alternative method to shadow prices

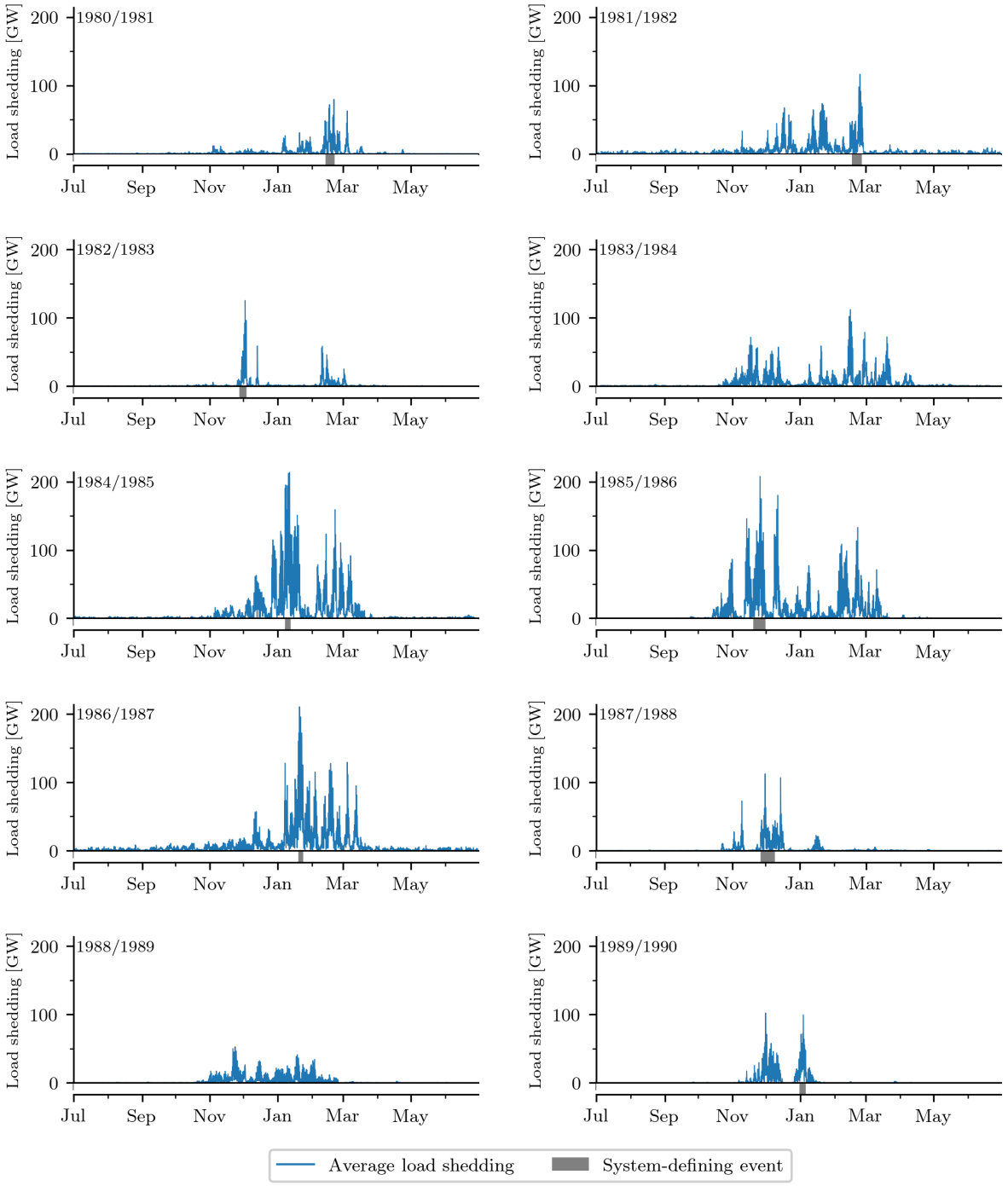

Figure S14: Average load shedding (across all networks) for the weather years 1980–1990. System-defining events are marked.

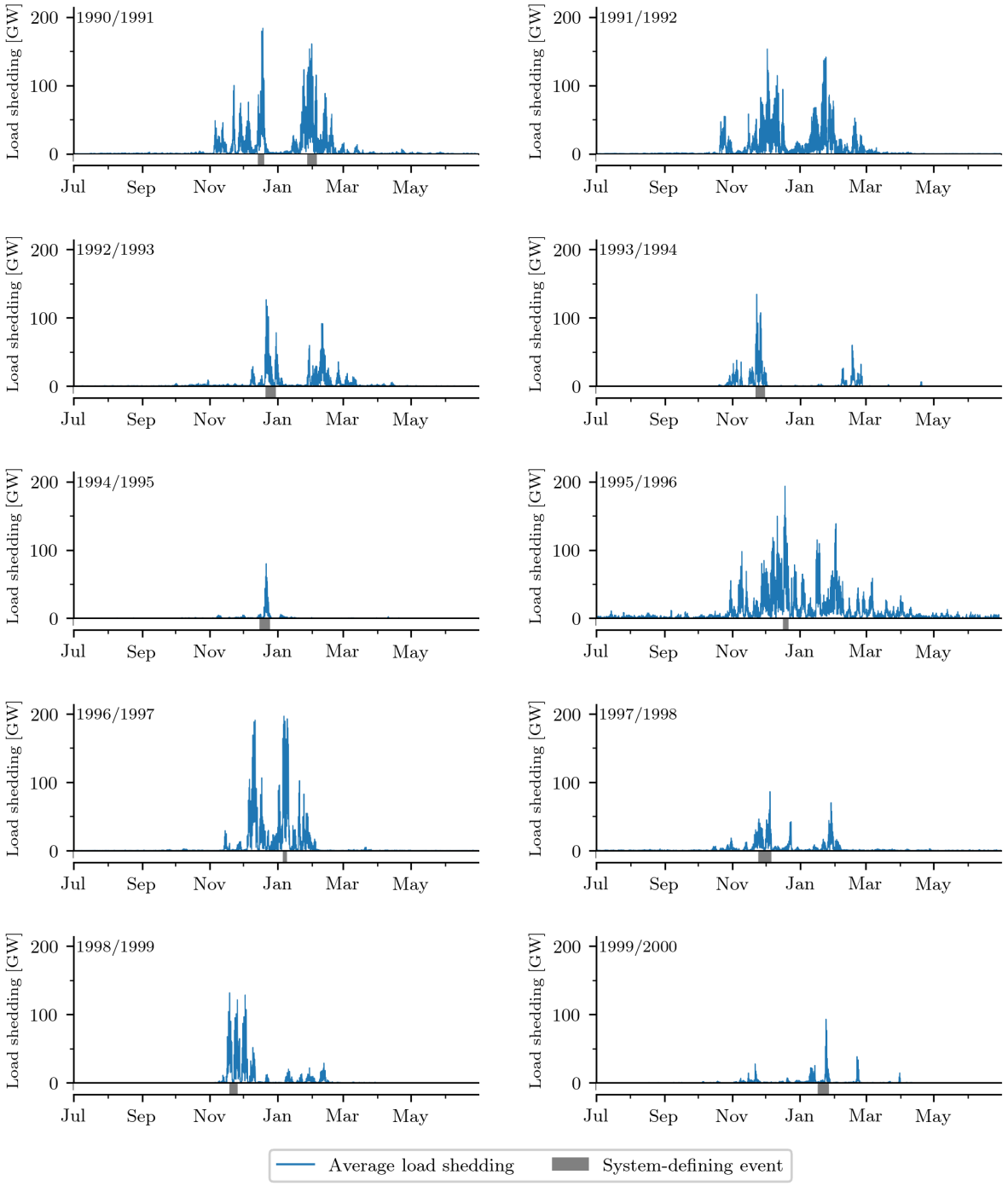

Figure S15: Average load shedding (across all networks) for the weather years 1990–2000. System-defining events are marked.

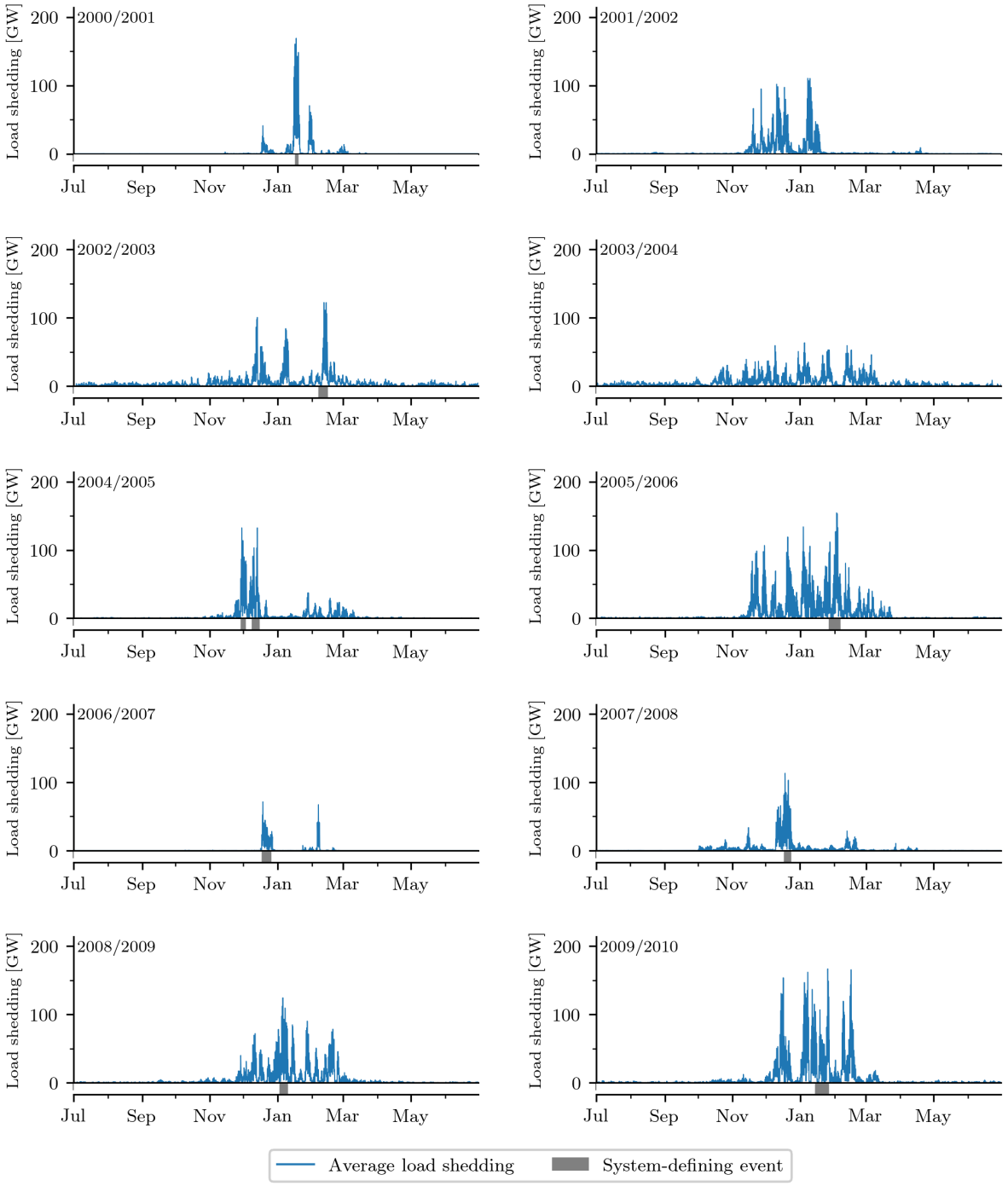

Figure S16: Average load shedding (across all networks) for the weather years 2000–2010. System-defining events are marked.

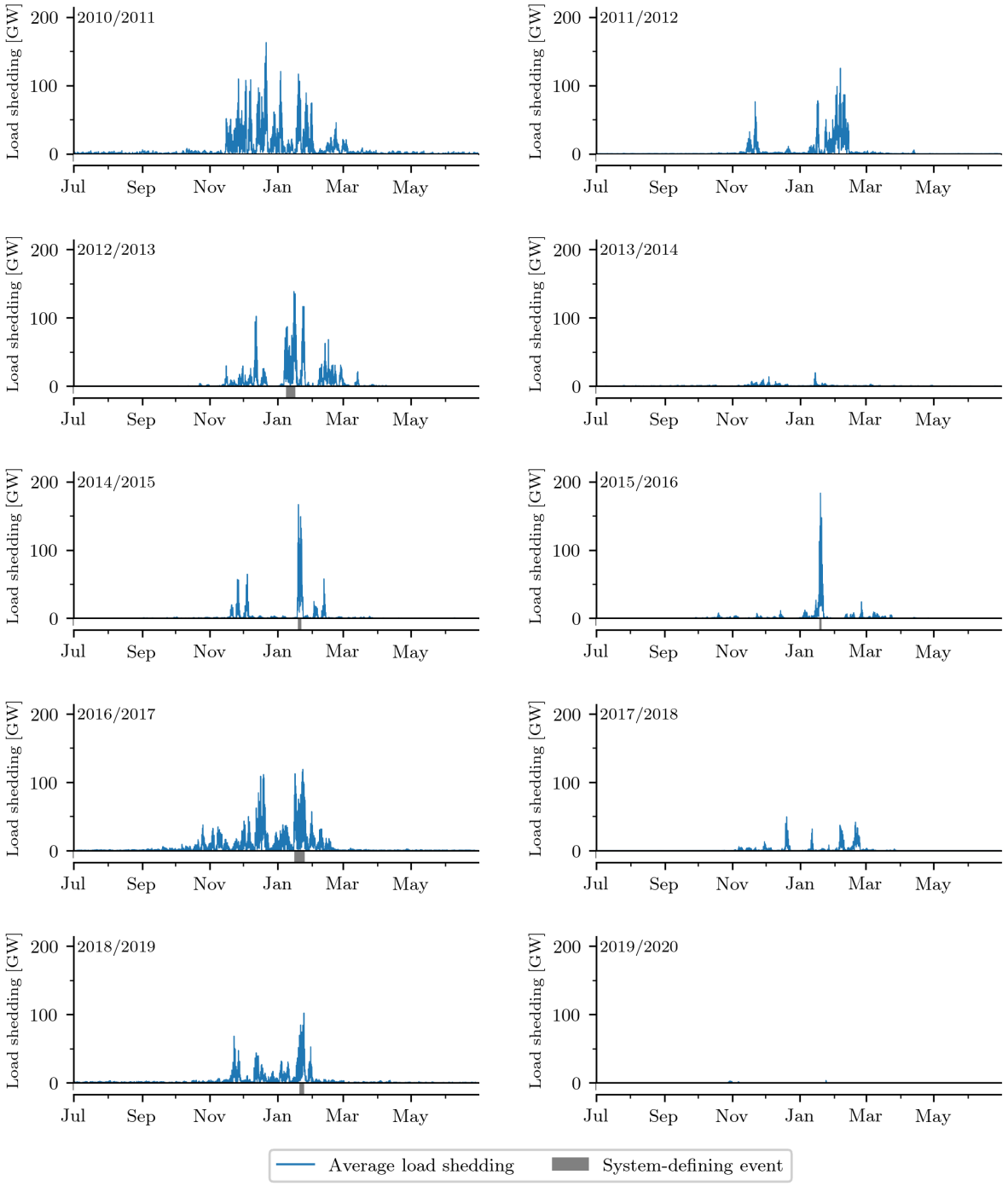

Figure S17: Average load shedding (across all networks) for the weather years 2010–2020. System-defining events are marked.

References

[1] Brown, T., Hörsch, J. & Schlachtberger, D. PyPSA: Python for Power System Analysis. *Journal of Open Research Software* **6**, 4 (2018).

[2] Biggar, D. R. & Hesamzadeh, M. R. (eds.) *The Economics of Electricity Markets* (John Wiley & Sons Ltd, Chichester, United Kingdom, 2014).

[3] Crampes, C. & Trochet, J.-M. Economics of stationary electricity storage with various charge and discharge durations. *Journal of Energy Storage* **24**, 100746 (2019).

[4] Williams, O. & Green, R. Electricity storage and market power. *Energy Policy* **164**, 112872 (2022).

[5] Grochowicz, A., van Greevenbroek, K., Benth, F. E. & Zeyringer, M. Intersecting near-optimal spaces: European power systems with more resilience to weather variability. *Energy Economics* **118**, 106496 (2023).

[6] Bloomfield, H. C., Suitters, C. C. & Drew, D. R. Meteorological Drivers of European Power System Stress. *Journal of Renewable Energy* **2020**, e5481010 (2020).

Article 3: “Trade-offs”

K. van Greevenbroek *et al.* «Enabling agency: Trade-offs between regional and integrated energy systems design flexibility.» arXiv: 2312.11264 [cs, eess, math]. (Dec. 18, 2023), pre-published

Trade-offs between regional and continental energy system design flexibility

Koen van Greevenbroek*†[1], Aleksander Grochowicz*[2], Marianne Zeyringer[3], and Fred Espen Benth[2]

[1]*Department of Computer Science, UiT The Arctic University of Norway, Postboks 6050 Langnes, 9037 Tromsø, Norway*
[2]*Department of Mathematics, University of Oslo, P.O. Box 1053 Blindern, 0316 Oslo, Norway*
[3]*Department of Technology Systems, University of Oslo, P.O. Box 70, 2027 Kjeller, Norway*

14th June 2024

Abstract

European countries have many alternatives to reach carbon neutrality by 2050. We use novel near-optimal modelling techniques illuminating trade-offs and interactions between national and continental energy transitions under uncertainty. Our results reveal extensive and robust flexibility at a regional level, few truly indispensable technologies (solar around the Adriatic and wind on the British Isles and in Germany) and variance of energy balance around the North and Baltic Seas beyond 1,000 TWh. Although most regions can refrain entirely from any particular form of renewable generation, cost-effective systems in Europe need investment of at least 60 bn EUR/a in either onshore wind or solar power. However, stronger commitment to solar in Southern Europe and Germany (for instance) unlocks more design options for the remaining system. Quantifying regional trade-offs in energy system planning is crucial in order to facilitate a more meaningful policy discussion than is possible with cost-minimality paradigms.

The European energy system is gearing up for a massive transformation towards net carbon neutrality which will deeply change the production and flow of energy both at the domestic and international level. Having enshrined greenhouse gas neutrality by 2050 in the European Climate Law[1], the EU plans to achieve the transition through a mix of the European Green Deal[2] and national policy. Modelling studies have shown that there is flexibility in regional and national investment choices and have explored the spatial diversity of potential carbon-neutral system designs[3–6]. The regional dynamics of decision making are thus important for investment planning[7–9], but systematic studies delineating the design spaces of individual regions embedded in a larger system are missing.

Energy system optimisation models play an important role in investigating how to best reach European and national climate targets, but their strict focus on cost-optimality limits the perspectives and insights for policymakers. Large varieties of system designs can be described by the near-optimal space of an energy system model[10–13] where the geometrical description aids in providing a systematic overview. Without such a complete overview, long-term planning can result in systems that lack resilience, are socially unacceptable or operationally inadequate.

Going beyond cost-optimality, what are the characteristics of the robust design spaces of regional European energy systems, and how do they interact with the continental energy landscape? To address this question, we use near-optimal methods with a sector-coupled energy system optimisation model to conduct a rigorous study of the effects of regional decision-making on the future European energy system and vice versa. Using a diverse set of scenarios to ensure robustness to uncertainty, we obtain results for 7 similarly sized *focus regions* embedded in the European energy system. This enables a comparison of regional design flexibility, export potentials and minimum investment levels subject to various system-wide investment decisions.

We find a strikingly large degree of design flexibility — on the continental, but even more so on the regional level. If renew-

*Contributed equally
†Corresponding author, koen.v.greevenbroek@uit.no

able generation is sufficient, policymakers may make trade-offs between different objectives among many cost-effective alternatives. Investment in certain technologies and regions affects overall system design flexibility much more than others, with for example solar power in Germany providing flexibility to the transition both domestically and system-wide. Wind and hydrogen investment, meanwhile, can be geographically shifted relatively freely, revealing investment opportunities for individual regions to become renewable energy exporters or hydrogen powerhouses. This significantly expands the understanding of design flexibility within the renewable electricity [13,14] or energy sector [4] in Europe, precisely describing the considerable trade-offs between solar, onshore wind and offshore wind at a regional resolution.

Our innovation is to map out near-optimal spaces in a set of dimensions representing investment in key technologies both *inside* and *outside* a given region. This allows us to quantify changes in regional robust design spaces resulting from continental decision-making and vice-versa. We concentrate on solar, onshore wind, offshore wind and hydrogen infrastructure (production, storage, conversion, transportation), resulting in a total of 8 dimensions (4 inside, 4 outside). Approximations of the resulting joint near-optimal design spaces [13] are then computed for each of the 7 focus regions separately. Crucially, we ensure robustness of the results against influential uncertainties such as technology costs, land use restrictions, and weather variability by intersecting near-optimal spaces. For the remainder of this work, we refer to the intersection of near-optimal spaces as the *robust design space*, and to points therein as *robust solutions/designs*. The intersection technique has previously only been applied to weather years [13]; our approach involving a variety of scenarios (Methods) provides a novel blueprint for future studies of robust system design.

Results

Ample opportunities for regional energy supply and exports

On the system-wide continental level and especially on the regional level, there is significant flexibility in how investment can be distributed onto the technologies explored in this study (solar, on- and offshore wind, hydrogen infrastructure — see Methods). Setting the present results apart from previous studies using near-optimal methods [4,14] is that this flexibility holds even while taking into account uncertainties in costs, weather years and land use restrictions. Indeed, we only consider so-called robust solutions that are feasible and cost-effective under all considered scenarios (Methods). Our results are given for a total system cost slack of $\varepsilon = 5\%$, but see Supplementary Table S1 for a sensitivity analysis of key figures under different slack levels. Relatively speaking, individual regions enjoy significantly more planning flexibility than we see for the overall system (Figure 1).

We see that any robust European system design needs at least around 60 bn EUR investment in onshore wind and solar power each, amounting to ∼500 GW and ∼1250 GW of installed onshore wind and solar capacity, versus 188 GW [15] and 209 GW [16] in EU-27 in 2022, respectively. This combination of wind (500 GW) and solar power (1250 GW) is not enough; remaining investment (of at least 340 bn EUR continent-wide) can be distributed in many different ways (Figure 1 (a)–(c)). Details on technologies beyond wind and solar are given in Supplementary Figure S1. All costs are annualised with a 7% discount rate and given in 2023 EUR.

We model for net zero CO_2 emissions and limit CO_2 sequestration to 200 Mt/a (following Neumann et. al. [17]) — this slashes natural gas use to 7% of 2021 levels [18,19] and renders fossil oil obsolete in the model (Supplementary information). Still, Europe overall can fully supply all energy demand from the residential, services, transportation and industry sectors using only local renewable generation, existing nuclear power and marginal use of abated natural gas. For comparison, in 2022 the fraction of imported energy in the EU27 countries was 63% [20] and the goal for 2040 lies at 26–34% [21].

At a regional level, we observe a remarkable variety of robust and cost-effective combinations of regional investments in solar power and onshore wind (Figure 1 (d)–(j)). As a matter of fact, most focus regions can get away entirely without any onshore wind or without any solar power. Figure 2 shows that a number of regions need a certain minimum investment in wind power of any kind, but as wind resources tend to be more abundant in coastal proximity, the balance between onshore and offshore wind can be adjusted relatively freely. Locally reducing overall investment in renewables is also possible, though for the purposes of this study we enforce a net self-sufficiency level of 75% for every country in the model (Methods; see the Supplementary information for a sensitivity analysis). The minimum investment levels for any kind of renewable seen in Figure 2 largely reflect this constraint. Partial self-sufficiency does not drastically increase total system cost but prevents the unnecessary exploration of system designs in which individual regions heavily rely on imports — we consider such designs unlikely to be realised.

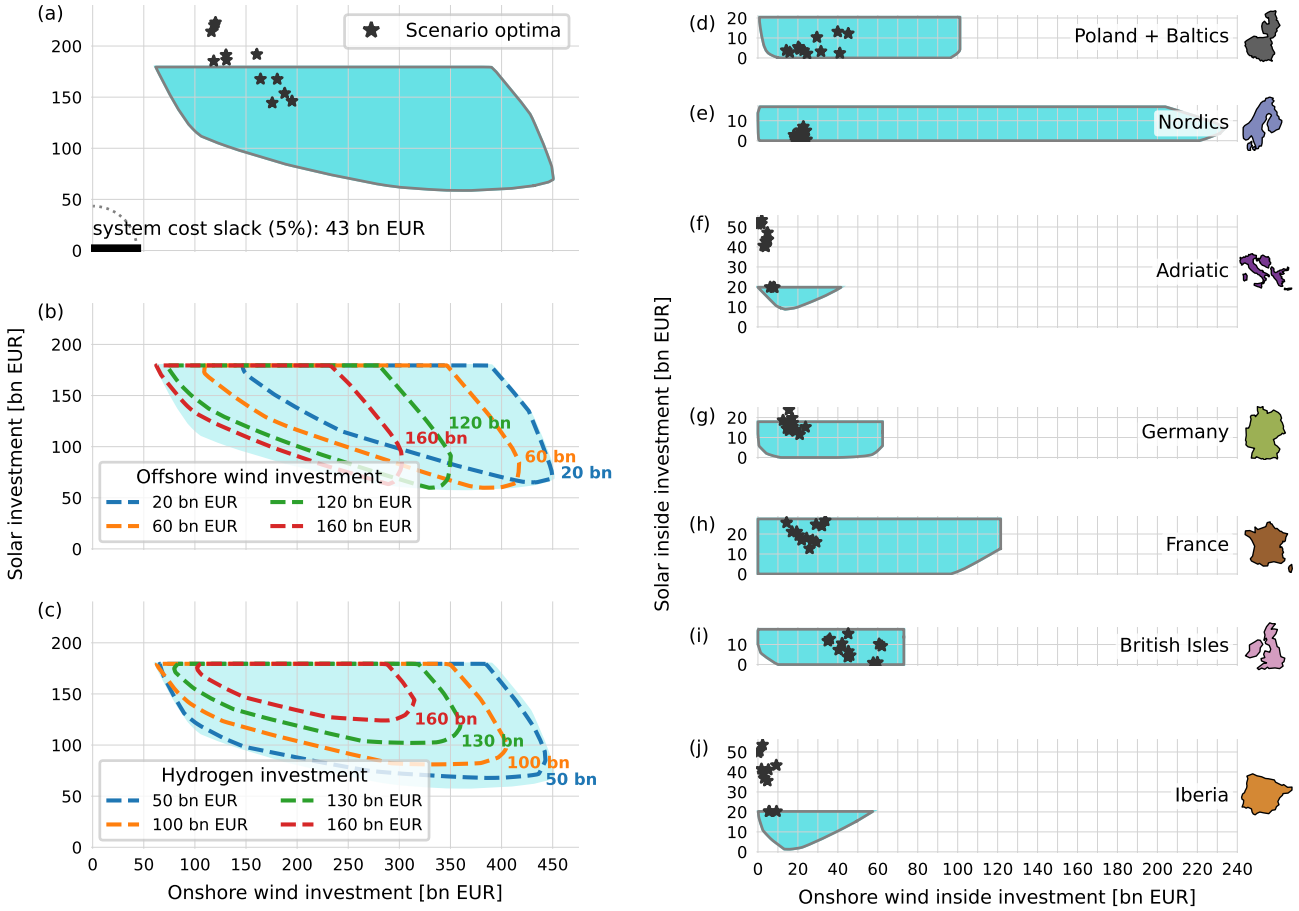

Figure 1: Robust trade-offs between annualised onshore wind and solar investment in Europe, consistent with the net-zero emissions target for 2050. (a) shows the overall robust design space projected onto the onshore wind and solar dimensions, with the cost slack marked, as well as the optima in all the individual scenarios marked. Note that the optima from individual scenarios are not necessarily robust (i.e. may not be feasible or near-optimal in other scenarios). (b) – (c) show how the robust design spaces changes (in dashed lines) subject to various levels of investment in offshore wind and hydrogen infrastructure respectively. For instance, investing only 20 bn EUR into offshore wind requires more investment in solar and/or onshore wind. Note that as cost-optimal European-wide hydrogen infrastructure investment is on average 67 bn EUR, investment beyond this level takes away cost slack from other technologies (here, solar and onshore wind) and forces their values closer to optimum, reducing the extent of the design space. (d) – (j) show the trade-offs between investment in solar PV and onshore wind for the different focus regions and display the vast opportunities of robust and cost-effective onshore wind-solar substitution.

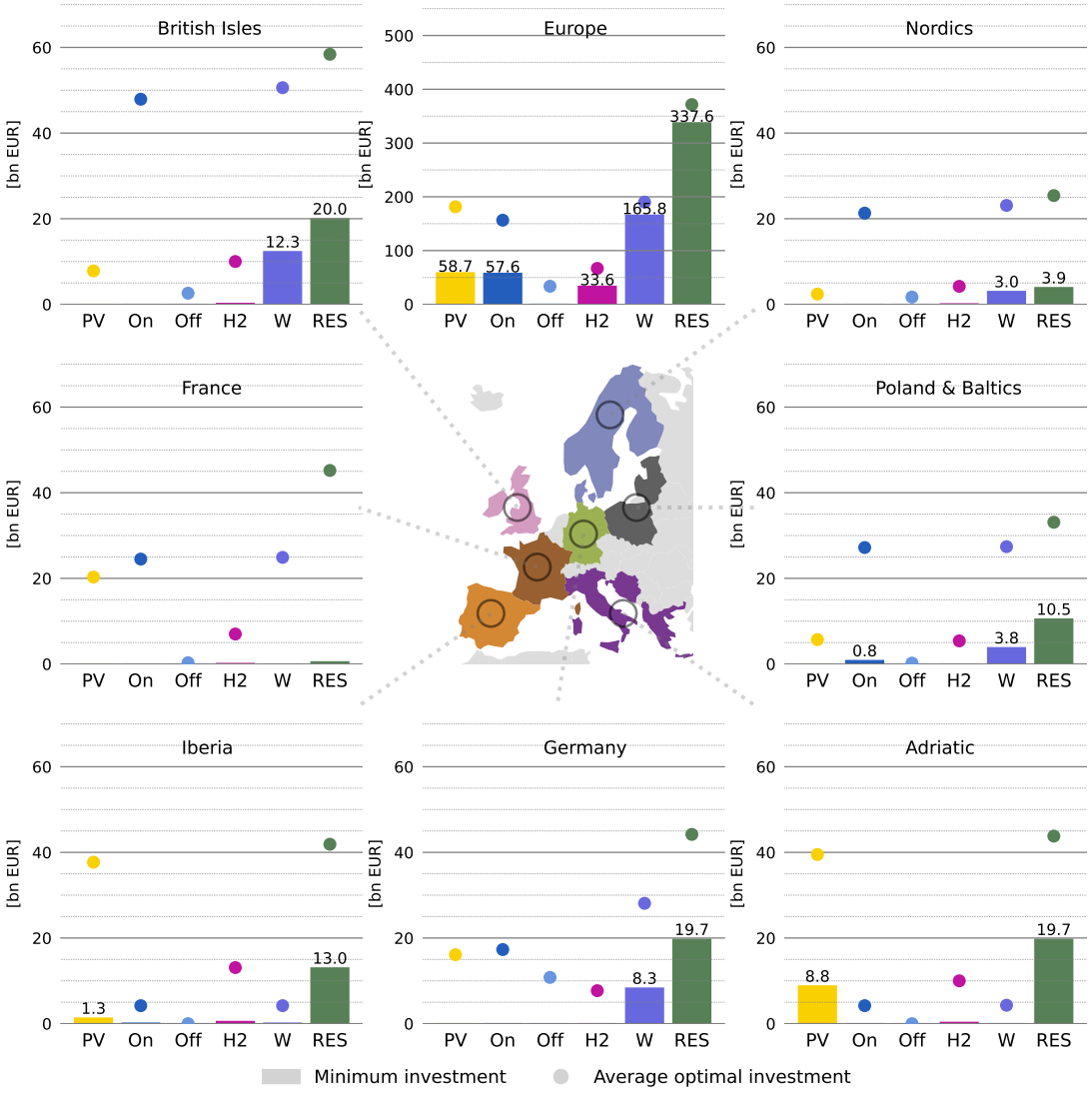

Figure 2: Comparison of minimal regional and European robust investment (in bn EUR, annualised) and average optimal investment across all scenarios. We present the investment levels in the four key technologies required for all robust designs as well as minimal total investment in wind power (on- and offshore wind) and in renewable generation (solar, onshore wind and offshore wind). The European investment values are the minimum across all focus regions' robust solutions (for the average optimal investments, they are the average across all scenarios and focus regions). Only indispensable investments above 1 bn EUR are annotated. For example, across robust system designs Germany requires investment of at least 19.7 bn EUR in total renewable generation, 8.3 bn EUR of which in wind power. Neither of solar, onshore or offshore wind power on its own is strictly necessary in Germany. Across the 12 scenarios (Methods), German optimal investment in renewable generation is on average 44.2 bn EUR.

Although hydrogen infrastructure is crucial for decarbonisation when carbon sequestration potential is limited and needs investment within Europe of at least 34 bn EUR in all robust designs, any *individual* region can forego hydrogen infrastructure entirely. Thanks to transportation at lower cost than electricity , we find that every studied region can become a hydrogen powerhouse, accumulating tens of billions of hydrogen infrastructure investment and reducing (but not eliminating) the need for hydrogen infrastructure in the rest of the system. Across robust system designs, we find total annual green hydrogen production in the range of about 2800–3900 TWh (comparable to an EU+UK natural gas consumption of around 4500 TWh in 2022[18,19]). The variations in total green hydrogen production reflect its potential (but not indispensable) role as a provider of operational flexibility; system cost slack levels above 5% further increase the range.

In a similar fashion, we find robust designs in which some regions may choose to export energy in significant quantities even as all other countries cover three quarters of their annual net energy demand locally. A striking example is provided by the Nordics, which have the potential for annual energy exports of up to 2000 TWh based on annualised investment of over 230 bn EUR (∼1800 GW of onshore wind compared to currently installed 30 GW). This is due to plentiful wind resources as well as large availability of land area for wind power — even if the political feasibility is doubtful. For comparison, the three regions of Poland and the Baltic countries, France and the British Isles are each found to have the potential for 1200–1300 TWh of annual exports. In contrast, Germany remains dependent on energy imports from the European grid (as the national energy and climate plan foresees for 2050[22]). Because of its high energy demand, Germany remains an energy net importer in any robust design, being limited by conservative assumptions on land area available for utility-scale solar PV. A complete overview over export/import ranges is given in Supplementary Figure S6; the exact figures can depend on total system cost slack as well as the self-sufficiency constraint.

Some technologies and combinations are locally indispensable

The 75% net energy self-sufficiency constraint we add to the model means that some regions need certain minimum investment levels in renewables; other regions have sufficient existing low-carbon power generation. The competitive edge due to high capacity factors make solar energy in Southern Europe and wind power particularly in the British Isles and Germany indispensable (Figure 2). In the case of the UK and Germany, some (onshore) wind investment is seen to be the only alternative in order to supply their significant energy demands, lacking other cost-effective low-carbon alternatives.

As a specific example, Figure 3 (a) shows ranges of robust local investments in wind power in the British Isles. We see that neither offshore wind nor onshore power are strictly speaking necessary; policymakers can weigh the trade-offs between cheaper onshore wind power against less visible capacities offshore. Low investment in hydrogen infrastructure allows vast ranges of investments in the different wind technologies (also depending on solar investments, not shown). A strong commitment to hydrogen in the UK, however, relies on higher investment in wind power (especially onshore) and reduces the design space. This shows that the UK could host a large hydrogen industry, which is only competitive in the presence of abundant renewable energy and relies on energy exports[23]. Overall, robust designs need at least 20 bn EUR of annualised renewable investment in the UK and Ireland, and at least 12.3 bn EUR in wind power — a tripling of today's capacity to about 100 GW[15] (Figure 2).

The Nordics or France on the other hand, with significant existing capacities of hydropower and/or nuclear power, can meet 75% of their domestic demand with fewer additional renewables, and without any single essential technology. This is in part due to electrification (including a switch to heat pumps) and the resulting reduction in primary energy demand. Furthermore, our implementation of the self-sufficiency constraint in terms of yearly net balance, counting energy content in terms of lower heating value for non-electricity carriers, allows e.g. France to export electricity and import high grade synthetic fuels, essentially outsourcing efficiency losses in hydrogen and derivative fuel production. The observed minimal investment levels for France and Nordics (Figure 2), though robust and cost-effective from a system perspective, are below current national targets for renewable expansion and ambitions for energy exports[26–31].

Regional policies can have an oversized effect on the rest of the European energy system

While Europe's net-zero transition must inevitably be upheld by a patchwork of national strategies, we find that investment in some regions and technologies has a much larger impact on the success of the overall transition than others. On one hand, lack of renewable generation in one region can lead to an inefficient

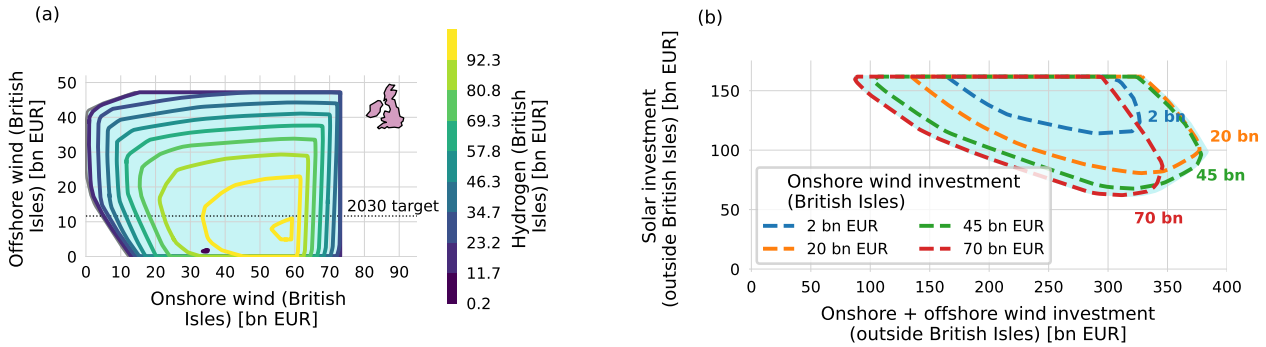

Figure 3: Internal dynamics between wind power and hydrogen on the British Isles (a) and the effects of British wind power on continental renewable investment (b). The left panel shows that low investment in wind power on the British Isles (of at least 12.3 bn EUR as by Figure 2) is connected with low investment in hydrogen infrastructure, as sufficient affordable electricity for green hydrogen is lacking. The annotated 2030 target represents the sum of UK[23] and Irish[24] offshore wind goals amounting to 50 GW and 5 GW respectively. Existing onshore and offshore capacities (at the end of 2023) are retrieved from IRENA[25] and sum to 20.3 GW of onshore wind and 14.8 GW of offshore wind. In both cases, capacities in GW are converted to annualised investment in bn EUR using the capital cost assumptions also used elsewhere in the model. The right panel shows the significant impact that British onshore wind has on robust invest levels in renewables in continental Europe. Renewable investment outside the British Isles is decomposed into onshore + offshore wind (x-axis) and solar (y-axis); the full space of robust solutions is shaded in turquoise. The dashed lines show how this design space changes depending on onshore wind investment on the British Isles. Very low onshore wind investment in the British Isles reduces the overall design flexibility of the rest of the system: the 2 bn EUR level shows a much smaller space. At the highest levels, on the other hand, the maximum viable wind investment in continental Europe is reduced.

overall system design, increasing the chance of continental cost overruns. On the other hand, high regional investment can outcompete similar investments elsewhere.

To start with an example, the British Isles have much potential for onshore wind development; enough to significantly impact minimum and maximum robust renewable investment in the remainder of Europe. Figure 3 (b) shows that for robust, cost-effective system design, lack of onshore wind power on the British Isles forces continental Europe to compensate with additional renewable power (either solar or wind).

Investment decisions in some regions can also significantly restrict or enable design flexibility in the rest of the continent, leaving either many different or rather few robust options for a European net-zero energy system by 2050. For example, Figure 4 shows how low renewable generation in Germany leaves little room to manoeuvre among remaining cost-effective robust solutions. Allocating an additional 35 bn EUR/a (4% of total system costs) to onshore wind and solar in Germany, however, frees up wide ranges of robust investment choices in the rest of Europe — despite the decrease of capital available to the rest of the system. Mapping our near-optimal spaces thus provides policymakers with useful information on the robustness of energy system designs.

In order to systematically quantify the effect of regional choices on the rest of the system, we introduce a system-wide design flexibility indicator based on the size of the space of robust European energy solutions subject to a given investment level in a particular region and technology (Methods). A low score on this indicator means that the given regional investment level leaves few robust solutions for the rest of Europe, increasing the chance of energy shortage or cost overruns. Figure 5 shows the system-wide flexibility indicator across the robust investment ranges for different technologies in our seven focus regions.

Solar in Iberia and in the Adriatic region stands out as a critical piece in the European energy transition. Lacklustre solar power expansion in either of these regions drastically reduces planning flexibility for the whole rest of the continent. Other critical pieces include solar power in Germany and, to a lesser extent, onshore wind power in Poland and the Baltic countries, Germany and the British Isles. The disproportional importance of solar in southern

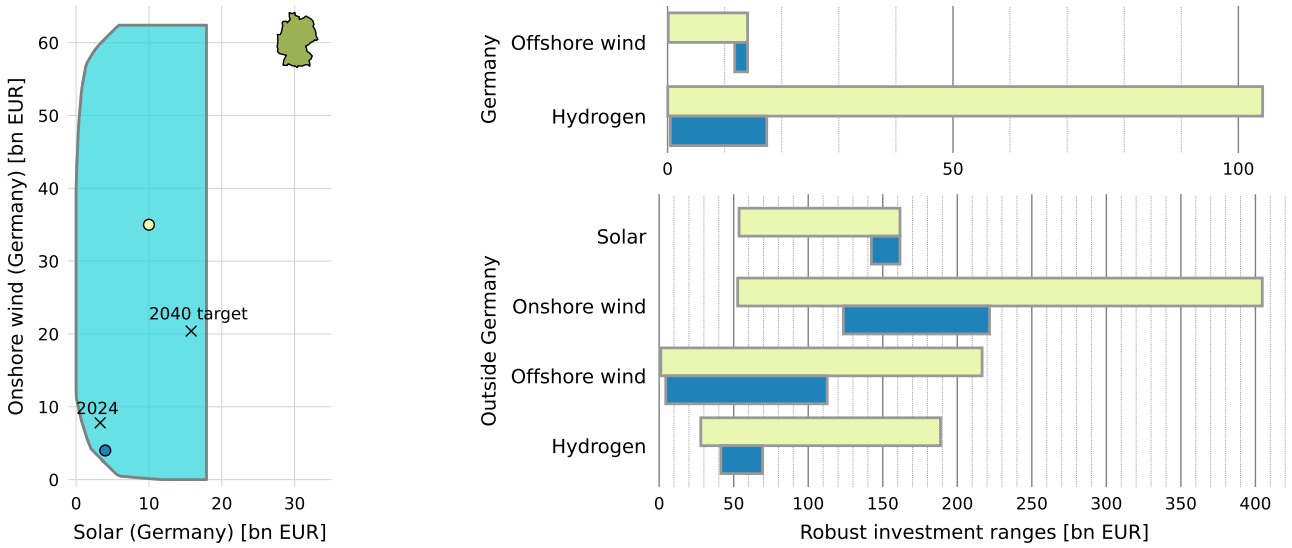

Figure 4: Left, the robust design space for solar and onshore wind inside Germany, with two particular designs / points marked as blue and yellow dots. Current (April 2024)[32] and targeted capacities for 2040[22] are marked with crosses; these are converted from GW to bn EUR annualised investment using the technology-specific capital costs also used elsewhere in the model. Right, robust investment ranges for remaining technologies inside Germany and all technologies under consideration outside Germany, at the investment levels in onshore wind and solar inside Germany given by the two points on the left. Blue bars correspond to the blue point and likewise for yellow. The ranges are expected to be of similar relative proportions but wider or narrower with higher or lower slack levels, respectively. Observe that the investment ranges for the blue point, being located closer to the boundary of the robust design space, are significantly smaller (as in Figure 5). German as well as European policymakers have an interest in ensuring large near-optimal feasible investment ranges (i.e. a large near-optimal space), as this translates to greater design robustness.

Europe can be explained by its low cost (meaning that alternatives are relatively expensive and not near-optimal) and limited land availability (meaning that lacking solar power in one region cannot easily be compensated for in another region).

Other regional renewable expansion has a remarkably low impact on the rest of the system. Solar power anywhere in northern Europe but notably also in France does not change the equation much for the rest of the system — both low and high investment in solar in these regions still leave plenty of different options for the rest of the system. For onshore wind, we observe wide ranges of robust regional investment that maintain high system-wide flexibility.

European policy sets the limits for regional energy design space

Conversely, regional investment decisions are sometimes also strongly impacted by policies in the rest of Europe. This in itself is not surprising given the inter-connected nature of the energy system. We generally see two distinct effects: in instances where the rest of Europe invests heavily in (certain kinds of) renewables, most — but not all — individual regions' potential for becoming major energy exporters is shrunk. If European investment is weak, some regions must compensate to achieve a robust and cost-effective system design.

Figure 6 illustrates both effects. The massive potential for wind power development in both Poland and the Baltic countries as well as in the Nordics decreases steadily with rising wind investment in the rest of Europe. At the same time, each of these two regions is individually forced to compensate strongly if the respective rest of the system falters in wind power. This dynamic results from low domestic demand but plentiful wind resources and makes large-scale wind development generally export-dependent. As outside developments determine what becomes over- or under-investment, coordination of wind power expansion around the North and Baltic seas may be required in order to ensure adequate and cost-effective system designs.

Elsewhere, regions with high domestic demand are less affected by wind investment in the rest of the continent, which makes wind power less susceptible to cost-inefficient lock-ins and over-investment: the *potential* wind investments in France, Germany and the British Isles remain stable even if wind power is expanded continent-wide (Figure 6). Moreover, the British Isles and especially Germany *need* wind investment to cover large shares of domestic demand almost regardless of the wind development in the rest of Europe. These regions stand apart as requiring the highest minimum investment in wind power across any robust system design (Figure 2). The British Isles also have the potential to export wind power and this exposes local wind investment to some competition, but these exports are never completely outcompeted by continental wind investment. Joint mapping of regional and continental robust design spaces thus provides local policymakers with a unique perspective on how exposed their energy goals are to outside developments.

Discussion

Comparison to existing literature and policy

We demonstrate that within an integrated European energy system, single countries or regions have large flexibility in designing their contribution to joint cost-effective decarbonisation policies. Trade-offs and broad ranges of options have been previously shown for the European electricity[11,14] and energy sector[4], and play out even stronger for individual regions. With only few exceptions, policymakers can cost-effectively substitute most single technologies if, for instance, they face delays or controversy.

However, the design space of individual regions does not exist in a vacuum but is strongly coupled with the surrounding system. We consistently see that European energy integration is only expected to deepen due to benefits of increased transmission capacities[33–36] as well as a hydrogen pipeline network[17]. For the first time, we quantify the interaction between national and continental policies laying out how both sides can increase or decrease the extent of the design space of the other, respectively. In general, investment in wind power and hydrogen infrastructure can be shifted geographically rather freely, but solar power less so. From a system perspective, there is a vested interest to pursue and coordinate regional long-term plans leading to larger design spaces — the benefits being higher robustness (lower vulnerability to uncertainty) or more flexibility and adaptability. We highlight particularly onshore *and* offshore wind power around the North- and Baltic seas as an area that may need coordination in order to prevent over- or under-investment: the Ostend Declaration[28] covering North Sea offshore wind and targeting at least 300 GW by 2050 is a step in the right direction.

This study reveals land use restrictions for solar power as a critical factor which cuts down the number of robust solutions (when including scenarios allowing 1% instead of 3% of available land);

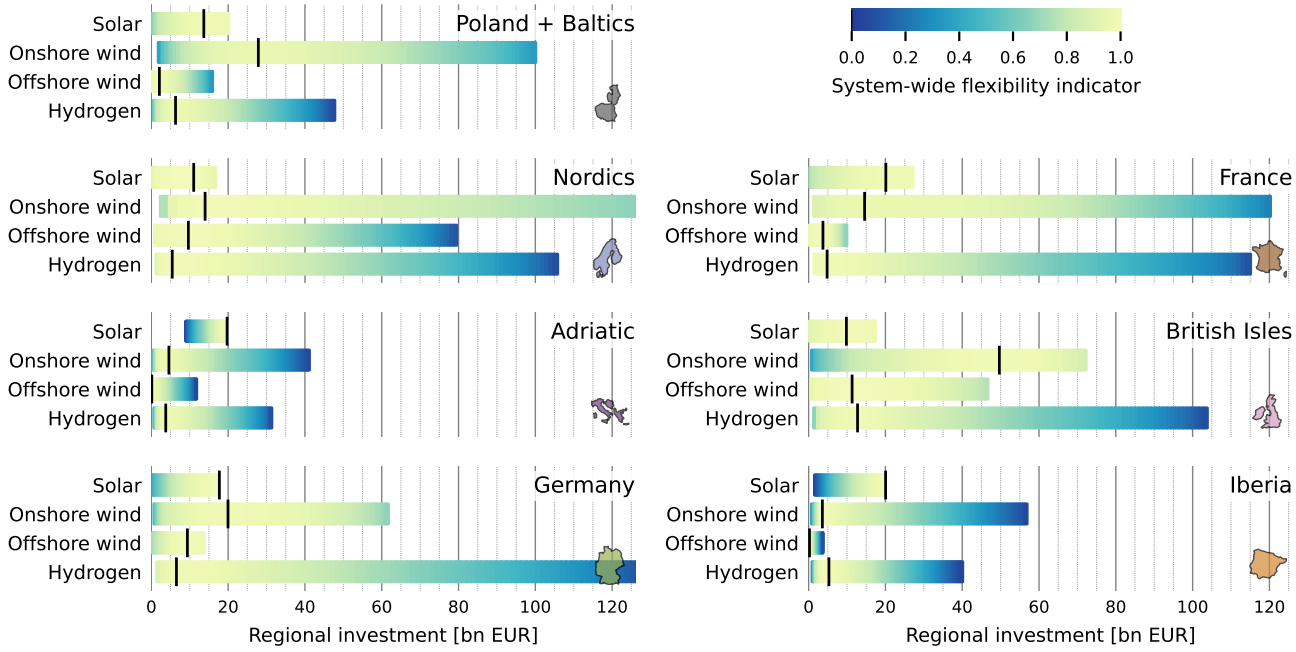

Figure 5: Effects of regional investment decisions on the design flexibility of the rest of the European system. The calculation of the flexibility indicator (where 1 is maximally flexible) that is plotted is explained in the Methods. The levels of regional investment leading to maximal outside flexibility are marked with black vertical bars. For instance, investment in solar in Poland and the Baltic countries has a positive effect on design flexibility in the rest of the system from 0 and up to about 14 bn EUR, with only a marginal decrease in flexibility upon further investment. The blue and yellow dots in Figure 4 are also examples of designs with low and high flexibility indicators, respectively. Robust onshore wind investments in the Nordics are cut off at 130 bn EUR (Figure 1(e)). While robust investment ranges widen with increasing slack levels, the investment levels maximising system-wide flexibility are not expected to change significantly under alternative slack levels. Supplementary Figure S8 shows an alternative, more detailed version of this figure. Moreover, Supplementary Figure S7 shows the "converse" to this figure, with inside and outside dimensions swapped.

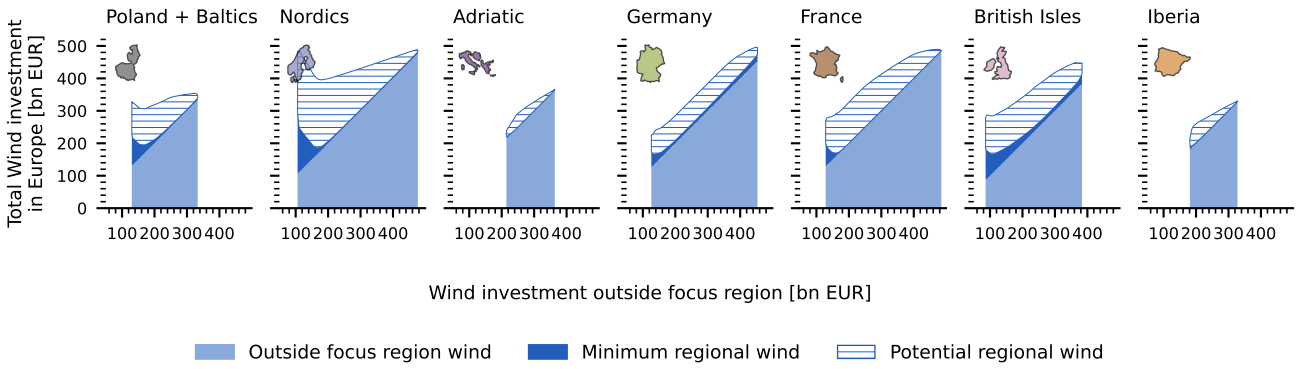

Figure 6: Minimum and maximum potential ranges of total wind power investment in different regions, as a function of wind power investment outside the respective regions. In all cases, "wind power" means onshore and offshore wind combined. Note that each subplot represents separate results from differently focused models, hence the disagreement on maximum overall viable wind power investment. Supplementary Figures S10–S11 show the corresponding regional potential of solar and hydrogen investment, respectively.

previously, weather years have already been identified as having a major impact on the energy system design space[13]. Moreover, overall design flexibility is found to be uniquely sensitive to solar investment in southern Europe and Germany, with for instance the greatest benefits unlocked by around 400 GW of solar on the Iberian peninsula — a quadrupling of the 2030 target of around 100 GW[37,38]. Germany is on a comparatively good track, already targeting 400 GW of solar by 2040[22]. By allotting enough land area for utility solar power in southern Europe, policymakers can lower the risk of energy supply shortage or cost overruns.

Moreover, we show the extent to which energy investment in individual countries and regions, while flexible, is affected by the direction of the rest of the system. Any of the studied regions can be energy net importers (or exporters, except for Germany), but not all at the same time. The EU as well as individual countries have come forward with hydrogen strategies in recent years[27,39–41], with domestic production and imports of 10 Mt each of green hydrogen being the EU target for 2030 — concrete targets for 2050 are outstanding. Our results point at the need for somewhere around 100 Mt of green hydrogen by 2050, amounting to a minimum annualised investment of 34 bn EUR in overall hydrogen sector; however, *where* these investments occur is very flexible. All in all, neither individual countries nor the EU can plan the transition to net-zero emissions without taking the tapestry of energy strategies across the European continent into account.

Possible limitations and future research directions

We choose an approach based on intersecting near-optimal spaces of different scenarios — as opposed to sensitivity analysis or stochastic programming — as it allows us to account for uncertainty both in inputs and outputs. This systematic mapping of near-optimal spaces[12,13] facilitates the use of other objectives beyond cost minimality compared to more classical modelling-to-generate-alternatives (MGA) like min/max-[11] or hop-skip-jump approaches[10,42]. The joint modelling of both each focus region and the outside system allows the examination of regional dynamics while preserving global near-optimality. The extent of the robust design space studied here does depend on the set of scenarios under which each design must be feasible, and our scenario selection is more of a starting point than a canonical selection.

The approximation of the design spaces requires many model optimisations (we use 450 for each region and scenario), which is why we restrict ourselves to mapping out the design space in only 8 key variables at a time. Moreover, robust design spaces depend on the cost slack (ε) by definition; our sensitivity analysis shows that robust design spaces mainly increase in extent with increasing slack but that their shapes remain similar. This means the natures of revealed trade-offs generally hold across different slack levels. The 5% cost slack throughout this analysis remains a choice by the modellers and does not necessarily reflect willingness-to-pay of stakeholders (where stated preferences can

differ from realised ones[43]).

A number of important factors and assumptions have not been explored through additional sensitivity or other methods for brevity and for computational reasons. These include alternative emissions targets, demand response, energy imports from outside the modelled European system, technological learning, regional differences in (static) technology costs, carbon sequestration potential and alternative fossil fuel limitations among others.

Increasing the spatial resolution in each of the 7 focus regions separately means that there may be slight variations in European-wide modelling results between differently focused model instances. This could be alleviated in future research by using a uniformly high spatial resolution for the entire modelling region. While our analysis is restricted to overnight investments, multi-horizon modelling could be of great value to policymakers. Lastly, inviting policymakers and stakeholders to interact with near-optimal modelling tools would be a major development in participatory modelling.

Conclusions

The methods advanced in this article allow us to systematically analyse more adaptable and acceptable solutions while achieving cost-effective net-zero systems in which all countries cover 75% of their annual demand. We present techniques that achieve higher resilience by incorporating scenarios reflecting a mix of meteorological, technological and societal impediments.

The vast planning flexibility we demonstrate underlines the agency of single regions and countries in shaping energy policy: if onshore wind is socially unacceptable, for example, many regions can substitute it with other technologies. On a continent with different transition speeds[44] and levels of ambition[45], almost all countries have the possibility to benefit from building up new industries through electricity or hydrogen exports. However, certain trade-offs between regions are unavoidable and must be considered in light of social and political priorities that are difficult to quantify. To overcome opposition to climate mitigation and strengthen a fair decarbonisation, accounting for diverging interests in a panoply of transition alternatives is possible and necessary.

Methods

Modelling framework

For this study, we use the open-source energy system model PyPSA-Eur-Sec 0.6.0[33] (since merged into PyPSA-Eur) which represents the European energy system including the power, heating, industry, transport and agricultural sectors. It includes a detailed representation of the existing electricity transmission and gas networks, as well as generation sites and spatially resolved demand of different sectors. With the aim of a 100% CO_2 emission reduction in the European power, heating, transportation and industrial sectors, the model finds investment and operational decisions for generation, transmission and storage in order to minimise total annualised system costs and meet projected 2050 energy demand. For a precise description of the model formulation see Brown et. al.[33] and the supplemental experimental procedures of Neumann et. al.[46].

Estimates of fixed and operational costs for 2050 are taken from `https://github.com/PyPSA/technology-data`, a repository collecting cost data and learning curves from various sources. All capital costs are annualised with a discount rate of 7%; this discount rate is chosen because it is the default in PyPSA-Eur, hence making the results more directly comparable across studies. While costs in the above repository are given in 2015 EUR, we have converted all cost data to 2023 EUR for the purposes of this study, using inflation data for the Euro area up to October 2023[47], amounting to a 24.5% increase compared to `technology-data`.

The model is run with a partial greenfield approach, where existing transmission and gas networks (2019) as well as nuclear (except for Germany), biomass, and hydropower generation (2022) are included at today's capacities. The above infrastructure was included because of its relatively long lifetime (including potential lifetime extensions), making existing capacities likely to approximately persist until 2050. The gas and transmission networks may additionally be reinforced beyond today's capacities in the model; for transmission this is limited to 125% of current levels (see sensitivity analysis in the Supplementary information). Nuclear, biomass and hydropower generation, on the other hand, are entirely fixed (i.e. not subject to optimisation) and are not included in total system costs.

The main technologies whose expansion is optimised from scratch include solar, onshore wind and offshore wind generation, gas turbines, combined heat and power plants with and without carbon capture and storage (CCS), boilers, battery storage, hydrogen

and heat storage, various power to X and other energy conversion technologies (electrolysis, steam methane reformation, methanation of hydrogen, ammonia and methonol production from hydrogen, synthetic fuel generation, biogas), direct air capture and carbon sequestration. The model includes all major potential components of a European energy system anno 2050, including the electricity, heating, transportation and industry sectors. See the accompanying code and data as well as PyPSA-Eur documentation and a recent study on the potential of a European hydrogen network[17] for more details.

We choose a spatial resolution of 60 nodes for 33 European countries, however, the exact allocation of nodes varies between the differently focused models (see below). In order to reduce the computational burden further, we use a non-uniform, sequential time step aggregation[48,49] setting in PyPSA-Eur with 1500 time segments (which we have tested to be more accurate than a comparable 6-hourly time resolution).

For all countries represented, we impose a 75% net self-sufficiency constraint for annual energy demand (see Supplementary Figure S3 and sensitivity analysis in the Supplementary information). It prevents the unnecessary exploration of technically robust system designs where individual regions are heavily dependent on imports — we consider such designs unlikely to be realised. At the same time, it can be seen as a measure to strengthen energy security and a more equal burden between different European countries in the joint decarbonisation efforts. The implementation of such a self-sufficiency constraint is a novelty in the context of sector-coupled energy system models for Europe; previously this was merely implemented for the electricity-only version of the model (PyPSA-Eur). The constraint is implemented bounding the ratio between total yearly local energy production and total yearly energy imports. Following the notation used to originally introduce PyPSA[50], let $g_{n,r,t}$ be the operational decision variables for generators (indexed by bus n, generator r and time step t) and $f_{\ell,t}$ be the operation decision variables for branch components, both passive (i.e. AC transmission lines) and active (DC transmission as well as transfer of other quantities than electricity between buses). Let $\mu_{\ell,t}$ be the efficiency of each branch component. All quantities tracked and transferred in a PyPSA-Eur model are energy carriers (electricity, natural gas, hydrogen, oil, etc.) except CO_2; the unit for energy is always MWh, measured in lower heating value for thermal energy carriers. For a country C, let

$$\alpha_{C,\ell,t} = \begin{cases} -1, & \text{if branch } \ell \text{ starts inside } C \text{ and ends outside of } C, \\ & \quad \text{and the bus that } \ell \text{ ends at tracks an energy carrier,} \\ \mu_{\ell,t}, & \text{if it start outside of } C \text{ and ends inside } C, \\ & \quad \text{and the bus that } \ell \text{ ends at tracks an energy carrier,} \\ 0, & \text{otherwise.} \end{cases}$$

Then the net yearly imports of country C are measured by

$$I_C = \sum_{\ell,t} \alpha_{C,\ell,t} f_{\ell,t}. \tag{1}$$

Letting

$$\delta_{C,n} = \begin{cases} 1, & \text{if bus } n \text{ is located inside country } C \\ 0, & \text{otherwise.} \end{cases}$$

be the indicator function of country C for buses, the total yearly amount of energy produced inside country C is

$$L_C = \sum_{n,r,t} \delta_{C,n} g_{n,r,t}. \tag{2}$$

Then, a self-sufficiency degree of γ for country C can be ensured by adding the following linear constraint to the capacity expansion formulation:

$$I_C \leq \frac{1-\gamma}{\gamma} L_C, \tag{3}$$

provided $\gamma > 0$. The actual implementation used in this paper is slightly complicated by the presence of multi-branch components (i.e. links connecting more than two buses, controlled by a single operational decision variable per time step), but equivalent to the above. Apart from the self-sufficiency constraint, we refer to the publication introducing PyPSA[50] for an exact mathematical formulation of the full optimisation problem.

Regional studies

Our results are based on studying the joint space of robust system designs of the European energy system, reduced to total investment in four key technologies both inside and outside 7 selected focus regions. For the approximations of these 7 robust design spaces, we use the same model of the European energy system, except that we distribute the spatial nodes of the model differently in order to allocate more spatial resolution to each respective focus region. Moreover, we also allocate slightly more nodes to countries neighbouring each focus region. Our focus regions are

- Poland and Baltic countries (EE, LT, LV, PL) with 20+25+15 nodes,
- Nordics (DK, FI, NO, SE) with 20+25+15 nodes,
- Adriatic (AL, BA, GR, HR, IT, MT) with 30+20+10 nodes,
- Germany (DE) with 20+25+15 nodes,
- France (FR) with 20+25+15 nodes,
- British Isles (IE, UK) with 15+25+20 nodes,
- Iberia (ES, PT) with 20+15+25 nodes,

with the corresponding number of nodes inside the region, for neighbouring countries and for remaining countries (further removed than distance 1), respectively, all adding up to 60 nodes. The increased spatial resolution inside the focus region allows us to capture renewable potential and effects like transmission bottlenecks in better detail. See Supplementary Figure S12 for a visual representation of the networks.

Scenario selection

For each focus region, we consider different scenarios across input uncertainties that we deem particularly impactful on energy modelling results. For each of these scenarios (and for each focus region), we approximate the corresponding near-optimal feasible space using the methods introduced by Grochowicz et al.[13]. For each focus region, then, we consider as robust design space the *intersection* of the near-optimal spaces arising from the scenarios under consideration (see below).

The factors we vary across scenarios and which we consider most impactful to modelling results include weather years[13,51], cost assumptions[14], and land use[52] availability. Following Grochowicz et al.[13], we select three difficult weather years (1985, 1987, 2010) and thus are particularly restrictive (and also significantly more expensive than other weather years) and well-suited for resilience considerations. We define three cost scenarios, one "baseline" scenario with standard cost assumptions, and two scenarios with higher capital expenditure costs for solar PV (39% more expensive) and wind power (24% more expensive) respectively; these ranges are taken from cost projections by the Danish Energy Agency[53]. Points in the robust design space (i.e. the intersection of the near-optimal spaces arising from the different scenarios) are defined in terms of investment levels in solar, onshore- & offshore wind and hydrogen infrastructure. This means that a single robust design with, say, x bn EUR investment in solar, would have different total solar capacities in GW in scenarios where solar has different capital costs, since the same amount of money will buy less capacity when solar is more expansive. Still, by definition, the design being located in the intersection of the near-optimal spaces means that the given investment levels are feasible even in the scenario with higher capital costs and thus lower total installed capacity.

Lastly, we restrict the available land area for utility solar PV in comparison to the standard assumptions in PyPSA-Eur-Sec to one third (from 3% to 1% of available land area after excluding unsuitable areas[54]). The restricted land availability scenario inhibits expansion of solar PV significantly: for instance, Germany's installation potential is capped at approximately 440 GW while the German government is targeting installed capacities of 400 GW until 2040[55].

All in all, this gives us 12 scenarios, as we pair the three different weather years with the three cost scenarios and the restriction on land use for utility solar ($3 \cdot (3+1) = 12$).

Near-optimal spaces

The near-optimal space for each of the above scenarios and focus regions, consists of feasible, alternative solutions to a cost-optimal solution which can be preferable over the cost optimum for other reasons. Energy system optimisation models are usually formulated mathematically as linear programs of the form $\min cx$ subject to $Ax \leq b$ in which case the *design space*, more formally *ε-near-optimal feasible space*[10,11,13], is defined as $\mathcal{F}_\varepsilon = \{x \in \mathbb{R}^n \mid Ax \leq b \text{ and } cx \leq (1+\varepsilon) \cdot c^*\}$ where c^* is the optimal objective (minimum cost) of the original linear program.

For the purposes of this study, we use a cost slack of $\varepsilon = 5\%$. See the Supplementary information for a sensitivity analysis on the cost slack. However, for each focus region we compute a uniform cost bound for all scenarios based on the optimum system cost for the most expensive scenario (roughly following[13]). More precisely, let r be a region and S a set of scenarios, such that we get a linear program $A_{r,s}x \leq b_{r,s}$ with objective $c^*_{r,s}$ for each $s \in S$. Then we define the near ε-near-optimal space for scenario s as

$$\mathcal{F}^{r,s}_\varepsilon = \{x \in \mathbb{R}^n \mid A_{r,s}x \leq b_{r,s} \text{ and } c_{r,s}x \leq (1+\varepsilon) \cdot \max_{s' \in S} c^*_{r,s'}\}$$

Defining near-optimal spaces for a set of scenarios as above allows for more direct comparisons, since all spaces are defined with respect to same absolute bound on total system costs.

In models of similar size to PyPSA-Eur-Sec (with n significantly greater than 10^6), the near-optimal spaces which can be analysed effectively are projections onto a few key dimensions from the high-dimensional space $\mathcal{F}_\varepsilon^{r,s}$. This is because an accurate approximation of such a near-optimal space is computationally demanding (one vertex is obtained through one optimisation of the linear program) in high dimensions[12,13]. Following previously introduced notation[13], we consider the reduced, low-dimensional near-optimal space $\mathcal{A}_\varepsilon^{r,s} \subset \mathbb{R}^k$; related to the full-dimensional space by a linear map $\sigma : \mathcal{F}_\varepsilon^{r,s} \to \mathcal{A}_\varepsilon^{r,s}$. In our case, we map down to $k = 8$ key dimensions: the total investments *inside* and *outside* the focus region in utility solar, onshore wind, offshore wind, and hydrogen infrastructure. Hydrogen infrastructure investments consist of investment in electrolysis, fuel cells, pipelines (both new and retrofitted from existing gas pipelines), synthetic methane and fuel production from hydrogen (methanation, Fischer-Tropsch process respectively) and steam methane reforming plants (with or without carbon capture) as well as hydrogen storage.

An accurate approximation of the near-optimal space geometry can inform policymakers about trade-offs between regional and continental investment, alternative technologies, and how much flexibility can be gained through the introduction of a cost slack of ε. Solutions beyond it are no longer near-optimal, which can mean that they are deemed infeasible by the model or no longer cost-effective (but feasible). For a more detailed description of the approximation methodology and validation see[13]; in this case, we conduct 450 optimisations for a satisfying approximation of each near-optimal space. See Supplementary Figures S13–S14 for a visualisation of the individual near-optimal spaces as well as their intersection for one of the focus regions.

Robust solutions

To find cost-effective solutions that are feasible (and near-optimal) notwithstanding the uncertainties encoded in our selection of scenarios, we look for investment decisions that lie in the near-optimal space for each scenario. We formally define the space of *robust solutions* (or robust design space) as points in $\mathbb{R}^k$ that lay within the intersection of the reduced near-optimal spaces for every scenario $s \in S$ under consideration:

$$\mathcal{I}_\varepsilon^r = \bigcap_{s \in S} \mathcal{A}_\varepsilon^{r,s}.$$

We refer to[13] for an extensive overview of the intersections of near-optimal feasible spaces with all due details.

By considering the geometry of the space of robust solutions (as in Figures 1 and 3, for example), we are able to study trade-offs between investments in different technologies both inside a given focus region and in the rest of Europe. One should keep in mind that the formulation in terms of near-optimality adds a slack of 5% on top of the optimal total system costs which corresponds to an additional investment of around 45 bn EUR (depending on the focus region) which can be allocated in different ways in order to enlarge the alternative robust options. (See Table S1 in the Supplementary information for alternative figures for slack levels of 2, 10 & 20%.) Note that monetary investments are robust across scenarios, however they might translate to different capacities in the scenarios with higher costs for solar PV or wind power.

The flexibility indicator

For Figure 5 we introduce a flexibility indicator based on the *mean width* of the robust design space (defined in more detail below). The mean width of the robust design space in the 4 outside investment dimensions is a simple metric for the variety of robust solutions and serves as a quantification of design flexibility of policymakers. The values between 0 and 1 for each regional investment dimensions show which investment levels allow for most robust solutions from a continental perspective. For instance, investing ca. 5 bn EUR/a in onshore wind in the Adriatic gives the rest of Europe the largest flexibility, whereas onshore wind investment in the order of 40 bn EUR/a — while still being robust — restricts the alternatives for the remainder of the system. In the Supplementary information, we present additional figures (S8–S9) for the derivative of mean width, which can identify at which investment levels most flexibility can be gained or lost.

For a precise mathematical definition, consider the space of robust designs $\mathcal{I}_\varepsilon^r$ for focus region r. Let $A = \{a_1, a_2, a_3, a_4\}$ and $B = \{b_1, b_2, b_3, b_4\}$ be the sets of inside and outside key dimensions, respectively, i.e. a_1, a_2, a_3, a_4 are investment in solar, onshore wind, offshore wind and hydrogen infrastructure in bn EUR inside the focus region r, respectively (and similarly for B outside the focus region). Now, let

$$\mathcal{I}_{\varepsilon,a_i=c}^r = \{x \in \mathcal{I}_\varepsilon^r \mid a_i = c\} \quad \text{where } x = (a_1, a_2, a_3, a_4, b_1, b_2, b_3, b_4) \tag{4}$$

be the subset of $\mathcal{I}_\varepsilon^r$ for which a_i equals a constant c. Then we define the *mean width of* $\mathcal{I}_\varepsilon^r$ *at* $a_i = c$ as

$$d_i^r(c) = \frac{1}{|B|} \sum_{b \in B} \left(\max\{b \mid x \in \mathcal{I}_{\varepsilon,a_i=c}^r\} - \min\{b \mid x \in \mathcal{I}_{\varepsilon,a_i=c}^r\} \right), \tag{5}$$

where we use the convention that $\min \emptyset = \max \emptyset = 0$. That is, $d_i^r(c)$ is the mean of the widths of $\mathcal{I}^r_{\varepsilon,a_i=c}$ in each of the outside dimensions B, and equals 0 when $\mathcal{I}^r_{\varepsilon,a_i=c} = \emptyset$. Finally, we define the flexibility metric f_i^r as the normalisation of d_i^r, namely

$$f_i^r(c) = \frac{d_i^r(c)}{\max_{c\in\mathbb{R}} d_i^r(c)}. \tag{6}$$

This is what is plotted in Figure 5 for each combination of region r and inside dimension a_i; we cut the plots off where $f_i^r(c) = 0$. The converse (the flexibility metric for regional investment based on fixed continental investment) is presented in Figure S6.

Code and data availability

The code to reproduce the results of the present study, as well as links to the data used, are available at https://github.com/koen-vg/enabling-agency/tree/v0. All code is open source (licensed under GPL v3.0 and MIT), and all data used are open (various licenses).

Acknowledgements

A.G., F.E.B. and M.Z. acknowledge funding by UiO:Energy and Environment (SPATUS).

ERA5 reanalysis data[56] were downloaded from the Copernicus Climate Change Service (C3S)[57].

The results contain modified Copernicus Climate Change Service information 2020. Neither the European Commission nor ECMWF is responsible for any use that may be made of the Copernicus information or data it contains.

Declaration of interests

The authors declare no competing interests.

References

[1] Regulation (EU) 2021/1119 of the European Parliament and of the Council of 30 June 2021 establishing the framework for achieving climate neutrality and amending Regulations (EC) No 401/2009 and (EU) 2018/1999 ('European Climate Law'), June 2021. URL http://data.europa.eu/eli/reg/2021/1119/oj/eng.

[2] European Commission, Secretariat-General. Communication from the Commission to the European Parliament, the European Council, the Council, the European Economic and Social Committee and the Committee of the Regions: The European Green Deal. Communication COM/2019/640, European Commission, 2019. URL https://eur-lex.europa.eu/legal-content/EN/TXT/?qid=1576150542719&uri=COM%3A2019%3A640%3AFIN.

[3] Francesco Lombardi, Bryn Pickering, Emanuela Colombo, and Stefan Pfenninger. Policy Decision Support for Renewables Deployment through Spatially Explicit Practically Optimal Alternatives. *Joule*, 4(10):2185–2207, October 2020. ISSN 25424351. doi:10.1016/j.joule.2020.08.002.

[4] Bryn Pickering, Francesco Lombardi, and Stefan Pfenninger. Diversity of options to eliminate fossil fuels and reach carbon neutrality across the entire European energy system. *Joule*, 6(6):1253–1276, June 2022. ISSN 2542-4351. doi:10.1016/j.joule.2022.05.009.

[5] Tim T. Pedersen, Mikael Skou Andersen, Marta Victoria, and Gorm B. Andresen. Using Modeling All Alternatives to explore 55% decarbonization scenarios of the European electricity sector. *iScience*, 26(5):106677, May 2023. ISSN 2589-0042. doi:10.1016/j.isci.2023.106677.

[6] Jan-Philipp Sasse and Evelina Trutnevyte. Cost-effective options and regional interdependencies of reaching a low-carbon European electricity system in 2035. *Energy*, 282:128774, November 2023. ISSN 0360-5442. doi:10.1016/j.energy.2023.128774.

[7] Mario Kendziorski, Leonard Göke, Christian von Hirschhausen, Claudia Kemfert, and Elmar Zozmann. Centralized and decentral approaches to succeed the 100% energiewende in Germany in the European context – A model-based analysis of generation, network, and storage investments. *Energy Policy*, 167:113039, August 2022. ISSN 0301-4215. doi:10.1016/j.enpol.2022.113039.

[8] Goran Durakovic, Pedro Crespo del Granado, and Asgeir Tomasgard. Powering Europe with North Sea offshore wind: The impact of hydrogen investments on grid infrastructure and power prices. *Energy*, 263:125654, January 2023. ISSN 0360-5442. doi:10.1016/j.energy.2022.125654.

[9] Claudia Strambo, Måns Nilsson, and André Månsson. Coherent or inconsistent? Assessing energy security and climate policy interaction within the European Union. *Energy Research & Social Science*, 8:1–12, July 2015. ISSN 2214-6296. doi:10.1016/j.erss.2015.04.004.

[10] Joseph F. DeCarolis. Using modeling to generate alternatives (MGA) to expand our thinking on energy futures. *Energy Economics*, 33(2):145–152, March 2011. ISSN 0140-9883. doi:10.1016/j.eneco.2010.05.002.

[11] Fabian Neumann and Tom Brown. The near-optimal feasible space of a renewable power system model. *Electric Power Systems Research*, 190:106690, January 2021. ISSN 0378-7796. doi:10.1016/j.epsr.2020.106690.

[12] Tim T. Pedersen, Marta Victoria, Morten G. Rasmussen, and Gorm B. Andresen. Modeling all alternative solutions for highly renewable energy systems. *Energy*, 234:121294, November 2021. ISSN 0360-5442. doi:10.1016/j.energy.2021.121294.

[13] Aleksander Grochowicz, Koen van Greevenbroek, Fred Espen Benth, and Marianne Zeyringer. Intersecting near-optimal spaces: European power systems with more resilience to weather variability. *Energy Economics*, 118:106496, January 2023. ISSN 0140-9883. doi:10.1016/j.eneco.2022.106496.

[14] Fabian Neumann and Tom Brown. Broad Ranges of Investment Configurations for Renewable Power Systems, Robust to Cost Uncertainty and Near-Optimality. *iScience*, 26(5):106702, April 2023. ISSN 25890042. doi:10.1016/j.isci.2023.106702.

[15] WindEurope. Wind Energy in Europe: 2022 Statistics and the outlook for 2023-2027, February 2023. URL https://windeurope.org/intelligence-platform/product/wind-energy-in-europe-2022-statistics-and-the-outlook-for-2023-2027/.

[16] Michael Schmela. European Market Outlook for Solar Power 2022-2026. Technical report, SolarPower Europe, 2022. URL https://www.solarpowereurope.org/press-releases/new-report-reveals-eu-solar-power-soars-by-almost-50-in-2022.

[17] Fabian Neumann, Elisabeth Zeyen, Marta Victoria, and Tom Brown. The potential role of a hydrogen network in Europe. *Joule*, 7(8):1793–1817, August 2023. ISSN 2542-4351. doi:10.1016/j.joule.2023.06.016.

[18] Eurostat. Supply, transformation and consumption of gas, 2023. URL https://ec.europa.eu/eurostat/databrowser/view/nrg_cb_gas/default/table?lang=en.

[19] Department for Energy Security & Net Zero (UK). Natural gas supply and consumption, 2023. URL https://assets.publishing.service.gov.uk/media/65130c71b23dad000de706d5/ET_4.1_SEP_23.xlsx.

[20] Eurostat. Energy imports dependency (nrg_ind_id), 2024.

[21] European Commission. Europe's 2040 climate target and path to climate neutrality by 2050 building a sustainable, just and prosperous society. Technical report, 2024. URL https://eur-lex.europa.eu/resource.html?uri=cellar:6c154426-c5a6-11ee-95d9-01aa75ed71a1.0001.02/DOC_1&format=PDF.

[22] German Government. Germany - Draft Updated NECP 2021-2030 - European Commission. Technical report, 2023. URL https://commission.europa.eu/publications/germany-draft-updated-necp-2021-2030_en.

[23] British Government. British energy security strategy. Technical report, 2022. URL https://www.gov.uk/government/publications/british-energy-security-strategy.

[24] Irish Government. Ireland - Draft Updated NECP 2021-2030 - European Commission. Technical report, 2023. URL https://commission.europa.eu/document/download/4b741649-7249-47d6-b62a-b123edd49ae5_en?filename=Ireland%20-%20Draft%20updated%20NECP%202021-2030%20EN.pdf.

[25] IRENA. Electricity statistics (MW/GWh) by Country/area, Technology, Data Type, Grid connection and Year, 2024. URL https://pxweb.irena.org/pxweb/en/IRENASTAT.

[26] French Government. France - Draft Updated NECP 2021-2030 - European Commission. Technical report, 2023. URL https://commission.europa.eu/publications/france-draft-updated-necp-2021-2030_en.

[27] Olje- og energidepartementet og Klima- og miljødepartementet. Regjeringens hydrogenstrategi - på vei mot lavutslippssamfunnet. Technical Report Y-0127 B, Norwegian Government, 2020.

[28] Minister of Climate, Energy and Utilities of the Kingdom

of Denmark, Minister for Energy of the Kingdom of Belgium, The Minister for Climate and Energy Policy of the Netherlands, and The Minister for Economic Affairs and Climate Action of the Federal Republic of Germany. The Declaration of Energy Ministers on The North Sea as a Green Power Plant of Europe, 2022. URL https://www.bmwk.de/Redaktion/DE/Downloads/Energie/20220518-declaration-of-energy-ministers.pdf?__blob=publicationFile&v=10.

[29] Swedish Government. Sweden - Draft Updated NECP 2021-2030 - European Commission. Technical report, 2023. URL https://commission.europa.eu/document/download/bdd2bbe5-eefd-4d22-a729-2a74cbb30e1f_en?filename=EN_SWEDEN%20DRAFT%20UPDATED%20NECP.pdf.

[30] Danish Government. Denmark - Draft Updated NECP 2021-2030 - European Commission. Technical report, 2023. URL https://commission.europa.eu/document/download/31895e48-37c3-46fe-8a8f-8f61fbff6724_en?filename=EN_DENMARK%20DRAFT%20UPDATED%20NECP.pdf.

[31] Finnish Government. Finland - Draft Updated NECP 2021-2030 - European Commission. Technical report, 2023. URL https://commission.europa.eu/document/download/78c7f4bd-a3ca-4e83-8732-65f1e0d0baaa_en?filename=DRAFT%20NECP%20update_Finland.pdf.

[32] Arbeitsgruppe Erneuerbare Energien-Statistik. Monatsbericht zur Entwicklung der erneuerbaren Stromerzeugung und Leistung in Deutschland. Technical Report Stand: 11.04.2024, 2024. URL https://www.umweltbundesamt.de/sites/default/files/medien/372/dokumente/04-2024_agee-stat_monatsbericht_final_neu.pdf.

[33] T. Brown, D. Schlachtberger, A. Kies, S. Schramm, and M. Greiner. Synergies of sector coupling and transmission reinforcement in a cost-optimised, highly renewable European energy system. *Energy*, 160:720–739, October 2018. ISSN 0360-5442. doi:10.1016/j.energy.2018.06.222.

[34] David P. Schlachtberger, Tom Brown, Stefan Schramm, and Martin Greiner. The benefits of cooperation in a highly renewable European electricity network. *Energy*, 134:469–481, September 2017. ISSN 0360-5442. doi:10.1016/j.energy.2017.06.004.

[35] Jonas Hörsch and Tom Brown. The role of spatial scale in joint optimisations of generation and transmission for European highly renewable scenarios. In *2017 14th International Conference on the European Energy Market (EEM)*, pages 1–7, Dresden, Germany, June 2017. IEEE. ISBN 978-1-5090-5499-2. doi:10.1109/EEM.2017.7982024.

[36] Tim Tröndle, Johan Lilliestam, Stefano Marelli, and Stefan Pfenninger. Trade-Offs between Geographic Scale, Cost, and Infrastructure Requirements for Fully Renewable Electricity in Europe. *Joule*, 4(9):1929–1948, September 2020. ISSN 2542-4351. doi:10.1016/j.joule.2020.07.018.

[37] Spanish Government. Spain - Draft Updated NECP 2021-2030 - European Commission. Technical report, 2023. URL https://commission.europa.eu/document/download/9ea170ec-fdce-49cb-9424-4ee95db33a4a_en?filename=EN_SPAIN%20DRAFT%20UPDATED%20NECP.pdf.

[38] Portuguese Government. Portugal - Draft Updated NECP 2021-2030 - European Commission. Technical report, 2023. URL https://commission.europa.eu/document/download/bbcdfa78-5d50-474d-bd7f-16bd804a8388_en?filename=EN_PORTUGAL%20DRAFT%20UPDATED%20NECP.pdf.

[39] European Commission. Communication from the Commission to the European Parliament, the Council, the European Economic and Social Committee and the Committee of the Regions: A hydrogen strategy for a climate-neutral Europe. Communication COM/2020/301, European Commission, 2020. URL https://eur-lex.europa.eu/legal-content/EN/TXT/?uri=CELEX:52020DC0301.

[40] Secretary of State for Business, Energy & Industrial Strategy. UK Hydrogen Strategy. Technical report, UK Government, 2021.

[41] Bundesministerium für Wirtschaft und Klimaschutz. Fortschreibung der Nationalen Wasserstoffstrategie. Technical report, German Government, Berlin, 2023. URL https://www.bmwk.de/Redaktion/DE/Wasserstoff/Downloads/Fortschreibung.pdf?__blob=publicationFile&v=4.

[42] James Price and Ilkka Keppo. Modelling to generate alternatives: A technique to explore uncertainty in energy-environment-economy models. *Applied Energy*, 195:356–369, June 2017. ISSN 0306-2619. doi:10.1016/j.apenergy.2017.03.065.

[43] Evelina Trutnevyte. Does cost optimization approximate

the real-world energy transition? *Energy*, 106:182–193, July 2016. ISSN 0360-5442. doi:10.1016/j.energy.2016.03.038.

[44] María de la Esperanza Mata Pérez, Daniel Scholten, and Karen Smith Stegen. The multi-speed energy transition in Europe: Opportunities and challenges for EU energy security. *Energy Strategy Reviews*, 26:100415, November 2019. ISSN 2211-467X. doi:10.1016/j.esr.2019.100415.

[45] Andrea Tosatto, Xavier Martínez Beseler, Jacob Østergaard, Pierre Pinson, and Spyros Chatzivasileiadis. North Sea Energy Islands: Impact on national markets and grids. *Energy Policy*, 167:112907, August 2022. ISSN 0301-4215. doi:10.1016/j.enpol.2022.112907.

[46] Fabian Neumann, Elisabeth Zeyen, Marta Victoria, and Tom Brown. The Potential Role of a Hydrogen Network in Europe, March 2023.

[47] Eurostat. Harmonised Indices of Consumer Prices (HICP) - all items, 2023. URL https://ec.europa.eu/eurostat/databrowser/view/teicp000/default/table?lang=en.

[48] Salvador Pineda and Juan M. Morales. Chronological Time-Period Clustering for Optimal Capacity Expansion Planning With Storage. *IEEE Transactions on Power Systems*, 33(6):7162–7170, November 2018. ISSN 1558-0679. doi:10.1109/TPWRS.2018.2842093.

[49] Leander Kotzur, Peter Markewitz, Martin Robinius, and Detlef Stolten. Impact of different time series aggregation methods on optimal energy system design. *Renewable Energy*, 117:474–487, March 2018. ISSN 0960-1481. doi:10.1016/j.renene.2017.10.017.

[50] Thomas Brown, Jonas Hörsch, and David Schlachtberger. PyPSA: Python for Power System Analysis. *Journal of Open Research Software*, 6(1):4, 2018. ISSN 2049-9647. doi:10.5334/jors.188.

[51] Marianne Zeyringer, James Price, Birgit Fais, Pei-Hao Li, and Ed Sharp. Designing low-carbon power systems for Great Britain in 2050 that are robust to the spatiotemporal and inter-annual variability of weather. *Nature Energy*, 3(5): 395–403, May 2018. ISSN 2058-7546. doi:10.1038/s41560-018-0128-x.

[52] Neha Patankar, Xiili Sarkela-Basset, Greg Schivley, Emily Leslie, and Jesse Jenkins. Land use trade-offs in decarbonization of electricity generation in the American West. *Energy and Climate Change*, 4:100107, December 2023. ISSN 2666-2787. doi:10.1016/j.egycc.2023.100107.

[53] Danish Energy Agency. Technology Data for Generation of Electricity and District Heating, 2016.

[54] Jonas Hörsch, Fabian Hofmann, David Schlachtberger, and Tom Brown. PyPSA-Eur: An open optimisation model of the European transmission system. *Energy Strategy Reviews*, 22:207–215, November 2018. ISSN 2211-467X. doi:10.1016/j.esr.2018.08.012.

[55] German Bundestag. Gesetz zu Sofortmaßnahmen für einen beschleunigten Ausbau der erneuerbaren Energien und weiteren Maßnahmen im Stromsektor, 2022. URL https://dejure.org/BGBl/2022/BGBl._I_S._1237.

[56] Hans Hersbach, Bill Bell, Paul Berrisford, Gionata Biavati, Andás Horányi, Joaquín Muñoz Sabater, Julien Nicolas, Carole Peubey, Raluca Radu, Iryna Rozum, Dinand Schepers, Adrian Simmons, Cornel Soci, Dick Dee, and Jean-Noël Thépaut. ERA5 hourly data on single levels from 1940 to present, 2018.

[57] Copernicus Climate Change Service (C3S). ERA5 hourly data on single levels from 1940 to present, 2023.

Supplementary Information

Total system cost distribution

Overall optimal system costs in our different focus models and scenarios (before near-optimal studies) have a range of 734–880 bn EUR (not including existing transmission, nuclear and hydropower infrastructure; Methods). The plot below shows a complete overview of total system costs in robust system designs considered in this study (i.e. those laying inside the intersection of near-optimal spaces for different scenarios). For each category, the figure indicates the range between the minimum and maximum system-wide cost in that category observed in any robust network (in this case coming from the German-focused model). Comparable costs found in the baseline cost-optimal solutions (for weather years 1985, 1987, 2010) are shown with white stars. Note that these cost-optimal solutions are not necessarily robust; indeed this figure as well as Figure 1 of the article show that e.g. solar investments in the cost optima are not feasible in all scenarios. The top four categories represent the dimensions which have been explored explicitly — in this figure "inside" and "outside" costs have been aggregated. The two starred categories, nuclear and hydro(power), have been included in this figure, but represent capacities that are not subject to optimisation and rather included at today's levels. There is nevertheless some variation in nuclear costs since marginal costs in the form of uranium supply can vary depending on operations, which are optimised, and included in the nuclear category.

The cost ranges in this plot have been calculated on the basis of optimisations of 300 robust system designs with total inside- and outside solar, onshore wind, offshore wind and hydrogen investment fixed at random vertices on the boundary of the robust design space. This is the same basis on which the export ranges in Figure 3 in the main text have been computed (Experimental procedures).

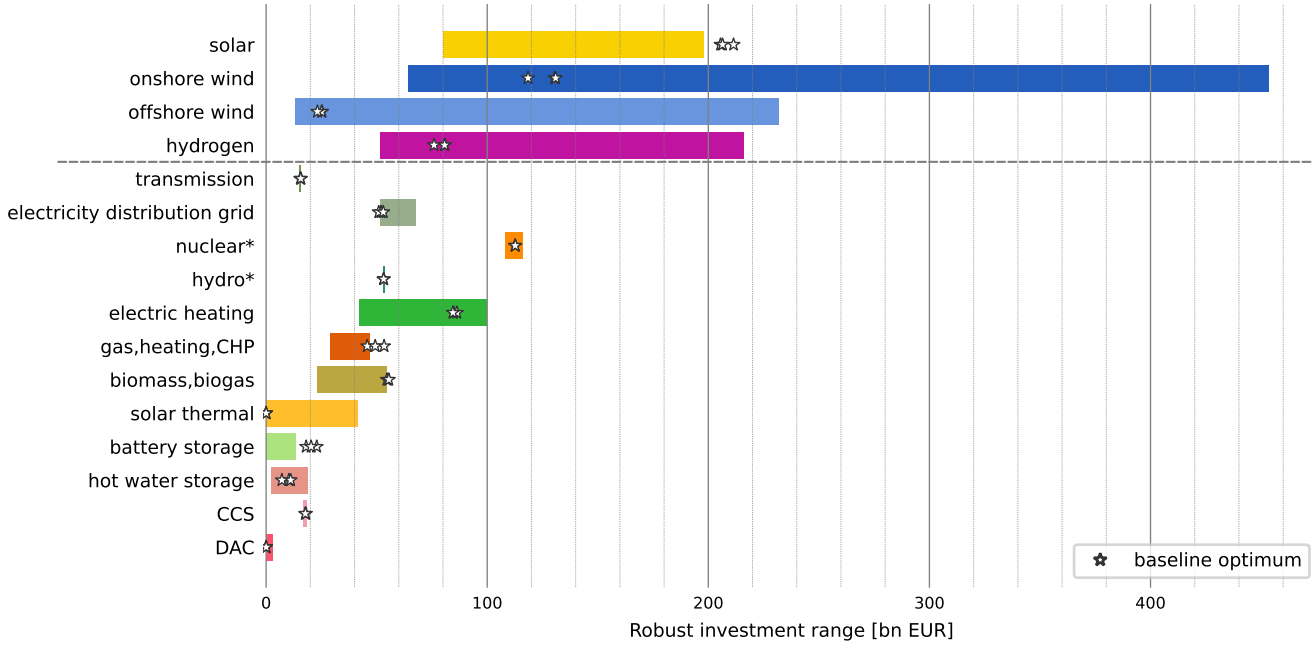

Figure S1: Ranges robust system costs by category.

Representation of fossil fuels and the carbon cycle

We strictly enforce net-zero emissions in all model runs. In order to achieve this, some use of negative emissions is necessary. However, optimal system design can depend strongly on assumed carbon sequestration potential. In this study, we assume a yearly sequestration capacity of 200 Mt CO_2, following [4]. This limit on sequestration effectively limits the use of fossil fuels in the model.

Natural gas use in Europe amounted to approximately 5271 TWh in 2021, with 4417 TWh in the EU27 area [2] and 854 TWh in the UK [1] (using gross calorific values). In all robust model solutions, we see a total natural gas use of around 363 TWh in the modelling region (which includes Switzerland, Norway and the Balkan in addition to the EU and the UK). This is about 6.9% of the EU+GB natural gas demand in 2021. The use of fossil oil is not found to be competitive in any robust model solution.

Natural gas and oil as well as non-feedstock emissions are the only way for carbon to enter the modelled cycle, and sequestration is the only way to leave the cycle. Since CO_2 sequestration potential as well as non-feedstock emissions (mainly from the cement industry) are fixed in the model, this also fixes the total amount of fossil gas and oil that may enter the system.

Impacts of different slack levels/near-optimality constraints

In the present study, we use a near-optimality constraint (slack level) of 5% on top of the most expensive of the 12 investigated scenarios. We have conducted a sensitivity analysis for one of the focus regions (Germany) to capture how the robust design spaces changes depending on the slack levels of 2%, 5%, 10%, and 20%. Table S1 presents an overview over how key results depend on the slack level. Figure S2 shows that although the size of the robust design spaces increases, the shape of the projections remains similar. This indicates that the trade-offs and insights presented in the main text are robust throughout different slack levels. Note that with increasing slack, the nested intersections increase in size and therefore the quality of the approximation decreases (as more than the constant 150 iterations would be needed to account for this). This explains why the approximated robust design space based on 20% slack does not contain the other robust spaces fully — in theory, it should.

European robust investment [bn EUR]	2% slack (∼ 15.6 bn EUR)	5% slack (default) (∼ 39 bn EUR)	10% slack (∼ 78 bn EUR)	20% slack (∼ 156 bn EUR)
Solar	98.0 – 179.5	58.7 – 179.5	45.3 – 179.5	49.6 – 180.5
Onshore wind	64.9 – 374.5	57.6 – 315.7	59.7 – 523.4	68.3 – 604.0
Offshore wind	5.0 – 176.2	0.1 – 158.6	3.1 – 213.5	1.5 – 179.1
Hydrogen infrastructure	37.5 – 236.1	33.6 – 118.6	29.8 – 326.1	25.5 – 441.0
Wind investment	181.3 – 381.9	165.8 – 329.2	167.2 – 517.8	152.0 – 586.6
Renewable generation	353.5 – 521.1	337.6 – 461.0	336.3 – 612.3	325.7 – 686.5

Table S1: Sensitivities of European robust investment to chosen slack level. The robust investment consists of the investment inside and outside the focus region. Note that the values for 2%, 10%, and 20% are based on 150 iterations with Germany as the focus region, whereas the 5% values are consistent with Figure 2 in the main text. The values in the robust range for 5% are minimal across all 7 focus regions and are based on 450 iterations. Note that as the slack level (and therefore the robust design space) increases, the quality of the approximation decreases. This explains the counterintuitive lower limits of solar and onshore wind and upper limit of offshore wind for 20% slack. If approximated in sufficient detail, these spaces are nested, i.e. the robust space for 20% contains the one for 10%.

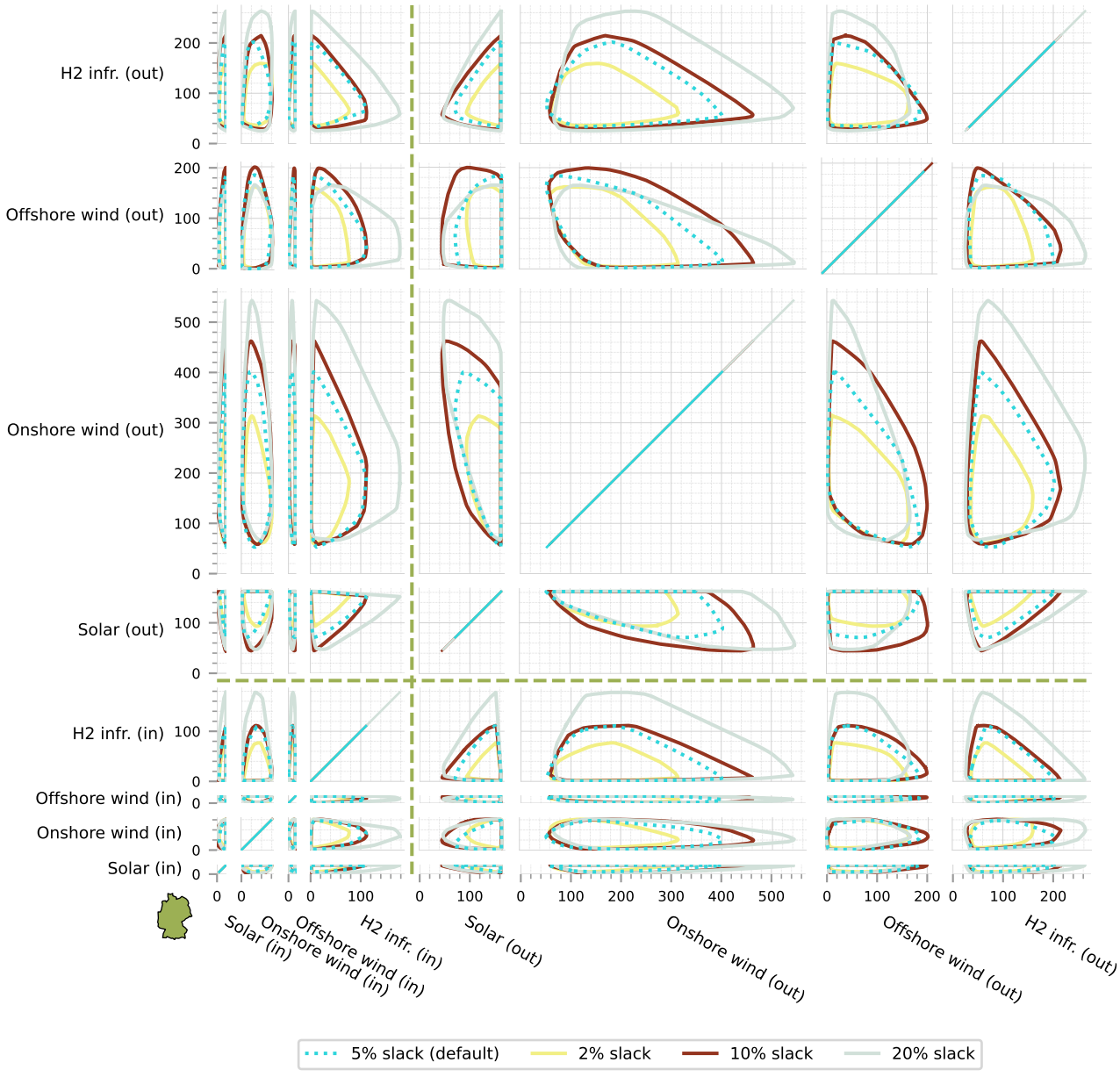

Figure S2: Projections of the intersection of near-optimal spaces for the German-focused model with different slack levels (2%, 10%, 20% compared to the 5% we use in the study). All four intersections are based on 150 iterations per near-optimal space (for the 5%-near-optimal spaces we only took the first 150 of the 450 iterations used in the study).

Impacts of self-sufficiency constraint

In the present study we introduce for the first time a self-sufficiency constraint to PyPSA-Eur-Sec; this constraint having originally only been implemented for PyPSA-Eur (the electricity-only version of the model). The self-sufficiency is accounted for on a yearly basis, that is, a self-sufficiency level of $x\%$ means that that total yearly energy production of every country must equal at least $x\%$ of the total yearly energy demand of that country (see precise definition in the Experimental procedures). Below, we present a simple sensitivity analysis of total system cost with respect to given self-sufficiency levels. We see that requiring self-sufficiency levels above 90% gets increasingly expensive; we choose a level of 75% for the present study.

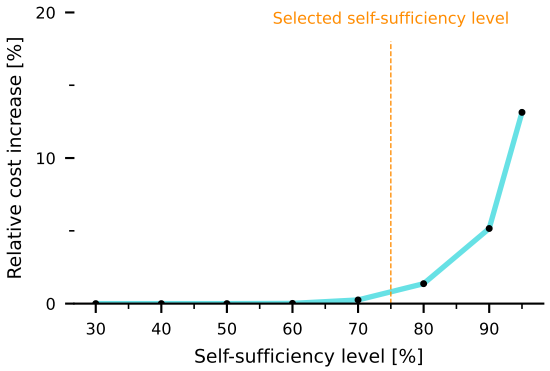

Figure S3: Relative increase of total system costs of an optimal network depending on different levels of net self-sufficiency (see Experimental procedures).

Furthermore, we have conducted a sensitivity analysis for one of the focus regions (Germany) to investigate the impact of the self-sufficiency constraint (75%) on the robust design spaces. Note that the robust design spaces in Figure S4 are smaller when dropping the self-sufficiency constraint: the total system costs are lower when the constraint is not enforced, which reduces the upper bound on near-optimality from the definition of the design spaces ($\mathcal{F}_{\varepsilon}^{r,s}$ in Experimental procedures). The reduction in available capital has a larger impact on the robust solution space than being able to rely more on imports.

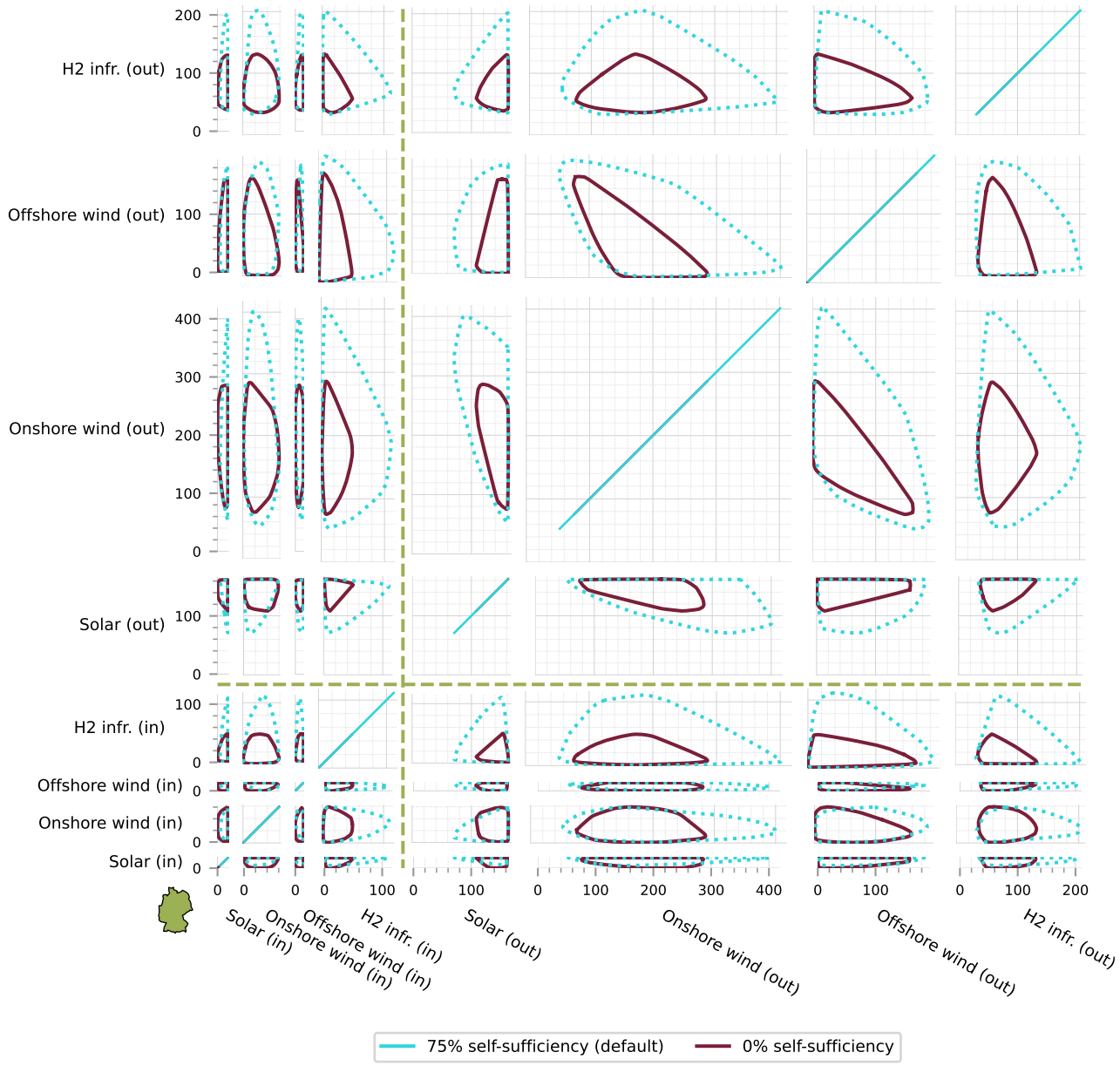

Figure S4: Projections of the intersection of near-optimal spaces for the German-focused model depending on whether the self-sufficiency constraint is enforced. Note that with relaxing the self-sufficiency constraint the reduction of total system costs makes less money available for near-optimal solutions, shrinking the robust design space. The intersections are based on 150 iterations per near-optimal space (for the near-optimal spaces with 75% self-sufficiency we only took the first 150 of the 450 iterations used in the study).

Sensitivity of transmission expansion limitations

The main results in the present study are based on optimisations in which we limit the transmission volume to 125% of the currently existing transmission in Europe. Single transmission lines or links can still be expanded freely as long as the total volume of transmission in the system adheres to the 125% constraint. We choose this conservative constraint, as most benefits in the power system are reaped at this level (Fig. 6 in Hörsch & Brown [3]); still, hydrogen transportation can still lead to significant energy transportation across the system.

We have conducted a sensitivity analysis for one of the focus regions (Germany) to investigate the impact of different transmission constraints (150%, 200%, 300%, 400% compared to the default 125%) on the robust design spaces and key system values (Table S2). Note that in Figure S5 the robust design spaces are smaller for higher transmission levels: the total system costs are lower when transmission can be expanded more, which reduces the upper bound on near-optimality from the definition of the design spaces ($\mathcal{F}_{\varepsilon}^{r,s}$ in Experimental procedures). The reduction in available capital has a larger impact on the robust solution space than being able to expand transmission more.

Optimal investment (bn EUR)	125% trans. (default)	150% trans.	200% trans.	300% trans.	400% trans.
Solar	182.7	178.6	172.6	167.6	167.6
Onshore wind	149.9	150.3	150.6	153.0	153.0
Offshore wind	28.5	28.9	30.1	29.7	29.7
Hydrogen infrastructure	67.8	63.1	56.8	54.6	54.6
Wind investment	178.5	179.2	180.6	182.8	182.8
Renewable generation	361.1	357.8	353.5	350.3	350.3
Total system costs	779.6	761	754.5	752.9	752.9

Table S2: Optimal investment in Europe (average across the 12 scenarios) depending on the upper limit of transmission expansion: 125%, 150%, 200%, 300%, 400% compared to current levels. The sensitivity analysis is conducted with Germany as the focus region. European investment is therefore the sum of inside (German) and outside (rest of the system) investments in solar, onshore and offshore wind and hydrogen infrastructure.

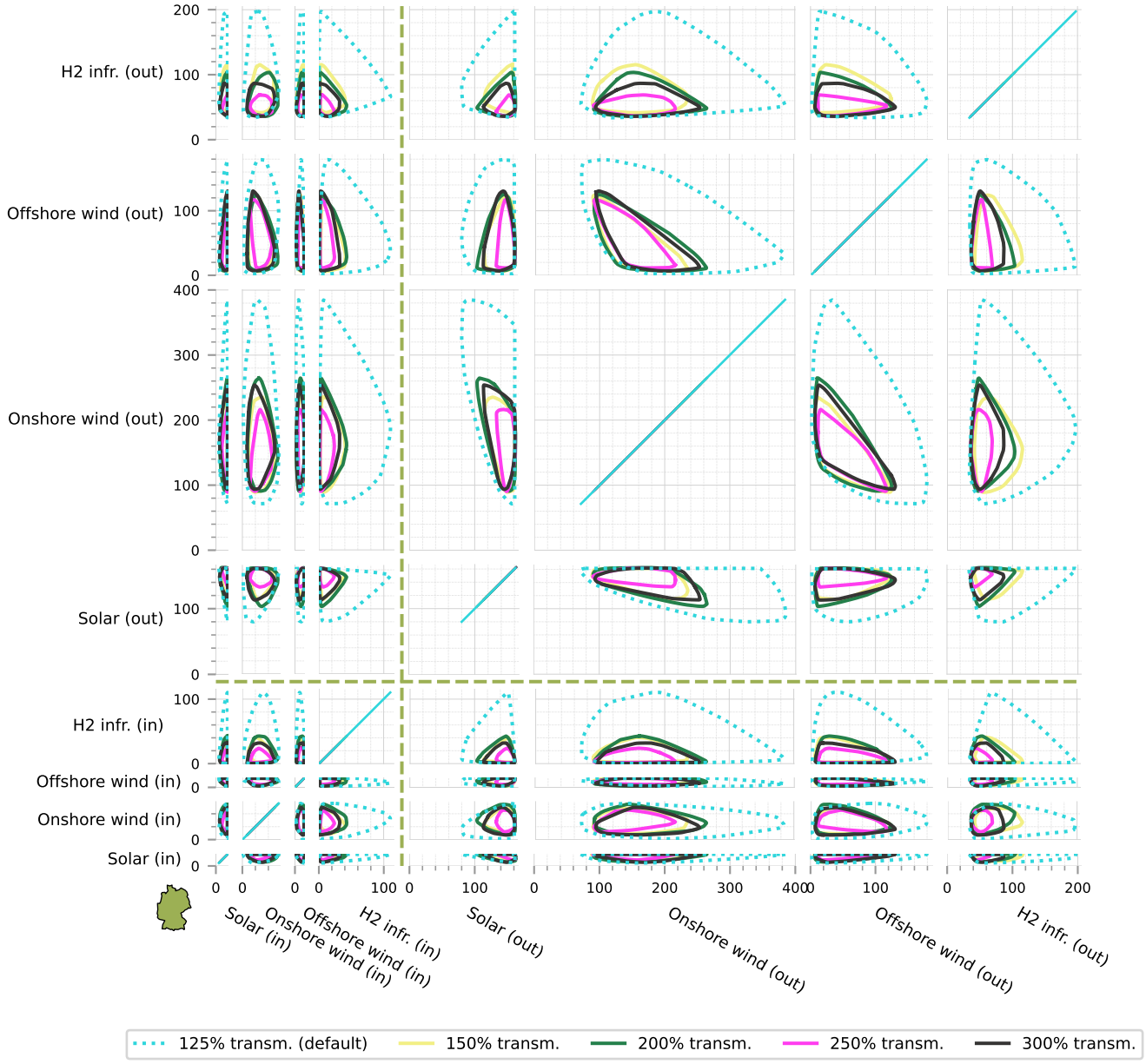

Figure S5: Projections of the intersection of near-optimal spaces for the German-focused model depending on the constraint of transmission expansion. Note that for higher allowed transmission expansion the reduction of total system costs makes less money available for near-optimal solutions, shrinking the robust design space. All five intersections are based on 140 iterations per near-optimal space (for the near-optimal spaces with 125% transmission expansion we only took the first 140 of the 450 iterations used in the study).

Robust export ranges

Figure S6 shows robust ranges of exports/imports observed for the 7 different focus regions. To compute export potential, we need a representative sample of full system designs (including operations) laying inside $\mathcal{I}_\varepsilon^r$ for each region r (Methods). This is because the geometric shape of $\mathcal{I}_\varepsilon^r$, which we compute as an intersection of near-optimal spaces, only contains information about total investment in solar, onshore wind, offshore wind and hydrogen (inside and outside r), but no total export figures. Thus, for each r, we sample 300 points in $\mathcal{I}_\varepsilon^r$, and run model optimisations where total solar, onshore wind, offshore wind and hydrogen investment are fixed to the coordinates of the 300 points. We can then calculate total imports / exports for each model and region; the results are shown in Figure S6. The 300 points are sampled randomly on the boundary of $\mathcal{I}_\varepsilon^r$, except the first 24 which consist of those points which min- and maximise each individual of the 8 key dimensions (16 total) and those that min- and maximise the system-wide solar, onshore wind, offshore wind and hydrogen dimensions (8 total).

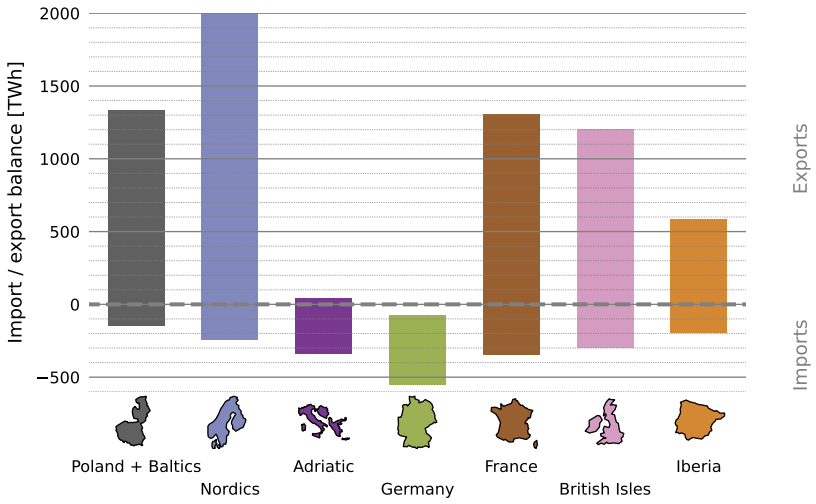

Figure S6: Robust ranges of net annual energy balance per focus region. Specifically, the bars indicate the minimum and maximum energy trade balances observed across a large sample of robust solutions. All regions can be net importers (while adhering to the 75% self-sufficiency) and most can also be net exporters to various degrees. While the lower ends of the ranges essentially reflect the imposed constraint of 75% self-sufficiency, the upper ends are determined by a combination of competitive renewable generation potential and access to export destinations. The absolute values of maximum possible exports may change with the system cost slack level (here 5%) where export potential is limited by profitability and not land-use.

Impact of regional/European investment on the near-optimal space

In Figure 7, we present the impact of regional investment on robust European investment through a flexibility indicator (defined in the Experimental procedures). The flexibility indicator in this case is based on the mean width of the space of robust designs (projected onto the 4 key dimensions of European investment), depending on (robust) investment levels for each regional key dimension. In other words, for a given inside investment level (say, a 10 bn EUR investment in onshore wind in the Nordics), we compute outside design flexibility as the mean of the differences between maximum and minimum outside investment in solar, onshore wind, offshore wind and hydrogen. The following plot shows the "converse": the impact of continental investment on regional design flexibility. The plot is analogous to Figure 7, but the roles of "inside" and "outside" have been swapped.

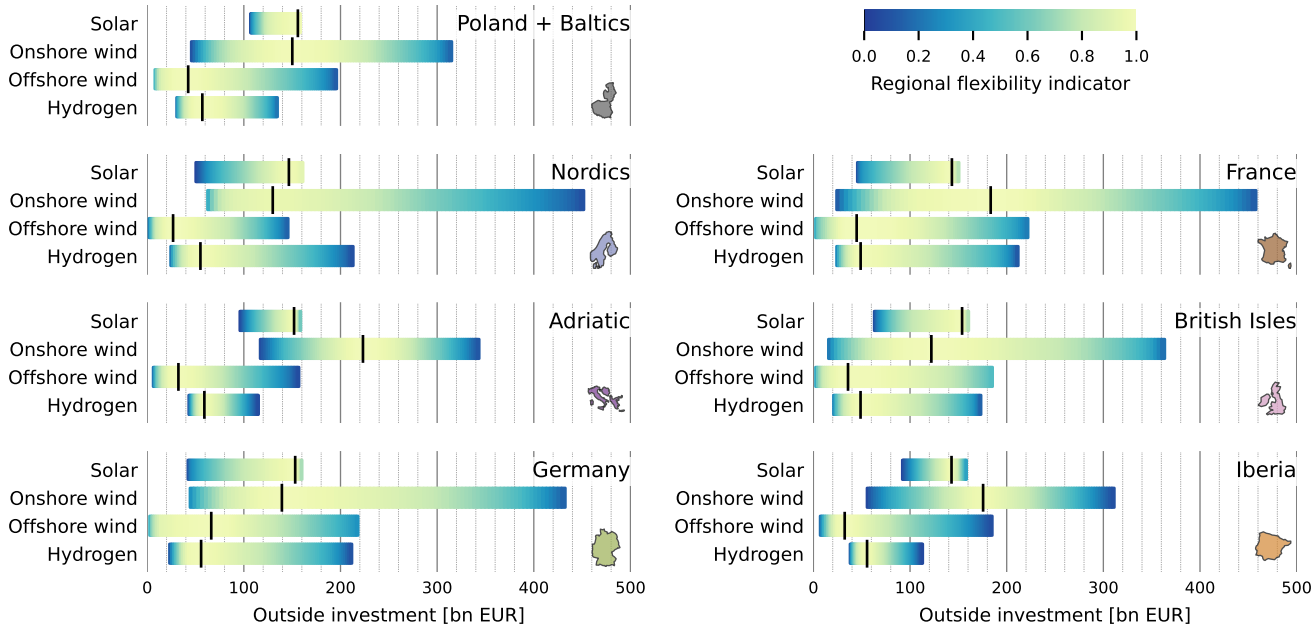

Figure S7: Effects of continental investment decisions on the design flexibility of the focus regions. The calculation of the flexibility indicator (where 1 is maximally flexible) that is plotted is explained in the Experimental procedures. The levels of continental investment leading to maximal regional flexibility are marked with black vertical bars. For instance, European investment in onshore wind has a positive effect on design flexibility in Poland and the Baltic states from 40 and up to about 150 bn EUR, with only a marginal decrease in flexibility upon further investment. Related to Figure 7.

Related to this, it is possible to identify at what (regional or continental) investment levels the largest gains or losses of design flexibility are realised: by taking the derivative of the mean width of the robust design space — formally the derivative of the absolute (not relative as in Figure 7 and Figure S7) flexibility indicator. By varying technology investment levels *inside* a focus region as in Figure S8 we capture the increasing or decreasing mean width of the projection onto European investments *outside* the focus region. These increases and decreases of flexibility are shown as derivatives in Figure S8 and for the converse (based on outside investment variations) in Figure S9.

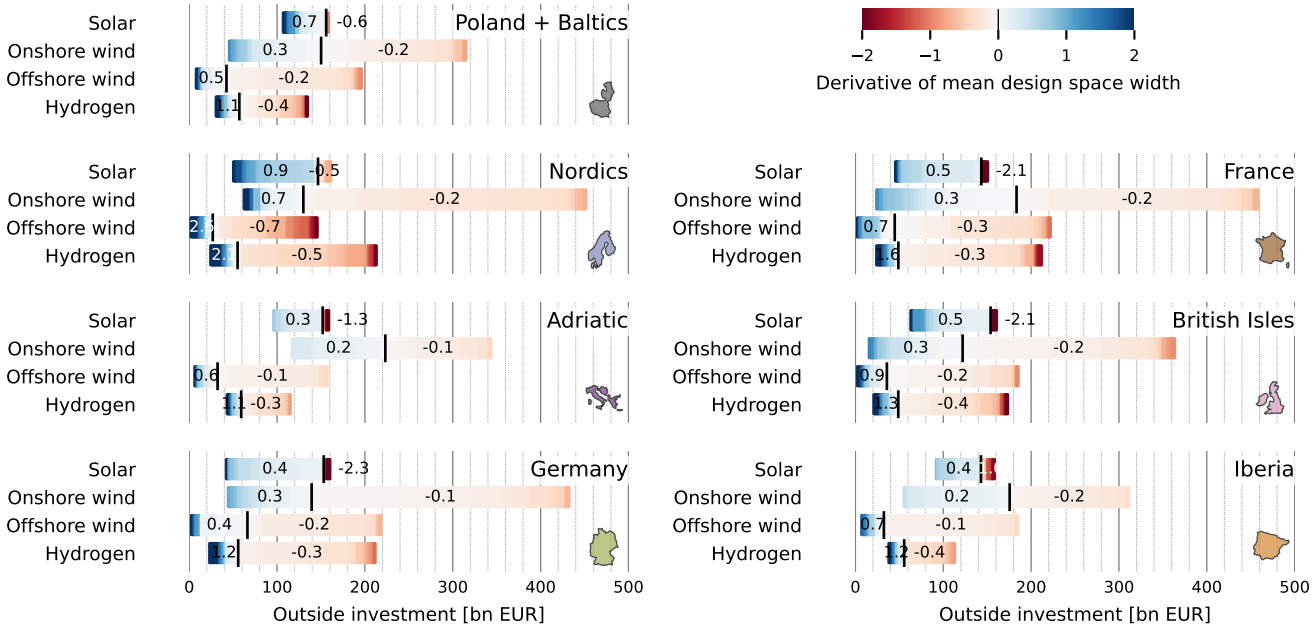

Figure S8: Derivative of mean width of focus region design space with respect to changes in investment outside the focus region. The levels of outside investment leading to maximal regional flexibility (where the derivative is zero) are marked with black vertical bars. On either side, the derivative of mean width of the robust design space of the given focus region, with respect to outside investment in solar, onshore- and offshore wind and hydrogen, is indicated using a colour scale. A positive derivative indicates that additional marginal investment in a given technology (outside a focus region) enlarges the design space, thus the flexibility, of the focus region. For each region and technology, the mean derivatives up to maximum flexibility and beyond this point (which are positive and negative respectively) are annotated. Related to Figure S7.

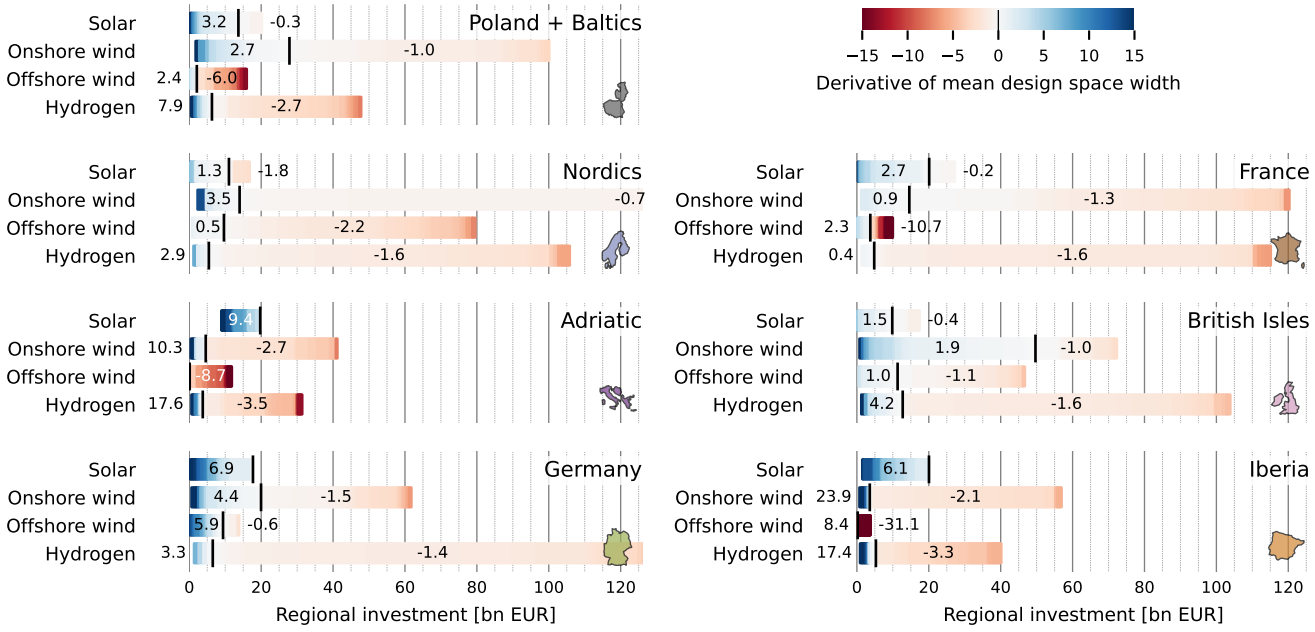

Figure S9: Derivative of mean width of the design space outside the focus region with respect to changes in investment inside the focus region. The levels of inside investment leading to maximal system-wide flexibility (where the derivative is zero) are marked with black vertical bars. On either side, the derivative of mean width of the robust design space outside the given focus region, with respect to inside investment in solar, onshore- and offshore wind and hydrogen, is indicated using a colour scale. A positive derivative indicates that additional marginal investment in a given technology (inside a focus region) enlarges the design space, thus the flexibility, outside the focus region. For each region and technology, the mean derivatives up to maximum flexibility and beyond this point (which are positive and negative respectively) are annotated. Related to Figure 7.

Regional vs. continental investment

The following two plots are analogous to Figure 8 in the main text, but for utility solar and hydrogen investments respectively.

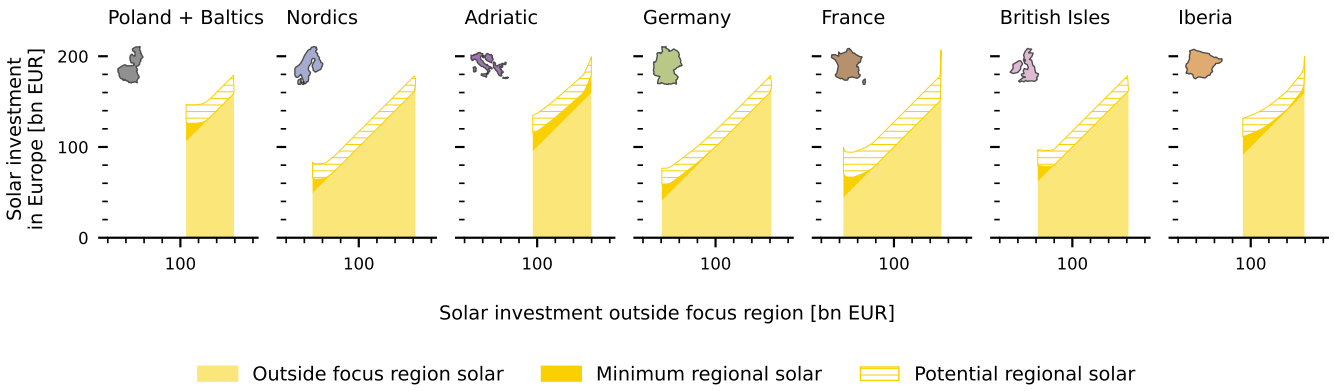

Figure S10: Minimum and maximum potential ranges of total solar power investment in different regions, as a function of solar power investment outside the respective regions. Note that each subplot represents separate results from differently focused models, hence the disagreement on maximum overall viable solar power investment. Related to Figure 8.

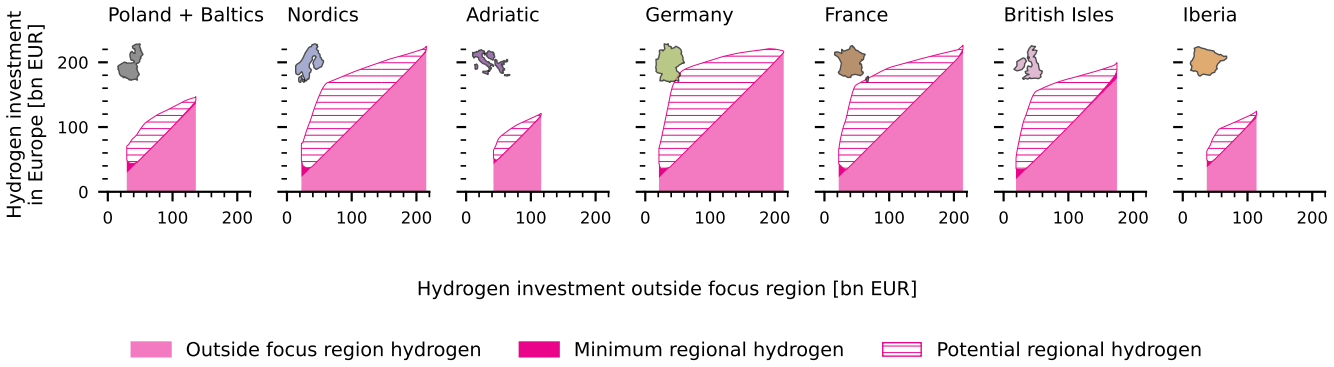

Figure S11: Minimum and maximum potential ranges of total hydrogen infrastructure investment in different regions, as a function of hydrogen infrastructure investment outside the respective regions. Note that each subplot represents separate results from differently focused models, hence the disagreement on maximum overall viable hydrogen infrastructure investment. Related to Figure 8.

Modelling regions

As described in the Experimental procedures section, we use different spatial layouts of the same model for our different focus regions. This is in order to better represent spatial variability and transmission bottlenecks in the respective focus regions, while reducing the overall spatial resolution of the model for computation reasons.

For each focus region, we "distribute" 60 nodes of spatial resolution by giving a certain number of nodes to each of the focus region itself, the countries bordering the focus region, and the remaining countries. The exact numbers of nodes allocated to each of these three categories depends on the focus region, and are listed in the Experimental procedures section of the main text. Note that there may sometimes be fewer nodes than countries in the modelling area not bordering on the focus region; in this case whole countries may be clustered together (e.g. Germany, Czechia and Poland in the Adriatic-focused model).

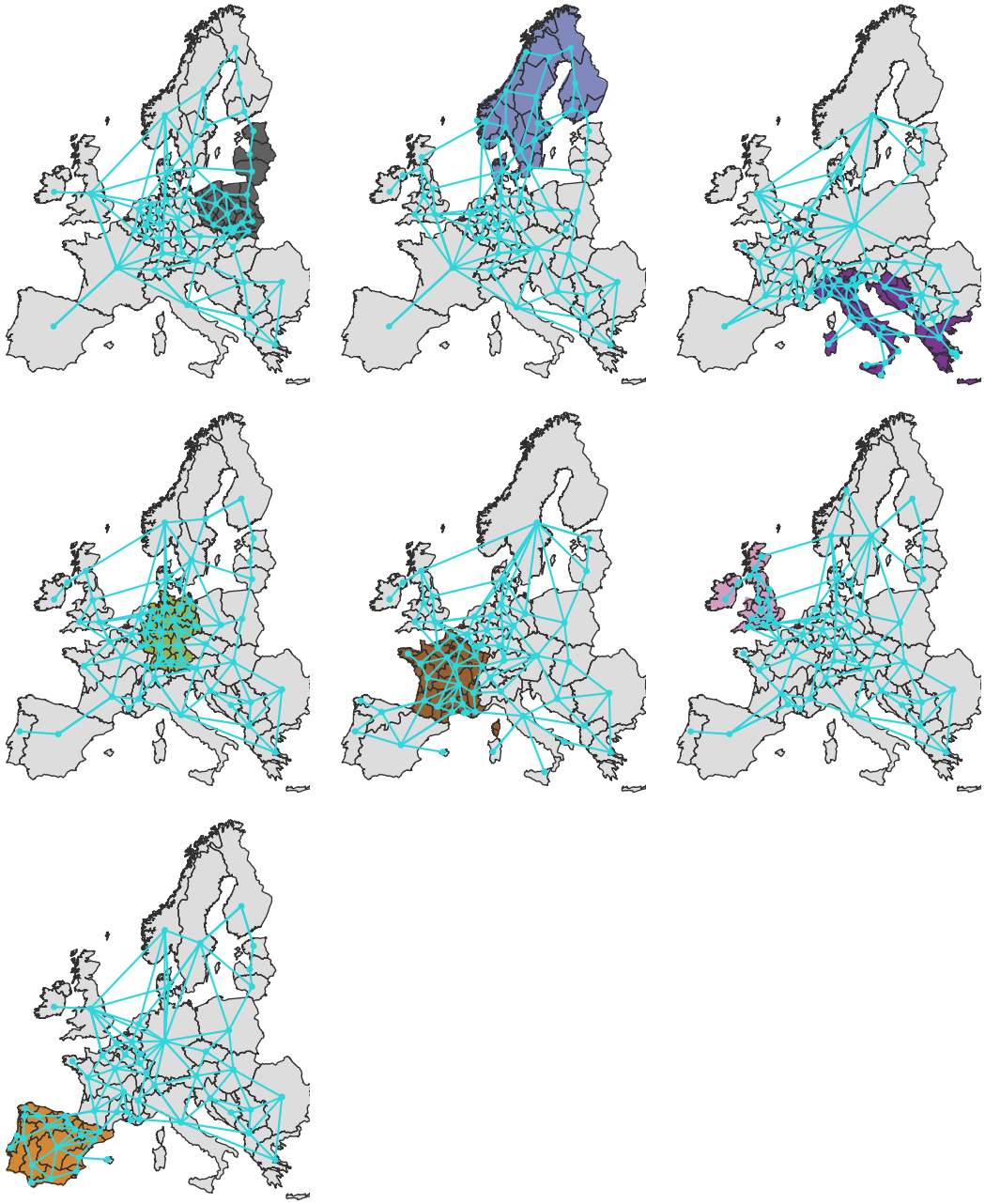

Figure S12: Network topology for the various focus models. The plots only illustration spatial resolution: bus and line sizes do not carry any significance in this plot.

Near-optimal spaces

Below, we show projections onto each pair of the 8 dimensions

$$\{\text{Solar, Onshore wind, Offshore wind, Hydrogen}\} \times \{\text{inside, outside}\}$$

of the robust design space for the German-focused model (Figure S13). Recall that this robust design space is the intersection of near-optimal spaces arising from 12 different scenarios. In the next figure, Figure S14, we show projections of these 12 near-optimal spaces, this time aggregating the inside and outside dimensions.

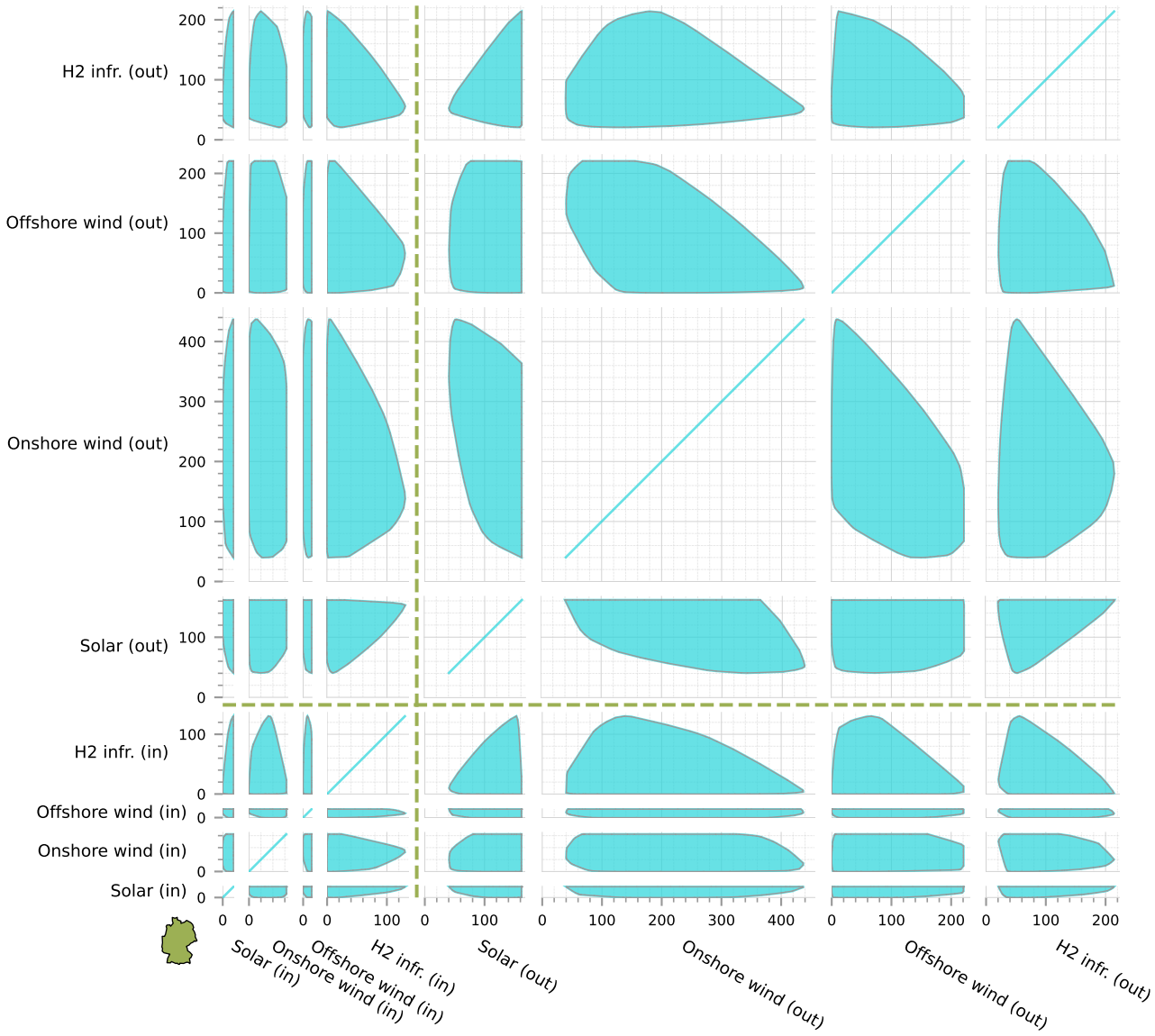

Figure S13: Projections of the intersection of near-optimal spaces for the German-focused model.

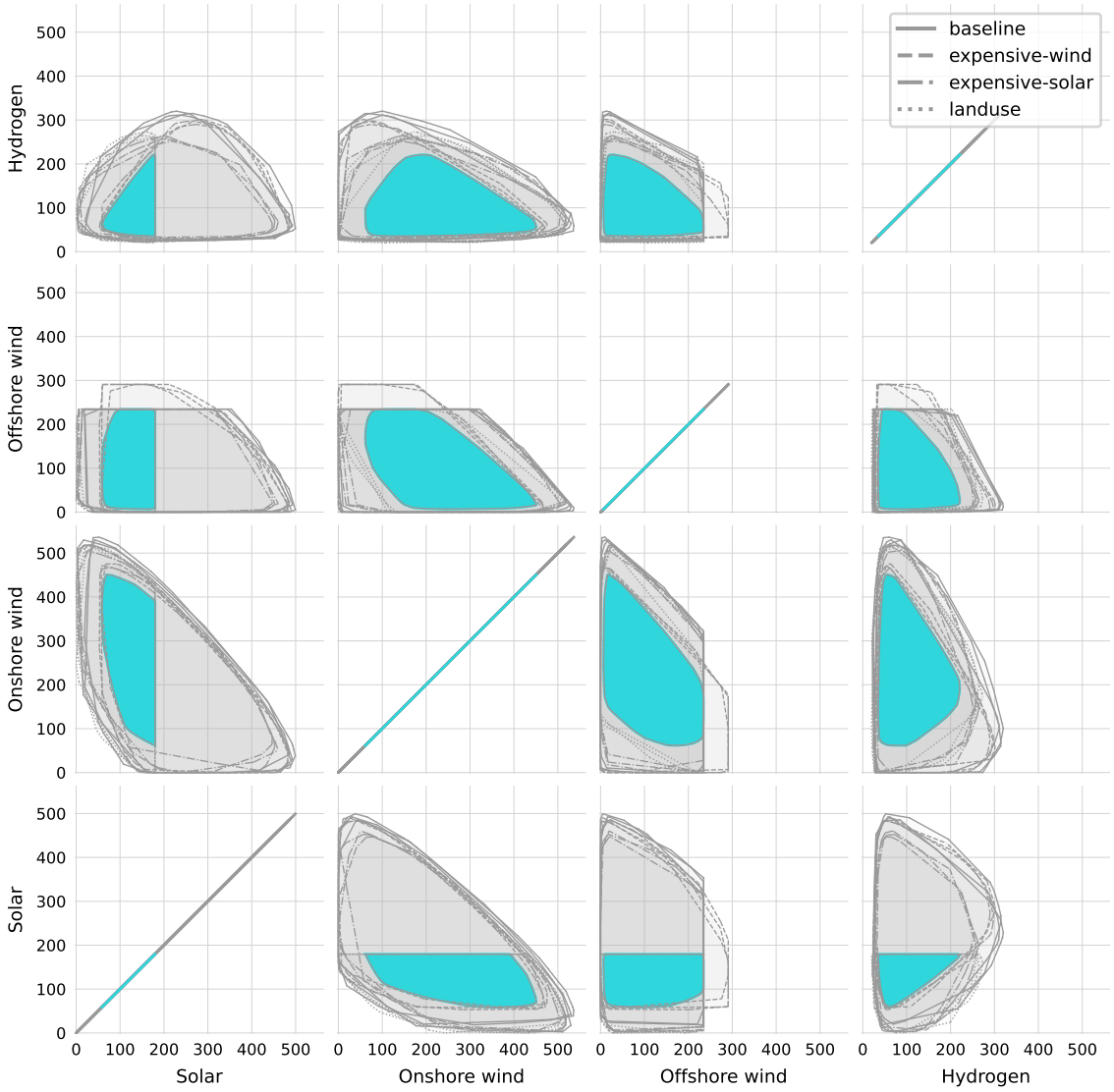

Figure S14: Projections onto four major dimensions of approximations of the near-optimal scenarios corresponding to 12 scenarios of the German-focused model (grey) as well as projections of the intersection of these scenarios (turquoise). Scenario categories are indicated with different line styles (see legend); for each category there are three different near-optimal spaces corresponding to the weather years 1985, 1987 and 2010. Each of the dimensions shows in this plot (solar, onshore wind, offshore wind, hydrogen) represent aggregations of the respective "inside" and "outside" dimensions.

References

[1] Department for Energy Security & Net Zero (UK). Natural gas supply and consumption, 2023. URL: https://assets.publishing.service.gov.uk/media/65130c71b23dad000de706d5/ET_4.1_SEP_23.xlsx.

[2] Eurostat. Supply, transformation and consumption of gas, 2023. URL: https://ec.europa.eu/eurostat/databrowser/view/nrg_cb_gas/default/table?lang=en.

[3] Jonas Hörsch and Tom Brown. The role of spatial scale in joint optimisations of generation and transmission for European highly renewable scenarios. In *2017 14th International Conference on the European Energy Market (EEM)*, pages 1–7, Dresden, Germany, June 2017. IEEE. doi:10.1109/EEM.2017.7982024.

[4] Fabian Neumann, Elisabeth Zeyen, Marta Victoria, and Tom Brown. The potential role of a hydrogen network in Europe. *Joule*, 7(8):1793–1817, August 2023. doi:10.1016/j.joule.2023.06.016.

Article 4: “Pathways”

K. van Greevenbroek *et al.* «Diverse pathways for green hydrogen production in Europe.» (2024), pre-published

Diverse pathways for European green hydrogen production

Koen van Greevenbroek*[1], Johannes Schmidt[2], Marianne Zeyringer[3], and Alexander Horsch[1]

[1]*Department of Computer Science, UiT The Arctic University of Norway, Postboks 6050 Langnes, 9037 Tromsø, Norway*
[2]*Institute for Sustainable Economic Development, University of Natural Resources and Life Sciences, Feistmantelstraße 4, 1180 Vienna, Austria*
[3]*Department of Technology Systems, University of Oslo, P.O. Box 70, 2027 Kjeller, Norway*

26th June 2024

Green hydrogen is seen by the EU as a key technology in the energy transition; the Commission has committed to domestic production and imports of 10Mt each by 2030. Domestic production harnesses local renewable energy, but faces competition from fossil fuels combined with carbon capture and storage (CCS). Earlier studies have demonstrated the uncertainty in future development of green hydrogen. We show that significantly larger ranges of European green hydrogen production are viable than previously thought, based on allowing solutions that are marginally more expensive than cost-optimal in any given scenario. Its domestic production can be eliminated with little additional cost in most scenarios; only restrictions on CCS and green fuel imports force green hydrogen production. The level of production, however, has a deep impact on all surrounding sectors of the European energy system, meaning that an early commitment to *some* green hydrogen strategy is crucial.

As Europe undergoes the transition to net-zero emissions by 2050, hydrogen is seen as a key technology enabling a shift away from fossil fuels. Green hydrogen, produced from renewable electricity by water electrolysis, can be used as a carrier for storing and transporting energy and act as a partial substitute for fossil fuels in industry and transportation. It can also act as the feedstock for the production of other fuels such as ammonia, methanol and synthetic gas and oil. The European Union has set a target of 10 Mt ($\sim$ 330TWh in lower heating value) green hydrogen production and imports each by 2030 [1].

The long-term future of green hydrogen is, however, nowhere near set in stone. Various studies have projected European green hydrogen production in 2050 at 75 Mt [2], 4 Mt [3], 0–120 Mt [4].

Hydrogen is notoriously difficult to represent correctly in energy system models [5]; requirements include adequate spatial and temporal resolution combined with a sufficient representation of sector-coupling and demand flexibility. This difficulty may explain some of large gap between different hydrogen prognoses above. Regardless, we are also faced with significant uncertainty around future technological development and costs. These factors significantly impact the competitiveness of hydrogen with alternative energy carriers. Green hydrogen in particular competes with fossil fuels, whose viability in a net-zero energy system in turn depends on the successful deployment of large-scale carbon capture and storage [6]. As such, small variations in costs and constraints can potentially lead to large swings in cost-optimal pathways for green hydrogen.

Indeed, in assessing reasonable pathways for scaling up green hydrogen production, we posit that looking at cost-optimality is not enough. Historically, energy systems have not developed in cost-optimal manners [7]. Recent work on near-optimal modelling (also known as *Modelling to Generate Alternatives* — MGA) has shown that considering systems design even just 5% more expensive than cost-optimal opens up a wealth of different options [8, 9, 10, 11, 12, 13], with room for political compromise, investment in robustness and other factors that are difficult to include in cost-optimisation models outright.

We propose that the prospects for green hydrogen production should similarly be considered from a near-optimal perspective. Only beyond strict cost-optimality is it possible to map out the full ranges of options available to policy-makers. We use a novel combination of MGA applied to European green hydrogen production within a multi-horizon optimisation framework in order to study possible pathways from 2025 to 2050. The results show vast ranges of near-optimal alternatives, with green production production typically bottoming out at 0 and or more than tippling compared to cost-optimal solutions, all within a 5% total system cost slack.

In order to the investigate the effects of some of the most important factors influencing green hydrogen production, we conduct an extensive global sensitivity analysis over electrolyser cost, carbon capture and storage cost and potential, renewable land use restrictions and green fuel imports. All scenarios conform to net-zero emissions by 2050. Our most striking result is that green hydrogen production can be en-

*Corresponding author, koen.v.greevenbroek@uit.no

	A	B
Electrolysis	Capital cost of electrolysers **-50%**	Capital cost of electrolysers **+50%**
CCS	• Capital cost of carbon capture **-10%** • CO_2 sequestration **€15/tCO_2** • CO_2 sequestration potential **2000 MtCO_2/a**	• Capital cost of carbon capture **+50%** • CO_2 sequestration **€30/tCO_2** • CO_2 sequestration potential **400 MtCO_2/a**
Imports	Green fuel imports **disabled**	Green fuel imports **enabled**
Land use	**-50%** available for renewables compared to baseline	Baseline (maximum installable capacity of ∼8.3TW onshore wind, ∼10.4TW solar in modelling region)
Weather year	**2020** (easy)	**1987** (hard)

Table 1: An overview over the scenarios used for this study. Near-optimal paths for green hydrogen production at 2%, 5% and 10% total system cost slack levels were generated for each of the $2^5 = 32$ different combinations of A/B settings. Note that the "cost of carbon capture" technologies multipliers are applied to the full capital cost of any technology incorporating carbon capture, such as industrial processes or combined heat and power plants. The factor of -10% brings these costs down to nearly the same level as the corresponding alternatives *without* carbon capture.

tirely eliminated at low cost in most scenarios under consideration. This is primarily due to competition with fossil fuels, and secondarily green fuel imports. Only in scenarios where the use of both fossil fuels and imports is restricted, is green hydrogen production essential. The surprising part of this result is not that green hydrogen production can be avoided, but that it can be avoided at only very modest increases of total system cost of 2–5%.

Mapping out green hydrogen production pathways

The subsequent results are based on large number of energy system model optimisations covering the period of 2025–2050 in 5-year steps. In order to fully capture the potential roles played by hydrogen, this model (based on PyPSA-Eur [14, 15]) includes representations of the electricity, gas, heating, transportation and industry sectors, and is run at high spatial and temporal resolution (Methods). We repeat the optimisations for 32 scenarios, representing all possible combinations of A/B settings in five categories shown in Table 1. The scenarios have been chosen to represent a broad range of future uncertainty, focusing on factors closely related to green hydrogen production. As illustrated in Figure 1, green hydrogen production is minimised and maximised subject to total system cost increase limits of 2%, 5% and 10% at each time horizon and for each scenario separately.

Large ranges of cost-effective European green hydrogen

Figure 2 shows the extent of feasible and near-optimal pathways for green hydrogen production from 2030 to 2050. While the hatched green area, representing the range of cost-optimal pathways, already shows annual production ranging from 0 to 54Mt (∼1780TWh in lower heating value) by 2050, the range becomes much larger when allowing for slight deviation from cost optimality. At a 2% total system cost slack, this ranges increases to 0–83Mt; the maximum amount of green hydrogen production over all scenarios at 10% cost slack is 122Mt.

Total annualised system costs across the scenarios range from 736–798 bn EUR (2030) to 679–888 bn EUR (2050), meaning that a 5% total system cost slack amounts to 37–44 bn EUR depending on the time-horizon and scenario. For the green hydrogen maximisations, the dual variable of the total system cost constraint (as shown in Figure 1) indicated how much more green hydrogen could be produced if the cost constraint was relaxed by one unit; from this was can derive the implied green hydrogen subsidy which would induce the upper ranges of green hydrogen production. This subsidy is at 1.21 EUR/kgH_2 on average over the whole time horizon and all scenarios (with a standard deviation of 0.31), decreasing from 1.55 to 1.03 EUR/kgH_2 from 2030 to 2050. Thus, by 2050, a total subsidy of 1 bn EUR could be expected to induce the production of approximation 1Mt of additional green hydrogen. Subsidies carry diminishing marginal returns, however, with the required subsidy level to produce more green hydrogen rising from 0.81 through 1.01 to 1.27 EUR/kgH_2 at system cost slack levels of 2%, 5% and 10%, respectively.

The future of fossil fuels is intertwined with green hydrogen

Looking at four specific examples (Figure 3), we see the substantial direct and indirect impacts of different green hydrogen production pathways. The figure shows the outcomes of green hydrogen minimisation and maximisation in two different scenarios at the 2050 time horizon: one with pessimistic CCS assumptions (top row) and one with optimistic CCS assumptions (bottom row). Mainly by limiting the CO_2-sequestration potential, the models in the pessimistic CCS scenarios can only use a limited amount of fossil fuels; here, the 400Mt limit on CO_2-sequestration leads to a maximum possible combined use of oil and natural gas equivalent to ∼1300 TWh. However, we see that the balance between oil and natural gas is diametrically opposite between the min- and maximisation of green hydrogen production. When green hydrogen production is encouraged, a significant fraction is used as a feedstock for synthetic fuel production by the Fischer-Tropsch process (represented in Figure 3 as the link from "Hydrogen" to "Oil"). Under green hydrogen minimisa-

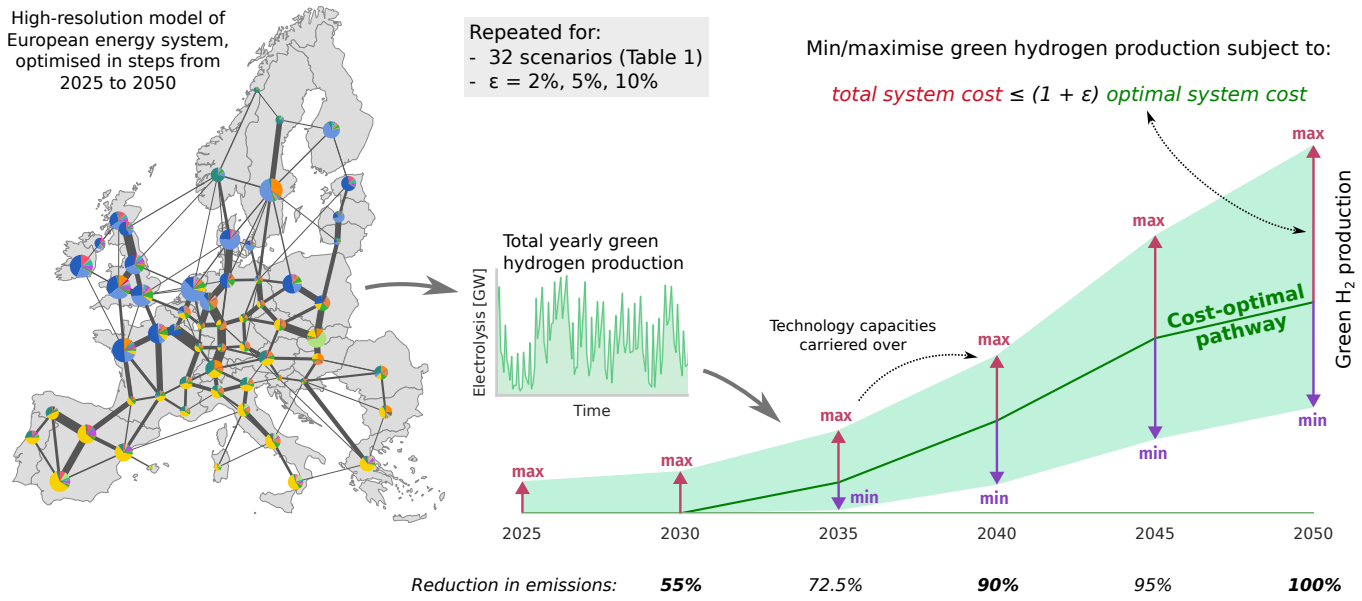

Figure 1: Illustration of model layout and the sequences of optimisations used to obtain ranges of green hydrogen production. In the middle, the cost-optimal pathway, consisting of a sequence of cost-optimisations at 5-year intervals, where capacities from each optimisation are carried over to the next (minus capacities that are phased out). Blue and red arrows illustrate the minimisations and maximisations (respectively) of green hydrogen at each time horizon; total system costs are not allowed to exceed $(1 + \varepsilon)$ times the optimal system cost for each time horizon. This sequence of optimisations is repeated for each of the 32 considered scenarios, and with $\varepsilon = 2\%, 5\%, 10\%$.

tion, almost all oil demand switches to fossil instead of synthetic, with hydrogen prioritised for essential (exogenously specified) demand in ammonia and methanol production. In this case, natural gas is almost eliminated from the system, with batteries supplying a significant amount of operational flexibility.

In the optimistic CCS scenario, green hydrogen production similarly displaces fossil oil. However, the effect on natural gas is reversed: minimal green hydrogen production (in this case, zero) is complemented with *more* natural gas use. In this scenario, fossil fuel use more than doubles from green hydrogen maximisation to minimisation; the ratio of renewables to fossil primary energy goes from about 4 : 1 to about 1 : 1. The use of fossil fuels is compensated for by generous use of carbon capture and storage.

While synthetic fuel production is most heavily affected by changes in green hydrogen production, other demand changes as well. In model runs with maximal green hydrogen production, we consistently see some switching from batteries to hydrogen fuel cells in the transportation sector. Hydrogen is used to some degree for heating as well. Of the examples in Figure 3, only in the case of green hydrogen production with pessimistic CCS assumptions do we see any use of grid-connected fuel cells to deliver backup generation using hydrogen as an energy storage medium. Green hydrogen thus mainly provides flexibility to the system indirectly, with electrolysers operating when renewable energy is available, and serving as a feedstock for synthetic fuel, ammonia and methanol which are cheap to store and transport.

We see that green hydrogen production, fossil oil and fossil gas are tightly intertwined in a decarbonised energy system consistent with the 2050 time horizon. The use of any one of these could approach (or stay at) zero by 2050 within a narrow range of total cost. Without any commitment to a combined hydrogen / gas / oil strategy, this could lead to great uncertainty in the European energy sector.

Fossil fuel limitations most consequential for viable green hydrogen levels

By performing a multi-variable linear regression on green hydrogen production in 2050 as a function of scenario settings (Table 1), we can quantify which scenario categories have the most impact on green hydrogen. Figure 4 (a) shows that assumptions on carbon capture and storage have the largest impact by some margin, though allowing imports is nearly as impactful for green hydrogen minimisation. The difference between settings A and B for the CCS category amount to a 30-35Mt difference in optimal and maximum green hydrogen production. Optimal and even more so maximum green hydrogen production levels are also impacted significantly by electrolyser costs, with the ±50% difference in captital cost assumption leading to 10-20Mt of additional production on average.

As seen in Table 1, the difference between optimistic and pessimistic CCS assumptions comprises three different factors: the capital cost of carbon capture infrastructure (i.e. the cost of installing carbon capture technology in power plants, industry, cement production, etc.), the marginal cost of CO_2 sequestration and the total annual potential for CO_2 sequestration. Figure 4 unpacks the sensitivities of green production

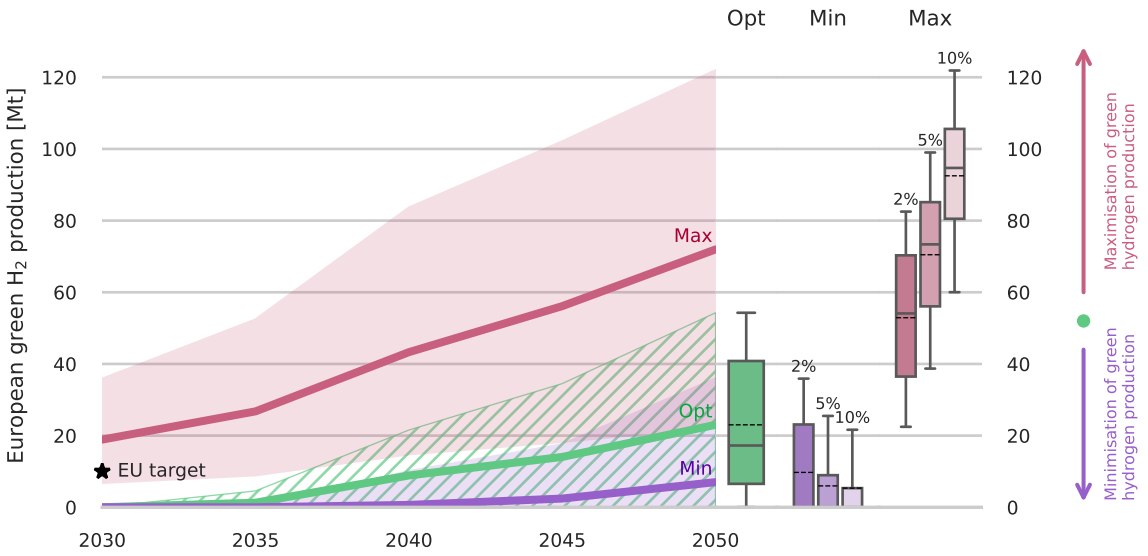

Figure 2: The range of pathways for European green hydrogen production across the scenarios studied. Shown are the cost-optimal trajectories (green, hatched) as well as trajectories under green hydrogen minimisation (blue) and maximisation (red). The solid lines show the mean, while the bands show the minimum and maximum across scenarios. The box plot on the right shows the distribution of green hydrogen production at the 2050 planning horizon, with the whiskers indicating the extreme ranges (0th and 100th percentile). Means are shown with dotted lines. For the min- and maximisations, the ranges are shown for 2%, 5% and 10% total system cost slack levels.

to these individual categories, as well as the additional factor of natural gas price. The CO_2 sequestration potential clearly has the largest impact, with sequestration cost and carbon capture capital cost nearly insignificant in comparison.

Figure 5 zooms in on near-optimal feasible ranges of green hydrogen production across the two most significant categories for minimal green hydrogen production: CCS and imports. The CCS setting (orange vs. pink) has an increasing effect on both minimal, optimal and maximum production starting in 2035; green fuel imports only have an impact on optimal pathways in 2045 and especially 2050. Looking at minimum green hydrogen production specifically, we see that the combination of pessimistic CCS assumption *and* no green fuel imports allowed (the rightmost bar) is the only case where any green hydrogen production is *necessary*. In all other cases, green hydrogen production can be kept at 0 even within the 2% total system cost bound.

Robust corridors of green hydrogen production

Some green hydrogen production levels are near-optimal for all included scenarios, depending the total system cost slack level. Figure 6 shows these robust "corridors" for three different slack levels. Notably, there is no single level which is within 2% of cost-optimal for all scenarios by 2050; the optimal pathways in different scenarios have diverged too much by then. The 2%-corridor is already narrow in 2040-45, rising between 10 and 20Mt — the 2030 EU target for 10Mt is on the high side for 2030. A much wider range is robustly near-optimal within 5% and 10%, however. Our results indicate that ~30Mt or more of European green hydrogen production would be a sensible target for 2050. It should be noted that, as per Figure 4, the lower ranges of the robust corridors are highly sensitive to the potential for imports and CO_2 sequestration.

Discussion & Conclusions

There is no real agreement in the literature on the "right" target for European green hydrogen production going forward[2, 3, 4]; to some extent this depends on uncertain and unknowable factors. This work demonstrates that while there may have been disagreement around cost-optimal pathways, much of the disagreement could be explained by the fact that large ranges of alternatives are near-optimal.

The European energy system could be powered by almost exclusively renewable power and green hydrogen by 2050, or keep relying on significant fractions of fossil fuels. We show that these different directions, and different roles for green hydrogen, can be realised at surprisingly similar total system cost. This similarity, however, betrays the far-reaching differences in energy flow, with flexibility services, the heating sector and synthetic oil production being particularly volatile. Given the lead time of over-turning energy infrastructure, this uncertainty presents a significant challenge to the energy transition.

In many scenarios, we see that European green hydrogen production can be entirely eliminated even while achieving net-zero emissions. However, a target of an annual domestic production around 30Mt would hedge against failing CCS efforts and lack of import options. A much higher production could also be feasible and would improve European energy self-sufficiency, but requires more renewable power which

(a) Low CCS, Minimum green H_2

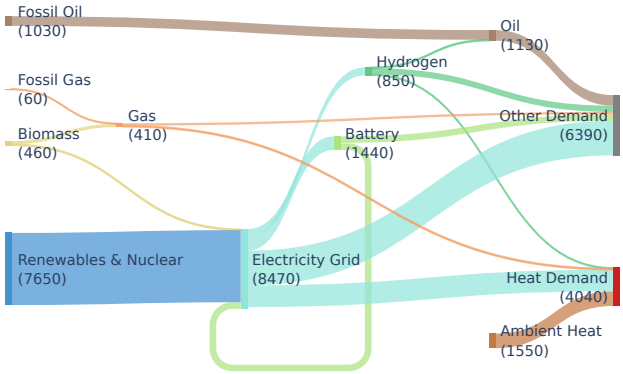

(b) Low CCS, Maximum green H_2

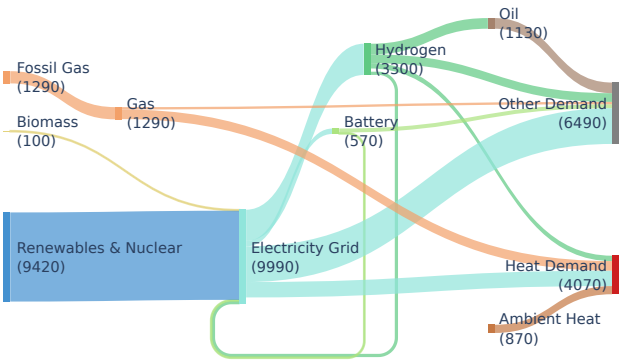

(c) High CCS, Minimum green H_2

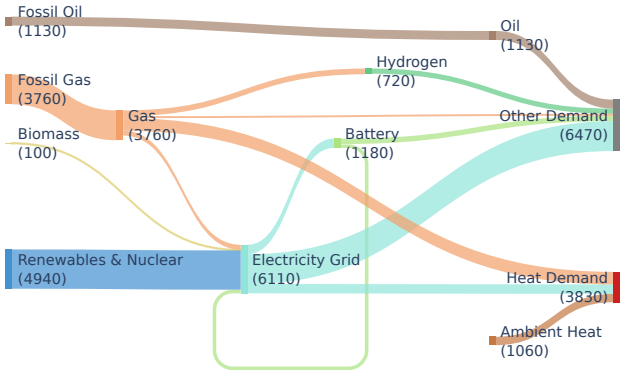

(d) High CCS, Maximum green H_2

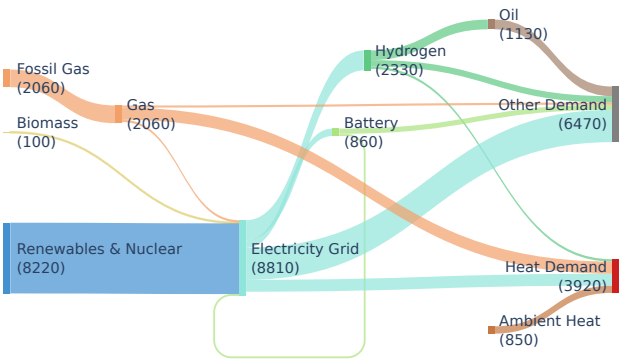

Figure 3: Comparison of energy flows in two different scenarios (top and bottom) under minimisation and maximisation of green hydrogen production (left and right, respectively). This figure displays energy flows at the 2050 planning horizon, with a 5% total system cost slack for green hydrogen min/maximisation. Total energy input to each node is displayed in TWh, rounded to the nearest multiple of 10. Green hydrogen production amounts to approximately 25 Mt (a), 95 Mt (b), 0 Mt (c) and 70 Mt (d) in the respective panels (converting from TWh to Mt in terms of lower heating value); note that (c) includes about 24 Mt of blue hydrogen production from natural gas, but no green hydrogen production. Note that energy losses are not explicitly shown or annotated here, resulting in slight discrepancies between energy input and output. Moreover, total demand is slightly different in the different panels because part of the demand is endogenous and can change between optimisations, such as direct air capture technology.

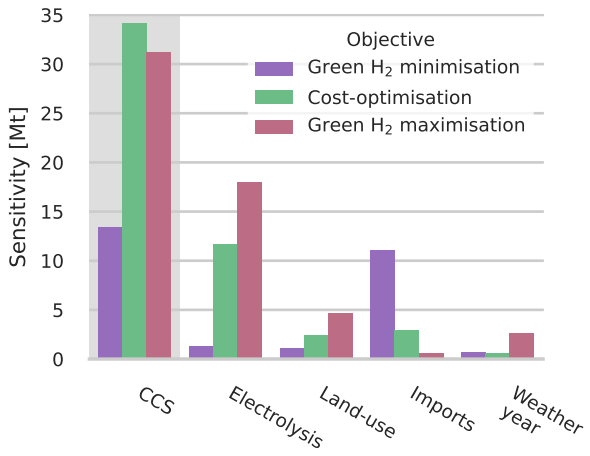

(a) Sensitivity of green hydrogen production in 2050 to the scenarios in Table 1. For the purposes of this sensitivity analysis, a multivariate linear regression was used to determine the impact of toggling each scenario category between A and B on minimum, optimum and maximum green hydrogen production. Since "A" and "B" were treated as 0 and 1 in this regression, the sensitivity coefficient can be interpreted as the amount by which minimum/optimum/maximum green hydrogen production changes between settings A and B (in Mt) for each category. For example, enabling imports reduces minimum green hydrogen production by just over 10Mt as predicted by the multi-linear regression.

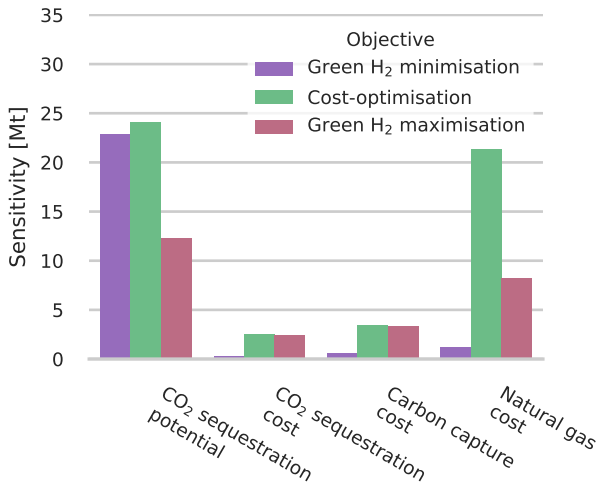

(b) Sensitivity of green hydrogen production in 2050 to more fine-grained parameters affecting use of CCS, i.e. the category highlighted in (a). The first three parameters (sequestration potential and cost, carbon capture cost) are set jointly for settings A and B of the CCS scenario (Table 1). The fourth parameter (natural gas cost) is not varied at all in the main scenarios, but included in this fine-grained sensitivity analysis for comparison.

Figure 4: Sensitivity of green hydrogen production in 2050 to scenarios and CCS-related parameters.

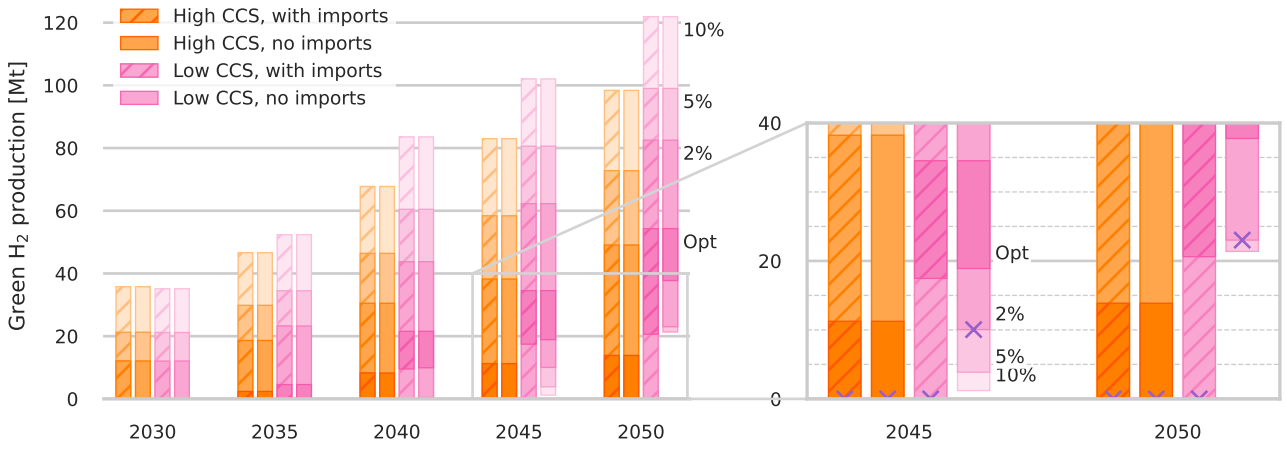

Figure 5: The ranges of pathways for European green hydrogen production under a combination of CCS and green fuel imports scenarios. The different shades show the observed ranges across near-optimal results at the 10%, 5% and 2% total system cost slack levels (from minimisation to maximisation of green hydrogen production), as well as the range of cost-optimal results. Orange and pink indicate scenarios with high and low CCS potential, respectively, while the hatched pattern indicates the availability of green fuel imports. In the zoomed-in portion, blue crosses mark the minimised green hydrogen production levels at 2% total system cost slack. We see that only in the scenarios with low CCS potential and no green fuel imports, are substantial volumes of green hydrogen production required.

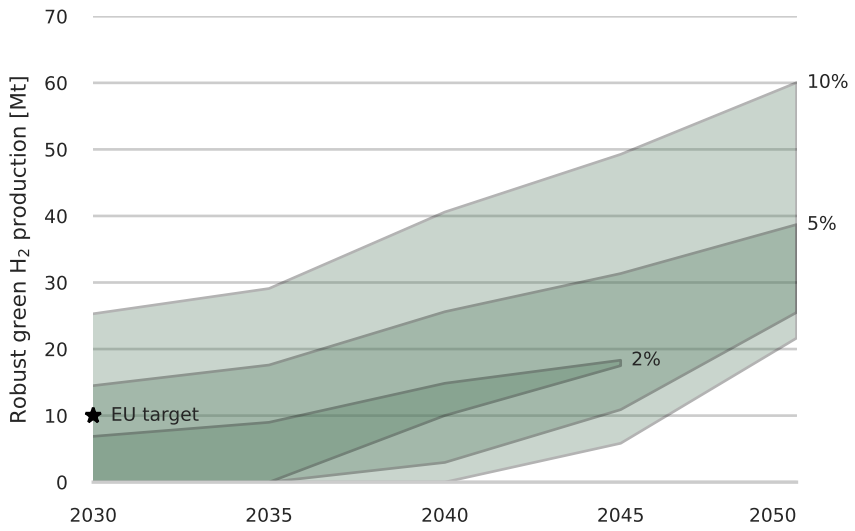

Figure 6: Corridors of green hydrogen production that are feasible and near-optimal in all scenarios. These robust corridors are shown at 2%, 5% and 10% total system cost slack levels. For example, 20Mt of green hydrogen production in 2040 is feasible and within 5% of cost-optimality for all scenarios, but not within 2% of cost-optimality for all scenarios. The robust corridor for 2% cost slack not extending beyond 2045 means that any green hydrogen production level is both below the minimum near-optimal level (at 2% cost slack) for some scenarios and above the maximum near-optimal level for other scenarios. This corresponds to overlap between the spread of minimum and maximum levels in Figure 2.

could face challenges related to land-use and social acceptance. On the other hand, continued use of fossil fuels will *require* extensive use of CCS technology in order to reach climate target.

The methodology used in this study has a few limitations, one of which is incomplete representation of technological learning; instead, costs of some technologies are assumed exogenously to fall in line with expect estimates. In reality, heavier initial investment in e.g. electrolysers could drive down costs faster. Imports are represented in limited detail; in particular, different import origins, seasonally varying prices and imports of other energy-related goods apart from fossil- and green fuels are not considered.

A clear European strategy for green hydrogen beyond 2030 is currently lacking. The same goes for oil- and gas use. Our work shows that the roles of fossil fuels and green hydrogen are so intertwined that they respective evolutions towards 2050 should be planned jointly and in a consistent manner. While the market-based Emissions Trading Scheme is effective at reducing emissions, an overarching vision for the balance between hydrogen and fossil fuels could provide predictability and stability to the energy transition.

Code and data availability

The code to reproduce the results of the present study, as well as links to the data used, are available at https://github.com/koen-vg/eu-hydrogen/tree/v0. All code is open source (licensed under GPL v3.0 and MIT), and all data used are open (various licenses).

Acknowledgements

M.Z. acknowledge funding by UiO:Energy and Environment (SPATUS).

ERA5 reanalysis data [16] were downloaded from the Copernicus Climate Change Service (C3S).

The results contain modified Copernicus Climate Change Service information 2020. Neither the European Commission nor ECMWF is responsible for any use that may be made of the Copernicus information or data it contains.

Declaration of interests

The authors declare no competing interests.

Methods

Model set-up

We use the capacity expansion model PyPSA-Eur [14, 15] (version 0.10 with slight modifications) to generate feasible energy system designs at planning horizons $Y = 2025, 2030, 2035, 2040, 2045, 2050$. The model includes representations of the electricity, heating, transportation and industrial sectors, maintaining energy balances across electricity, hydrogen, natural/synthetic gas, fossil/synthetic oil, biomass, ammonia and methanol. Energy demand is retrieved from Eurostat at 2019 levels and largely kept fixed over time; see the PyPSA-Eur documentation* for more details. The electricity, heat, hydrogen and gas energy carriers are spatially resolved; oil, biomass, ammonia and methanol are not. The model is configured with a spatial scale of 60 nodes (see Figure 1 to represent the modelling region, which consists of the EU excluding Cyprus, Luxembourg and

*https://pypsa-eur.readthedocs.io/en/latest/supply_demand.html

Malta but including Norway, Switzerland and the United Kingdom; k-means clustering is used to cluster smaller regions corresponding to transmission substations down to 60 regions based renewable energy capacity factor and electricity load time series. In the temporal dimension, we aggregated hourly time-steps (8760 over one year) down to 2000 time-steps using a segmentation approach [17], which is known to be more accurate than the equivalent ~4.4-hourly uniform aggregation [18].

The model is solved several times in sequence to obtain system designs for the planning horizons under consideration; optimised and existing capacities from one planning horizon are carried over to the next, except for components which have reached the end of their lifetime by the next planning horizon. This approach is called "myopic foresight optimisation" in the context of PyPSA-Eur; "myopic" refers to capacity expansion only being done one time horizon at a time. Operationally, the model has perfect foresight over one year for each optimisation. At the first planning horizon of 2025, currently existing infrastructure, including renewable, nuclear, gas and coal power plants (except those reaching the end of their lifetime by 2025) are included in a brownfield optimisation. Solar, wind (onshore, bottom-fixed offshore, floating offshore), nuclear and gas power plants are expandable at each planning horizon; coal and hydro power plants are not. Infrastructure related to the production, storage, transportation and use of hydrogen (green as well as blue and grey) is expandable at each horizon. The same goes for the capture, storage / sequestration and utilisation of CO_2, including direct air capture and geological storage. Expansion of the transmission grid is capped 50% over the current grid on a global basis (individual lines may be reinforced more).

CO_2 emissions are capped at 65% of 1990 levels for the first modelling horizon of 2025 (compared to recorded emissions at 70.8% of 1990 levels in 2022 [19]). Thereafter the cap is reduced to 45%, 10% and 0% of 1990 levels at the 2030, 2040 and 2050 planning horizons in accordance with committed EU policy. Caps are linearly interpolated at the 2035 and 2045 planning horizons.

Costs are given in 2023 EUR; investment costs are annualised with a discount rate of 7%. Technology costs are parameters are retrieved from the `technology-data` repository[†], version 0.6.2. They are not modified beyond the scenario parameters in Table 1.

Near-optimal modelling

In order to explore different options for green hydrogen production, we exploit near-optimal solutions. Near-optimal modelling was first applied to energy systems modelling by DeCaroris [9] in 2011 under the name *Modelling to Generate Alternatives* (MGA) and has subsequently been applied in various contexts [8, 11, 12, 20, 21] to reveal the range of options that are available for energy system designs when cost-optimality is relaxed slightly.

We develop a novel methodology to apply the near-optimal perspective to sequential optimisation over multiple planning horizons ("myopic foresight multi-horizon optimisation"). Following Grochowicz et. al. [12], let $\mathcal{F}_\varepsilon = \{x \in \mathbb{R}^n \mid Ax \le b \text{ and } (1+\varepsilon)c \cdot x \le c^*\}$ be the ε-near-optimal space of an energy system model defined by the linear program $\min c \cdot x$ s.t. $Ax \le b$ with optimal value c^*. For multiple planning horizons with capacities carried over from one to the next, let $x_1^*, x_2^*, \ldots$ be cost-optimal solutions at planning horizons $1, 2, \ldots$, and let x_0^* be the state of the current energy infrastructure before the first planning horizon. Then the capacity expansion problem at horizon i depends on x_{i-1}^*; let $\min c_i x_i$ s.t. $A_{i|x_{i-1}^*} x_i \le b_{i|x_{i-1}^*}$ be the corresponding linear program. We define the ε-near-optimal space at the ith planning horizon as

$$\mathcal{F}_\varepsilon^{(i)} = \Big\{x_i \in \mathbb{R}^n \mid \exists x_{i-1} \in \mathcal{F}_\varepsilon^{(i-1)} \text{ s.t. } A_{i|x_{i-1}} x_i \le b_{i|x_{i-1}} \text{ and } (1+\varepsilon)c_i \cdot x_i \le c_i^* b\Big\}. \tag{1}$$

That is, each element in $\mathcal{F}_\varepsilon^{(i)}$ must be near-optimal with respect to optimal sequence of solutions $x_1^*, x_2^*, \ldots$ (hence the constraint $(1+\varepsilon)c_i \cdot x_i \le c_i^* b$), and must be feasible in the linear program $A_{i|x_{i-1}} x_i \le b_{i|x_{i-1}}$ based on *some* solution x_{i-1} in the near-optimal space $\mathcal{F}_\varepsilon^{(i-1)}$ from previous horizon.

Instead of working with the full-dimensional spaces $\mathcal{F}_\varepsilon^{(i)}$, we project down to the single variable of interest: the annual sum of green hydrogen production (specifically, the sum of hydrogen production from electrolysis) across the entire model. Under this projection, the image of $\mathcal{F}_\varepsilon^{(i)}$ is a line segment. The extreme points of this line segment can be found by minimising and maximising the sum of green hydrogen production, respectively. In this study, we furthermore assume that minimum/maximum green hydrogen production at horizon i is obtained by starting with the optimised capacities from a green hydrogen minimisation/maximisation at horizon $i-1$.

[†] https://github.com/PyPSA/technology-data

References

[1] European Commission. Commission staff working document implementing the REPowerEU action plan: Investment needs, hydrogen accelerator and achieving the bio-methane targets [SWD/2022/230 final] (2022).

[2] Seck, G. S. *et al.* Hydrogen and the decarbonization of the energy system in europe in 2050: A detailed model-based analysis. *Renewable and Sustainable Energy Reviews* **167**, 112779 (2022).

[3] Sgobbi, A. *et al.* How far away is hydrogen? Its role in the medium and long-term decarbonisation of the European energy system. *International Journal of Hydrogen Energy* **41**, 19–35 (2016).

[4] Blanco, H., Nijs, W., Ruf, J. & Faaij, A. Potential for hydrogen and Power-to-Liquid in a low-carbon EU energy system using cost optimization. *Applied Energy* **232**, 617–639 (2018).

[5] Quarton, C. J. *et al.* The curious case of the conflicting roles of hydrogen in global energy scenarios. *Sustainable Energy & Fuels* **4**, 80–95 (2020).

[6] Mignone, B. K. *et al.* Drivers and implications of alternative routes to fuels decarbonization in net-zero energy systems. *Nature Communications* **15**, 3938 (2024).

[7] Trutnevyte, E. Does cost optimization approximate the real-world energy transition? *Energy* **106**, 182–193 (2016).

[8] Neumann, F. & Brown, T. The near-optimal feasible space of a renewable power system model. *Electric Power Systems Research* **190**, 106690 (2021).

[9] DeCarolis, J. F. Using modeling to generate alternatives (MGA) to expand our thinking on energy futures. *Energy Economics* **33**, 145–152 (2011).

[10] Pickering, B., Lombardi, F. & Pfenninger, S. Diversity of options to eliminate fossil fuels and reach carbon neutrality across the entire European energy system. *Joule* **6**, 1253–1276 (2022).

[11] Neumann, F. & Brown, T. Broad Ranges of Investment Configurations for Renewable Power Systems, Robust to Cost Uncertainty and Near-Optimality. *iScience* 106702 (2023).

[12] Grochowicz, A., van Greevenbroek, K., Benth, F. E. & Zeyringer, M. Intersecting near-optimal spaces: European power systems with more resilience to weather variability. *Energy Economics* **118**, 106496 (2023).

[13] Millinger, M. *et al.* Diversity of biomass usage pathways to achieve emissions targets in the European energy system (2023).

[14] Hörsch, J., Hofmann, F., Schlachtberger, D. & Brown, T. PyPSA-Eur: An open optimisation model of the European transmission system. *Energy Strategy Reviews* **22**, 207–215 (2018).

[15] Brown, T., Schlachtberger, D., Kies, A., Schramm, S. & Greiner, M. Synergies of sector coupling and transmission reinforcement in a cost-optimised, highly renewable European energy system. *Energy* **160**, 720–739 (2018).

[16] Hersbach, H. *et al.* ERA5 hourly data on single levels from 1940 to present (2018).

[17] Pineda, S. & Morales, J. M. Chronological Time-Period Clustering for Optimal Capacity Expansion Planning With Storage. *IEEE Transactions on Power Systems* **33**, 7162–7170 (2018).

[18] Kotzur, L., Markewitz, P., Robinius, M. & Stolten, D. Impact of different time series aggregation methods on optimal energy system design. *Renewable Energy* **117**, 474–487 (2018).

[19] Eurostat. Net greenhouse gas emissions (2024).

[20] Pedersen, T. T., Victoria, M., Rasmussen, M. G. & Andresen, G. B. Modeling all alternative solutions for highly renewable energy systems. *Energy* **234**, 121294 (2021).

[21] van Greevenbroek, K., Grochowicz, A., Zeyringer, M. & Benth, F. E. Enabling agency: Trade-offs between regional and integrated energy systems design flexibility (2023). 2312.11264.

Article 5: “Exports”

C. Cheng *et al.*, «The competitive edge of Norway’s hydrogen by 2030: Socio-environmental considerations,» *International Journal of Hydrogen Energy*, vol. 85, pp. 962–975. Oct. 4, 2024, ISSN: 0360-3199. DOI: 10.1016/j.ijhydene.2024.08.377

International Journal of Hydrogen Energy 85 (2024) 962–975

Contents lists available at ScienceDirect

International Journal of Hydrogen Energy

journal homepage: www.elsevier.com/locate/he

The competitive edge of Norway's hydrogen by 2030: Socio-environmental considerations☆

C. Cheng [a], K. van Greevenbroek [b,*], I. Viole [c]

[a] Department of Social Sciences, UiT The Arctic University of Norway, 6050, Langnes, 9037, Tromsø, Norway
[b] Department of Computer Science, UiT The Arctic University of Norway, 6050, Langnes, 9037, Tromsø, Norway
[c] Department of Technology Systems (ITS), University of Oslo, Gunnar Randars Vei 19, 2007, Kjeller, Norway

ARTICLE INFO

Handling Editor: Prof. J. W. Sheffield

Keywords:
Hydrogen economy
Integrated assessment
Norway
Hydrogen exports
Blue hydrogen
Green hydrogen
Social transition

ABSTRACT

Can Norway be an important hydrogen exporter to the European Union (EU) by 2030? We explore three scenarios in which Norway's hydrogen export market may develop: A Business-as-usual, B Moderate Onshore, C Accelerated Offshore. Applying a sector-coupled energy system model, we examine the techno-economic viability, spatial and socio-economic considerations for blue and green hydrogen export in the form of ammonia by ship. Our results estimate the costs of low-carbon hydrogen to be 3.5–7.3€/kg hydrogen. While Norway may be cost-competitive in blue hydrogen exports to the EU, its sustainability is limited by the reliance on natural gas and the nascent infrastructure for carbon transport and storage. For green hydrogen exports, Norway may leverage its strong relations with the EU, but is less cost-competitive than countries like Chile and Morocco, which benefit from cheaper solar power. For all scenarios, significant land use is needed to generate enough renewable energy. Developing a green hydrogen-based export market requires policy support and strategic investments in technology, infrastructure and stakeholder engagement, ensuring a more equitable distribution of renewable installations across Norway and national security in the north. Using carbon capture and storage technologies and offshore wind to decarbonise the offshore platforms is a win-win solution that would leave more electricity for developing new industries and demonstrate the economic viability of these technologies. Finally, for Norway to become a key hydrogen exporter to the EU will require a balanced approach that emphasises public acceptance and careful land use management to avoid costly consequences.

Abbreviations

CCS	Carbon Capture and Storage
DENA	German Energy Agency
EU	European Union
H_2	Hydrogen
HHV	Higher Heating Value
LCOE	Levelised costs of electricity
LCOH	Levelised costs of hydrogen
LHV	Lower Heating Value
Mt	Million tonnes
NVE	Norwegian Water Resources and Energy Directorate (Norges vassdrags- og energidirektorat)
PEM	Proton-Exchange Membrane
PyPSA-Eur	Python for Power System Analysis — European energy system
SMR	Steam Methane Reforming

1. Introduction

The European Union has the ambition to be climate-neutral by 2050 [1]. As an intermediate goal to bolster its energy security and reduce its dependence on Russian natural gas (hereinafter gas) imports, the EU plans to replace parts of its gas consumption with 20 million tons (Mt) of green hydrogen by 2030, of which half will be produced domestically and half will be imported [2]. As the EU transitions away from fossil fuel imports, countries that depend on petroleum exports to the former will need to find a new market to tap into. One such country is Norway, whose petroleum exports represent 73% of the total country's exports value in 2022. Of this volume, 67% was exported to the EU [3]. In terms

☆ The authors have contributed equally and are listed alphabetically by last name.
* Corresponding author.
E-mail address: koen.v.greevenbroek@uit.no (K. van Greevenbroek).

https://doi.org/10.1016/j.ijhydene.2024.08.377
Received 18 May 2024; Received in revised form 20 August 2024; Accepted 22 August 2024

of availability of natural resources, political stability and regulatory status, economic resources, industrial know-how and adaptability, Norway is ranked as one of the top ten potentially most competitive hydrogen exporters in the world [4]. Should Norway succeed in realising this potential, it would be able to maintain its economic growth despite a transition away from fossil fuel exports [5]. However, this would require abundant renewable electricity to ensure minimal greenhouse gas emissions and price-competitiveness [5,6]. Yet, the power surplus of around 13 TW h (TWh) that Norway has been enjoying averagely in the last decade [7] could turn into a deficit by 2030 if the increased electricity demand resulting from the electrification of sectors is not followed by a proportionate expansion of the domestic renewable electricity capacity [8]. As pointed out by Cheng [6], timing is important in taking advantage of the window of opportunity for an energy transition. The point of departure of this work is that Norway should aim to become an important EU hydrogen supplier by 2030 and the main objective of this work is to evaluate this potential. This is measured by the cost-competitiveness against other non-EU hydrogen exporters, the environmental impacts on land use and the associated social implications.

Several techno-economic studies on the potential for low-carbon hydrogen export to the EU focused solely on the production costs. However, this could be misleading as the transportation costs could affect the overall cost-competitiveness of the exports, as highlighted by Refs. [9–11]. The transportation costs may vary due to the travelling distance and the form in which the hydrogen is being transported. In contrast, a value chain approach that includes the costs implicated in the transportation of hydrogen export would provide a better overview of the cost-attractiveness of hydrogen as an export commodity [11]. This approach has been adopted by Galimova et al., Roos, Seiti et al., Okunlola et al., Wietschel and Hasenauer for the export of blue and green hydrogen from non-EU countries in North and South America, Africa, Northern Europe to Europe, including Germany [11–14]. Additionally, three studies concern the export of blue or green hydrogen from Norway to Germany. Andressen et al. [15] evaluated the feasibility of exporting green liquid hydrogen from Norway (Glomfjørd) to German cities (Berlin, Munich, Magdeburg) via the ports of Hamburg, Bremerhaven or Rostock. Stiller et al. [16] compared the costs of exporting blue and green hydrogen from Southern and Northern Norway to Northern Germany (Hamburg) via eight different pathways, of which two considered production in Southern Norway before being transported through hydrogen pipelines, and two considered production in Northern Norway before being exported by liquid hydrogen ships. Ishimimoto et al. [17] compared the techno-economic cost of large-scale production and transport of blue liquid hydrogen and liquid ammonia from Northern Norway (Hammerfest) to Rotterdam and Tokyo.

The techno-economic assessments mentioned above were quantified based on static values on the electricity prices and capacity factors that are applied to renewable electricity technologies. While this provides a high-level view of the economic potential of hydrogen exports to the EU, the reality is that electricity prices and renewable energy generation can vary significantly from site to site [18]. To capture this reality, the energy system optimisation model, PyPSA-Eur, is used to derive the costs of hydrogen exports from Stavanger (Southern Norway), Trondheim (Central Norway) and Tromsø (Northern Norway), each representing different geographical points and electricity price zones in Norway. Further, it is critical to consider the volume of hydrogen exports targets, which impacts the amount of renewable energy required, and thereby demands the use of more natural resources like land. In Norway, the future renewable energy expansion is likely to rely on either onshore or offshore wind [8]. By allowing the expansion of renewable energy capacity in the model, it is possible to calculate the amount of land or sea area needed for the production of hydrogen. For hydrogen exports to be a viable alternative for Norway's post-petroleum future, we assume that Norway should aim to secure the same market share as its gas exports as its hydrogen exports, that is 20% market share of the EU's hydrogen import demand in 2030. This equates to an export of 2 Mt hydrogen, and aligns well with the assumption taken by Espegren et al. [5] on the role of hydrogen exports in Norway to transition away from petroleum exports.

Given the joint-declaration by Norway and Germany to cooperate closely on developing a hydrogen value chain [19], this article focuses on the export route between the two countries. While the recent hydrogen value chain feasibility studies by DENA and Gassco on the construction of a hydrogen pipeline between Norway and Germany concluded that "no technical showstoppers have been identified", there remain substantial barriers concerning costs, regulatory framework, environmental impacts and financing model [20, p. 24]. Considering the timeline to 2030, we opt to evaluate the export of hydrogen in the form of ammonia, which can be safely transported on existing chemical and semi-refrigerated liquefied petroleum gas tankers and can leverage an established intercontinental transmission and distribution network [21]. Furthermore, it is considered the most cost-attractive carrier for shipping hydrogen [22]. The receiving terminal is assumed to be the port of Wilhelmshaven, where a new hydrogen pipeline could potentially be built in the vicinity and facilitate further distribution inland [20].

The novelty of this article builds on several pillars. (i) This article is the first study in Norway which models both blue and green hydrogen in a technology-open manner to study system-wide impacts of cost-optimal export pathways. (ii) The model allows for an analysis of the distribution of renewable energy and hydrogen from different regions of Norway and the discussion on the energy needs, land-use and associated social consequences at a regional level. (iii) Further, our results build on a broad cost-sensitivity analysis addressing the fundamental uncertainty in future costs of technologies including carbon capture and storage, electrolysis and offshore wind turbines.

The key research question for this article is "What is the potential for Norway to be an important hydrogen supplier to the EU?". Guiding the analysis are the following sub-questions:

1) How fast does Norway need to ramp up the expansion of its renewable energy capacity to meet the EU's hydrogen import needs?
2) What are the economic and environmental trade-offs between blue and green hydrogen production in Norway, considering current infrastructure and future energy policy needs?
3) What are the socio-economic impacts of expanding onshore and offshore wind capacity in different regions of Norway, and how can policy address potential disparities?

These research questions are investigated through the lens of three different scenarios involving blue and green hydrogen as described in the Methods section. There, we dive into specifics of the foreseen hydrogen pathways, and then discuss how we adapted the PyPSA-Eur model for this article. In particular, we extend PyPSA-Eur with additional components and linear constraints forcing hydrogen exports; a relatively novel concept in the context of capacity expansion model. We further give an overview of relevant cost assumptions and present social and environmental concerns of hydrogen export pathways. The Results section then discusses the accruing costs in the different scenarios, defines the needed willingness-to-pay to evade social acceptance issues, and marks down the land use needs and power system changes in Norway following the different hydrogen export pathways and variations in costs. This paper is rounded up by a Discussion and Conclusion.

2. Methods

2.1. Hydrogen pathways

This article examines the potential for hydrogen exports based on three scenarios from Norway to Germany: "A Business-as-usual", "B Moderate Onshore", "C Accelerated Offshore". We use an integrated energy system optimisation model to investigate a range of outcomes

Table 1
Description of scenarios and their implementation in the energy system model.

Scenario	Model implementation	Description
A: Business-as-usual	No restriction to baseline model.	Aligns with current policies where only blue hydrogen is produced for export.
B: Moderate onshore	Steam methane reforming (SMR) not allowed.	Green hydrogen export using the cost-effective renewable electricity source.
C: Accelerated offshore	SMR not allowed, total yearly offshore wind power production must be at least the total yearly electrolysis demand in Norway.	Green hydrogen export using offshore wind power.

(including hydrogen cost, land use and subsidy levels) in three different scenarios, see Table 1. At the basis of all scenarios lies the fixed target for Norway to supply 2 Mt of hydrogen (derivatives) annually to continental Europe. The scenarios and modelling assumptions are tailored to a 2030 planning horizon.

Where the scenarios differ is in the methods and energy sources for hydrogen production. See Table 1 for a brief summary. Scenario A (*Business-as-usual*) explores the export of both blue and green hydrogen while allowing the expansion of the lowest-cost renewable energy. That is, hydrogen may be produced through the conventional method, steam methane reforming (SMR), combined with Carbon Capture and Storage (CCS) technology at 90% capture rate, as well as through water electrolysis via Proton-Exchange Membrane (PEM) electrolysers that are powered by renewable energy. In practice, this leads the model to invest in SMR with CCS in most cases since this is significantly cheaper than electrolysis at baseline 2030 technology cost assumptions. In Scenario B (*Moderate onshore*), only green hydrogen production is allowed based on the potential for expansion of renewable energy generation in Norway. This leads the model to invest in a significant variable renewable portfolio in Norway in order to supply the electrolysis; renewable investment is dominated by onshore wind in this case. Given the low social acceptance towards onshore wind installations in Norway [23], Scenario C (*Accelerated offshore*) assumes the same but the production of green hydrogen relies on an accelerated roll-out of offshore wind turbines in Norway. In this scenario, we add the constraint that offshore wind power (as opposed to onshore wind and solar) must supply all the electricity for electrolysis; this is however only accounted for on a net yearly basis. For all scenarios, we assume high prioritisation of energy security in Norway in that it may not become an electricity importer on a net yearly basis. Fig. 1 illustrates the value chain of ammonia exports considered in the scenarios, from the energy sources in Norway to the transport of ammonia to the receiving terminal in Germany.

As mentioned above, this article considers marine shipping of ammonia from Norway to continental Europe. We model power requirements and losses in the production of ammonia, but do not consider ammonia cracking to convert the exports back to hydrogen; rather, we model the exports of an amount of ammonia having the energy content (measured in lower heating value) of 2 Mt of hydrogen, being 66.7 TWh. We disregard ammonia cracking due to the large uncertainty in final end-use of imported green hydrogen. A recent projection of green hydrogen demand by 2030 in Germany [24] notes that there is already a 1 Mt hydrogen demand (currently grey) in the chemical industry for the production of ammonia; demand from the transportation and shipping sectors may also be in the form of ammonia or other synthetic fuels. Including conversion losses in ammonia cracking would overestimate costs if the resulting green hydrogen is to be converted back to a liquid fuel. Given the nascent stage of the use of ammonia as a fuel in ships, we assume that the transport of ammonia will be by container ships running on conventional fuel in 2030.[1] Hydrogen pipelines are excluded in the scenarios due to potential delays in funding and approval processes for the constructions, (despite being considered as technically possible by 2030 [25]).

In the model, the export pathways are modelled as three separate corridors characterised by having a capital investment cost (representing the cost of an ammonia production plant), efficiency losses (representing imperfect conversion from hydrogen to ammonia), a running power requirement (representing the electricity required to run the ammonia production plant) and a marginal export cost (representing the cost of shipping ammonia; dependant on the shipping distance). While we have based these parameters on ammonia as an energy carrier (see Table 2 for the parameters used in the present study), the model formulation itself would be equivalent to an alternative carrier such as liquid hydrogen. As discussed below, the modelling results are not particularly sensitive to shipping costs.

2.2. Choice of modelling framework

In order to generate plausible system solutions in each of our three scenarios, we employ an energy system optimisation model covering the electricity, transportation, heating and industrial sectors. The specific tool we use is PyPSA-Eur, an open-source sector-coupled model for the European energy system [26,27]. At the core, this is a capacity expansion model; a type of optimisation model where both investment and operation decisions are subject to optimisation. The model is equipped with an objective function representing total system cost (as a sum of annualised investment costs and yearly operating costs). Investment variables subject to optimisation include onshore and offshore wind capacities, solar capacities, conventional natural gas and nuclear power generation, energy storage capacities (batteries, hydrogen storage, hot water storage), transmission expansion, heating infrastructure (combined heat and power plants, gas boilers, heat pumps, resistance heaters) and power-to-X capacities including electrolysis, ammonia and methanol synthesis and fischer-tropsch liquid fuel production. The model also includes existing capacities of the above technologies with lifetimes beyond 2030. Existing hydro, coal and oil power plants are similarly included, but with fixed capacities that cannot be expanded. For a complete overview of the technologies included and optimised in the model, see the official PyPSA-Eur documentation.[2]

In a typical capacity expansion model such as PyPSA-Eur, the adequacy of feasible model solutions is ensured by including in the model formulation a simulation of system operations over one full year at sub-daily time resolution. Demand for electricity and other energy carriers is fixed in advance for each node and time step in the model; dispatch and optimal power flow problems for each time step are included in the overall problem formulation. Thus, both operational and investment decision variables are subject to optimisation jointly. PyPSA-Eur (as well as many other capacity expansion models) is formulated as a linear program, meaning that both constraints and the objective function are linear in the decision variables. This entails simplifications of non-linear real-world effects but makes the optimisation model tractable to solve at high spatial and temporal resolution.

[1] Note that shipping costs (see Fig. 4) only play a minor role in final exported hydrogen costs, meaning that shipping fuel choice is unlikely to have a large effect on our results.

[2] https://pypsa-eur.readthedocs.io/en/latest/introduction.html.

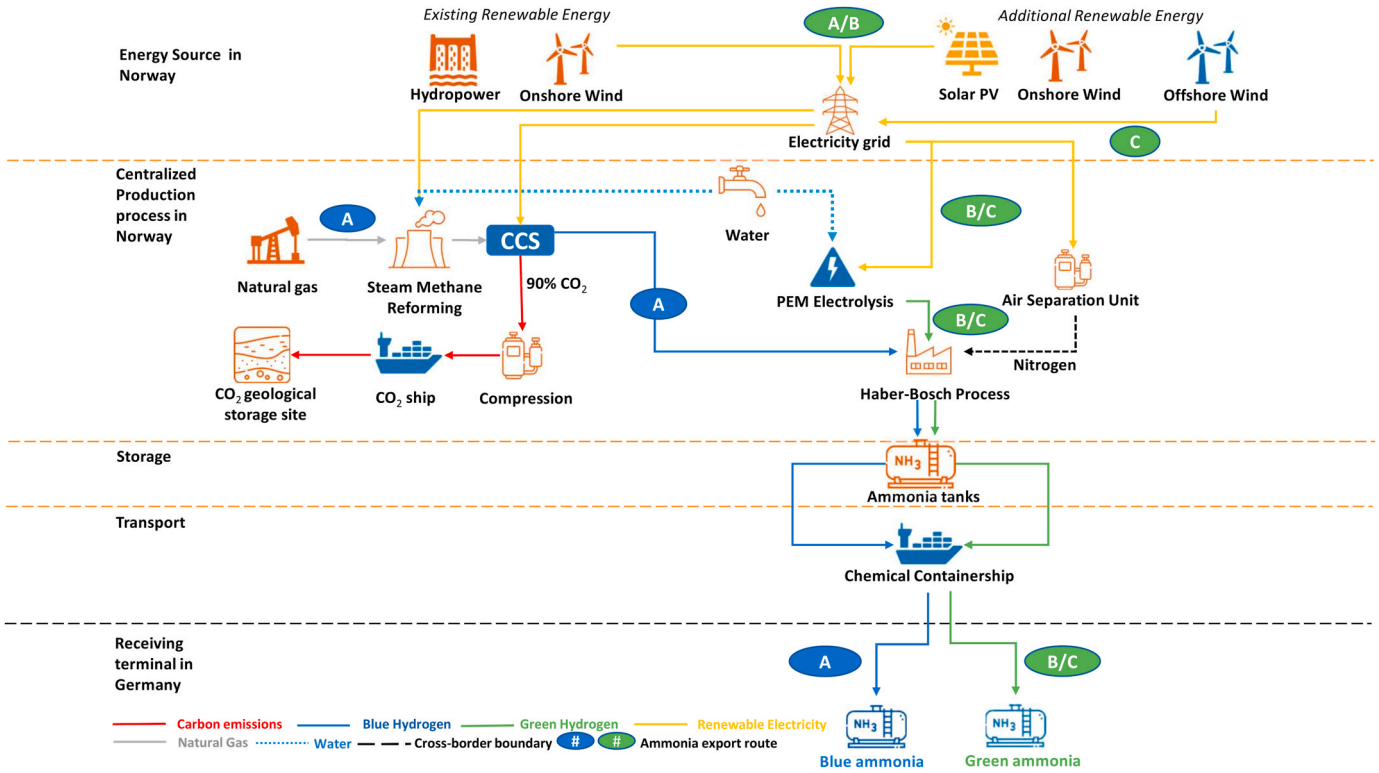

Fig. 1. Simplified ammonia export value chain from Norway to Germany in 2030[1]
[1]Clipart source: flaticon.com.

2.3. Modelling setup

We restrict PyPSA-Eur to the countries around Norway and the North Sea, namely Norway, Sweden, Denmark, Finland, the UK, the Netherlands and Germany. We choose a 20-node spatial resolution at the transmission and demand level, but allocate only one node per synchronous zone and country for Denmark, the UK, the Netherlands and Germany, while modelling Sweden with 2 nodes and Norway with the remaining 11 nodes (see Fig. 2). This ensures adequate representation of transmission bottlenecks in and around Norway. In order to better capture variations in renewable energy availability, we model renewable generation at a spatial resolution of 60 different regions; each region being connected to the closest of the 20 transmission nodes. We obtain the desired network resolution using the built-in hierarchical clustering function of PyPSA-Eur [28] based on onshore wind capacity factor profiles — starting from small initial regions, nearby nodes with similar onshore wind capacity factors are successively merged. Furthermore, the temporal resolution of the model is reduced using the segmentation approach introduced in Ref. [29] to a total of 1000 time steps. The model is run over the single weather year of 2013 [30] — this weather year is close to average in terms of total system costs compared to the 1980–2020 period and is the default in PyPSA-Eur, making the results easier to compare to other studies. Total yearly CO_2 emissions over the entire modelling region are subject to a 55% reduction compared to 1990 levels in accordance with the EU and Norway's climate target for 2030. This reduction is implemented as a constraint on total model-wide CO_2 emissions; the model then finds the most cost-effective solution to meet this constraint while satisfying the given energy demand. Following the PyPSA-Eur default [31], renewable expansion is restricted to a selection of CORINE land use types [32].

We add a number of new components and linear constraints to PyPSA-Eur in order to model our hydrogen export scenarios. These are as follows:

1. A new network bus with attached store/stockpile representing continental hydrogen demand, and three links from the Norwegian export hubs to this bus, as described above.
2. A constraint forcing the hydrogen demand stockpile to be filled with the equivalent of 2 Mt of hydrogen (amounting to 66.7 TWh of ammonia in our case) by the end of the year.
3. A constraint forcing Norway to remain a net electricity exporter on a yearly basis. Specifically, the total net electricity exports (i.e. the difference between total yearly exports and imports) is constrained to be greater than 0. This constraint maintains the current status quo of Norway's role as an electricity exporter, but also crucially prevents the import of electricity only for this to be used in electrolysis and exported again as green hydrogen.
4. In Scenario C, a constraint is added forcing total yearly Norwegian offshore wind production to match total yearly electrolysis electricity consumption.

Thus, our scenarios are based on using an optimisation model to explore cost-optimal solutions for exporting hydrogen from Norway, without making assumptions about exactly where and when this hydrogen is produced, or with which power (except for Scenario C, forcing the use of offshore wind).

2.4. Technology costs and sensitivity analysis

Table 2 shows the complete overview of the baseline cost assumptions in our model. All costs are given in 2023 euros, and technology costs and efficiencies are given for 2030, wherever possible. When necessary, we convert between NOK and EUR based on an average 2023 exchange rate of 1 EUR = 11.302 NOK [33]. It is noteworthy that e.g. PEM electrolysis efficiency is forecasted to increase by at least 5%-points in the decades beyond 2030 [34] (subject to uncertainty), which would decrease the Levelised Cost of Hydrogen (LCOH) for model runs set in later years than 2030. In the model, capital investment costs are

Table 2
Overview of baseline cost assumptions for hydrogen production and transportation chain. All costs are given in 2023 euros; older cost data are converted using the Eurostat Harmonised Index of Consumer Prices.

Technology	Baseline assumption	Range	Source
Onshore wind investment	€1413/kW	±20%	[35]
Bottom-fixed offshore wind investment (excluding connection)	€2921/kW	±20%	[35]
Floating offshore wind investment (excluding connection)	€5269/kW	±20%	[35]
Steam-methane reformation with 90% carbon capture rate	€728/kW_{CH_4}	±20%	[36]
Steam-methane reformation conversion efficiency[a]	69%	fixed	[37]
Natural gas	€30/MWh_{th}	±20%	[38]
CO_2 sequestration[b]	€36.50/tCO_2	±20%	[39]
PEM electrolysis	€429/kW_e	±20%	[40]
PEM electrolysis efficiency[c]	65%	61%–69%	[34]
Ammonia synthesis[d]	€1570/kW_{th}	±20%	[36]
Ammonia synthesis hydrogen consumption[e]	1.15 MWh_{H_2}/MWh_{NH_3}	fixed	[41]
Ammonia synthesis electricity consumption[f]	0.25 MWh_{el}/MWh_{NH_3}	fixed	[41]
Ammonia shipping	€1.47/MWh_{th}/1000 km	±20%	[42]

[a] Efficiency is given in terms of LHV, and is lower than the reference value of 76% for non-CC SMR from the same source due to the additional energy requirement for the carbon capture process.
[b] Sequestration cost includes the levelised cost of both transportation of CO_2 and injection into depleted gas fields, but not the cost of capturing CO_2 (which is included in the capital cost of SMR plants with carbon capture).
[c] Efficiency is given in terms of LHV; this value corresponds to an efficiency of 77% in terms of high heating value (HHV). The range of efficiencies tested corresponds to 72%–82% in terms of HHV.
[d] Capital cost includes the air-separation unit needed for N_2 feedstock. The cost is per kW of hydrogen input capacity.
[e] Using lower heating values and assuming 178 kg H_2 input per 1000 kg NH_3 output.
[f] Using the lower heating value for ammonia, not including the electricity needed for the air-separation unit.

annualised with a 7% discount rate. Since all costs under consideration are subject to considerable uncertainty, we perform an extensive global sensitivity analysis in order to determine both which costs are most important for final hydrogen prices as well as to determine likely ranges of prices and system configurations across many cost combinations. In particular, our global sensitivity analysis consists of taking intervals of ± 20% around each baseline cost (listed in Table 2), and randomly sampling 500 points in the resulting parameter space. Then, we run the model for each of these 500 combinations of cost assumptions and each scenario. The resulting 1500 model solutions are used throughout the results section.

3. Results

The key results are summarised in Table 3; in the following sections we go into more detail.

3.1. Competitiveness of Norwegian hydrogen

Fig. 3 shows the distributions of Norwegian Levelised Cost of Hydrogen (LCOH) observed for each scenario across the 500 model optimisations, following the sensitivity analysis as described above. Under Scenario A (*business-as-usual*), only blue ammonia is being exported from Norway to Germany due to the cheaper cost associated with the production method, SMR and CCS, entailing the capture and storage of about 23 Mt of CO_2 annually.[3] Consequently, the cost of producing hydrogen and exporting it in the form of ammonia is the cheapest among the three scenarios, with a median cost (between 5th–95th percentiles) of €3.87 (3.50–4.27)/kgH_2 in 2030. Limiting the production to only green hydrogen, the cost of hydrogen export becomes around 34% higher in Scenario B (*moderate onshore*) at €5.18 (4.61–5.72)/kgH_2 and 65% higher in Scenario C (*accelerated offshore*) at €6.39 (5.54–7.25)/kgH_2. The cost uncertainty is found to be greater for green hydrogen, especially in Scenario C, which is completely reliant on offshore wind power. These costs include both production, ammonia synthesis (with resulting efficiency losses) and transportation. Note that we report costs in €/kgH_2-equivalent in terms of lower heating value energy content even though exports are modelled as using ammonia. Without ammonia synthesis and transportation, we find hydrogen production costs of €2.34 (2.05–2.63), €3.43 (2.95–3.83) and €4.51 (3.78–5.17) for Scenarios A, B & C respectively.

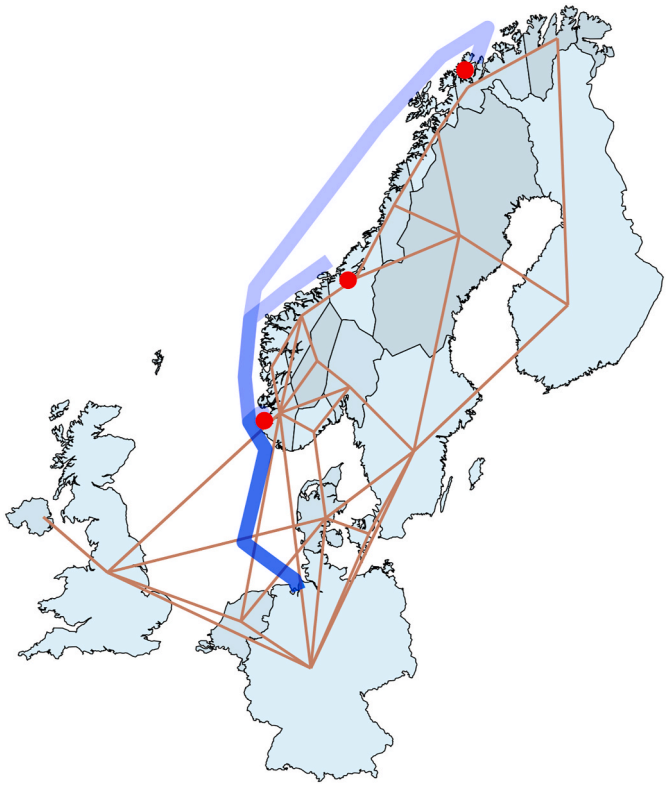

Fig. 2. The spatial layout of the model used in this study. The distinct model regions are shown, with the connecting lines indicating transmission grid connections. The thick blue lines illustrate the export corridors from Tromsø, Trondheim and Stavanger, marked with red dots. (For interpretation of the references to colour in this figure legend, the reader is referred to the Web version of this article.)

Fig. 4 shows the sensitivities of the final Norwegian LCOH to the various parameters subject to variation in the global sensitivity analysis. It should be highlighted that the first parameter relates to the efficiency rate of electrolysers, while the rest of the parameters relate to the different cost components in the supply chain. Although the electrolyser efficiencies have the same baseline value of 65% in both Scenarios B (*moderate onshore*) and C (*accelerated offshore*), the effects on the cost of hydrogen are higher in the latter due to the higher cost of electricity. A

[3] See Section 4.1 for a more detailed discussion of CO_2 capture and storage in Scenario A.

Table 3
Summary of key results. All ranges indicate the 5th and 95th percentiles over the sensitivity analysis. The production-only LCOH is taken as the average locational marginal price of hydrogen in Norway, whereas the LCOH including conversion and export is taken as the average locational marginal price of ammonia (given in kgH_2-equivalent units in terms of energy content) in the model node representing continental hydrogen demand. The total electricity requirement includes the electricity requirement for ammonia synthesis (16.3 TWh in total) and, in Scenarios B and C, the electricity requirement for hydrogen electrolysis. The average electricity cost represents a demand-weighted average of the locational marginal prices of electricity in the Norwegian model nodes.

	Scenario A (*Business-as-usual*)	Scenario B (*Moderate onshore*)	Scenario C (*Accelerated offshore*)
Norwegian LCOH (production only) [€/kgH_2]	2.05–2.63	2.95–3.83	3.78–5.17
Norwegian LCOH (incl. conversion to ammonia and export) [€/kgH_2-equivalent]	3.50–4.27	4.61–5.72	5.54–7.25
Total electricity requirement for exports [TWh]	16.3	126	126
Average electricity cost (Norway) [€/MWh]	48.9–62.0	56.5–71.2	51.5–65.9
Onshore wind capacity, Norway [GW]	8.4–25.4	34.5–62.7	12.6–19.9
Offshore wind capacity, Norway [GW]	0–8.8	0–13.0	27.9–33.5
Bottom-fixed [GW]	*0–8.8*	*0–9.9*	*0–19.7*
Floating [GW]	*0–4.1*	*0–4.1*	*10.6–32.5*
Onshore wind land area demand [km^2]	979–2959	4007–7291	1462–2309
% of open land areas in Norway[a] [44]	0.9–2.6%	3.6–6.5%	1.3–2.1%

[a] Open land areas in 2023, defined as undeveloped areas excluding forest, marshland, permanent snow, ice and glacier areas, as well as bodies of water [43].

drop of 1% in electrolyser efficiency could lead to an average cost increase of €0.042/kgH_2 in Scenario B whereas the increase in hydrogen cost is €0.052/kgH_2 in Scenario C. Natural gas cost is the single main factor determining the cost of hydrogen production in Scenario A (*business-as-usual*), where an 1% increase in natural gas prices may lead to an average increase of €0.016/kgH_2. The next two important factors are the capital cost for SMR installation and CO_2 sequestration cost (including transportation). In Scenario B, the cost of hydrogen production is highly dependent on the capital cost of onshore wind, where an increase of 1% leads to an average increase of €0.045/kgH_2. The export capital costs refer to the cost of converting hydrogen into the exportable ammonia.

The model differentiates between bottom-fixed and floating offshore wind, and the final LCOH is highly sensitive to the cost of floating offshore wind in Scenario C (*accelerated offshore*). The reliance on floating offshore wind is explained by the relatively low potential for bottom-fixed offshore wind by the Norwegian coast, with only about 55 GW of maximum installable capacity available along the entire Norwegian coastline (based on a maximum depth of 60 m and density of 2 MW/km^2 for bottom-fixed offshore wind), less than a third of which is located below 62°N — the preferred location for offshore wind in the model (see Fig. 6).

Table 4 summarises the production and shipping costs of hydrogen and its derivatives in the existing literature to Germany. The cost of blue hydrogen production in Norway is higher than in Canada, which could be due partly to the slightly lower carbon capture rate (85% instead of 90%) and gas prices assumed in the latter countries (roughly half of the value assumed in our model). This may be attributed to the fact that the studies were conducted before the recent energy crisis triggered by the

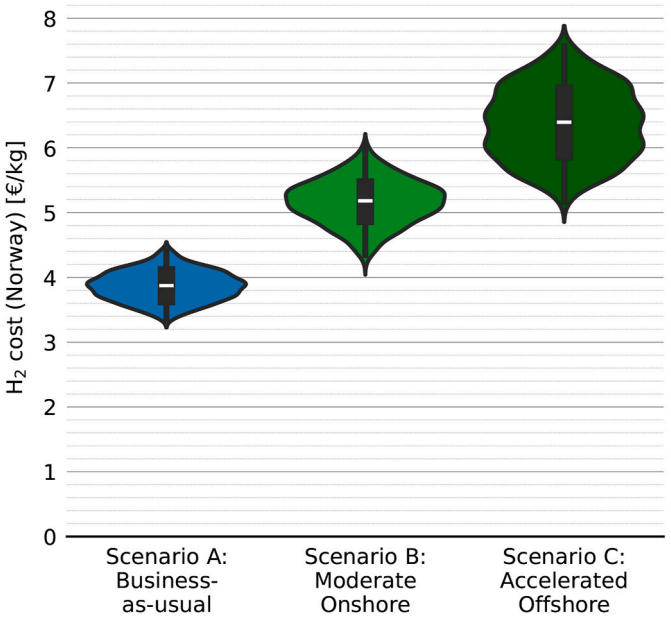

Fig. 3. Distributions of levelised costs of Norwegian hydrogen seen across 500 model runs in each of the three scenarios. These include production, conversion to ammonia and transportation and correspond to the figures in the second row of Table 3. The median costs are marked in white, and the 75th and 95th percentiles are marked with thick and thin black lines respectively. The coloured areas show kernel density estimations for the probability distributions of the costs.

Russian invasion of Ukraine and did not take into account the aftereffects of the ongoing war. Adjusting for these effects, Norway's total export cost for blue ammonia is likely to be cheaper than that of Canada.

As for green hydrogen production cost, Norway's cost ranges in Scenarios B (*moderate onshore*) and C (*accelerated offshore*) are higher than those of other countries including Morocco, Argentina, Chile and Australia. This could be attributed to the type of renewable energy technologies used to produce renewable electricity as well as market effects. The Levelised Cost of Electricity (LCOE) of solar PV is lower than onshore and offshore wind, which results in lower electricity costs. Given the high sensitivity of hydrogen production cost to electricity prices, it is not surprising that Morocco, Argentina and particularly Chile could have a cost advantage over Norway for green hydrogen production. Further, we assume the use of proton exchange membrane (PEM) electrolysers in our study as they allow for a modular scale-up of the operation — being able to start with small units and scale up later can reduce investment risk. Nevertheless, as shown in Fig. 4, the impact on the overall cost contributed by the electrolyser capital cost is small compared to that of the electrolysis efficiency rate. Moreover, Norwegian electricity prices, though falling from 2023-levels, are still affected by high prices in neighbouring countries (see also Table 6); such effects are not taken into account in the studies considered in Table 4. Overall, green ammonia exports from Norway in both Scenarios B and C are less cost-competitive than the considered alternatives.

3.2. How fast do we need to ramp up renewable energy expansion?

Diving into the green hydrogen scenarios, Fig. 5 shows the installed capacities of onshore and offshore wind required in Norway across the three different scenarios. Scenario A (*business-as-usual*) requires a total installed renewable capacity of 21 GW on average across the sensitivity analysis, of which 8–25 GW (5th–95th percentiles) is onshore wind, depending on the volume of offshore wind installations (0–9 GW, 5th–95th percentiles). The additional electricity generated is used mostly for the decarbonisation of various sectors in Norway, but also

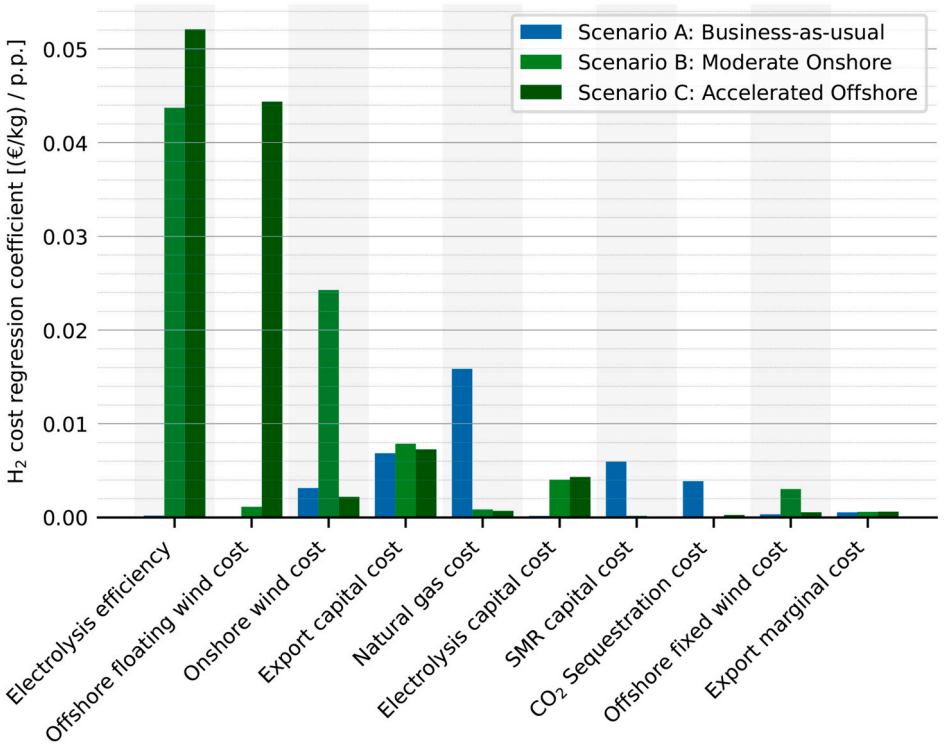

Fig. 4. Sensitivities of Norwegian H_2 export costs in Scenarios A, B & C to variations in technological parameters. The sensitivities are calculated as the coefficients of the parameters in a multi-dimensional linear regression model fitting parameters to H_2 cost. The combination of parameters predicts hydrogen cost linearly with R^2 values of 0.997, 0.981 and 0.998 for the three scenarios respectively. The coefficients are expressed in LCOH (€/kgH_2) per percentage point (p.p.) change in respective technological parameters. For example, the figure shows that in Scenario B (light green), a cost increase in onshore wind of 1% would increase H_2 costs by €0.024/kg on average. For more details on the technological parameters, see Table 2. (For interpretation of the references to colour in this figure legend, the reader is referred to the Web version of this article.)

Table 4
Comparison of LCOH at production and delivery between the present study and other comparable studies. All figures are inflation-adjusted to 2023 EUR where necessary. Cost ranges arise from sensitivity analyses performed in the cited studies where applicable. All studies assume Hamburg, Germany to be the European port of delivery. "Electrolysis" is shortened to "Elec.".

Origin	Transport medium	Production method	Hydrogen Production cost [€/kgH_2]	Cost of delivered hydrogen [€/kgH_2]
Norway[a]	Ammonia	Scenario A: SMR + CCS (90%)	2.05–2.63	3.50–4.27
	Ammonia	Scenario B: Elec.	2.95–3.83	4.61–5.72
	Ammonia	Scenario C: Elec. (offshore wind)	3.78–5.17	5.54–7.25
Western Canada[b] [12]	Ammonia	SMR + CCS (85%)	1.85	5.56
	Ammonia	Elec. (onshore wind)	2.68	6.39
Morocco [11]	H_2 pipeline	Elec. (onshore wind & solar)	1.59–3.07	3.54–5.71
Chile [11]	Liquid H_2	Elec. (onshore wind & solar)	1.29–2.53	2.67–4.47
Argentina [45] [c]	Ammonia	Elec. (on- and offshore wind & solar)	–	2.72–4.02
Australia [45]	Ammonia	Elec. (on- and offshore wind & solar)	–	3.32–4.93

[a] Present study. Note that conversion of ammonia to hydrogen upon delivery is not included; cost is in kgH_2-equivalent in terms of energy content.
[b] Based on 2020 conversion rate 1 EUR = 1.53 CAD (https://www.ecb.europa.eu/).
[c] The numbers given for this study likewise do not include conversion of ammonia to hydrogen at destination.

Table 5
Land use requirement for onshore wind installations in different scenarios by region, following the results presented in Fig. 6. We assume 8.6 km^2/MW to calculate the area. The regions are defined as in Fig. 6.

	2023		Scenario A (*business-as-usual*)		Scenario B (*moderate onshore*)		Scenario C (*accelerated offshore*)	
	GW	Area [km^2]	GW	Area [km^2]	GW	Area [km^2]	GW	Area [km^2]
North	0.7	82	5.6	659	8.9	1035	7.4	860
Central	1.8	204	0.9	101	2.8	326	0.9	105
South	2.5	296	13.1	1528	40.6	4721	8.1	942
Total	**5.0**	**582**	**19.6**	**2278**	**52.3**	**6082**	**16.4**	**1907**

ammonia synthesis (16.3 TWh annually). The electricity for blue hydrogen production is assumed to be generated using natural gas and thus will not impact the current electricity grid. Nevertheless, the need for renewable electricity expansion is significant, compared to the current onshore wind capacity of 5 GW [46]. Without offshore wind installations, the deployment of onshore wind turbines would need to be

Table 6
Average electricity prices by region in different scenarios compared to 2023. 5th to 95th percentile ranges across the sensitivity analysis are shown in brackets. The regions "North", "Central'' and "South" are defined in Fig. 6 for Scenarios A–C, whereas they correspond to the respective (group of) Nordpool pricing zones for 2023 prices.

€/MWh	2023	Scenario A *(business-as-usual)*	Scenario B *(moderate onshore)*	Scenario C *(accelerated offshore)*
North	30	56 *(50–62)*	64 *(56–70)*	59 *(52–66)*
Central	49	56 *(49–62)*	67 *(58–74)*	59 *(51–66)*
South	90	56 *(49–63)*	64 *(56–71)*	59 *(52–66)*
Overall average	70	56 *(50–63)*	64 *(56–71)*	59 *(52–66)*

increased by 2030 by 5 times compared to the installations done in the last 6 years, during which 925 wind turbines with a total capacity of 3.8 GW were installed [46].

To meet the demand for green hydrogen exports in Scenario B (*moderate onshore*), the total installed renewable energy capacity needs to increase more significantly than in Scenario A as this requires the generation of additional electricity for the electrolysis process (around 109 TWh a year). This entails an increase in the onshore wind capacities to at least 27 GW with some offshore wind installations, or to as high as 64 GW without any offshore wind installation (see Fig. 5). Although offshore wind installations are permitted in Scenario B, the model consistently proposed higher proportions of onshore wind installations than offshore wind installations as the former has a lower LCOE. On the other hand, Scenario C is constrained to only use power from offshore wind plants to produce the green hydrogen and sees a minimum offshore wind capacity of 28 GW. This is almost the same as the national ambition of 30 GW for offshore wind installations for 2040 [47] — the present study, however, targets 2030.

Fig. 6 shows the mean deployment of onshore wind and offshore wind in each of the model regions in Norway. In all the scenarios, the model proposed that the majority of the additional RES capacity should be installed in southern Norway. As good wind conditions can be found in the North and South, and marginal export costs (which are higher for exports from the North) are relatively insignificant for final LCOH, the preference for wind power in Southern Norway is likely due to a stronger transmission grid and greater hydropower capacity making it easy to maintain a high capacity factor for electrolysis, as well as avoiding wind power curtailment in periods of high wind power production.

Note that despite the lower demand for electricity in Scenario A, where the energy for blue hydrogen production is assumed to be generated from natural gas, there is still an average of 13 GW of onshore wind power in Southern Norway and about 6 GW in Northern Norway. This is mainly attributed to an increase in renewable electricity demand due to the constraint to meet a 55% reduction in CO_2 emissions. Increased Norwegian wind power production in Scenario A mostly feeds into a combination of partial electrification of transportation and industry. Today's installed onshore wind capacities in Southern Norway and Northern Norway stand at around 2.2 GW and 1.1 GW respectively [46]. This means that decarbonisation is expected to lead to a 6-fold increase in onshore wind power from a cost-minimisation perspective.

To produce green hydrogen, electrolysis plant capacity in both Scenarios B and C needs to reach around 14 GW. Thanks to the abundance of existing hydropower plants in Norway, the electrolysers can leverage the flexibility of hydropower and run at a high capacity factor of around 0.97 to balance the intermittent energy production inherent to variable renewable energy technologies. This flexibility, also including the transmission grid (including cross-border connections to the UK and continental Europe) is one of the reasons for the model preference for both onshore and offshore wind capacities primarily in Southern Norway, as seen in Fig. 6. In addition, the modelling results include an

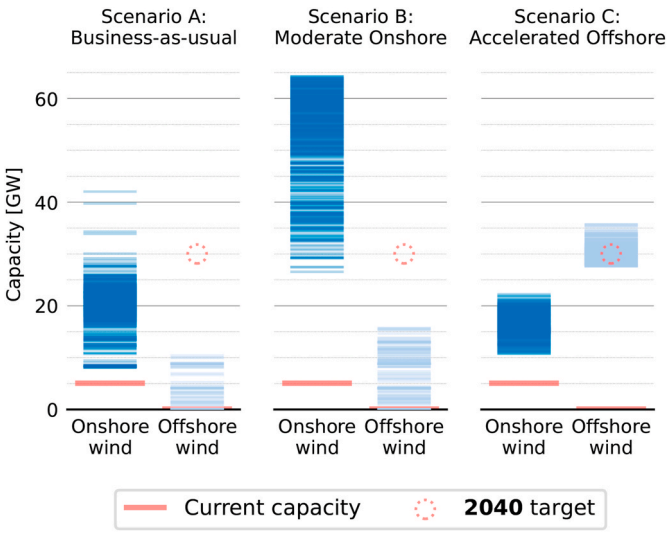

Fig. 5. Installed onshore and offshore wind capacities in Norway across Scenarios A, B & C. The plotted ranges indicate all observed capacities in the sensitivity analysis over 400 model runs.

average of 7.5 GW and 1.2 GW of solar installation in Scenarios B and C respectively, which is not shown in Fig. 6.

3.3. Social and environmental impacts

3.3.1. Land use requirement for onshore wind farms

The land area in Norway excluding Svalbard measures about 324,000 km^2, of which 42.5% (equivalent to 138,000 km^2) was classified as "undeveloped open land"[4] in the National Land Resource Map in 2021 [48], a first approximation of which areas could be perceived as suitable for wind power development. Breaking this down by region (using the latitude-based definition from Fig. 6), the open land areas in Southern Norway, Central Norway and Northern Norway are around 58,000 km^2, 25,000 km^2 and 55,000 km^2 respectively. The deployment of renewable energy technologies requires more land areas than fossil fuel. According to the Norwegian Water Resources and Energy Directorate (NVE), the *directly affected area* ("direkte påvirket areal") of onshore wind installation is estimated to be around 8.6 MW/km^2 [49]. In a study by the same, a country-wide total area of 16,705 km^2 was identified as potentially suitable for wind power development based on a number of exclusion criteria [50].

Based on the average onshore wind capacity needed for ammonia production, the land area required for the installation of the turbines in each of the Scenarios is shown in Table 5. The results show regional differences in the land impacts from renewable energy expansion and electricity impacts on the local communities in Norway, where Southern Norway is expected to be more affected than Northern Norway. In Scenario A (*business-as-usual*), the average of 20 GW of wind installations necessitates around 2278 km^2 of land area, equating to around 2.6% of open land area in Southern Norway and 1.2% in Northern Norway. Scenario B (*moderate onshore*) requires a significant amount of land area that represents about 8.2% of open land in Southern Norway and 1.9% in Northern Norway; the total land use amounts to 36% of the area identified as potentially suitable for wind development by a 2019 NVE report [50]. Scenario C (*accelerated offshore*) shows an

[4] Also known as "snaumark", area code 50 in the National Land Resource Map, corresponding to classes 18 (open firm ground) and 20 (bare rock, gravel and blockfields) in Ref. [44]. This includes areas used for reindeer husbandry. The total of 138,000 km^2 is based on the author's own calculations using the AR250 dataset.

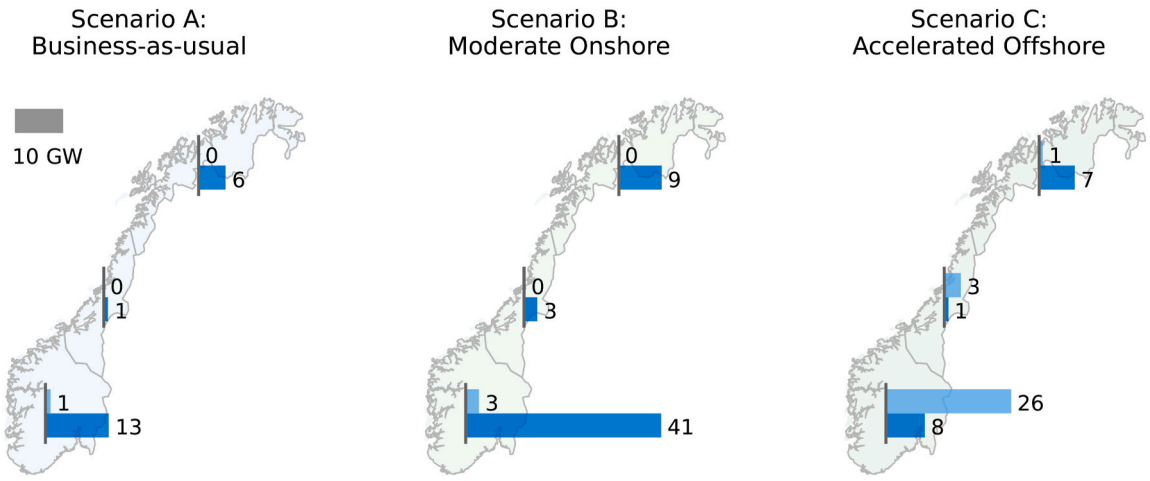

Fig. 6. Spatial distribution of onshore wind (dark blue) and offshore wind (light blue) capacities in Norway (in GW) between the different scenarios. The values shown are averagely over the 500 model runs used for sensitivity analysis. The bar in the top left is shown for scale. The capacities are given for Southern, Central and Northern Norway respectively; the regions correspond to groups of model nodes (as shown in Fig. 2) located south of, between and north of the 63°N and 67°N parallels. (For interpretation of the references to colour in this figure legend, the reader is referred to the Web version of this article.)

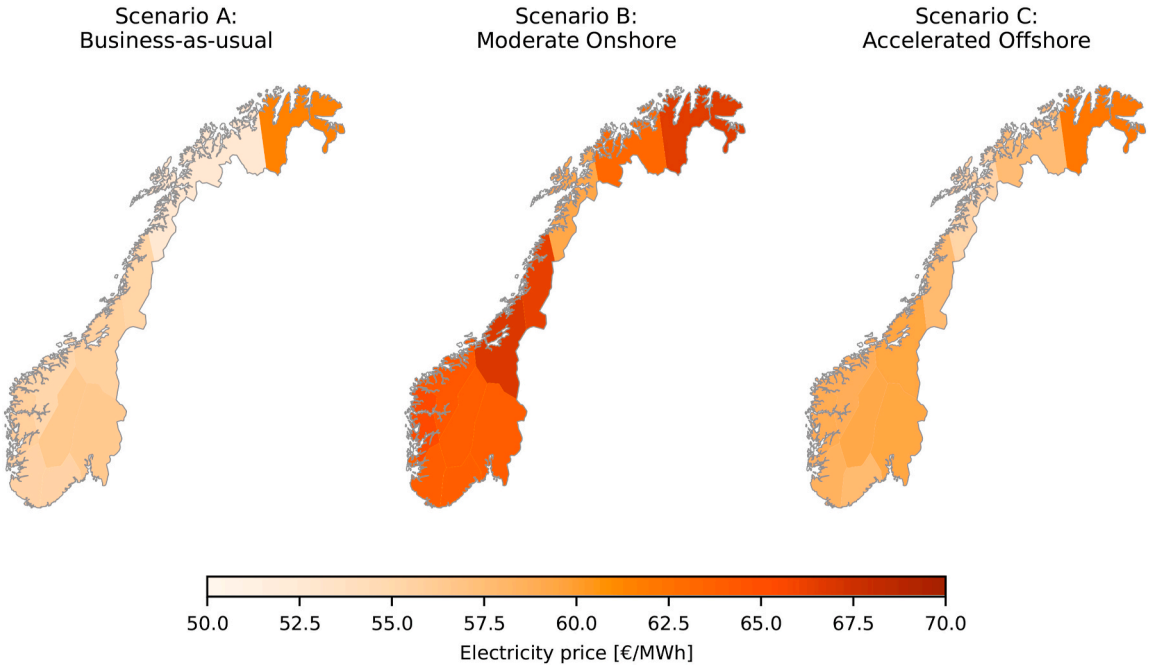

Fig. 7. Yearly mean electricity prices observed in the different scenarios by model region in Norway. These are the average prices observed across all sensitivity analysis model runs for each region. Note that prices are shown for model regions/nodes, not Nordpool pricing zones. See Table 6 for price ranges observed across the sensitivity analysis, presented by aggregated regions.

equal distribution of onshore wind between the South and the North, which represents about 1.6% of open land in each region.

To put things in perspective, the biggest city of Norway, Oslo, measures 454 km^2 in land area. The amount of land needed for reducing Norway's carbon emissions to be in line with its 2030 climate goal would require about 1907 km^2 (as shown in Scenario C), approximately about 4–5 times the size of Oslo. Achieving Scenario B would required a land area of 6082 km^2, that is more than 13 times the size of Oslo. Of this, the green hydrogen export industry requires 4175 km^2, equivalent to 9 times the size of Oslo.

3.3.2. *Electricity prices for the local communities*

The electricity prices in Norway are divided into 5 pricing zones: NO1 (South-east), NO2 (South), NO5 (South-west), NO3 (Central) and NO4 (North). Historically, NO1, NO2 and NO5 tend to share similar electricity prices due to the strong flows of electricity between the zones, but higher than in NO3 and NO4, due to the close connection with the grid in Continental Europe. In 2023, the average electricity price in Southern Norway (NO1, NO2 and NO5) was around €89.77/MWh, whereas the average electricity prices in Central Norway and Northern Norway were €48.54/MWh and €30.24/MWh respectively [51]. Note that the electricity prices include taxes except for Northern Norway where the electricity tax of 25% is exempted.

Electricity prices can be extracted from energy system optimisation models as the shadow prices of the set of constraints enforcing that electricity demand is met; these are optimisation outputs similar to electricity market prices. The results can indicate general trends but don't necessarily capture all market dynamics governing current-day

electricity prices (see also Limitations). Fig. 7 shows that in all scenarios, the regional differences in electricity prices become less prominent in 2030 compared to the average electricity prices in 2023. At the national level, the overall mean electricity prices for all scenarios are lower than in 2023. However, the implications for each region vary. Taking the mean value of the electricity prices calculated in Scenario A (*business-as-usual*), the increase in renewable energy installations in the south is expected to lead to a drop in the average electricity prices by −38% versus 2023, whereas the electricity prices in Central Norway are likely to increase by around 14% (refer to Table 6). Across all the scenarios, Northern Norway's electricity prices are expected to almost double the electricity prices in 2023.

The large increase in electrolysis-induced electricity demand in Scenario B (*moderate onshore*) leads average Norwegian electricity prices to jump from 50 to 63 €/MWh to 56–71 €/MWh compared to Scenario A. Even then, Southern Norway's electricity prices in 2030 are expected to be lower than in 2023 in Scenario B. Both Central and Northern Norway are expected to face higher electricity prices compared to 2023 prices and Scenario A. Green hydrogen exports are thus seen to have an equalising effect on electricity prices, with any low-price regions being exploited for exports by the model until the price matches other regions. Some of the price equalisation may however also be due to limitations in modelling transmission bottlenecks.

Shifting electricity production to offshore wind (Scenario C) is shown to be feasible, but necessitates total annual subsidies for offshore wind of €3.2 billion on average, equivalent to subsidising each kg of H_2 by €1.62, or a feed-in tariff of €27.9/MWh for offshore wind.[5] The subsidy leads to lower electricity prices in Scenario C than in Scenario B, even if the total system cost (and LCOH) is significantly higher. The total required subsidy could be compared with the willingness to pay around €22.4 (NOK 253) per household per month to shift wind production from onshore to offshore shown in Ref. [52], which would amount to a total annual subsidy of approximately €6,99 billion (counting 2.6 million households in Norway). However, the same study notes a comparable willingness to pay to ensure that wind development serves local or national needs but is not used for export purposes. Ensuring local/national ownership induces an even higher willingness to pay.

3.3.3. Alternative Scenario B for more onshore wind expansion in Northern Norway

In Section 3.3.1, the modelling results of Scenario B proposed a significant number of onshore wind turbines to be installed in Southern Norway, based on a cost-minimisation principle. To explore alternatives, we imposed a sequence of limitations on the onshore wind capacity in the Southern half of Norway (here defined as south of 65°N): 5, 10, 20, 30, 40, 50 and 60 GW (Fig. 8). The results show that southern onshore wind can be replaced by a combination of onshore wind in the North as well as offshore wind in the South; the balance between the two is relatively sensitive to technology costs. This shift, however, results in a higher LCOH on average, rising by €0.57/kgH_2 from the least to most restrictive case and further threatening the profitability of Norwegian green hydrogen.

[5] The offshore wind subsidy is calculated based on the dual variable of the model constraint that all electricity used for Norwegian hydrogen electrolysis comes from offshore wind on a net yearly basis (constraint 4 in Section 2.3); the value of this dual variable is €27.9/MWh on average across the cost sensitivity analysis. This is an output of the optimisation, and indicates how binding the offshore wind constraint is; it is equivalent to a subsidy in the sense that €27.9/MWh is the feed-in-tariff for offshore wind power production which would make it cost-optimal to build enough offshore wind power to supply all electrolysis demand, as per Scenario C. The value was multiplied by the total offshore wind power production figure to arrive at the total subsidy figure of €3.2 billion.

3.4. Limitations

Our model is based on a single weather year (2013) rather than multiple weather years. Previous research has shown that total system costs resulting from a capacity expansion model as in this study can vary significantly between weather years [30], meaning that the present study is likely to underestimate weather-induced variations in green hydrogen price. Moreover, the impacts of climate change are not reflected in our results. The aggregated nature of our model means that transmission bottlenecks may be imperfectly captured. The geographical scope is limited to Norway and neighbouring countries, meaning that the energy sectors of neighbouring countries themselves (and especially energy trade outside the model region, e.g. with France) is not perfectly modelled. Our model has perfect foresight over the entire year of operations, meaning that especially hydropower may be operated in a more optimal than realistic fashion. Moreover, our model does not include real-life time-dependent constraints on hydropower reservoir levels and downstream river flow, meaning that reservoir hydropower in the model can operate more flexibly than in real life. These factors combined could induce systematic biases in total system cost, electricity prices and LCOH.

Some assumptions regarding the choice of hydrogen pathway to model are open to uncertainty and could not all be subjected to sensitivity analysis. We choose to disregard the cost of and losses involved in ammonia cracking to produce hydrogen at the destination port; as explained in Section 2.1 this is because green hydrogen is often expected to be used as a feedstock for the production of liquid fuels such as ammonia. Still, this choice may cause final costs to be underestimated. On the other hand, we limit our analysis to ammonia shipping as the hydrogen transportation vector; hydrogen exports costs would improve once a pipeline is in place. These systematic effects are not considered in the determination of likely cost ranges based on sensitivity analysis.

Energy demands of various sorts (electricity, gas, heat, oil) in Norway and neighbouring countries are estimated for 2030 in this study using the sector-coupled version of PyPSA-Eur but left unchanged save for the additional 2 Mt hydrogen demand. This projection is, however, subject to uncertainty; a specific uncertainty pertaining to Norway is the degree of electrification of the offshore oil and gas industry. This uncertainty has not been specifically investigated in the present study but could impact especially the results on minimum onshore/offshore wind capacities required in Norway while meeting climate targets and not becoming a net electricity importer.

4. Discussion

4.1. Norwegian cost-competitiveness as a blue hydrogen exporter

As a blue hydrogen exporter to the EU, the analysis shows that Norway has some price advantage over Canada, mainly due to the transportation cost. The cost of production of hydrogen in Canada in Ref. [12] was calculated based on half the value of the natural gas prices assumed in our model and a lower carbon capture rate of 85%. Given that natural gas prices represent 45–70 % of grey hydrogen production [53] and the sensitivity of hydrogen production cost to natural gas prices, adjusting for these prices could allow Norway to be even more cost-competitive in blue hydrogen exports to the EU. While the transport of the CO_2 and sequestration in depleted fields is included in our model, this was computed as a fixed cost per ton of CO_2 at around €36.50/tCO_2, due to the uncertainty of the distance between the source of CO_2 and the potential CO_2 storage site. This cost is comparable to that estimated by a recent pilot CCS study, where the shipping costs of CO_2 in Norway by a CO_2 ship over a distance of between 433 km and 600 km was between €18–42/tCO_2 [54](€0.16–0.37/kgH_2 based on 8.9 kgCO_2/kgH_2 [55]).

The SMR in Scenario A involves an annualised investment of €1.5 billion, which is expected to capture about 23 Mt of CO_2 annually; almost half the total territorial GHG emissions in Norway in 2022 [56].

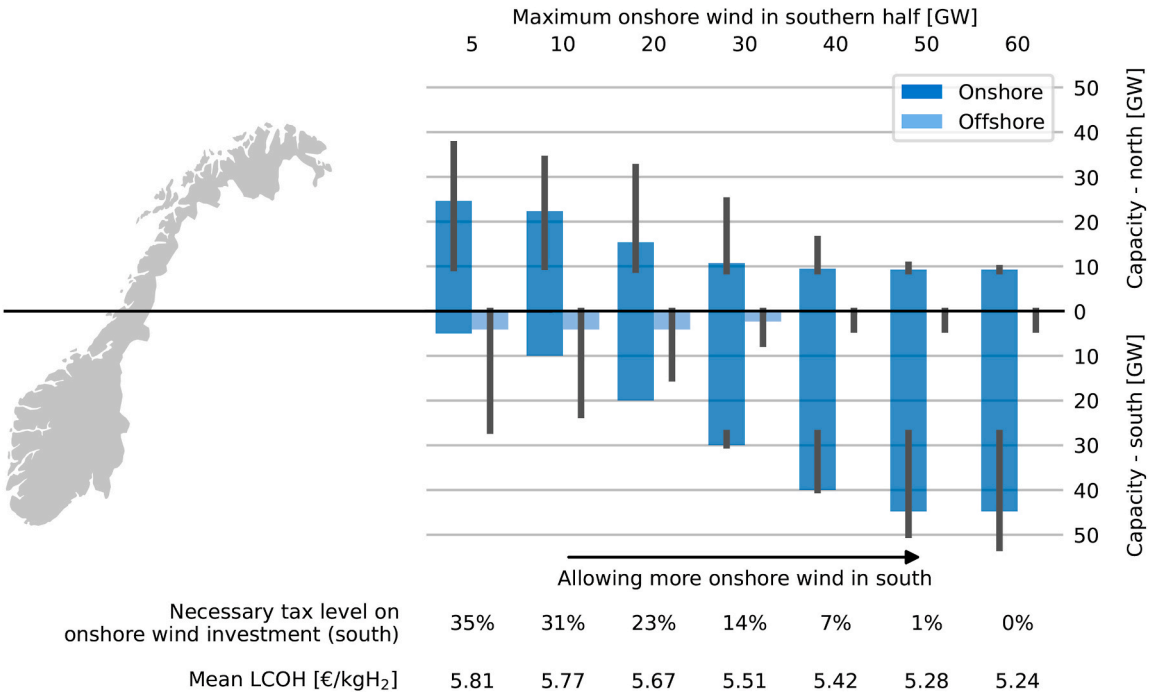

Fig. 8. Alternatives for the distribution mix of renewable energy capacity expansion for Scenario B. For the purpose of this figure, cost-optimisations for Scenario B (*moderate onshore*) are run with various caps on the total allowed onshore wind capacity in the southern half of Norway (south of 65 N), from 5 GW to 60 GW. The bar chart shows the resulting distribution of onshore wind and offshore wind installed south and north of 65 N, showing that onshore wind investment could be shifted to the north of Norway to some extent. The error bars show the 5th–95th percentile ranges over a cost-sensitivity analysis as described in Section 2.4. The first of the bottom two rows of the figure indicates the tax level on the onshore wind in the southern half of Norway required to make the given distribution profitable. These figures are derived from the shadow prices of the regional capacity constraints; outputs of the optimisations which indicate (in €/MW) how much the total system cost would be reduced if one additional MW of onshore wind were allowed in the south of Norway. The shadow price is also equivalent to the additional tax on onshore wind in the south (in €/MW) which would make the given total capacity cost-optimal. Dividing this number by the assumed capital cost of onshore wind (Table 2) gives a relative figure. The second row displays the resulting mean LCOH.

Despite a high CO_2 capturing rate of 90% at steam methane reformation plants, the blue hydrogen production would nevertheless result in 2.6 Mt of CO_2 emissions to the atmosphere. Based on an assumed carbon tax of €200/tCO_2 in 2030 [57], p. 14], the total carbon tax per year amounts to a hefty €4.6 billion. For reference, the shadow price of CO_2 in our model[6] is €85.6/tCO_2 in Scenarios B & C, and €89.1/tCO_2 in Scenario A — this is the model-wide carbon tax that would be required to lower emissions by 55% in the model.

Moreover, the feasibility of blue hydrogen export is contingent on the infrastructure for CO_2 transport from mainland Norway to potential CO_2 storage sites, which do not exist with the storage volumes required for this study today. The transport and storage of CO_2 in subsea reservoirs in Norway is subject to the Storage regulations of 5 December 2014 No. 1517 [58]. In 2022, two exploration licences for CO_2 storage were awarded, one in the North Sea, (outside of Bergen in the South) and one in the Barents Sea (outside of Hammerfest in the North) [59]. The exploration licences awarded are valid for four and three years respectively, and can be extended up to a maximum of ten years [58]. An exploitation licence may subsequently be granted before any installation of the necessary infrastructure can begin. When this will happen will depend on the results of the exploration licences, which are expected to expire in 2025 and 2026.

4.2. Norwegian cost-competitiveness as a green hydrogen exporter

Norway has historically enjoyed relatively cheaper electricity prices than continental Europe and this is expected to remain so in 2030 [60]. This implies that green hydrogen imported from Norway could be cheaper than that produced in continental Europe. Furthermore, the demand for hydrogen in Germany is higher than can be produced domestically, which makes Norway's green hydrogen export attractive. However, compared to other potential green hydrogen exporters like Chile, Morocco, Australia and Argentina, Norway is less cost competitive, mainly due to the electricity generation from solar PV, whose LCOE is known to be lower than onshore and offshore wind, as well as possibly electricity market effects.

Nevertheless, Norway has a long-standing relationship with the EU as an important strategic trading partner and the joint-statement on hydrogen cooperation between Norway and Germany indicates that this will likely remain unchanged [19]. Therefore, Norway could still be an important green hydrogen exporter for the EU, but the size of the market share depends highly on the amount of renewable energy Norway can generate in the next 6 years.

4.3. Energy policy implications

With fast-depleting petroleum resources [61], Norway needs to explore new avenues to secure a post-petroleum future. Given the dependence on gas to produce blue hydrogen, it is destined to play a temporal role in the low-carbon energy future. In the long-run, the EU plans to reduce its dependence on fossil fuel, which makes green hydrogen a better market to tap into. As the results in Section 3.3.1 show, substantial amount of land is needed to develop an export market based on green hydrogen using onshore wind. Careful planning and allocation of resources is required to ensure efficient use of land which provides long-term benefits to the communities in Norway that can last beyond the petroleum future. According to Norway's power system

[6] The shadow price of CO_2 is an optimisation output, being the dual variable of the global CO_2 emissions constraint. Its level indicates the marginal cost of reducing total CO_2 emissions by one tonne.

operator, Statnett, the electrification of petroleum offshore platforms requires about 20 TWh [62]. Based on an average wind capacity factor of 30%, this equates to about 7.6 GW onshore wind capacity (884 km^2 of land area), accounting for almost half of the decarbonisation power needs assumed in our model for 2030. If this power demand can be supplied by either the use of gas with carbon capture or with offshore wind power, this would provide the petroleum industry the opportunity to demonstrate its leadership in both technologies. Meanwhile, the land-use impact of the green hydrogen export industry would be reduced. This would be a win-win solution for Norway to develop three potential markets in the post-petroleum future.

The expansion of renewable energy is needed to ensure that overall electricity prices will remain competitive in Norway for Norwegian end-users in spite of the production of green hydrogen exports. If the roll-out of renewable energy follows the cost-optimisation results, the electricity prices between the regions will be more homogeneous, which would benefit Southern Norway the most. Central Norway will see some increase in electricity prices and Northern Norway would lose its long-time advantage of being the region with the lowest electricity prices. Overall, Norway will risk eroding its competitiveness as a potential hydrogen exporter, if the production of blue and green hydrogen for export is not followed by the expansion of renewable energy proposed by the model. This will also likely affect other energy-intensive industries in Norway which are dependent on cheap electricity prices to compete in the global market.

The lower electricity prices in Southern Norway in the scenarios may be due to the proposed installation of most of the onshore and offshore wind turbines in the South of Norway. Part of the reason is due to the weak transmission network in Northern Norway. However, concentrating the growth of new industries in Southern is likely to accentuate the problem of declining population in Northern Norway [63]. Maintaining a permanent population in Northern Norway is crucial for Norway's national security due to its proximity to the Russian border, a concern that has intensified following the war in Ukraine. Therefore, it is essential to promote more equitable distribution of renewable energy development across Norway. This can be achieved by upgrading the existing transmission grid in the North and providing government grants and incentives to enhance economic viability of onshore and offshore wind parks in Northern Norway.

Historically, onshore wind parks were often built in windy and exposed, but scenic locations due primarily to political concerns for power supply and cost-effectiveness, rather than less cost-effective but visually less intrusive locations [64]. This fostered the perception that public opinion about nature conservation concerns were ignored, thereby fuelling popular resistance against onshore wind [64]. Part of the resistance may also be due to the perceived erosion of local self-determination rights, where national and/or international interests take precedence over local concerns [65]. A case in point is the Fosen Vind conflict with the Sámi reindeer herders, where the Supreme Court of Norway ruled that the concession of two wind parks of the former violated the rights of the former as indigenous people to conduct their cultural practices, reindeer husbandry [66]. This case proved that failing to address these concerns adequately could be costly for all stakeholders; the reindeer herders suffered a significant loss of reindeer winter grazing pastures [66]; the international credibility of the Norwegian government as an environmental leader was tarnished, which could affect its prospects securing a market for its green products including green hydrogen; the financial compensation to the former will cost Fosen Vind millions of kroner [67]. The ruling further implies that future wind power expansion in Central and Northern Norway will face a permanent constraint from the spatial sovereignty claims of the indigenous community [65], making it more difficult to realise all three scenarios in these regions.

Nevertheless, while the public opinion towards onshore wind still trends negatively, it has improved slightly since the war in Ukraine [68,69]. This may be because of the perceived need for greater energy security following the energy crisis in Europe resulting from the war. The reverse trend in public opinion demonstrates that it is not static and could evolve depending on people's perceptions of the need for renewable energy expansion. Future energy policies may thus have better success in expanding renewable energy if the locals' needs and concerns are identified and addressed adequately prior to implementation.

Compared to onshore wind, offshore wind is more well-received by the public across all the regions in Norway, with more than 70% positive responses in a national survey on opinions about offshore wind [23,52]. Although bottom-fixed offshore wind is assumed to cost almost half of that of floating offshore wind (see Table 2), the modelling results suggested significantly more installations of the latter. The reason is due to the limited amount of suitable area (sea beds of less than 60 m deep) for bottom-fixed offshore wind installations. In any case, floating offshore wind is socially and politically more popular, not least due to less visual impact on the seascape and lower negative environmental impacts [70]. Floating offshore wind technologies are seen as more compatible with the existing Norwegian energy political paradigm thanks to the transferable competences and knowledge from the petroleum and maritime industries [70]. The distribution of offshore wind installations suggested in the model is similar to that of the allocated areas for offshore wind installations in Southern Norway [71] and the potential areas identified as technically feasible with minimal risk of conflicts with other sea users by NVE [72], where thirteen out of twenty are in Southern Norway. The results show that subsidies amounting to €27.9/MWh would be needed to make Norwegian offshore wind competitive with onshore wind. This is double the amount of subsidies that is allocated to the recently auctioned 1500 MW floating offshore wind project Sørlige Nordsjøen II, that has a lifetime cap of 23 billion NOK [73] which translates to an expected €13.9/MWh (assuming a lifetime of 20 years and capacity factor of 0.559 [74]). The development of a green hydrogen-based export market in Norway depends on both onshore and offshore wind expansion. To accelerate the development of the offshore wind, thereby securing its market share as an important supplier of green hydrogen export to the EU, more financial support is needed from the Norwegian government.

5. Conclusion

The modelling results show that all the scenarios are technically and economically feasible. However, each scenario requires some trade-offs between the short-term and long-term costs and benefits. While Norway seems to have a cost advantage over its competitors for blue hydrogen exports, this entails the continued dependence of natural gas, which is fast-depleting in Norway. To secure a post-petroleum future, Norway needs to leverage its technological competencies and other resources to accelerate the development of new industries. As leaders in both CCS and offshore wind technologies, the Norwegian petroleum industry is well-positioned to decarbonise its offshore platforms and produce both blue and green hydrogen at large scale, without significant need for electricity from the mainland grid. Succeeding in the feat would allow the industry to demonstrate the viability of both technologies and gain a foothold in exporting those technologies globally.

If the annual power from Norway's mainland grid meant for decarbonising offshore platforms (20 TWh) is used for developing new industries like green hydrogen export, the amount of land area required for onshore wind expansion will be reduced by 884 km^2 (about twice the size of Oslo). Nonetheless, a significant expansion of onshore wind installations will be necessary until offshore wind technology is mature, to maintain relatively low electricity prices for both existing and new energy-intensive industries, such as green hydrogen export. While the model favours the installation of onshore wind turbines in Southern Norway based on cost-optimisation principles, developing new industries in Northern Norway may help address the problem of declining population and enhance Norway's national security in the North, which

shares the border with Russia. Therefore, it is critical to promote a more equitable distribution of renewable energy development across Norway. This may be achieved through upgrading the existing transmission infrastructure and providing government support schemes to enhance the economic viability of onshore wind turbines in the North. Further, the development of renewable energy capacity should proceed with adequate care and attention to locals' needs and concerns as failure to do so can be very costly for all stakeholders.

Lastly, if Norway wants to gain a foothold as an important green hydrogen exporter to the EU, it is essential to advance the technological maturity of offshore wind, particularly floating offshore wind. Our results show that the current subsidies of ~€14/MWh for the offshore wind industry is insufficient. A doubling of the subsidies is needed to make Norwegian offshore wind competitive with onshore wind.

Data and code availability

All data and code needed to reproduce the results and figures in this work can be found at https://github.com/koen-vg/pypsa-eur/tree/hydrogen-exports-v0.1.

CRediT authorship contribution statement

C. Cheng: Writing – review & editing, Writing – original draft, Visualization, Methodology, Investigation, Formal analysis. **K. van Greevenbroek:** Writing – review & editing, Writing – original draft, Visualization, Software, Methodology, Investigation, Formal analysis, Data curation, Conceptualization. **I. Viole:** Writing – review & editing, Writing – original draft, Methodology, Investigation, Formal analysis, Data curation, Conceptualization.

Declaration of competing interest

The authors declare the following financial interests/personal relationships which may be considered as potential competing interests: Isabelle Viole reports financial support was provided by European Union (Horizon 2020). If there are other authors, they declare that they have no known competing financial interests or personal relationships that could have appeared to influence the work reported in this paper.

Acknowledgements

This work was inspired by cooperation within the Norwegian research school on hydrogen and hydrogen-based fuels (HySchool). Isabelle Viole further acknowledges funding from the European Union's Horizon 2020 research and innovation programme under grant agreement No 951815 (AtLAST project). The authors are grateful to Berit Kristoffersen (Department of Social Sciences, UiT The Arctic University of Norway) and Marianne Zeyringer (Department of Technology Systems, University of Oslo) for their helpful comments on the manuscript drafts.

References

[1] European Commission, Directorate-General for Climate Action. Going climate-neutral by 2050 – a strategic long-term vision for a prosperous, modern, competitive and climate-neutral EU economy [Online]. Available: https://op.europa.eu/en/publication-detail/-/publication/92f6d5bc-76bc-11e9-9f05-01aa75ed71a1; 2019.

[2] European Commission. Commission staff working document implementing the REPowerEU action plan: investment needs, hydrogen accelerator and achieving the bio-methane targets [SWD/2022/230 final] [Online]. Available: https://eur-lex.europa.eu/legal-content/EN/TXT/?uri=SWD%3A2022%3A230%3AFIN; May 18, 2022.

[3] Norwegian Petroleum Directorate. Exports of oil and gas [Online]. Available: https://www.norskpetroleum.no/en/production-and-exports/exports-of-oil-and-gas/; 2023.

[4] Hjeij D, Bicer Y, Al-Sada M bin S, Koç M. Hydrogen export competitiveness index for a sustainable hydrogen economy. Energy Rep 2023;9:5843–56. https://doi.org/10.1016/j.egyr.2023.05.024.

[5] Espegren K, Damman S, Pisciella P, Graabak I, Tomasgard A. The role of hydrogen in the transition from a petroleum economy to a low-carbon society. Int J Hydrogen Energy Jul. 2021;46(45):23125–38. https://doi.org/10.1016/j.ijhydene.2021.04.143.

[6] Cheng CSW. Does time matter? A multi-level assessment of delayed energy transitions and hydrogen pathways in Norway. Energy Res Social Sci Jun. 2023;100:103069. https://doi.org/10.1016/j.erss.2023.103069.

[7] Statistics Norway, "08307: produksjon, import, eksport og forbruk av elektrisk kraft (GWh), etter år og statistikkvariabel." [Online]. Available: https://www.ssb.no/statbank/table/08307/tableViewLayout1/; 2024.

[8] Statnett. Langsiktig markedsanalyse: norge, norden og europa 2022-2050 [Online]. Available: https://www.statnett.no/contentassets/723377473d80488a9c9abb4f5178c265/langsiktig-markedsanalyse-norden-og-europa-2020-50—final.pdf; 2023.

[9] Seck GS, et al. Hydrogen and the decarbonization of the energy system in europe in 2050: a detailed model-based analysis. Renew Sustain Energy Rev Oct. 2022;167:112779. https://doi.org/10.1016/j.rser.2022.112779.

[10] Heuser P-M, Ryberg DS, Grube T, Robinius M, Stolten D. Techno-economic analysis of a potential energy trading link between Patagonia and Japan based on CO2 free hydrogen. Int J Hydrogen Energy May 2019;44(25):12733–47. https://doi.org/10.1016/j.ijhydene.2018.12.156.

[11] Galimova T, Fasihi M, Bogdanov D, Breyer C. Impact of international transportation chains on cost of green e-hydrogen: global cost of hydrogen and consequences for Germany and Finland. Appl Energy Oct. 2023;347:121369. https://doi.org/10.1016/j.apenergy.2023.121369.

[12] Okunlola A, Giwa T, Di Lullo G, Davis M, Gemechu E, Kumar A. Techno-economic assessment of low-carbon hydrogen export from western Canada to eastern Canada, the USA, the asia-pacific, and europe. Int J Hydrogen Energy Feb. 2022;47(10):6453–77. https://doi.org/10.1016/j.ijhydene.2021.12.025.

[13] Roos TH. The cost of production and storage of renewable hydrogen in South Africa and transport to Japan and EU up to 2050 under different scenarios. Int J Hydrogen Energy Oct. 2021;46(72):35814–30. https://doi.org/10.1016/j.ijhydene.2021.08.193.

[14] Sleiti AK, Al-Ammari WA, Musharavati F, Azizur Rahman M. Techno-economic assessment of low-carbon hydrogen exports from the Middle East to the Asia-Pacific, and Europe. Energy Sources B Energy Econ Plann Dec. 2023;18(1):2254764. https://doi.org/10.1080/15567249.2023.2254764.

[15] Andreassen K, Buenger U, Henriksen N, Oyvann A, Ullmann O. Norwegian hydro energy in Germany (NHEG). Int J Hydrogen Energy Apr. 1993;18(4):325–36. https://doi.org/10.1016/0360-3199(93)90047-E.

[16] Stiller C, et al. Options for CO2-lean hydrogen export from Norway to Germany. Energy Nov. 2008;33(11):1623–33. https://doi.org/10.1016/j.energy.2008.07.004.

[17] Ishimoto Y, Voldsund M, Nekså P, Roussanaly S, Berstad D, Gardarsdottir SO. Large-scale production and transport of hydrogen from Norway to Europe and Japan: value chain analysis and comparison of liquid hydrogen and ammonia as energy carriers. Int J Hydrogen Energy 2020;45. https://doi.org/10.1016/j.ijhydene.2020.09.017.

[18] Terlouw T, Bauer C, McKenna R, Mazzotti M. Large-scale hydrogen production *via* water electrolysis: a techno-economic and environmental assessment. Energy Environ Sci 2022;15(9):3583–602. https://doi.org/10.1039/D2EE01023B.

[19] Norway Office of Prime Minister and Norwegian Ministry of Energy, "Joint Statement - Germany – Norway - Hydrogen," Government.no. Accessed: February. 9, 2024. [Online]. Available: https://www.regjeringen.no/en/whatsnew/dep/smk/press-releases/2023/closer-cooperation-between-norway-and-germany-to-develop-green-industry/joint-statement-germany-norway-hydrogen/id2958105./.

[20] Deutsche Energi-Agentur GmbH, Gassco AS. German-Norwegian energy cooperation joint feasibility study - hydrogen value chain summary report [Online]. Available: https://gassco.eu/wp-content/uploads/2023/11/GER-NOR-Joint-feasibility-study-report-Hydrogen-23.11.2023.pdf; 2023.

[21] IEA. The Future of Hydrogen: seizing today's opportunities. 2019.

[22] IRENA. Global hydrogen trade to meet the 1.5 °C climate goal: Part II – technology review of hydrogen carriers. Int Renew Energy Agency, Abu Dhabi 2022 [Online]. Available: https://www.irena.org/-/media/Files/IRENA/Agency/Publication/2022/Apr/IRENA_Global_Trade_Hydrogen_2022.pdf.

[23] Tvinnereim Endre, Faleid Ingrid Kvåle. Hva mener folk om vindkraft på land og til havs? [Online]. Available: https://www.uib.no/sites/w3.uib.no/files/attachments/tvinnereim_og_faleide_-_hva_mener_folk_om_vindkraft.pdf; 2023.

[24] Wasserstoffrat Nationaler. Treibhausgaseinsparungen und der damit verbundene Wasserstoffbedarf in Deutschland [Online]. Available: https://www.wasserstoffrat.de/fileadmin/wasserstoffrat/media/Dokumente/2023/2023-02-01_NWR_Grundlagenpapier_H2-Bedarf_2.pdf; 2023.

[25] Energie-Agentur Deutsche, Gassco. German-Norwegian joint energy cooperation feasibility study report [Online]. Available: https://gassco.eu/wp-content/uploads/2023/11/GER-NOR-Joint-feasibility-study-report-Hydrogen-23.11.2023.pdf; 2023.

[26] Hörsch J, Hofmann F, Schlachtberger D, Brown T. PyPSA-Eur: an open optimisation model of the European transmission system. Energy Strategy Rev Nov. 2018;22:207–15. https://doi.org/10.1016/j.esr.2018.08.012.

[27] Brown T, Schlachtberger D, Kies A, Schramm S, Greiner M. Synergies of sector coupling and transmission reinforcement in a cost-optimised, highly renewable European energy system. Energy 2018;160:720–39. https://doi.org/10.1016/j.energy.2018.06.222.

[28] "A comparison of clustering methods for the spatial reduction of renewable electricity optimisation models of Europe | Energy Inform! Full Text." Accessed: August. 15, 2024. [Online]. Available: https://energyinformatics.springeropen.com/articles/10.1186/s42162-022-00187-7.
[29] Pineda S, Morales JM. Chronological time-period clustering for optimal capacity expansion planning with storage. IEEE Trans Power Syst Nov. 2018;33(6):7162–70. https://doi.org/10.1109/TPWRS.2018.2842093.
[30] Grochowicz A, van Greevenbroek K, Benth FE, Zeyringer M. Intersecting near-optimal spaces: European power systems with more resilience to weather variability. Energy Econ Feb. 2023;118:106496. https://doi.org/10.1016/j.eneco.2022.106496.
[31] Hörsch J, Hofmann F, Schlachtberger D, Brown T. PyPSA-Eur: an open optimisation model of the European transmission system. Energy Strategy Rev Nov. 2018;22:207–15. https://doi.org/10.1016/j.esr.2018.08.012.
[32] European Environment Agency, "CORINE land cover 2012," EEA geospatial data catalogue. Accessed: April. 22, 2024. [Online]. Available: doi.org/10.2909/a84ae124-c5c5-4577-8e10-511bfe55cc0d.
[33] European Central Bank. Norwegian krone/Euro, Annual. ECB Data Portal; 2023 [Online]. Available: https://data.ecb.europa.eu/data/datasets/EXR/EXR.A.NOK.EUR.SP00.E.
[34] International Energy Agency. The future of hydrogen. Paris: International Energy Agency; 2019 [Online]. Available: https://www.iea.org/reports/the-future-of-hydrogen. [Accessed 9 August 2022].
[35] NVE. Kostnader for kraftproduksjon [Online]. Available: https://www.nve.no/energi/analyser-og-statistikk/kostnader-for-kraftproduksjon/; 2023.
[36] Danish Energy Agency. Technology data for renewable fuels [Online]. Available: https://www.ens.dk/teknologikatalog. [Accessed 9 January 2024].
[37] International Energy Agency, "Special Report on Carbon Capture Utilisation and Storage - CCUS in clean energy transitions," IEA. Accessed: February. 16, 2024. [Online]. Available: https://www.iea.org/data-and-statistics/charts/global-average-levelised-cost-of-hydrogen-production-by-energy-source-and-technology-2019-and-2050.
[38] Fulwood Mike. A new global gas order? (Part 1): the outlook to 2030 after the energy crisis, NG 184. Oxford Institute for Energy Studies; 2023. https://www.oxfordenergy.org/wpcms/wp-content/uploads/2023/07/NG-184-A-New-Global-Gas-Order-Part-1.pdf.
[39] Killingland Magnus, Boge Matias Krogh, Magneschi Guido. Potential for reduced costs for carbon capture, transport and storage value chains (CCS), vols. 2019–1092. DNV GL Energy; 2020. p. 2. Rev [Online]. Available: https://ccsnorway.com/app/uploads/sites/6/2020/10/Potential-for-reduced-cost-for-carbon-capture-2019.pdf.
[40] Mongird Kendall, Viswanathan Vilayanur, Alam Jan, Vartanian Charlie, Vincent Sprenkle, Baxter Richard. Grid energy storage technology cost and performance assessment. US Department of Energy, DOE/PA-0204, 2020; 2020.
[41] Alexis Michael Bazzanella, Ausfelder Florian. Low carbon energy and feedstock for the European chemical industry. DECHEMA; 2017.
[42] Salmon N, Bañares-Alcántara R. Green ammonia as a spatial energy vector: a review. Sustain Energy Fuels Jun. 2021;5(11):2814–39. https://doi.org/10.1039/D1SE00345C.
[43] Statistics Norway. Standard for classification of areas for statistical purposes [Online]. Available: https://www.ssb.no/en/klass/klassifikasjoner/118. [Accessed 20 February 2024].
[44] Statistics Norway. Table 09594: land use and land cover (km^2), by region, area classification, contents and year [Online]. Available: https://www.ssb.no/en/statbank/table/09594/tableViewLayout1/, ; 2024.
[45] Hampp J, Düren M, Brown T. Import options for chemical energy carriers from renewable sources to Germany. PLoS One Feb. 2023;18(2):e0262340. https://doi.org/10.1371/journal.pone.0281380.
[46] NVE. Vindkraftdata [Online]. Available: https://www.nve.no/energi/energisystem/vindkraft/vindkraftdata/; 2023.
[47] Norwegian Government. Kraftfull satsing på havvind [Online]. Available: https://www.regjeringen.no/no/aktuelt/kraftfull-satsing-pa-havvind/id2912297/; May 11, 2022.
[48] Heggem ESF, Mathisen H, Frydenlund J. AR50 – arealressurskart i målestokk 1:50 000. Et heldekkende arealressurskart for jord- og skogbruk. NIBIO; 2019 [Online]. Available: https://nibio.brage.unit.no/nibio-xmlui/handle/11250/2626573. [Accessed 25 April 2024].
[49] NVE. Direkte påvirket areal - NVE [Online]. Available: https://www.nve.no/energi/energisystem/vindkraft/arealbruk-for-vindkraftverk/direkte-paavirket-areal/. [Accessed 26 February 2024].
[50] Bjerkestrand Erlend. Forslag til nasjonal ramme for vindkraft. Norges vassdrags- og energidirektorat. 2019.
[51] Forbrukerådet, "Historiske strømpriser," Forbrukerrådet. Accessed: February. 27, 2024. [Online]. Available: https://forbrukerradet.no/strompris/.
[52] Linnerud K, Dugstad A, Rygg BJ. Do people prefer offshore to onshore wind energy? The role of ownership and intended use. Renew Sustain Energy Rev Oct. 2022;168:112732. https://doi.org/10.1016/j.rser.2022.112732.
[53] IEA. 07 cross-cutting: hydrogen [Online]. Available: https://www.cceguide.org/wp-content/uploads/2020/08/07-IEA-Cross-cutting.pdf; 2020.
[54] Jordal Kristin, et al. The CCS Midt-Norge cluster - industrial CCS collaboration for exploring synergies and common interests. SINTEF; 2023, 00230.
[55] Collodi G, Azzaro G, Ferrari N, Santos S. Techno-economic evaluation of deploying CCS in SMR based Merchant H2 production with NG as feedstock and fuel. Energy Proc Jul. 2017;114:2690–712. https://doi.org/10.1016/j.egypro.2017.03.1533.
[56] Statistics Norway. Table 13931: greenhouse gases, by source, energy product and pollutant, GWP-values due to Paris agreement (AR5) 1990 - 2022 [Online]. Available: https://www.ssb.no/en/statbank/table/13931/tableViewLayout1/. [Accessed 28 February 2024].
[57] Norwegian Ministry of Climate and Environment. Norway's climate action plan for 2021-2030 [white paper] [Online]. Available: https://www.regjeringen.no/contentassets/a78ecf5ad2344fa5ae4a394412ef8975/en-gb/pdfs/stm202020210013000engpdfs.pdf; 2020.
[58] Norwegian Ministry of Energy. Forskrift om utnyttelse av undersjøiske reservoarer på kontinentalsokkelen til lagring av CO2 og om transport av CO2 på kontinentalsokkelen [Online]. Available: https://lovdata.no/dokument/SF/forskrift/2014-12-05-1517?q=Forskrift+om+utnyttelse+av+undersj%C3%B8iske. [Accessed 15 February 2024].
[59] Norwegian Offshore Directorate. "Announcement 2021, round 1," Licences for carbon storage [Online]. Available: https://www.sodir.no/en/facts/carbon-storage/licences-for-carbon-storage/2021/. [Accessed 15 February 2024].
[60] NVE. Rapport nr. 25/2023 - Langsiktig kraftmarkedsanalyse 2023 : energiomstillingen – en balansegang. 2023.
[61] Norwegian Petroleum Directorate. Resource report 2022 [Online]. Available: https://www.npd.no/en/facts/publications/reports/resource-report/resource-report-2022/; 2022.
[62] Statnett. Forbruksutvikling i Norge 2022-2050 - delrapport til Langsiktig markedsanalyse 2022-2050 [Online]. Available: https://www.statnett.no/om-statnett/nyheter-og-pressemeldinger/nyhetsarkiv-2023/forventer-kraftig-vekst-i-kraftforbruket-avhengig-av-nett-og-mer-kraftproduksjon/. [Accessed 10 May 2024].
[63] Vennerød Ø, Scjøtt-Pedersen KE. The Impending population decline in northern Norway: implications and demographic challenges. Arctic Review 2023;14(Sep). https://doi.org/10.23865/arctic.v14.5465.
[64] Moe E, Hansen ST, Kjær EH. Why Norway as a green battery for europe is still to happen, and probably will not. In: Midford P, Moe E, editors. New challenges and solutions for renewable energy. Cham: Springer International Publishing; 2021. p. 281–317. https://doi.org/10.1007/978-3-030-54514-7_12. International Political Economy Series.
[65] Hansen ST, Moe E. Renewable energy expansion or the preservation of national energy sovereignty? Norwegian renewable energy policy meets resource nationalism. Polit Geogr Nov. 2022;99:102760. https://doi.org/10.1016/j.polgeo.2022.102760.
[66] Norwegian Supreme Court I. Statnett SF v. Sør-Fosen sijte, Nord-Fosen siida & Fosen Vind DA, II) Fosen Vind DA v. Sør-Fosen sijte & Nord-Fosen siida, III) Sør-Fosen sijte v. Fosen Vind DA 2021 [Online]. Available: https://www.domstol.no/globalassets/upload/hret/avgjorelser/2021/oktober-2021/hr-2021-1975-s.pdf.
[67] Opsal K, Mudenia Håkon, Skartland Ellinor, Saxrud Myrvang, Frida. Fosen-saken: Enighet om mellom Nord-Fosen siida og staten. NRK; Mar. 06, 2024 [Online]. Available: https://www.nrk.no/trondelag/enighet-om-mellom-nord-fosen-og-roan-vind-1.16792292. [Accessed 10 May 2024].
[68] Vågerö O, Bråte A, Wittemann A, Robinson JY, Zeyringer M, Sirotko-Sibirskaya N. Machine learning of public sentiments towards wind energy in Norway. Wind Energy Feb. 2024;2902. https://doi.org/10.1002/we.2902.
[69] Cicero. Vindkraft på land [Online]. Available: https://cicero.oslo.no/no/ciceros-klimaundersokelse/Oppfatninger-om-virkemidler-og-tiltak/Vindkraft-pa-land. [Accessed 1 March 2024].
[70] Dahl IR, Tveiten BW, Cowan E. The case for policy in developing offshore wind: lessons from Norway. Energies Feb. 2022;15(4):1569. https://doi.org/10.3390/en15041569.
[71] Ministry of Petroleum and Energy. "Three new offshore wind areas considered for opening and tender in 2025," Government [Online]. Available: https://www.regjeringen.no/en/aktuelt/tre-nye-havvindomrade-aktuelle-for-opning-og-utlysing-i-2025/id2993904/, . [Accessed 4 March 2024].
[72] NVE. Foreslår å utrede disse 20 områdene for havvind [Online]. Available: https://www.nve.no/nytt-fra-nve/nyheter-energi/foreslaar-aa-utrede-disse-20-omraadene-for-havvind/. [Accessed 4 March 2024].
[73] Olje- og energidepartementet. Utlysning av konkurranse om et prosjektområde i Sørlige Nordsjø II til fornybar energiproduksjon til havs [Online]. Available: https://www.regjeringen.no/contentassets/bd4d260de2c242beb661494550b8d7a3/utlysningsdokumenter-for-konkurranse-om-et-prosjektomrade-i-sorlige-nordsjo-ii.pdf. [Accessed 23 April 2023].
[74] Noregs vassdrags- og energidirektorat. Beregning av kraftproduksjon for de identifiserte områdene [Online]. Available: https://veiledere.nve.no/havvind/identifisering-av-utredningsomrader-for-havvind/metode-og-vurderinger/beregning-av-kraftproduksjon/. [Accessed 23 April 2024].